Molecular Orientation and Relaxation Behavior in Flexible Water-Blown Polyurethane Foams

by

John C. Moreland

Thesis submitted to the Faculty of the

Virginia Polytechnic Institute and State University

in partial fulfillment of the requirements for the degree of

Master of Science

in

Chemical Engineering

APPROVED:

G.L. Wilkes, Chairman

M.E. Davis

W.G. Glasser

February, 1989

Blacksburg, Virginia

Molecular Orientation and Relaxation Behavior in Flexible Water-Blown Polyurethane Foams

by

John C. Moreland

G.L. Wilkes, Chairman

Chemical Engineering

(ABSTRACT)

A set of flexible water-blown slabstock polyurethane foams and their respective compression molded plaques as well as a chemically similar polyurea-urethane elastomer, PUUE, were studied to better understand the relaxation behavior and the molecular orientation upon deformation in these systems. The two main experimental techniques used in this investigation were stress relaxation in tension and deformation-IR dichroism. The stress relaxation in the foams and their respective plaques increased with hard segment content. The stress relaxation in the foams also appeared to depend very little on its anisotropic cell geometry and hence, mainly on the material comprising the cell-wall struts and windows. Segmental orientation was measured as a function of elongation, and relaxation, as well as hysteresis behavior for several of the plaques and the PUUE elastomer. The orientation changes upon deformation in the soft segments of both materials were small. Small changes in orientation with time and upon cyclic straining were also observed for the soft segments. The orientation at the interface of the hard and soft segments was influenced more by the soft segments in comparison to the hard segments in the plaques and in the PUUE elastomer. Significant transverse orientation upon deformation was observed in the hard segments of the plaques and up to elongations of 100 percent for the PUUE elastomer. Based on this transverse orientation behavior, the polyurea aggregates in the plaques were thought to possess a lamellar-like structure with the long axis of the aggregates aligning in the stretch direction. Relaxation and hysteresis behavior were observed upon following the orientation of the hard segments of the PUUE elastomer, but were negligible in that of the hard segments of the plaques.

Acknowledgements

I would like to thank my advisor, Dr. G.L. Wilkes, for his guidance, patience and encouragement, without I would not have completed this work.

I would also like to thank Dr. Glasser and Dr. Davis for their willingness to serve on my committee, for the interest they showed in my research, and for reading my thesis.

I would like to thank Riley Chan and Billy Williams for their assistance in designing and building the rheo-optical stretching apparatus, without their help this work would not have been completed.

I am grateful to Dow Chemical for supporting me and this research project. I would like to especially thank Bob Turner of Dow Chemical for his assistance and the interest he expressed in this project.

I would like to thank the research group of Dr. Wilkes for their interest in this work, helpful discussions, support, encouragement and for all the good times in the lab as well as away from the lab.

Finally, I am grateful for the support and encouragement that I received from my family and other close friends during the time that I was writing this thesis.

Table of Contents

List of Illustrations v

List of Tables vi

1.0 Introduction 1

2.0 Literature Review 4

2.1 Chemistry 4

2.1.1 General Chemical Reactions 4

2.1.2 Formulation Components 6

Diisocyanates 6

Polyols 7

Chain Extenders 9

Catalysts 9

Blowing Agents 10

Surfactants 11

2.1.3 Foam Process 13

2.1.4 Reaction Sequences in Foam Formation 14
2.2 Morphology 17
2.2.1 Macroscopic Structure 18
2.2.2 Thermal Characterization 19
2.2.3 Microphase Structure 19
2.2.4 Extraction Study 20
2.2.5 Wide and Small Angle X-Ray Scattering 21
2.3 Mechanical Properties 23
2.3.1 Stress-Strain Behavior 24
2.3.2 Ultimate Properties 26
2.3.3 Hardness 27
2.3.4 Viscoelastic Properties 28
2.4 Summary 33

3.0 Linear IR-Dichroism 36
3.1 Introduction 36
3.2 Linear Dichroism Theory 37
3.3 Application 40
3.3.1 Polyurethane Elastomers 41
Orientation-Elongation Behavior 41
Orientational Hysteresis 44
Orientation Time Study 45
Temperature Effects on Orientation 46
3.3.2 Polyurea-urethane Elastomers 47
MDI-Based Urea-Urethanes 47
2,4-TDI Based Urea-Urethanes 51
3.4 Summary 52

4.0 Experimental **53**

4.1 Materials 53

4.2 Experimental Techniques 55

4.2.1 Stress Relaxation 55

4.2.2 WAXS 57

4.2.3 Dynamic Mechanical Spectroscopy 57

4.2.4 IR Dichroism 57

Design Criteria 58

Rheo-optical Stretching Device 59

Mounting of the Sample and Sample Considerations 60

Rotation of Polarizer 61

Thermal Chamber 61

Procedures for Obtaining Orientation Data 62

5.0 Results and Discussion **65**

5.1 Stress Relaxation 65

5.1.1 Foams 65

5.1.2 Compression Molded Plaques 68

5.1.3 Temperature Effects 70

5.2 Characterization of Samples used in the IR-Dichroism Study 72

5.2.1 Pretreatment Effects on Plaques 72

5.2.2 Polyurea-urethane Elastomer-PUUE 74

5.2.3 Plaques 1-lc0 and 3-lc 75

5.3 IR-Dichroism with Mechanical Response 76

5.3.1 Treatment of IR and Mechanical Data 77

Band Assignments 77

IR Sample Spectra and Dichroic Measurements 78

Mechanical Evaluation 79

5.3.2 Evaluation of Rheo-Optical Stretching Apparatus 79
5.3.3 IR-Dichroism Studies of Compression Molded Plaques and the PUUE Elastomer .. 81
Orientation-Elongation Behavior 82
Orientational Hysteresis Behavior 91
Orientation Time Study 93
5.4 Summary 95
5.5 Conclusions and Recommendations 100
5.5.1 Conclusions 100
5.5.2 Recommendations 103

References **106**

Components for Stretching Apparatus **189**

Computer Program for Stretching Device **191**

Components for Thermal Chamber **194**

Possible Explanation for Biaxial Orientation **195**

Vita **200**

Acknowledgements ..... **iii**

List of Tables

Table 3.1. Absorbing Frequencies for Polyurethane Elastomers* 111

Table 3.2. Absorbing Frequencies for Polyurea-urethane Elastomers* 112

Table 4.1. Formulation Components for Flexible Water-Blown Foams 113

Table 4.2. Formulation Amounts for the Foams 114

Table 5.1. Composition and Density of Foams 115

Table 5.2. Stress Decay Rates for Foams 1-4 116

Table 5.3. Stress Decay Rates for Plaques 1-4 117

Table 5.4. Absorbing Frequencies for Plaques and the PUUE Elastomer 118

List of Illustrations

Figure 2.1. Primary Reactions in Flexible Foam Formation 119

Figure 2.2. Secondary Reactions in Flexible Foam Formation 121

Figure 2.3. Stuctures of Diisocyanates Commonly Used in Manufacture of Foams and Elastomers 122

Figure 2.4. Repeat Units for the Most Common Polyether Polyols 123

Figure 2.5. Repeat Units for Most Common Polyester Polyols 124

Figure 2.6. Most Common Chain Extenders Used in Manufacture of Elastomers 125

Figure 2.7. SEM Micrographs of Foam 1(a) and 4(b) 126

Figure 2.8. Storage Moduli(a) and Tan Delta(b) Curves for Foams 1-4 127

Figure 2.9. Comparison of DMS spectra for Foam 3 and its Compression Molded Plaque . 128

Figure 2.10. Proposed Morphological Model for the Solid Portion of Flexible Water-Blown Foam 129

Figure 2.11. Cubic Models for Open-Celluar Materials 130

Figure 2.12. Typical Shape of the Compressive Stress-Strain Curve for a Foam 131

Figure 2.13. Stress-Strain Behavior for Flexible Foams in Compression,Shear, and Tension 132

Figure 2.14. Compressive Stress-Strain Curves for Four Different Flexible Foams 133

Figure 2.15. Characteristics of Compression Hardness and Indentation Hardness in Flexible Foams 134

Figure 2.16. Proposed Model for Humid Aged Flexible Foam 135

Figure 3.1. The Electric and Magnetic Fields for Plane Polarized Light 136

Figure 3.2. Coordinate Systems for Linear Dichroism 137

Figure 3.3. Two Spectra Technique for Measuring IR Dichroism 138

Figure 3.4. Examples of Transition Moments 139
Figure 3.5. Schematic Representation of Hard Domains in Polyurethane Elastomers 140
Figure 3.6. Proposed Mechanism for Deformation of Lamellar Hard Domains 141
Figure 4.1. Rheo-Optical Stretching Device in Nicolet 5DXB FTIR Chamber 142
Figure 4.2. Rheo-Optical Stretching Device in Nicolet 5DXB FTIR Chamber 143
Figure 4.3. Rheo-Optical Stretching Device 144
Figure 4.4. Sample Preparation Holder and Dogbone Die Cutter 145
Figure 4.5. Thermal Chamber with Stretching Device 146
Figure 4.6. Top View of Thermal Chamber with Stretching Device 147
Figure 5.1. Stress Relaxation Behavior for Foams 1-4 Stretched Parallel to Blow Direction 148
Figure 5.2. Stress Relaxation Behavior for Foams 1-4 Stretched Perpendicular to Blow Direction 149
Figure 5.3. Linearized Stress Relaxation Behavior for Foams 1-4 150
Figure 5.4. Effect of Hard Segment Content on Stress Decay Rates for Foams 1-4 151
Figure 5.5. Proposed Mechanism for Local Strain on Soft Segments during Stress Relaxation 152
Figure 5.6. Stress Relaxation Behavior for Plaques 1-4 153
Figure 5.7. Stress Relaxation Behavior for Foam 4 at Different Temperatures 154
Figure 5.8. Stress Relaxation Behavior for Plaque 4 at Different Temperatures 155
Figure 5.9. Stress Relaxation Behavior for Plaque 2 and Plaque 2-DMF 157
Figure 5.10. Storage Modulus Curves for Plaques 2 and 2-DMF 158
Figure 5.11. WAXS Patterns for Plaques 2(a) and 2-DMF(b) 159
Figure 5.12. Storage Modulus and Tan Delta Curves for the PUUE Elastomer 160
Figure 5.13. WAXS Patterns for the PUUE Elastomer(a) and for Plaque 3(b) 161
Figure 5.14. WAXS Patterns for Plaques 1-lc(a) and 3-lc(b) 162
Figure 5.15. Infrared Spectrum of a Polyether Urethane Elastomer 163
Figure 5.16. Infrared Spectrum of Polyurea-urethane 164
Figure 5.17. Orientation-Elongation Behavior for ET-2000-30 165
Figure 5.18. Simultaneous Stress-Strain Behavior for ET-2000-30 166
Figure 5.19. Orientation-Elongation Behavior for ET-1000-31 167

Figure 5.20. Mechanical Evaluation of Stretching Apparatus 168
Figure 5.21. Orientation-Elongation Behavior for Plaque 2-DMF 169
Figure 5.22. Orientation-Elongation Behavior for Plaque 2-THF 170
Figure 5.23. Orientation-Elongation Behavior for the PUUE Elastomer 171
Figure 5.24. Simultaneous Stress-Strain Behavior for Plaque 2-DMF 172
Figure 5.25. Simultaneous Stress-Strain Behavior for the PUUE Elastomer 173
Figure 5.26. Orientation-Elongation Behavior for Plaque 1-THF 174
Figure 5.27. Orientation-Elongation Behavior for Plaque 1 175
Figure 5.28. Orientation-Elongation Behavior for Plaque 1-lc(DMF) 176
Figure 5.29. Orientation-Elongation Behavior for Plaque 3-lc 177
Figure 5.30. Simultaneous Stress-Strain Behavior for Plaques 1-lc(DMF) and 3-lc 178
Figure 5.31. Suggested Modification of Proposed Morphological Model 179
Figure 5.32. Orientational Hysteresis Behavior for Plaque 2-DMF 180
Figure 5.33. Mechanical Response for Plaque 2-DMF during Cyclic Deformation 181
Figure 5.34. Orientational Hysteresis Behavior for the PUUE Elastomer 182
Figure 5.35. Mechanical Response for the PUUE Elastomer during Cyclic Deformation .. 183
Figure 5.36. Orientation Time Behavior for Plaque 1-THF 184
Figure 5.37. Orientation Time Behavior for Plaque 2-DMF 185
Figure 5.38. Simultaneous Stress Relaxation Behavior for Plaque 2-DMF 186
Figure 5.39. Orientation Time Behavior for the PUUE Elastomer 187
Figure 5.40. Simultaneous Stress Relaxation Behavior for the PUUE Elastomer 188

CHAPTER I

1.0 Introduction

Polyurethanes are often made by reacting an isocyanate group of an aromatic diisocyanate with a hydroxyl group of a polyether or polyester polyol. In polyurethanes, the urethane group (NH-CO-O) generally serves as the chemical linkage between the flexible unit(e.g. polyol) and the more rigid unit(e.g. aromatic diisocyanate). The different types of polyurethane products can be classified under foams, elastomers, adhesives, binders, coatings and paints. Within these categories there are a wide range of properties leading to numerous applications. Five of the most important areas of applications are automotive, furniture, construction, thermal insulation, and footwear. Of the different types of polyurethanes, flexible foams are dominant and have been chosen for this investigation because of their extensive usage. The focus of this thesis is on the structure-property relationships in flexible foams because this particular class of materials are very important and have received little attention due to their complex morphology.

From a historical point of view, urethane chemistry dates back to 1849 when the reaction between an isocyanate and hydroxyl compound was first reported. However, not until 1937 did the first commercial polyurethanes become available by Otto Bayer and co-workers. During World War II

polyurethane elastomers, coatings and adhesives were also developed due to the demand for new materials.

In 1953, the first flexible polyurethane foams were produced based on a Bayer patent system using toluene-diisocyanate (TDI) and a polyester polyol. It was in 1956 that the first polyether based-flexible polyurethane foam was developed in the United States using a two stage process. Three years later flexible foams were produced by mixing all chemical components at the same time and then dispensing the mixture. This process is better known as the "one shot" system and still remains the common way of producing flexible foams. In 1959 improvements in the polyether polyol were made that cut costs and brought about improved properties. One other major development for the advancement of flexible foam technology was the introduction of the silicone surfactant into the "one-shot" system. From here, improvements in the physical properties in flexible foams have been continuously made by several approaches. All of these improvements have resulted in flexible foams constituting 50% or more of the polyurethanes made today.

Flexible foams are manufactured either by a continuous method or by a batch operation. The batch operation consists of molding foams in a hot-cure or in cold-cure process. The most efficient batch operation is the cold-cure process and high-resilient (HR) foams are most often made by this process. These foams are used in the automotive and furniture industries. Molded foams make up about 20% of the flexible foams while slabstock foams make up the rest. Flexible slabstock foams are usually manufactured by a continuous method and in few cases by a batch operation (e.g. complex shapes and sizes). They are also used in the furniture and automotive industries as well as for packaging material.

As was mentioned earlier, improvements in the performance and in the physical properties of flexible foams have been made since their market introduction in the 1950's. Most of these improvements were made by adjusting the chemical and processing variables and these types of improvements are still being made today. However, the more recent approaches are beginning to focus on understanding why a particular physical property results. One of these approaches has

involved comprehending the sequence of reactions and their mechanisms that take place during the foam formation. Furthermore, studies have and are being carried out to model or predict mechanical behavior in hopes of understanding the contributions from the cell structure and the solid portion of flexible foams. More recent studies have concentrated on understanding the morphology of the solid portion of flexible water-blown polyurethane foams by utilizing several stuctural techniques.

In summary, the approach to obtaining more economical flexible foams possessing better physical properties has changed somewhat in the last ten to fifteen years. Instead of continuously changing the chemical and processing variables to obtain the preferred physical properties, foams are being studied on the macroscopic and the microscopic levels. With this in mind, Dow Chemical and Virginia Tech have initiated a joint venture to hopefully obtain a better understanding of the resulting physical properities in flexible water-blown polyurethane foams. A part of this venture is given in this thesis with the emphasis on the stress relaxation behavior and the molecular orientation with deformation of flexible polyurethane foams as well as the compression molded plaques of these same foams.

CHAPTER II

2.0 Literature Review

2.1 Chemistry

In this section, the focus will be on flexible polyurethane foams, although some comparisons to thermoplastic polyurethane elastomers are made in some instances. The general chemical reactions as well as the specific components and their significance in the foaming process are discussed. Furthermore, the foaming process and some of the most recent work concerning the chemistry of flexible water-blown polyurethane foams are also covered.

2.1.1 General Chemical Reactions

There are three primary reactions that take place in the formation of polyurethane foams. The first(see Figure 2.1a) takes place between an isocyanate group and water to give an unstable intermediate group, carbamic acid, which then degenerates to form a primary amine and carbon dioxide

gas. The carbon dioxide created from this reaction serves as the principal source of blowing the foam mixture. Thus, this reaction is commonly referred to as the blowing reaction. In the second as shown in Figure 2.1b, the primary amine created from the first reacts with another isocyanate group to give a disubstituted urea. This reaction serves as a means to chain extend the aromatic groups of the diisocyanates by urea linkages. These first two reactions are highly exothermic (1-3).

The third takes place between an isocyanate group and a hydroxyl group to give a urethane as shown in Figure 2.1c. The urethane serves as a link between the chains of a polyol and an aromatic diisocyanate. This reaction is called the gelling reaction due to its ability to develop a network from the polymerizing foam mixture. Furthermore, the gelling reaction is also highly exothermic.

Secondary reactions can also take place upon reaction of urea or urethane groups with isocyanate to give biuret or allophanate groups, respectively (see Figure 2.2). These reactions can cause further crosslinking in foams with the biuret formation being more likely of the two since urea groups are more reactive with isocyanates than urethanes. Furthermore, temperatures greater than 120°C in uncatalyzed systems are necessary to have any significant allophanate crosslinking. However, both of these reactions are less likely to occur in flexible polyurethane foams due to steric hindrance in the reacting components as will become clearer when the chemical structures of the formulation components in flexible foams are reviewed.

Polyurethane elastomers are made by a one or two step reaction. The two step procedure is the more preferred.The first step is similar to the gelling reaction described above and consists of reacting a polyol and diisocyanate to give an endcapped prepolymer. The prepolymer and the excess isocyanate mixture are then reacted with a chain extender to give the final product. This step is similar to the primary amine-isocyanate reaction given above. Depending on the type of chain extender, urea(diamine) or urethane(diol) linkages are formed between the aromatic groups of the diisocyanates. Thus, if a diamine is used, a polyurea-urethane is made; if a diol is used, a polyurethane is made.

The chemistry of foams and elastomers differ in several ways. First, two reactions are taking place simultaneously in the formation of foams, while it usually takes two separate stagewise reactions to form an elastomer. Also, the conditions for the foam reaction are less controllable in comparison to that of the polyurethane elastomers. This is due to the elastomer being formed in solution, where such conditions as temperature are more controllable. Furthermore, a network polymer is generally formed in flexible foams and a linear polymer forms in polyurethane elastomers. Some of the other differences and the similarities of the resulting chemistries for the two polyurethanes are covered later in this thesis.

2.1.2 Formulation Components

There are many different components that go into making polyurethane foams. The five major ones are diisocyanate, polyol, catalysts, surfactant, and blowing agent. The different chemical names as well as their function in the formation of the foams are given below. Comparisons to the formulation components of polyurethane elastomers are also provided in the following paragraphs.

Diisocyanates

The two most important diisocyanates are toluene diisocyanate (TDI) and diphenylmethane diisocyanate (MDI) with the latter being more dominant in the production of elastomers and the former in the manufacture of foams (1). TDI is manufactured from toluene via nitration and followed by phosgenation. It is mainly sold in the liquid form as a mixture of 2,4 and 2,6 isomers at ratios of 80:20 and 65:35, respectively. The structures of the two isomers are shown in Figure 2.3. The order of reactivity of the isocyanate groups from highest to lowest is as follows: (1) #4 group on the 2,4 isomer, (2) #2 and #6 groups of the 2,6 isomer and (3) #2 group of the 2,4 isomer. The

80:20 mixture of TDI which is called TDI-80 is used most often in producing flexible slabstock foams, and in some cases, hot-molded foams as well as cast elastomers (1-4).

Polymeric MDI (shown in Figure 2.3) and mixtures of polymeric MDI and TDI-80 are also used to manufacture flexible molded polyurethane foams. Pure MDI also shown in Figure 2.3 is used in making thermoplastic polyurethane and polyurea-urethane elastomers. The main difference in polymeric MDI and pure MDI is that the level of functionality is higher in the polymeric form (1,3).

In the production of flexible foams and in some cases for elastomers, the amount of isocyanate(s) used is expressed as the isocyanate index. An index of 110 indicates an excess of 10 percent diisocyanate over the stoichiometric amount required by the polyol and water (3). The iscocyanate index in flexible foams is generally over indexed in order to obtain optimum physical properties. The effect of isocyanate index on the physical properties in flexible foams will be discussed later in the literature review.

Polyols

The two most important polyols are hydroxyl terminated polyethers and hydroxyl terminated polyesters. Polyether polyols are generally chosen over polyester polyols because they are cheaper and more hydrolytically stable. Polyether polyols are generally made from cylic oxides of propylene(PO) and ethylene(EO). The repeat units for these polyether polyols are shown in Figure 2.4. Polyether polyols used in flexible foams are of functionalities from 2.5 to 3 and in the molecular weight range of 1000 to 4000. Polyether polyols used for manufacturing polyurethane elastomers are generally of functionality equal to 2 and in a molecular weight range of 1000 to 6500. An example of a commonly used polyol in polyurethane elastomers is polytetramethylene oxide (PTMO) and its repeat unit is shown in Figure 2.4 (1,2).

The first polyether polyol used to manufacture flexible foams was a 2900 molecular weight propylene oxide/glycerine initiated polyol (2). However, there have been modifications in composition to improve the polyol performance. Duffy and Whitman report that through the years modifications have been made by changing the functionality, using an ethylene/propylene oxide composition, capping polypropylene polyols with ethylene oxide, and using a glycerine/oxypropylene/oxyethylene polyol which contained essentially no primary hydroxyl groups (5). Today, most flexible polyurethane foam formulations use a copolymer made from an approximate 80:20 mixture of propylene and ethylene oxide which is then gylcerine intiated. Two important aspects in synthesizing this copolymer are the amount and the placement of the oxyethylene groups amongst the oxypropylene groups to give the particular foam of interest without any processing difficulties (1). One reason for this is that the reactivity of the secondary hydroxyl group of the oxypropylene groups is lower than that of the oxyethylene. Furthermore, the oxypropylene groups are more hydrolytically stable and thus they make up a higher percentage in the copolymer. A third aspect in synthesizing the above copolymer polyol is that PO is subject to the formation of unsaturated allyl end groups. These groups are undesirable due to increasing the molecular weight of the polyol and lowering its functionality. Furthermore, these unsaturated groups are not reactive with isocyanate groups.

Modifications on polyether polyols are generally made to provide foams of higher hardness. One example is the polyurea-modified polyols (PHD) which contain polyurea dispersions. These dispersed polyurea particles may react with an isocyanate group to give increased crosslinking i.e., higher hardness. Polyester polyols are also used in special instances where higher levels of tensile strength, stiffness, and compressive strength are necessary. These higher levels in the above physical properties are obtained due to hydrogen bonding between the ester carbonyl and urea and urethane groups (1). Furthermore, this hydrogen bonding also raises the soft segment glass transition temperature (T_g) by promoting phase mixing between the hard and soft segments (phase mixing is covered in more detail later in this thesis).

Most polyester polyols used in making flexible foams are lightly branched poly(diethylene adipates) An example of such a structure is shown in Figure 2.5. Polyester polyols are also used in the manufacture of polyurethane elastomers. They usually consist of adipates made from aliphatic diols(see Figure 2.5) and in some cases the more expensive polycaprolactone diols.

Chain Extenders

Chain extenders are used in the manufacture of thermoplastic polyurethane elastomers and are very rarely added to the formulation for flexible polyurethane foams. As stated earlier, chain extenders are either diols or diamines and serve as a link between chains in the diisocyanate-polyol prepolymer. An example of a diol is butanediol(BD) as shown in Figure 2.6. This diol is often utilized for elastomers. One common diamine is ethylenediamine(ED) - see Figure 2.6. The use of a diamine extender clearly produces a polyurea-urethane elastomer. Chain extenders also serve as curing agents and especially in TDI cast elastomers. The most commonly used curing agent was 3,3′ dichloro-4-4′- diaminodiphenylmethane (MOCA) until some years ago when it was considered a possible carcinogen (2,4). The structure of MOCA is also given in Figure 2.6.

Catalysts

The two main catalysts used in making flexible foams are a tertiary amine and an organotin compound. The importance of these catalysts are to balance the blowing and gelling reactions. The correct balance is needed due to the possibility of foam collapse if the blowing reaction is too fast. On the other hand, if the gelling reaction is too fast, foams with closed "crosslinked" cells result and foam shrinkage or "pruning" occurs. In general, a catalyst system should allow for a sufficient induction period, appropriate timing in the foaming reaction and the curing process, and the possibility to adjust the foam properties. The catalyst system should not affect the properties such as the stability of the foam (3,6).

The tertiary amine enhances the blowing reaction the most, since it is able to form stable hydrogen bonds with water. The reactivity of the tertiary amine increases with its level of basicity. On the other hand, the organotin compound acts as a Lewis acid that can attack the oxygen of a polyol and thus exhibits its ability to enhance the gelling reaction (6).

The tin and the amine catalyst can also activate the blowing and the gelling reaction, respectively as shown by Burkhart and co-workers (6). They have reported that the tin compound catalyzes the blowing reaction as much as the amine compound. Thus, the tin compound sets the reactivity of the formulation. On the other hand, the amine compound is referred to as a fine tuning catalyst and its level is adjusted most often to obtain the right balance between the two competing reactions (6).

Some of the different tertiary amines for flexible polyurethane foams are triethylenediamine (DABCO), trimethyl-hydroxylethyl ethylenediamine and diomethethylamine (DMEA). Stannous octate is the primary organotin compound used in making flexible foams.

Blowing Agents

Blowing agents are used to bring about the foaming and to help control the density of the foam. There are chemical and physical blowing agents. Water acts as the chemical blowing agent and reacts with an isocyanate group leading to the formation of a primary amine. By increasing the level of water in the formulation and adjusting other component levels the density of the foam will decrease because more CO_2 will be generated leading to a greater extent of the blowing reaction. Furthermore, the hard segment content in the foam is also increased due to reacting more water and isocyanate. However, the amount of water added to the formulation is limited by the exothermic heat of reaction which depends on numerous factors such as the scale of manufacture, rate of heat dissipation, and the amount of excess diisocyanate present (2).

Physical or auxiliary blowing agents are used to lower the density and thus produce softer foams. Auxiliary blowing reagents are low boiling solvents and are inert in the chemical reactions. Chlorofluorocarbons (CFC's) are most commonly used in flexible polyurethane foams. CFC 11 and in some cases CFC 12 are normally used, until recently when Dupont stopped producing both due to environmental hazards. CFC's in general have been reported as depleting the Earth's protective ozone layer - especially over the Antarctica (7). Replacements for the two CFC's used in foam manufacture are now in progress, but it may be a few years until the replacements are produced on a large scale. One alternative is methylene chloride which has been used in the past. The main drawbacks with methylene chloride are its higher toxicity, lower volatility, and high solubility in the foam which limits the amount of additional blowing it can create. Furthermore, methylene chloride does not leave a pleasant odor at high levels (5 parts per 100 parts of polyether polyol). However, the one advantage is it is cheaper than CFC 11 (2).

Surfactants

With the introduction of the "one-shot" system versus foam systems based on prepolymers, new surfactants were developed for producing flexible polyurethane foams. The new surfactants are primarily siloxane-polyether block and graft copolymers. Their introduction was necessary due to the lower viscosity in the foam mixture and the need for foam stabilization. Thus, the surfactants used today serve many functions in the production of one-shot flexible polyurethane foams. Some of which are not well understood and agreed upon. For the most part, surfactants help in stabilizing the foam structure and the cell size. In doing so, the surfactants play an important role in many of the stages in the foam formation as shown below.

The first stage in the foam process is nucleation and here the surfactants act as a dispersion agent by regulating the air bubbles in the liquid mixture. In the second stage, called creaming, the air bubbles are enlarged and the surfactant acts in a similar manner as in the first stage. The foam now begins to rise as more gases are given off and the foam mixture becomes more viscous. The

surfactant acts as a stabilizing agent hereby reducing the surface tension; thus preventing the bubbles from coalescing. The mechanism(s) by which the surfactants performs this role are not well understood. One mechanism that seems to hold true is the surfactant slows the drainage of the cell membranes into the plateau borders by increasing the surface viscosity. This delay in the thinning of the struts enables the foam to gain some of its mechanical strength before bubble breakage occurs. Another possible mechanism that could be taking place due to surface viscosity build-up, is the Gibbs-Marangoni effect. This effect calls for elasticity in the membrane which serves to maintain the membrane at uniform thickness; thus preventing rupture (10). Rossmy et. al. have also suggested that upon precipitation of polyurea (more explanation on the development of precipitated polyurea is given later) the stability of the rising foam was affected (8). In order to overcome this instability, the surfactant becomes a dispersing agent by incorporating the precipitated polyurea into the liquid foam matrix. The last two events in the formation of the foam are the blow-off or cell rupture point which establishes the full rise in the foam and the gelation step (3). The surfactants role in these steps has not been reported on heavily. Howerer, it is believed that the surfactants possibly assist in the cell opening process, but the actual mechanism is not known. Finally, the surfactant is thought to help to control the precise timing in the foam process (2-3).

The amount of surfactant used in the formulation governs the quality of the final foam. For example, if too much surfactant is used a closed cell foam results due to the possibility of little drainage in plateau borders; thus preventing cell rupture. On the other hand, if not enough surfactant is added the foam collapses due to cell opening occurring to soon (3).

As mentioned earlier, surfactants used today in flexible polyurethane foams are generally polysiloxane-polyoxyalkylene block and graft copolymers. These surfactants generally have two different structures. The first is a linear polysiloxane with attached polyoxyalkylene chains. The second is a branched trifunctional polysiloxane polymer which contains pendant polyether chains. The surfactants used in flexible foams are usually non-hydrolyzable and thus consist of Si-C linkages between the polyether and the siloxane. The polyether portion of the surfactants are adjusted

to meet the requirements of the particular foam being produced (9,11). Generally the polyether consists of 75 percent or more of oxypropylene and the rest oxyethylene (4).

2.1.3 Foam Process

The flexible polyurethane foam formation is a difficult process to follow in detail. However, most of the main mechanisms in the foam process are understood and for the most part agreed upon. A discussion of the foam process from the mixing of the five or more chemical components, until the final product is obtained is given below.

Flexible polyurethane foams are made by a "one-shot" process. The chemical components are usually metered into a mixing head in appropriate quantities and at well controlled temperature conditions. During mixing it is essential that nucleation sites are formed. The level of nucleation is reflected in the cell size and the cell structure. Normally in flexible foam formation, the amount of nucleation is controlled by bubbling air or nitrogen gas into the mixing head through a polyol or isocyanate meter. The mixing agitation speed is also important in the level of nucleation.

After mixing for less than one second, the nucleated liquid mixture is dispensed into a mold or onto the bottom lining of a continuous trough. For a short induction period, the bubbles begin to grow and decrease in number. Furthermore, the mixture turns opaque at the end of the induction period(6-15 seconds) and this time is referred to as the "cream time." The longer the "cream time" the larger the cell size. Furthermore, by using a surfactant the bubble loss is lowered due to reducing the surface tension and thus lowering the pressure differential between the dissolved gas and the dispersed gas. By increasing the catalyst levels, the cream time is shorter and the cells are fewer in number and in size.

After the cream time, the foam mixture begins to rise and the small spherical bubbles are elongated. The expansion of the bubble is in the blow direction and is caused by the increasing amounts of

CO_2 that are produced by the isocyanate-water reaction. The bubbles will continue to expand until they eventually contact to form planar membranes, if the bubbles are equal in size (usually the case for water-blown slabstock foams). The planar membrane is formed by three bubbles and produces a triangular shape rib at the point of contact.

At temperatures near 100°C, the wall-membranes of the cells rupture and the gas is released. The temperature of the cell opening depends on the foam formulation. However, the actual mechanism that brings about the cell opening is not well understood. At the point of cell opening which is also known as blow-off, the foam reaches full rise. This time generally occurs 100-200 seconds after mixing the chemical formulation.

The remaining isocyanate groups continue to react after blow off and furthermore, the temperature of the foam continues to increase. After the maximum temperature is reached (30 minutes- 1hour), the foams are taken to storage areas where they cure. The time for curing will depend on the size of the foam. Large foams which are generally produced in a continuous process take approximately forty-eight hours. The smaller foams (e.g. molded cushions) could take up to seven days before the properties stabilize (1-4).

2.1.4 Reaction Sequences in Foam Formation

As was alluded to earlier, the chemical reactions are difficult to follow in polyurethane foams due to the high rates of reaction, the large exotherms, the high rate of viscosity and volume changes, and the heterogeneity of the reacting mixtures (2). Thus, it has only been in the last 10-15 years that steps toward a better understanding of the reaction sequences in foams has been obtained. Some of the techniques that have been used in following the sequence of reactions are FTIR, weight loss of certain components, and temperature profiles.

The water-isocyanate reaction has been observed by several investigators in the early stages of the foam reaction by using FTIR (8,9,12,14). Rossmy et. al. reported seeing at the beginning of the reaction an absorption at 1710 cm^{-1} which increased in the early stages of the reaction (8). They also observed absorptions at 1660 cm^{-1} at 50% of the rise time and for 75% of the rise time a band at 1645 cm^{-1} then appeared. Bailey and Critchfield also reported observing an absorption at 1710 cm^{-1} in the beginning of the reaction as well as at 1645 cm^{-1} at approximately 75% of the rise time (12). Both of the investigators agreed that the 1645 cm^{-1} band is due to a disubstituted urea, but they were not in full agreement on the band at 1710 cm^{-1}. It appears, as Rossmy et. al. first suggested, that the band at 1710 cm^{-1} is due to soluble urea while that at 1645 cm^{-1} is due to insoluble urea. This hypothesis was supported by Hauptman et. al. and Hocker who reported observing a IR shift from 1710 cm^{-1} to 1645 cm^{-1} for a diphenyl urea model compound dissolved in a good solvent(DMF) and a poor solvent (THF), respectively. Rossmy et. al. gave further justification by replacing the surfactant in their formulation with a defoamer. In this experiment, the authors observed the foam mixture going from a clear mixture to an opaque mixture at the same time they observed the 1645 cm^{-1} band in the regular foam mixture (8). Furthermore, in the clear mixture the IR absorption at 1710 cm^{-1} was only observed, and as the mixture turned opaque, the 1645 cm^{-1} was detected. Thus, with this evidence there appears that at some time during the foam reaction a precipitated urea phase is formed.

The isocyanate-polyol reaction has been reported as occurring in the later stages in the foam reaction (near blow-off) (8,9,12-15). Bailey and Critchfield reported observing during foam rise a slow increase in the urethane absorption band at 1730 cm^{-1} in comparison to the urea absorption band at 1645 cm^{-1} (12). A steady increase in the urethane absorption was observed after foam rise for 30 minutes while the urea absorption remained practically constant. Rossmy et. al. reported observing the urethane band at 1725 cm^{-1} for the first time at 75% of the foam rise.

In a different study, Illeger et. al. followed the relative weight loss of isocyanate and water. With this approach, it was also concluded that the isocyanate-water reaction was the dominant reaction in

the early stages of foam formation. They did report observing a small amount of isocyanate-polyol reaction at the beginning of the foam reaction as did Bailey and Critchfield.

Bailey and Critchfield also used gel/rise profiles to follow the foam formation. The gel/rise profiles give a qualitative idea of the balance of the gelling and blowing reactions, respectively (16). The rise profile measures the height of the rising foam mixture, while the gel profile gives a measure of the strength of the rising foam. The authors observed that the rate of rise was going through a maximum upon the first detection of the urea groups at 1645 cm^{-1} (16). It was suggested that the urea groups could be aggregating and thus retarding the foam rise. The gel profile occurred during the period of time when the urea formation was predominant and as the rate of rise was decreasing. This also suggested that the urea groups were forming domains due to the added strength in the foam mixture (12). Rossmy et. al. have also suggested in another study that the urethane formation does not play an important role in the foam stabilization (9).

Van Gheluwe and Leroux have followed the temperature rise during the foam formation (17). In doing so, they determined the maximum rate of temperature rise as a function of varying water content and tertiary amine catalyst concentration for two different polyether polyols. Two temperature curves were obtained for the two different chemical reactions. The temperature rate for the blowing reaction was generally greater than that of the gelling reaction. This observation further supports the fact that the blowing reaction is more reactive in the early stages of foam formation (17).

The results of Van Gheluwe and Leroux work also showed an increase in the temperature rate curves with increasing water content. This is expected due to more extensive blowing reaction occurring at higher water contents. However, they did note the temperature rate levels off at the higher water level contents for the blowing reaction, but a steady increase in the temperature rate was observed for the gelling reaction. This observation was not fully understood, but was related to the formation of the polyurea precipitates. An increase in the temperature rate was also seen with increasing levels of tin catalysts. On the other hand, only slight increases in temperature rate were

observed by increasing the levels of tertiary amine. These last two results suggest as stated earlier that the tin catalysts activate the gelling and blowing reactions more. Furthermore, the primary hydroxyl polyol exhibited higher temperature rates upon reaction than that of the secondary hydroxyl. This is to be expected since primary hydroxyls are more reactive (17).

In short, this section has provided a semi-quantitative outlook on the reaction sequences as well as some details on the foaming mixture for flexible foams. One of the basic conclusions is that the isocyanate-water reaction is dominant in the early stages of the foam formation. On the other hand, the gelling reaction becomes more effective when the foam approximately reaches its maximum height. One other important feature, is that the polyurea is soluble in the foam mixture in the early stages of foam formation and at 75% of the rise time it begins to aggregate as well as precipitate out of solution.

2.2 Morphology

Until recently very little work had been done towards understanding the morphology of flexible foams (18-20). In the past, the study of the morphology in polyurethanes has been concentrated on thermoplastic elastomers. A typical polyurethane elastomer consists of MDI chain extended hard segments and a linear polyether or polyester soft segment. The hard segments generally aggregate due to hydrogen bonding to form crystalline or amorphous domains. These domains serve as physical crosslinks in a soft segment matrix. Thus, a two phase morphology consisting of hard domains randomly dispersed in a soft segment matrix is normally depicted in polyurethane elastomers (1,21).

Recently, Dow Chemical and Virginia Tech have undertaken a joint venture to investigate the morphology of flexible water-blown polyurethane foams using many of the different techniques that

were also utilized in defining the morphology of polyurethane elastomers (19-21). The techniques that have provided the most useful information in this recent joint study have been scanning electron microscopy (SEM), transmission electron microscopy (TEM), dynamic mechanical spectroscopy (DMS), differential scanning calorimetry (DSC), wide angle X-ray scattering (WAXS) and small angle X-ray scattering (SAXS). A series of four TDI-80 - polypropylene oxide water blown foams of varying hard segment content(21 to 34 by wt%) were studied. These foams are referred to as 1-4 with one having the lowest hard segment content. Compression molded plaques of these same foams were also studied and were made by compressing the foams at 204°C for 10 minutes at 250 tons of pressure. A summary of this most recent work is given below.

2.2.1 Macroscopic Structure

The cellular structure of foams 1 and 4 are shown in Figure 2.7 looking down the blow direction and along the blow direction. Looking down or parallel to the blow direction the cells appear spherically shaped in both foams and more in foam 1. Along or perpendicular to the blow direction the cells appear ellipsoidal in shape with the major axis aligned with the blow direction. This anisotropy of the cells is reflected in the foam's properties. For example, the compressive strength parallel to the blow direction is generally much greater than that in the perpendicular direction.

The cells in foam 4 looking along the blow direction are more elongated in comparison to foam 1 (see Figure 2.7). This is due to more blowing action taking place in the formation of foam 4. With the increased blowing action, a more open foam (more ruptured windows) and thinner struts results. It was suggested that the above trends could also be attributed to greater nucleation taking place in the formation of higher water content foams as in the case of foam 4 (18).

2.2.2 Thermal Characterization

Spell et. al. used dynamic mechanical spectroscopy (DMS) to investigate the thermal behavior in foams 1-4 and the corresponding plaques (20). The DMS spectra for the foams are shown in Figure 2.8 and resemble the spectra of soft ideal elastomers. Each spectrum exhibits a fairly sharp glass transition, a rubbery modulus, and thermal stability up to 200°C. At or above 200°C the modulus drops off due to thermal degradation. The soft segment glass transition is approximately -40°C for for all the foams and thus did not change significantly upon increasing the hard segment content.

The DMS spectrum for the foams are similar to that of TDI-polyurea-urethane elastomers. This was somewhat surprising due to the network structure of the foams versus the linear segmented structure of the elastomers (19). However, as the authors pointed out, the intramolecular and the intermolecular forces that govern the two different polyurethane systems appear to be similar.

A comparison of the DMS spectra for foam 3 and plaque 3 is shown in Figure 2.9. The spectra are very similar with the plaque having a slightly lower soft segment T_g and higher temperature stability. The differences were attributed to the plaques having possibly better phase separation induced upon compression molding.

The differential scanning calirimetry results showed slightly higher soft segment T_g's for the foams. Again the difference in the soft segment T_g's was small, thereby suggesting that the plaques and the foams had still very similar morphologies (19).

2.2.3 Microphase Structure

Transmission and high magnification scanning electron microscopy were both used to detect any form of phase separation in the foams and the plaques. The TEM results for foam 1 showed a

diffuse grainy texture at the 100 nm level. It was thought, due to the weak contrast and different levels of contrast that the grains are randomly dispersed and can be attributed to features less than 120 nm in size. On the other hand, the contrast systematically improved in foams 2-4 showing what appeared to be larger urea based aggregations. The aggregates are randomly dispersed and vary in size. The largest aggregates in foam 2 were ca. 100 nm in diameter and for foam 4 were ca. 300 nm in diameter. Similar results as described for foams 1-4 were also observed in their respective plaques.

The SEM micrographs also gave evidence of a multiphase morphology on the cold fracture surfaces of the plaques. The micrograph of plaque 1 showed a smooth fracture surface indicating no observable microstructure at the 100 nm level. Increasing surface texture was observed in plaques 2-4. In plaques 3 and 4, 100-300 nm protuberances were observed. Further evidence of the microphrase morphology was seen in the compression molded plaques with the naked eye. Plaque 1 is transparent while the other plaques increase in opaqueness from plaque 2 to 4.

The microscopy results gave further indication that the precipitated urea phase, Rossmy and coworkers attributed the IR shift in the urea carbonyl region to, is probably real. Thus, it was speculated that the agglomerations observed in the TEM micrographs are due to this precipitated urea phase (19).

2.2.4 Extraction Study

The extraction studies were carried out after swelling foams 1-4 in THF and DMF to determine if such species as urea were apart of the polymer network (18). The sol fractions from both the DMF and THF solutions are small and increase with hard segment content with the highest fraction being 7 percent. The sol fractions were higher for the DMF extracts which indicated the hard segment was extracted the most. This observation was further supported by analyzing the extract with IR

and detecting that urea was the predominant species. Overall, the swelling study showed that there exists a well-formed network in all of the foams (18). However, at this point it is questionable how well the polyurea precipitates are incorporated in the network.

2.2.5 Wide and Small Angle X-Ray Scattering

The WAXS patterns for foams 1-4 exhibited a diffuse halo and a corresponding reasonably sharp diffraction peak at 0.45 nm. Foams 2-4 have another weaker peak at 0.59 nm. The sharpness of the peaks increased with hard segment content. The peaks were also distinct, thus indicating a certain degree of order and not just maxima of the amorphous halos. The plaques exhibited very similar patterns to that of the foams.

In comparison to the diffraction results of a TDI- 80 based water extended polyurea (23) and other WAXS studies of amorphous polyurea-urethane elastomers with similar hard segments (22), it was suggested that the amorphous halo was due to the randomness associated with the hard and soft segments. The diffraction peaks at 0.45 and 0.59 nm indicate an increase in the hard segment order. This was surprising due to the hard segments consisting of both 2,4 and 2,6 TDI isomers. The origin of these diffraction peaks, based on an earlier study of MDI-BD urethanes(24), were thought to be caused by hydrogen bonding in the hard segments (18-19).

The WAXS patterns did not appear to change significantly upon compression molding, thus indicating the thermal process did not have a significant effect on the hard segment order. However, after swelling plaque 4 in DMF, the hard segment ordering did appear to decrease due to the increased diffuseness in the diffraction pattern. It was suspected that the swelling removed some of the polyurea rich phase and/or may have disrupted the hydrogen bonding between the hard domains leading to some rearrangement in microphase separation.

The results from the SAXS study were obtained from the scattering profiles, the correlation function analysis and the interfacial boundary thickness between the hard and the soft segment regions. The scattering profiles for the foams and the plaques did not exhibit sharp peaks, but shoulders that appeared nearly in the same place for the foams or plaques. The shoulders were a result of the morphological features not having the same shape, size and distance from one another. Bragg's law was applied to the shoulders and estimates of the center-to-center (interdomain) spacing between the scattering particles, approximately equal to 10 nm for the plaques and 9 nm for the foams were obtained. The difference in the Bragg law spacings for the foams and the plaques can possibly be attributed to better phase separation and formation of slightly larger domains in the plaques (18,20).

The correlation functions (1-dimensional and 3-dimensional) also provide additional information on the scattering particles. In short, the correlation function gives the probability that a rod of length r will have both ends in the same electron density. The 3-dimensional(3-D) correlation function gives an estimate of the center-to-center particle spacing. The 1-dimensional(1-D) correlation function provides the distance between scattering centers assuming a lamellar morphology. The results of the 1-D and 3-D showed no long range order. The results of the first maxima in the 3-D correlation function were lower than that of the Bragg-spacing's and are believed to be a better estimate of the interdomain spacing.

In comparison to polyurea-urethanes of similar hard segment structure, the interparticle spacing in the foams and the plaques were 20-50 percent lower (20,25-26). This was attributed to the shorter and stiffer hard segments and the use of a trifunctional polyol in the foams. Where as in the urea-urethanes, an ethylenediamine chain extender exist in the hard segments and a linear soft segment is used (22).

The diffuse boundary between the hard and soft segments was characterized assuming a sigmodial gradient and by utilizing Porod's law. Such an analysis lead to an index of interfacial thickness, denoted as sigma, for which sigma represents half-width of the diffuse boundary where the smoothing function has a value of 0.606. The results showed an increase in sigma from 0.23 to 0.53

nm for increasing hard segment content. This trend, though unexpected, implies that the ends of the hard segments are more phase mixed with increasing water content due to the their asymmetry. One might predict, as the authors suggested, higher ordered domains with increasing hard segment content (21).

The plaques followed the same trend as the foams did with increasing water content, but with slightly higher sigma values. This again implies that larger domains are formed upon compression molding. The authors also pointed out that the sigma values are comparable to that of TDI-based urethane and urea-urethane elastomers (24-25). Furthermore, the results by the SAXS analysis suggested that the hard segment domains in the foams have some similar features to that of the urethane and urea/urethane elastomers (18-19).

With the above results in mind the authors proposed a simplified morphological model as shown in Figure 2.10 (21). The urea balls in the model represent the aggregates seen in the TEM micrographs and are believed to be bonded to the matrix. The remaining structure appears to be very similar to that of urea and urea/urethane elastomers. That is the smaller hard segments form amorphous domains through hydrogen bonding and are dispersed randomly in the soft segment matrix.

2.3 Mechanical Properties

Flexible polyurethane foams like other cellular materials are complex material systems which can be characterized as having a mechanical response that is a function of deformation, time and the surrounding conditions. The mechanical response also depends on the cell structure as well as the morphology of the cell matrix material. As was discussed earlier both are dependent on the foam formulation. This in itself exhibits the complexity of characterizing the mechanical response of

these materials and probably why very few systematic studies have been reported on the stress-strain properties of flexible polyurethane foams. As a result, many of the reports on these properties for flexible foams have involved theoretical analyses. In other studies, the formulation components influence on the different stress-strain properties have been evaluated. Two of the stress-strain properties that are discussed in this section are the ultimate properties and the load bearing properties. Furthermore, a few of the theoretical models are qualitatively presented to give a structural interpretation of the mechanical response as well as the structural dependence on the mechanical response. Finally, a section is devoted to the viscoelastic properties which become important when considering the long-term behavior of the physical properties in flexible foams. Where possible, some comparisons to polyurethane elastomers are also made.

2.3.1 Stress-Strain Behavior

The stress-strain behavior like many other mechanical properties of flexible foams are usually measured in compression. The compression stress-strain behavior is measured on a small rectangular piece of foam with uniform thickness and a width to thickness ratio of not less than 2 to 1. The rate of deformation in this test, as well as other mechanical tests, is important due to the viscoelastic nature of flexible foams. In the paragraphs to follow, the stress-strain behavior in compression is described using predictions from structural models and an empirical model analysis. In addition, some comparisons to stress-strain behavior in tension of flexible foams and polyurethane elastomers are given.

Gent and Thomas and more recently Gibson and Ashby have used structural models to predict the stress-strain behavior in compression (27-30). The authors generally evaluate the modes of deformation to model the stress-strain behavior for a given foam. Gent and Thomas used a cubic strut model (Figure 2.11a), while Gibson and Ashby used a similar model, but slightly different as shown in Figure 2.11b (27-29).

In modeling the behavior, two different deformation modes were developed to describe the stress-strain behavior as depicted in Figure 2.12 (30). The first mode occurs when the cells bend, and this represents the linear elastic region. This region occurs over the first 5-10 percent of compressive strain and is much higher in tension. The non- linear region represents the buckling of the cell walls for flexible foams. The buckling of the cell walls occurs elastically if the cell wall material does not have a plastic yield point. A plastic yield point is usually not observed in flexible foams, but is observed in rigid foams. The last region is the densification of the foam which occurs when the cell walls are crushed together. The differences in the stress-strain behavior in tension and compression as shown in Figure 2.13 are two-fold: (1) A longer linear-elastic region in tension and (2) only a small non-linear region in tension before rupture (29-31).

Rusch evaluated the effects of the structural features on the compressive stress-strain behavior of low density flexible foams using an empirical model (32). Some of his results are shown in Figure 2.14. Using his nomenclature, curves Q and L represent low density reticulated polyurethane foams that have a regular cell structure, for which Q is of higher density. Curve R is for a rubber latex foam that has irregular cell structure and a higher density than the other foams shown in Figure 2.14. Foam E is a nonreticulated polyurethane flexible foam which contains some closed cells and has an irregular cell structure.

From his empirical model analysis (given in ref. 32), Rusch came to some basic conclusions. First, the cell structure (specific matrix geometry) has the greatest effect on the compressive stress-strain behavior. This can be seen in Figure 2.14 by comparing the non- linear regions of foam L or Q to foam E and recalling the description given above for the different cell structures. The density or volume fraction of the matrix polymer and the cell size showed secondary effects on the stress-strain behavior. These effects are seen by comparing foam L and Q for which Q has the higher density and the smaller cell size.

One common industrial application of compressive stress-strain curves or the more commonly used indentation load-deflection curves (described later) is in predicting the performance of a cushion.

Generally speaking, a comfortable foam is represented by cushion curve that is characterized as having an increase in stress or load with increasing deflection. An example of a representative cushion curve, but with a slightly lower initial modulus is shown in Figure 2.14 for foam E (32). The cushion curve for foam E exhibits a constant force of "fight back" when compressed. In contrast, the cushion curve for foam L shows a sharp rise in stress and then reaches a constant level of stress which is indicative of a foam with a low comfort rating (31).

The shape of the stress-strain behavior in tension for polyurethane elastomers is similar in many cases to that in compression of the foams. The stress-strain curve has a small linear region and then becomes non-linear. The non-linearity in the elastomers is caused by stress softening which could be due to a number of factors. Three of these are;(1) disruption of hard segment domains by rearrangement of hydrogen bonding, (2) movement of polymer chains, crosslinks and entanglements and (3) the reformation of domains after being stressed mechanically and then taking on different geometrical configurations as a result.

2.3.2 Ultimate Properties

The tensile strength and the tear strength as well as the elongation of flexible polyurethane foams have been shown to increase by increasing the water content (hard segment content) up to a certain level (4 parts/100 parts polyol) and then leveling off (2,34). This of course assumes that the formulation is adjusted to obtain a reasonable foam. By normalizing these results based on the density of the foam, the tensile strength increases with water content. Thus, the decrease in density of the foam appears to have caused the leveling off of the ultimate properties.

Sung et. al. reported for a set of 2,4 TDI-ED-PTMO amorphous urea-urethane elastomers as having higher moduli and tensile strength with increasing hard segment content at a given PTMO MW(22). Cooper and Wang have also observed the same behavior for a set of MDI-ED-PTMO

urea-urethanes that have semicrystalline hard segments (33). Both investigators also observed lower elongation at break with increasing hard segment content.

2.3.3 Hardness

Another important mechanical property of flexible foams is their load bearing capacity which is measured by the hardness of the foam. The hardness is typically measured by indentation load deflection (ILD) and in some cases by compressive stress (compression hardness) which was discussed earlier. The difference between the two is illustrated in Figure 2.15. The indentation hardness is performed on a larger piece of foam (standard cushion size) as shown in Figure 2.15. Furthermore, the indentation hardness is reported as a load and not as a stress as in the case of compression hardness. Thus, the thickness of the sample, the tensile strength and the sample size effect the level of indentation hardness, but have little or no effect on the compression hardness. The rate of deformation is also of importance as stated earlier.

As mentioned earlier and shown in Figure 2.15, the indentation hardness can be reported in the form of ILD-deflection curves. The ILD value is also reported at different levels of deflection or at a percentage of the original height of the foam in the form of %ILD. An example of the latter, is by calculating the ratio of the 65% to 25% ILD values (sag factor) to give an indication of a cushion's expected performance. A sag factor of 2.8 or greater usually suggests a good cushion. However, it could be misleading without the ILD values when considering the level of comfort (31).

The hardness depends like some of the other stress-strain properties on different formulation variables (2-4,31,34-35). The hardness (40% ILD value) decreases with increasing water content (decreasing density) for flexible slabstock foams (2,4) and in high resilient(HR) foams (35). This trend, though somewhat different to that of the tensile strength, is explainable. First, the cell structure and possibly the density play a more important role in the compression mode than in tension. Fur-

thermore, there are two opposing factors with increasing water content; increasing modulus of the matrix and the decreasing density of the foam. It appears the density is the controlling factor. However, Patten and Seegfried showed if the density is held constant by using a physical blowing agent, the hardness increases with water content (35). This again shows the strength of the foam is effected greater by the urea content. Furthermore, this is also a good example of the difficulties that can arise if both the structure and the matrix material are not considered when evaluating the mechanical properties of foams.

Some of the other formulation variables that effect the hardness are the isocyanate index and the polyol structure. An isocyanate index of 105 or greater results in a harder foam due to the possible formation of biuret and allophanate structures. The level of hardness for high isocyanate indexes will also depend on the humidity during foam processing. With humid conditions, a decrease in the level of hardness is observed. A softer foam will be produced for either a lower functionality or higher molecular weight polyol.

One of the many factors of the foam geometry that effects the hardness as well as tensile strength is the direction of cell elongation. As mentioned earlier, the cells appear ellipsoidal in shape when looking perpendicular to the blow direction. The maximum loads in tension and compression occur by deforming along the major axis of these ellipsoidal cells as would be expected (2,31).

2.3.4 Viscoelastic Properties

In most cases, the viscoelastic properties of polymers are characterized by measuring the stress decay or strain increase with time at a constant strain or load, respectively. These two types of tests are better known as stress relaxation and creep. However, with flexible foams, tests that more realistically consider the application of foams have been used to characterize their viscoelastic nature. Such tests include compression set and indentation load(%ILD) loss. These tests are done in

compression under a constant load or constant deflection and also under dynamic conditions. Furthermore, these tests are carried out under accelerated conditions such as high temperature and humidity in order to predict the long term durability and/or fatigue resistance.

Before discussing the different responses, a brief description of each is necessary. Compression set is a measure of the recovery of the foam height after subjecting a foam to a constant deflection at a given set of conditions (usually 23 °C and 50% relative humidity) for an extended period of time (17-22 hours). The %ILD loss measures the load loss i.e., stress relaxation after subjecting a foam to similar conditions.

Several authors have measured the compression set in both slabstock and HR flexible foams (34-42). Most of these studies have concentrated on the effects of the formulation variables as well as temperature and humidity effects on compression set. The water content has shown the largest effect on compression set and especially under humid conditions (34-40). Herrington and Klarfeld reported humid aged compression set(HASET) values increasing with water content at 121°C and 50% compression with 100% relative humidity (36). Seefried and Patten as well as Saotome et. al. also observed a similar trend for slightly different conditions (34,37). The first two investigators also reported slight changes in compression set at different levels of density (constant water content) and isocyanate index (34,36). These results indicate that the urea content or the hard segment content has a significant effect on humid aged compression set. A possible mechanism will be given later.

Herrington and Klarfeld also observed that the foams recover with time upon removal from the compression jig, reaching a 10 percent loss in original height in about 120 hours (36). The time to reach the 10 percent loss was accelerated by storing the sample in a 70°C oven rather than at ambient conditions. These results suggest that the compression set is practically reversible and the bonding involved is mostly secondary and not primary. Furthermore, time-temperature superposition could be considered here in predicting the long term behavior.

Herrington and Klarfeld also reported that there was a drastic drop in the 50% HASET values upon humid aging at 104°C rather than at 121°C. Several other authors have also observed a decrease in compression set loss with decreasing temperature and with less time held at humid or high temperature conditions (35-36). These results possibly indicate that at elevated temperatures the hydrogen-bonding between the hard segments is weakened to a greater extent. This hypothesis is supported by IR-thermal studies. For example, Cooper et. al. reported observing a decrease in the absorption of the hydrogen bonded carbonyl group with increasing temperature for polyurethane elastomers (64).

Herrington and Klarfeld also discovered that there was a direct correlation between the urea concentration and the 50% HASET values. In explaining this result, the authors utilized attenuated internal reflectance-infrared spectroscopy (ATR-IR) and revealed a more distinct urea carbonyl at 1640 cm^{-1} for the humid aged sample. Thus, it was proposed, during humid aging that the hydrogen bonds to the urea carbonyls of the hard segments were replaced by water molecules as described schematically in Figure 2.16. From these results and the proposed model, a few conclusions can be drawn for the mechanism of humid aged compression set. It appears the local morphology on the molecular level of the foam has changed due to humid aging. Furthermore, upon compressing the foam the water molecules are broken which allows for chain slippage to take place. In the compressed state, a new equilibrium state is taken on by reforming hydrogen bonds. Therefore, upon release, the foam usually loses 40-50 percent of its original height (34).

Indentation load loss is affected in some similar ways to that of compression set. One way that the two differ is that the isocyanate index has a greater effect on the %ILD loss. Dwyer and Hilliard have shown an increase in fatigue resistance i. e., lower %ILD loss with increasing isocyanate indexes up to 115 (31,39). This could be attributed to the formation of allophanate structures and more likely biuret structures with increasing isocyanate index which allows for less rearrangement of the chemical network. In otherwards, less stress relaxation occurs with a greater crosslinked polymer system.

Patten and Seefried reported the %ILD loss not changing with increasing density at a constant water level. However, the authors did point out upon increasing the water level the %ILD values under humid conditions also increased (35) . Kane as well as Dwyer have reported the same trends under normal conditions and for static and dynamic tests, respectively (39-40). The increase in fatigue with increasing water content has been attributed to the higher levels of urea content; thus more hydrogen bonding is present in the foams (35). With more hydrogen bonding present, more hydrogen bonds are broken upon deformation which results in lower hardness values upon recovery. A somewhat similar situation was described above for compression set behavior.

In a different study, Lee measured the compression set and the hysteresis loss i.e., the energy loss during the compression set test for an HR foam (41). Lee concluded from his test that the compression set depends heavily on the hysteresis loss (41). Dwyer also observed that the %ILD loss was also related to the hysteresis loss (39). The hysteresis is attributed to the large amount of stress relaxation that takes place during the prolonged compression (22 hrs). Furthermore, the level of stress relaxation is enhanced by increasing the temperature of the test as several other investigators alluded to in their studies (36-39,41).

Reports on stress relaxation in polyurethane elastomers have shown that below 100°C, the soft segment dominates most of the stress relaxation taking place (39-40). This could possibly explain why Herrington and Klarfeld observed a significant difference in the HASET values when the test temperature was changed from 104°C to 121°C. The level of restoring force in the soft segments depends on the polyol functionality and the molecular weight. An elastic soft segment i.e., lower compression set values and %ILD loss in foams are obtained by having a high crosslinking density (up to a limit) and a long chain length between crosslinks. On the other hand, the hard segments exhibit little restoring force upon releasing the load as compared to the soft segments. Thus, by increasing the hard segment content when at high temperatures, one would expect greater stress relaxation and likewise higher compression set values and %ILD values as mentioned above.

A few investigators have reported on the stress relaxation behavior of foams in the compression mode (40,44-46). Ball and Doherty reported on a set of conventional slabstock foams with varying density, isocyanate index, and water levels (44). From the limited data that was reported, it could be concluded that the higher water content foams showed greater stress decay and thickness losses with time. This of course is consistent with the results shown above. Furthermore, Kane also reported an increase in stress relaxation with increasing urea content (40).

Ball and Doherty also showed that the data for the percent thickness loss and percent hardness loss over time could be described by the following general equation,

$$\Delta L = At^X \qquad [1]$$

where t is time, ΔL is the percentage loss of either thickness loss or hardness and A and X are constants. The constant X could be thought of as a "relaxation" time or rate of stress decay. Doherty and Ball did report a small increase in X with increasing water content (44).

Meincke also reported observing the same stress relaxation behavior as defined in Eq. (1) for a rubber-latex foam (flexible but generally denser foam than flexible polyurethane foams) (40). Furthermore, the relaxation rate was independent of the compression level when plotted on a log-log scale. Thus, a master curve was obtained and exhibited a linear relationship between log modulus and log time. This linear behavior has also been observed in 2,4 TDI-ED-PTMO urea-urethane elastomers (22). Sung et. al. reported observing a greater decay in stress for a lower molecular weight soft segment polyurethane elastomer. The faster rate was attributed to the lower soft segment MW sample having more solubilized hard segments which will lead to greater viscous flow.

Mitz and Raman have studied the stress relaxation behavior for a set of plastic packaging foams (semirigid foams) which consisted of two polyether bonded chip foams, a polystyrene foam, and a polyethylene foam (46). In their study, they have used a model developed by Peleg(47) to evaluate their data. In short, the model is empirical in orgin and the stress was normalized by the following equation,

$$Y(t) = \frac{F(0) - F(t)}{F(0)} \qquad [2]$$

where F(t) is the stress at a given time and F(0) is the initial stress. A linear relationship was obtained by plotting the inverse of Y(t) against time. The authors do point out that this linearity is satisfied if the modulus is only a function of time; therefore independent of strain. Two parameters evolve from the model by satisfying the above linearity for a given set of experimental data. They are the initial relaxation rate and an estimate of the residual (asymptotic) modulus at equilibrium conditions.

Mitz and Raman showed that the four semirigid foams studied fit the model well. Furthermore, the time required to obtain the data was only 30 minutes. Thus, this model provides a quick and simple method to obtain the initial relaxation rate and be able to predict the long term stress relaxation behavior in compression.

2.4 Summary

Flexible water-blown polyurethane foams are made in a "one-shot" continuous process by generally adding five different chemical components. These components are a diisocyanate, a polyether or polyester polyol, water, silicone surfactant, and tin and amine catalysts. A blowing reaction which consist of two primary reactions and a gelling reaction take place during the foam formation. In the early stages, the formation of disubstituted urea via the blowing reaction is the dominant species in the foam mixuture. Towards the end of the foam rise, disubstituted urea has been detected to precipitate out of solution. After the end of foam rise, the gelling reaction becomes more effective and the urethane linkages are for the most part formed at this time.

The morphology of the solid portion of flexible slabstock foams are similar to that of polyurea-urethane elastomers. For example, the SAXS results and the thermomechanical spectrum suggest similar morphologies. Both techniques detect a two-phase morphology. The DMS results exhibit a rubbery plateau and a fairly sharp soft segment glass transition which is independent of the hard segment content. The SAXS results detected scattering centers (hard domains) that were approximately 9 nm apart and contained fairly sharp phase boundaries. Furthermore, both techniques predicted better phase separation in the plaques. The TEM results showed evidence of large polyurea domains that increased in size from approximately 100 nm to 400 nm with increasing hard segment content. The solid morphology of the flexible slabstock foams on the molecular scale is represented best by Figure 2.10 based on the above results.

The mechanical properties are dependent on the above morphology of the solid portion of the foam as well as the cellular structure. The compressive stress-strain behavior goes through a linear elastic region (cell bending), a non-linear region (cell wall buckling), and then densification of the foam. The stress-strain behavior depends primarily on the cell regularity and the cell geometry, and secondarily on the cell density and cell size. The tensile strength and hardness of flexible foams increase with the hard segment content for a set of constant density foams. The isocyanate index, the structure of the polyol, and other formulation variables also have an effect on the stress-strain properties of foams.

The viscoelastic properties of flexible foams are also affected by the formulation components as well as by temperature and humidity. The water content has the greatest affect on the indentation load loss and the compression set at high temperatures and humidity. The isocyanate and the blowing agent levels have secondary effects on these viscoelastic properties. The loss in the properties can be attributed to stress relaxation. The compression stress relaxation behavior shows a linear relationship in a plot of log stress versus the log time.

Now that a better understanding of the molecular morphology as well as the mechanical properties of flexible foams exist, the next step is to associate the two. In other words, the structure-property

behavior at the molecular level of the solid portion of the foam needs to be investigated. In the next chapter, a technique that can help in reaching this goal is discussed.

CHAPTER III

3.0 Linear IR-Dichroism

3.1 Introduction

The structure-property relationships in polymers have been studied to obtain a better understanding of the resulting morphology as well as the mechanical properties. Rheo-optical techniques are often employed when obtaining such relationships. These techniques use electromagnetic radiation in studying the deformation of polymers and in many instances are utilized to probe the orientation in polymers on the molecular scale and at the superstructure level (e.g. spherulites) (48-49).

One rheo-optical technique used to obtain the degree of orientation in polymers is linear dichroism. Linear dichroism utilizes linearly polarized radiation to characterize the chromophoric groups of a molecule. The radiation used most often for dichroism is either ultraviolet, visible, or infrared (IR). Of the three, infrared radiation is most often used since many chromophoric groups common to polymers absorb energy in this region, where the frequencies of absorption in wavenumbers, typi-

cally range form about 6000 cm^{-1} to about 200 cm^{-1} (52). Thus, this discussion will concentrate solely on the utility of the IR region of the electromagnetic spectrum for orientation determination.

IR-dichroism is of particular interest when studying segmented and multiphase polymers due to its ability to separate the orientation behavior of the different segments or phases. For example, the separate orientation behavior can be obtained for the hard and soft segments in polyurethane elastomers and flexible foams. In multiphase polymers (e.g. semicrystalline polyethylene), the orientation of the amorphous and crystalline regions can also be separated. Before discussing some of the applications, the basic theory of linear IR-dichroism is reviewed.

3.2 Linear Dichroism Theory

Electromagnetic radiation consists of two oscillating fields, an electric and a magnetic, as shown in Figure 3.1 (48). The electric field is important when using IR-dichroism for two reasons. One, by polarizing the incident electromagnetic radiation, the direction in which the electric vector oscillates is governed. Secondly, the absorption of radiation in the infrared region occurs due to molecular vibrations. This involves the dipole moment of vibrating chromophoric groups of a molecule resonating with the electric field at a given wavelength of light or energy. The vector of the oscillating dipole moment for a given chromophoric group is the better known as the transition moment. Thus, the absorption, A, of polarized light for a given chromophoric group is written as

$$A \propto (\mu \cdot E)^2 = (\mu E)^2 \cos^2 \gamma \qquad [3.1]$$

where μ is the transition moment vector and E is the electric vector of the incident polarized radiation and γ is the angle between the two vectors.

The contributions from a given chromophoric group for a polymer made up of many molecules, n, is given by the absorption, A, such that

$$A \propto \int_n (\mu \cdot E)^2 dn \qquad [3.2]$$

As one may expect, if the orientation of the transition moments of a given chromophoric group is non-random, then a net absorbance will vary with the direction of the electric vector (51). This phenomena gives rise to linear dichroism.

The dichroic ratio, D, is defined as

$$D = \frac{A_{\parallel}}{A_{\perp}} \qquad [3.3]$$

where $A_{\parallel}$ and $A_{\perp}$ are the integrated absorbances of linear polarized radiation parallel and perpendicular to the stretch axis, respectively (see Figure 3.2). The peak heights are sufficient in measuring the absorbances as demonstrated in Figure 3.3. In relating the dichroic ratio to the orientation of the molecular chains in a polymer, an overview of Fraser's derivation is provided (50). Fraser, first derived a relationship between D and the transition moment angle, α, for perfect uniaxial order as shown in Figure 3.2a. By perfect axial order, one means the chains are perfectly aligned in one direction (e.g. draw direction) and the transition moments associated with the vibrations are cylindrically symmetrical about the chains. The dichroic ratio for this case is given as

$$D_o = 2\cot^2\alpha \qquad [3.4]$$

When α varies from 0 to $\frac{\pi}{2}$, D_o changes from ∞ to 0 and when $\alpha = 54.7°$, no dichroism is observed (50).

It is highly unlikely to have perfect axial order; thus Fraser considered a situation where only a fraction of the chains are perfectly ordered and the remaining are distributed randomly. Furthermore, he considered the case as shown in Figure 3.2b, where the chains are displaced from the draw direction by angle β. The following equation for D resulted using the coordinate system in Figure 3.2b;

$$D = \frac{(2cot^2\alpha)(\cos^2\beta) + \sin^2\beta}{(\cot^2\alpha)(\sin^2\beta) + \frac{(1+\cos^2\beta)}{2}} \qquad [3.5]$$

Using equation [3.4] and [3.5] and Herman's orientation function, f_h, where f_h is given as

$$f_h = \frac{3 < \cos^2\beta > - 1}{2} \qquad [3.6]$$

a relationship between the experimentally measured value of D and the second moment orientation function, f, is obtained. With some difficulty, the following expression can be derived which relates f to D_o and D,

$$f = (\frac{D_o + 2}{D_o - 1})(\frac{D - 1}{D + 2}) \qquad [3.7]$$

In evaluating Eq. [3.7], one needs to know the transition moment, α , and the experimentally measured dichroic ratio, D .

For $\alpha = 0°$, eq. [3.7] becomes

$$f = \frac{(D - 1)}{(D + 2)} \qquad [3.8]$$

and for $\alpha = 90°$ eq. [3.7] gives,

$$f = -2\frac{(D - 1)}{(D + 2)} \qquad [3.9]$$

The upper and lower limits of Eq. [3.7] are defined by Eq. [3.6] such that for parallel alignment of the chains, f equals 1 and for perpendicular alignment, f equals -0.5. In Eq. [3.9] the lower limit does approach -2 *as* D approaches infinity which appears to contradict the last statement. However, Eq. [3.6] is defined for uniaxial orientation only and thus the lower limit when assuming uniaxial orientation can be shown to be -0.5. Although, in the case of biaxial orientation of the chains, several authors have shown the lower limit of the orientation function to approach -1 (53-55).

By using linear IR-dichroism theory, one can determine the second moment average orientation in polymer systems that have chromophoric groups with known transition moments. Some examples of these groups and their respective transition moments are shown in Figure 3.4. The only experimental value needed is the dichroic ratio. Thus, with known transition moments and means to obtain their dichroic ratio, the orientation of different components or phases in multicomponent or multiphase polymers can in principle be determined.

3.3 Application

Over the past 20 plus years linear IR-dichroism has been used to evaluate the structure-property relationships in many polymeric materials. As mentioned earlier, segmented polymers can be characterized by utilizing IR-dichroism due to its selective absorption capabilities. The segmented polymers are also of particular interest since flexible polyurethane foams possess a phase-separated system as described earlier. Indeed, highly studied segmented polymer systems have been urethane and urea-urethane elastomers. The objectives involving the study of these materials, have been to obtain the orientation function given in Eq. [3.7], as a function of deformation, cyclic deformation, and time. Furthermore, some of these methods have been performed at different temperatures and in some cases directed towards understanding the hydrogen bonding behavior in polyurethanes. In

the paragraphs to follow, the application of IR-dichroism in response to different types of deformation is discussed with respect to both urethane and urea-urethane elastomers.

3.3.1 Polyurethane Elastomers

Polyether and polyester-urethanes have been studied using IR-dichroism as well as IR-thermal techniques (56-64). Most of the studies used MDI based hard segments with a butanediol (BD) chain extender. The soft segment was usually polytetramethylene oxide (PTMO) for the polyether urethanes and polytetramethylene adipate (PTMA) for polyester urethanes. If different chemical components, other than the above, are used in the following discussion they will be so stated. Furthermore, in characterizing the orientation of the hard and the soft segments as well as at the interface of these two segments, different chromophoric or absorbing groups with known transition moments were chosen. The hard segment orientation of the urethane elastomers was characterized by the $N-H$ group which is contained in the urethane linkage. For the polyether urethanes only, the urethane carbonyl groups, $(C=O)_b$ (hydrogen-bonded) and $(C=O)_f$ (not hydrogen-bonded), represented the hard segment orientation and the orientation at the interface of the hard and soft segments, respectively. The soft segment orientation for the urethanes was characterized by the CH_2 group. These absorbing groups along with their absorbing frequencies are summarized in Table 3.1. The orientation function in some cases is abbreviated for the different representative absorbing groups by the following nomenclature: e.g. $f_{(N-H)}$ represents the hard segment orientation level.

Orientation-Elongation Behavior

The orientation as a function of elongation for thin film polyether urethanes of different composition has been measured by Seymour et. al. (56,57). The authors reported observing higher levels

of orientation for the hard segments than the soft segments at the same level of deformation for 25 weight percent (wt%) to 50 wt% hard segment (HS) content samples (56-57). This is expected since the hard segments tend to retain their level of orientation upon deformation due to their rigidity, while the flexible soft segments are inclined to relax quickly. The level of orientation for the $(C=O)_b$ was higher than that of the $(C=O)_f$ as expected. This behavior was attributed to the $f_{(C=O)f}$ being affected by both the hard and soft segments. Furthermore, the orientation of the $(C=O)_f$ group was higher than that of the *CH* group (56-57). Bonart and Hoffman also reported observing similar orientation behavior for a similar polyether urethane elastomer (58).

Seymour et. al. reported observing similar levels of orientation for 1000 molecular weight (MW) PTMO samples with 31 wt% to 46 wt% HS content. However, for a 25 wt% HS - 1000 MW PTMO sample the level of orientation was much lower for both the hard and the soft segments due to phase mixing. On the other hand, a 50 wt% HS - 2000 MW PTMO sample which contained some crystalline hard domains, exhibited negative orientation for the hard segments at strains less than 100% and positive orientation was observed thereafter, but at much lower levels than the samples (28wt% to 38wt% -1000 MW PTMO) that contained amorphous HS domains. This negative orientation behavior was attributed to the crystalline domains and a possible mechanism to explain this behavior will be proposed in the following paragraph.

Bonart and Hoffman also reported observing similar hard segment orientation behavior for a 45 wt% HS-2000 MW PTMO polyether urethane in comparison to that of the 50 wt% HS-2000 MW PTMO sample just mentioned (58). In explaining this behavior, they proposed a model (see Figure 3.5) which consisted of small hard segment domains and large lamallae like hard segment domains. These HS domains could be of crystalline order, of para-crystalline order, and/or amorphous. The model in Figure 3.5 predicts that the small HS domains orient in the stretch direction upon being deformed. On the other hand, at the lower elongations the hard segments of the lamellae domains orient transverse to the stretch direction or likewise the long dimension of the domains orient in the stretch direction (see Figure 3.5). Thus, the orientation of the larger domains (lamellae-like) appeared to be dominating at the lower elongations for both the 50 wt% HS and 45 wt% HS samples.

However, at the higher elongations some of these domains are disrupted by local shear stresses applied by the soft segments; thus allowing for the hard segments that are separated from the hard domains to align in the stretch direction (54). This of course would result in the positive orientation observed by both Seymour et. al. as well as Bonart and Hoffman at higher elongations (100 percent) (56-58). These results have also been supported by WAXS studies that were carried out as a function of elongation (59).

Bonart and Hoffman also found that the more time permitted for solvent evaporation in preparing the thin films resulted in an increase in the level of transverse orientation. This increase was thought to be attributed to the formation of larger hard domains; thus suggesting the smaller domains contribute less to the orientation level i.e., positive orientation at lower elongations (58).

A set of non-hydrogen bonded polyurethanes with piperazine based hard segments have also been studied to determine the effects of hydrogen bonding in MDI based urethanes (60). The hard segments are partly crystalline for all compositions (32 to 52 wt% HS content) as shown by WAXS and DSC studies. Furthermore, negative orientation was observed for the hard segments at the smaller elongations. Allegreza et. al. also attributed this transverse orientation to the partly crystalline hard segment lamellae as described earlier by Bonart's model (60). In comparison to the hydrogen bonded polyurethanes that were discussed above, these samples exhibited higher levels of orientation at the higher strains. This behavior was attributed to the non-hydrogen bonded hard domains being disrupted easier than the hydrogen bonded hard domains due to less interchain interaction between the piperazine hard segments (60). Finally, the soft segment orientation did not differ signficantly between the hydrogen bonded and non-hydrogen bonded polyether polyurethanes.

The orientation behavior with deformation has also been studied in polyester urethanes (61-63). Estes et. al. reported observing similar orientation levels for both the hard and soft segments of a 46 wt% HS-1000 MW PTMA polyester urethane (61). The orientation of the soft segment was slightly higher than that of the hard segments up to 150% strain and then the reverse behavior was

observed until the sample broke at 325 percent strain. Siesler also reported observing similar orientation behavior for a set of polyester urethanes containing a 2000 MW PTMA soft segment with 35 to 60 wt% HS content. However, he only observed slightly higher levels of orientation of the soft segments up to strains of 200% (as high as was reported) (57-58). Siesler also reported a small increase in both the $f_{(N-H)}$ and the $f_{(CH_2)}$ with increasing HS content (62-63).

The difference in the orientation behavior between the polyester and polyether urethanes has been suggested to be possibly due to a higher level of phase separation for polyether urethanes of similar composition, that is, polyether soft segments are less compatible with the hard segment in comparison to polyester soft segments. This difference in compatibility can be attributed mostly to the interaction of the ester carbonyl with the $N-H$ group of the hard segment; thus permitting phase mixing to occur. This also explains why the orientation levels do not differ significantly between the hard and soft segments of the polyester urethanes. Furthermore, the crossover in the level of orientation observed by Estes et. al. at the higher elongations suggests that some dissociation of the hydrogen bonding to the soft segments is taking place. If so, this would allow for more soft segment relaxation and furthermore, lower $f_{(CH_2)}$ values than for $f_{(N-H)}$.

Orientational Hysteresis

Orientation behavior upon cyclic straining has been measured for polyether and polyester urethane elastomers (56-57,60-63). Cooper et. al. measured the orientation level(residual) at no load after subjecting a sample to a loading-unloading cycle and then allowing for it to relax for 5 minutes. The authors reported that the level of segmental residual orientation increased systematically with increasing cycle elongations up to 250 percent for both the hard and soft components of 46 wt% HS-1000 MW soft segment polyether and polyester urethanes (56-57, 60-61). Higher residual orientation behavior in the hard segments than in the soft segments was observed for these urethane elastomers. This behavior is expected due to the nature of the hard segment retaining their orien-

tation upon deformation. Seymour et. al. also suggested that the residual hard segment orientation plays a role in the mechanical hysteresis or stress softening in these materials (57).

Siesler followed the orientation behavior for a loading- unloading cycle on the same set of polyester urethanes discussed earlier. As mentioned earlier, he observed slightly higher orientation levels in the soft segments upon loading. However, he also observed that the hard segments retained a slightly higher state of orientation than that of the soft segments upon strain recovery (62-63). It was suggested that the orientation behavior was due to the soft segments relaxing quickly during unloading and thus limiting the recovery of the hard segments (62). Furthermore, higher levels of orientation(both hard and soft segments) and mechanical hysteresis were observed at the un-stretched state for the higher hard segment content samples. Thus, the increase in the irreversible orientation behavior of the hard and soft segments caused more energy to be lost upon cyclic deformation.

Orientation Time Study

The viscoelastic nature of polyether urethanes has also been evaluated in conjunction with orientation measurments by imposing a constant level of strain and then observing the orientation change as a function of time (56-58). Seymour et. al. reported observing similar orientation time behavior after stepping to a 150% level of strain for a set of samples with a 1000 MW PTMO soft segment varying in HS content from 30 wt% to 46 wt% (56-57). An increase in $f_{(C=O)b}$ and $f_{(N-H)}$ as well as a decrease in $f_{(C=O)f}$ and $f_{(CH_2)}$ were seen with time (56-57). The soft segment ($f_{(CH_2)}$) partially relaxes very quickly then gradually decreases under an entropy driven relaxation. The increase in the hard segment was attributed to a similar mechanism mentioned for Siesler's results during the unloading cycle. That is the relaxation of the soft segment exerts a tension on the hard segments; thus causing the hard segments to orient more in the stretch direction (56).

Bonart and Hoffman also reported observing similar orientation relaxation behavior for a 2000 MW PTMO - 40 wt% HS polyether urethane at a 60% constant strain level for the $N-H$ groups as well as for the $(C=O)_f$ and $(C=O)_b$ groups (58). However, the orientation of the hard segments returned to the initial level of orientation at very long times (10 hrs). The authors suggested that this return could indicate reformation of the hard domains that were disrupted during initial deformation.

Temperature Effects on Orientation

Cooper et. al. reported observing the level of orientation for a 5000 MW PTMO- 55 wt% HS polyether urethane and a 1000 MW PTMA-46 wt% HS polyester urethane going through a maximum (f_{max}) as a function of temperature (56,60). The temperature where f_{max} occurs is above the hard segment T_g which indicated the hard domains are more easily disrupted near their T_g i.e., the hard segments can align easier in the stretch direction. However, at temperatures greater than the maximum, the disruption of hydrogen bonding increases (observed in a separate IR-thermal study (64)) and the hard segments are able to relax more after being deformed (56). Furthermore, the degree of disruption of hydrogen bonding was found to be a function of the hard segment content and the MW of the soft segment for both polyether and polyester urethanes by IR thermal analysis (59).

Siesler also observed for a 2000 MW PTMA-60 wt% HS polyester urethane an increase in the $f_{(N-H)}$ at temperatures below the T_g of the hard segments (62). The increase was so significant that it surpassed the level of orientation of the soft segments at strains greater than 80% (remember at ambient $f_{(CH_2)} > f_{(N-H)}$ at all strains on loading). This behavior is also attributed to the hard segments softening near their T_g and thus orienting more in the stretch direction.

3.3.2 Polyurea-urethane Elastomers

Polyurea-urethanes have also been studied utilizing IR dichroism to gain a more complete understanding of their morphology in regards to strain and thereby leading to their mechanical behavior. The urea-urethane elastomers that are discussed in the paragraphs to follow, contained hard segments which were formed from either MDI or 2,4 TDI, while the soft segment consists of PTMO repeat units. The chain extender was ethylenediamine(ED), unless stated otherwise. In comparison to polyurethanes, polyurea-urethanes of similar composition have been generally reported as having better phase separation and different hard domain structure. This is attributed to the urea hard segment's greater incompatibility with the the soft segment and the development of a 3-dimensional hydrogen bonding network (21,65).

The IR bands which represented the different segments are somewhat similar to the urethane elastomers. However, the urea carbonyl ($(C=O)_{ur}$) group also represented the hard segment orientation, while the $(C=O)_b$ and $(C=O)_f$ both were used to characterize the orientation at the interface of the hard and soft segments. Once again $(C=O)_b$ stands for a hydrogen bonded urethane carbonyl and represents $(C=O)_f$ a non-hydrogen bonded urethane carbonyl. These absorbing groups along with their absorbing frequencies are summarized in Table 3.2.

MDI-Based Urea-Urethanes

Several investigators have studied the deformation-IR-dichroism behavior in MDI-ED-PTMO urea-urethanes (33,66-70). Hoffman and Bonart reported observing positive orientation in the soft segments as well as at the interface (both $(C=O)_f$ and $(C=O)_b$ groups) for 2000 MW PTMO - 17 and 21 wt% HS content samples (66-67). On the other hand, the hard segments ($(C=O)_{ur}$ and $N-H$ groups) exhibited transverse or negative orientation. The transverse orientation was observed up to strains near 200% and then a positive upturn in the orientation level was seen. A

maximum in the transverse orientation for the $(C=O)_{ur}$ groups was reported as low as -0.6 for the 21 wt% HS sample. This of course is below the lower limit allowed for uniaxial orientation. Thus, one must assume the possibility of biaxial orientation. In short, the authors suggested an azimuthal dependence of the transition moment about the chain axis which implies biaxial orientation (67). More details of the authors explanation and proposed theory are found in reference 67.

The value of $f_{(C=O)ur}$ was always less than that of $f_{(N-H)}$ even though both absorbing groups represent the hard segment orientation (66). However, the N-H group is also in the urethane linkage which exhibits positive orientation. Thus, the level of orientation is going to be slightly more positive than for $f_{(C=O)ur}$ due to a small contribution from the urethane N-H groups.

Ishihara et. al. as well as Cooper and Wang have also observed similar behavior for MDI-ED-PTMO urea-urethanes as discussed above (33,68-70). However, these two investigators did not observe negative orientation below -0.5 for the $(C=O)_{ur}$ as Bonart and Hoffman did. This may be attributed to a number of factors (e.g. different composition, sample preparation, sample size, and polymerization conditions). However, it appears the difference between Bonart's and Cooper's results are due to sample preparation (no information on Ishara's sample preparation is availible). Bonart and Hoffman apparently removed the solvent from their solution cast films slower than Cooper and Wang; thus possibly allowing for larger hard segment lamellae to form (33,66-67). As was mentioned earlier for the urethane elastomers, the size of the lamellae domains is suggested to play a role in the level of transverse orientation in the hard segments (58).

The investigators discussed above have contributed to the explanation of the transverse orientation behavior of the hard segments (33,66-70). First, it must be stated that Bonart et. al. as well as Ishihara et. al. have reported observing paracrystalline and crystalline hard segment lamellae by utilizing WAXS (68,70). All investigators appear to agree that at the smaller elongations (< 150% - 200%) the transverse orientation can be attributed to the long axis of the lamellae orientating in the stretch direction as depicted in Figure 3.6. Furthermore, at the higher strains some of the lamellae hard domains disrupt and begin to align in the stretch direction (see Figure 3.6b) which

gives the positive upturn in the orientation level. However, the method by which the hard domains disrupt is not well understood nor consistent among these investigators. Hoffman and Bonart state that the lamellae are disrupted by shearing forces which causes the hard segments to separate from one another and furthermore calls for a decrease in hydrogen bonding. On the other hand, Cooper and Wang reported observing only a slight decrease in the interurea carbonyl absorbance with strain. This suggests the disruption of the hard domains is gradual with strain and that the hard segments possibly do not separate as Bonart has suggested (33). It also appears from Ishihara's study, as depicted in Figure 3.6b at the higher strains, the hard domains become smaller in size, but still contain the hydrogen bonding between the segments as Cooper has suggested from the IR-strain study. As one may notice from the discussion, the exact mechanism is not fully understood for the hard segment behavior at the higher deformations. However, it is clear that the lamellar structure of the hard domains is causing the transverse orientaion at the smaller strains. This has been supported by WAXS and SAXS diffraction patterns of urea-urethane elastomers which showed X-ray diffractions in the equatorial zone indicating transverse alignment in the stretch direction of the lamellar domains at lower elongations. In contrast, a diffuse X-ray diffraction pattern was observed at higher elongations which suggested that some form of disruption in the hard domains was taking place (68,70).

In their IR dichroism study, Cooper and Wang concentrated on the effects of block length and the hard segment content on the morphology as well as the physical properties for a set of 2000 and 1000 MW PTMO polyurea-urethane elastomers with hard segment contents varying from 25 to 46 wt%(33). For comparable hard segment contents, the longer block length (2000 MW PTMO) samples exhibited greater transverse orientation behavior and furthermore, higher moduli and for the most part higher ultimate tensile strength. This was attributed to the longer block lengths i.e. higher interurea hydrogen bonding and thus better hard segment domain (segment-segment) cohesion. The higher MW soft segment samples exhibited a decrease in the orientation level with decreasing HS content. This was consistent with the stress hysteresis results which showed higher initial hysteresis values with increasing HS content. Thus, the mechanical hysteresis and the orien-

tation results indicate better hard domain interconnectivity and a higher degree of order with increasing HS content (33).

As mentioned earlier the urethane groups at the interface and the soft segment showed positive orientation. The urethane groups orient in the stretch direction due to the retractive force which is exerted on them by the soft segments (33). The orientation of the $(C=O)_f$ groups was generally found to be greater than that of the $(C=O)_b$ groups. This is expected since the $(C=O)_b$ is also influenced by the hard segments. Cooper and Wang did report observing in one instance the reverse behavior for the urethane carbonyls and suggested that the $(C=O)_b$ could be hydrogen bonded more to the ether groups of the soft segment than the N-H groups of the hard segment (33).

The level of orientation of the soft segment as well as the urethane C=O's decreased with decreasing hard segment content and block length. The storage modulus, E', at room temperature also decreased in a similar fashion. The higher E' and f values were attributed to less segmental relaxation and disorientation (33).

Orientational hysteresis behavior has also been reported for the MDI-ED-PTMO elastomers (66-67,69). The orientation behavior upon cyclic deformation for the soft segments and the urethane groups at the interface was approximately reversible up to strain levels of 400%. On the other hand, the hard segments exhibited irreversible orientation behavior to different extremes depending on the level of cyclic straining. At initial strain levels less than the maximum transverse orientation (f_{tmax}), the orientation behavior did not change considerably upon cyclic deformation. However, at initial strains greater than f_{tmax}, the retainment of the original orientation behavior became less and the hard segments begin to align more in the stretch direction (69). This behavior of the hard segments furthermore shows that at strain levels before f_{tmax}, the lamellae hard domains are more cohesive and the hard segments separate very little. On the other hand, at strain levels beyond f_{tmax}, some of the lamellae hard domains are disrupted (69).

2,4-TDI Based Urea-Urethanes

As mentioned earlier, IR-dichroism has also been utilized to study the orientation behavior in urea-urethanes with hard segments formed from 2,4 TDI instead of MDI (71-72). Sung and Hu reported on two *amorphous* 2,4 TDI-ED-PTMO samples with comparable composition, but with different soft segment molecular weights of 2000 and 1000. They reported that the two samples exhibited positive and comparable orientation-elongation behavior for both the hard and soft segments (71). The positive orientation in the hard segments was similar to that of the polyurethanes containing amorphous hard segments (56-57). The higher MW soft segment (PTMO 2000) sample has higher orientation values. These results suggested a better phase separated system and less interconnected domains for the PTMO 2000 sample. This observation is consistent with the mechanical properties which exhibited higher elongation at break, lower hysteresis, and slower rate of relaxation for the PTMO 2000 sample versus that of the PTMO 1000 sample (22).

Khranovskii and Gul'ko also reported on a similar urea-urethane but with a 4-4 diphenylmethanediamine (PM) chain extender (72). By replacing the ED chain extender with a PM extender, crystallinity in the hard domains was observed by utilizing WAXS. The orientation behavior was similar to that of MDI based polyurea-urethanes as described earlier. However, the authors chose not to explain the hard segment orientation behavior on the basis that lamellar hard domains were present in their samples. In short, they attributed the transverse orientation of the hard segments to conformation transitions in the hard segments and based their arguments on their WAXS results (72). Khranovskii and Gul'ko did report observing different WAXS patterns compared to those of Ishihara et. al. (70,72).

3.4 Summary

Infrared dichroism is a powerful rheo-optical technique due to its ability to selectively quantify the second moment orientation of different segments or phases in polymers. This has been demonstrated for the segmented urethane and urea-urethane elastomers which consist of hard segment domains in a soft segment matrix. The soft segments exhibited positive orientation in all cases as well as did the urethane groups at the interface of the hard and soft segments.

The orientation behavior of the hard segments, though difficult to explain in some instances, appears to depend on whether smaller domains or larger lamellar textured hard domains are present. These domains have been reported as possessing amorphous, paracrystalline, and/or crystalline order. It does appear that the lamellae hard domains normally possess paracrystalline or crystalline order. The samples containing the smaller hard domains generally exhibit positive orientation upon deformation, while the samples with the lamellae hard segments present showed transverse or negative orientation at the smaller strains and eventually positive orientation at the higher strains. The transverse orientation is attributed to the lamellar structure of the hard domains which upon deformation orient with their long axis in the stretch direction.

Linear IR-dichroism theory provides a simple method to obtain the second moment orientation function. However, the transition moment for a given representative absorbing group of a particular segment or phase must be known and the dichroic ratio must be obtained for the sample at hand. By obtaining the deformation-orientation behavior, a better understanding of the mechanical properties and a clearer morphological picture can be obtained as has been exemplified for the urethane and urea-urethane elastomers.

CHAPTER IV

4.0 Experimental

4.1 Materials

The flexible polyurethane foams used in this investigation were conventional slabstock water-blown foams. These foams were made in a homemade, boxfoaming operation. This operation consisted of a mixing container, a mechanical stirrer, and a wooden box. The mixing container was a 16 inch diameter carbon steel baffled tank that fits over an 8 inch diameter multiple blade stirrer. The stirrer was being driven by a motor. The wooden box was of 3 cubic feet and lined with a polyethylene bag (3,18).

The formulation components given in Table 4.1 were used to make the foams for this investigation and are also used on a commercial scale. These foams were processed by using the exact formulation amounts given in Table 4.2. The water, the polyether polyol, the surfactant, and the amine catalyst were first mixed for 30 seconds at 900 revolutions per minute. This was followed by addition of the tin catalyst and mixing for 30 more seconds at the same speed. The diisocyanate was

then added and mixing took place for 5 more seconds at 1200 rpms. The mixture was then poured in a lined wooden box and allowed to react. After the foams had cured, they were then trimmed. The remaining block was used for various testing analysis. All of the foams investigated were prepared in this manner (18).

Foams 1-4 are the same foams that were discussed earlier in the morphology section of the literature review. Foams 1-lc0 and 3-lc were made with the same amount of formulation components given in Table 4.1, but the actual amounts (except for the water content) are not presented in Table 4.2 due to proprietary reasons. The only difference in the formulation of foam 1-lc0 and 3-lc is that foam 3-lc has an extra proprietary component and foam 1-lc0 does not.

Compression molded plaques were also made from each foam by applying pressure for 10 minutes at 204°C. In some cases the foams were subjected to a pretreatment process before compression molding. The pretreatment process consisted of first soaking the foams in DMF or THF overnight. The foams were then patted dry and the excess solvent was taken off by storing the foams in a vacuum oven at 50°C for at least 24 hours. After this solvent removal treatment, the foams were then compression molded using the above conditions. The nomenclature used for the plaques prepared from the pretreated foams is as follows: e.g., plaque 1-DMF represents plaque 1 (made from foam 1) which was pretreated with DMF before compression molding.

A urea-urethane cast elastomer and a urethane elastomer were also used in this investigation. The urea-urethane elastomer was made from T-80 (see Table 4.1) and a 2000 MW polypropylene oxide diol (P2000) with a methylene-bis(2-chloroaniline) (MOCA) curing agent. The elastomer was prepared by first making a prepolymer. This was done by mixing P2000 and T-80 for 4hrs at 80°C. The prepolymer which contained 5% extra NCO groups was then mixed with MOCA. This mixture was then poured into a mold for 1 hr at 130°C and then allowed to cure for 16 hrs at 70°C. This urea-urethane elastomer contains a 31 wt% hard segment content and is referred to as the PUUE elastomer for this investigation.

The urethane elastomer was made from pure MDI and a 2000 MW PTMO with a butanediol chain extender. The elastomer was prepared by the two-step procedure described earlier in the chemistry section of the literature review. This elastomer is also known by its commercial name ESTANE®. It contains a 30 wt% of hard segment and will be referred to as ET-2000- 30.

4.2 Experimental Techniques

The two main objectives of this work were to evaluate the relaxation behavior and the molecular orientation with deformation of flexible slabstock polyurethane foams as well as the plaques of these same foams. The compression molded plaques were studied because they offer the advantage of analyzing the material comprising the foam independent of its geometry. As discussed earlier, the compression molding process does not alter the morphology of the solid material significantly. The two techniques that were utilized to meet these objectives are stress relaxation in tension and deformation-IR dichroism. Dynamic mechanical spectroscopy (DMS) and wide angle x-ray diffraction (WAXS) were also used to characterize the pretreated plaques, plaques 1-lc0 and 3-lc, and the PUUE elastomer.

4.2.1 Stress Relaxation

Stress relaxation in tension was used to follow the stress decay with time at ambient conditions and at high temperatures. The experiments were carried out on an Tensilon/UTM II Tensile Tester that was equipped with a homemade thermal chamber. The temperature was controlled by an OMEGA® miniature microprocessor temperature controller and a type K thermocouple. The relative humidity ranged from 20 to 40 percent depending on the time of year.

All samples were stretched with a strain rate of 40 mm/min to a constant elongation of either 25% or 40%. The samples were then held at the appropriate elongation for 3 to 4 hours while the load readings were collected by a chart recorder. The chart recorder was run for the first five minutes of stress relaxation and then readings were taken periodically for the next 3 to 4 hours. The experiment was repeated 3 or 4 times for a given sample and set of conditions. A fresh sample was used for each experiment.

Foams 1-4 were all tested using a dogbone shape sample with a thickness of 6.5 mm, a cross section of 1.55 mm, and a gauge length of 10 mm. The foams were cut in a manner so that the dogbone specimen would be stretched parallel($\sigma_{\parallel}$) or perpendicular($\sigma_{\perp}$) to the blow direction. This was done to check for mechanical anisotropy as well as the dependence of the cell structure on the stress relaxation. Both sets ($\sigma_{\parallel}$ and $\sigma_{\perp}$) of foams were tested at ambient conditions. The foams stretched parallel to the blow direction were also tested at 75°C and foam 4($\sigma_{\parallel}$) was tested at 125°C. The foams stretched perpendicular to the blow direction were only tested at ambient conditions due to similar stress relaxation behavior to that of the foams tested under parallel conditions. Most of the experiments were done at 40% elongation due to the loads exerted by the foams being small in comparison to the range of the load cell.

The compression molded plaques were tested to check for a anisotropic dependence of the cell geometry on the stress relaxation behavior for the foams. The same dogbone shape sample was used as described above. The thickness of the plaques ranged form 5 to 10 mils. The plaques were tested at ambient conditions and at 75°C. Plaque 4 was also tested at 125°C. Plaque 2-DMF was also tested at ambient conditions. These test were all done at 25% elongation in order to stay within the range of the load cell for all the plaques.

4.2.2 WAXS

Wide Angle X-ray diffraction patterns in general were obtained to help characterize the compression molded plaques and the urea- urethane elastomer. The WAXS setup consists of a Phillips Table-Top X-Ray Generator PW 1720 with a standard vacuum-sealed Statton Camera. The samples tested were 7 to 10 mils in thickness. The exposure times varied from 18 to 24 hours depending on the sample thickness. The sample to film distance was 6 cm or 7.8 cm depending on the test. WAXS patterns were obtained for plaques 2 and 2-DMF. WAXS patterns were also taken for plaque 1-lc0 and 3-lc as well as for the PUUE elastomer.

4.2.3 Dynamic Mechanical Spectroscopy

Dynamic Mechanical Spectroscopy was utilized to check for changes in the thermo-mechanical spectrum of the plaques due to using the pretreatment process. The test were carried out on an automated Rheometrics Model 7700 Dynamic Spectrometer. The temperature range was from -100°C to 200°C or 220°C at a heating rate of 2°C. The samples tested were plaques 2 and 3 (un-treated and pretreated with DMF). The PUUE elastomer was also tested.

4.2.4 IR Dichroism

As discussed earlier, IR-dichroism is an useful technique to obtain the molecular orientation for segmented polymers. This technique was utilized in this investigation for similar purposes to study the plaques of the flexible water-blown polyurethane foams. Such information would hopefully lead to a better understanding of the important physical properties such as compression set and fatigue.

Furthermore, a more complete morphological picture was also an objective of applying this method.

In order to obtain the molecular orientation by IR-dichroism as well as the simultaneous mechanical response, certain pieces of equipment were necessary. They were an infrared source (commonly an FTIR), a suitable polarizer, and an appropriate mechanical apparatus. It is such an apparatus that was constructed for the purposes of this investigation. The design criteria for this apparatus, a description and the operation of this apparatus, and the procedures for obtaining the dichroic data are given in the paragraphs to follow.

Design Criteria

The main objective for the above addressed rheo-optical system is to simultaneously collect polarized FTIR data and measure stress-strain properties of thin film samples. In order to do this, a mechanical apparatus was required to fit into a Nicolet 5DXB Spectrometer chamber. It was also believed that the stretching device should be able to deform a sample from both ends for purposes of maintaining a constant "sample zone." Variability of strain rate and level of elongation were also desired. Furthermore, it was desired to simultaneously monitor the stress and strain behavior of the polymer samples by an on-line computer during the orientation measurements. Also, a thermal chamber was desired to allow temperature control in the range of 20°C to 150°C. Finally, a simple method to rotate the polarizer accurately and refrain from damaging the polarizer had to be incorporated into the design.

Many of the above criteria were obtained by utilizing several of the design features of a system constructed and described by Siesler (63,73). His apparatus has the capability of measuring IR dichroism while performing various mechanical tests on thin polymer films as was alluded to earlier in the application of IR dichroism to polyurethane elastomers. Using the above criteria, the rheo-optical stretching apparatus was constructed and its features are now given in more detail.

Rheo-optical Stretching Device

The mechanical apparatus constructed is a versatile instrument for its size. The actual size of the stretching device is 7.5 cm by 19 cm by 8 cm. It was built to fit into a Nicolet 5DXB FTIR Spectometer chamber which is 21 cm by 27 cm by 19 cm. The stretching device and the polarizer are shown in Figures 4.1 and 4.2 in the FTIR chamber.

A close-up photograph of the stretching device along with the polarizer is shown in Figure 4.3. The different components in Figure 4.3 are the linear motors (1), a load cell (2), an amplifier (3), a grid polarizer (4), an arm used to rotate the polarizer (5) and a thin film sample (6). The manufacturers of these components along with other details are listed in Appendix A. A description of the linear motors and the load cell is given below.

Each of the linear motors are driven by a microstepping drive. The resolution is 25,000 steps per revolution or 25,000 steps per linear inch of travel. The number of steps that the motor travels and its velocity are computer controlled. A Basic program with simple input commands is used to control the movement of the motors. The distance the motors travel determines the strain or elongation.

Other computer commands (operator input) control the velocity i.e. the extension rate. The polymer sample is elongated from both sides in the stretching device. This is favorable when carrying out IR dichroism measurements since the IR beam penetrates approximately at the middle of the polymer sample. Thus, by stretching the sample from both ends the beam will remain at the center of the samples at all times.

The velocity of the separating sample clamps with both motors moving simultaneously, ranges from 20 to 60,000 mm/min. This is equivalent to extension rates ranging from 0.8 to 2400 %/min for a given initial clamp to clamp distance of 25 mm. The accuracy of the motor from step to step is ± 0.0001 cm and the overall accuracy is ± 0.00431 cm. Thus, by the precise control of the motor

system, the strain on the polymer can in turn be well controlled. It should be mentioned that the travel of the motors is very smooth even when applying a force on the motors. The maximum static load that each motor permits is 5 lbs. or 2.25 kg.

The resistance force that the polymer exerts upon stretching is also measured by the device. The force exerted is converted to an electrical signal and amplified by an attached load cell (see Figure 4.3). The amplified signal is then digitized by an analog to digital converter and then stored in the computer. The amplifier shown in Figure 4.3 further enhances the signal to the A/D converter, filters noise, and provides a power source for the load cell. The whole operation to obtain a digital reading of the force is computer controlled as in the case for the operation of the motors. The program for the A/D conversion is incorporated within the program for the motors. An example program is given in Appendix B.

The load cell is calibrated by using standard weights. A linear relationship exists between the force readings and the digital readings from the A/D converter. After obtaining the linear relationship, it is inserted into the Basic program to convert the digital readings to the force exerted by the thin film. The force measurements in turn are used to calculate the stress given the cross sectional area of the thin film.

Mounting of the Sample and Sample Considerations

The sample used possesses a dogbone shape in order to avoid clamp effects (see Figure 4.4). Before placing the sample into the apparatus, the sample is first premounted into the clamps as demonstrated in Figure 4.4. The clamps for the sample are then removed from the holder and transferred to the stretching device. The ends of the sample clamps possess a dovetail shape as shown by the arrow in Figure 4.4. This makes it easy for placement of the clamps in the stretching apparatus without damaging the sample or the polarizer.

Rotation of Polarizer

The grid polarizer(4) shown in Figure 4.3 is rotated the necessary 90° by the elbow shaped piece of plastic (5). This arm on the polarizer extends outside the FTIR chamber such that the polarizer can be rotated without having to open the chamber door.

Thermal Chamber

The final addition to the rheo-optical stretching apparatus was a thermal chamber which was also constructed. The thermal chamber material was of a polyphenylsulfide (PPS) thermoplastic composite material as shown in Figure 4.5 and 4.6 along with the stretching apparatus. The different components in Figure 4.5 are the removable lid (1) and teflon window holder for a 25 mm diameter salt plate (2). As shown in Figure 4.6 by the arrows, there are two windows for the IR beam to pass through the chamber walls. The thermal chamber is stationary and the arms with the sample clamps are able to move freely through the ends of the chamber as shown in Figure 4.6. The two components labeled in Figure 4.6 are a type-K thermocouple (1) and a silicone rubber flexible heater(2). Both of which are connected to a OMEGA® microprocessor temperature controller to provide for feedback temperature control of the thermal chamber.

The thermal chamber was also insulated with asbestos free milboard material and held together with nylon machine screws. The maximum operating temperature of the thermal chamber is limited to 150°C due to the maximum service temperature of the nylon screws. Furthermore, it is designed to limit the amount of heat loss since all of the above materials possess low thermal conductivities. The amount of heat that could escape was a major concern due to the temperature sensitive detector of the FTIR as well as the other components that make up the optics. More information on the materials used to construct the thermal chamber and the different components used are given in Appendix C.

Procedures for Obtaining Orientation Data

Thin Film Preparation

When using FTIR spectroscopy, the intensity of energy, I, that passes through the sample is defined by the Beer- Lambert law which states,

$$A = -\log(\frac{I}{I_o}) = abc \qquad [4.1]$$

where I_o is the incident intensity, a is absorption coefficient for a given chromophoric group and has the units of $liter\, g^{-1}\, cm^{-1}$, b is the thickness of the sample and has the units of cm, and c is the concentration of a given chromophoric group and has the units of *grams/liter*. For a given sample, a and c are generally fixed and the thickness becomes the governing factor for the amount of transmitted energy that reaches the detector. With this in mind, several different methods were attempted to obtain the thinnest films possible for the compression molded plaques. The best procedure was to cut a piece of foam 2 mm in thickness with a die. This thin piece of foam was then pressed or exposed to the pretreatment process first and then pressed. The thin films ranged from 1.1 mils to 2.5 mils. The thinnest films for the most part were obtained by using the pretreatment process prior to compression molding. The plaques that were prepared in the above manner for the IR-dichroism experiments were plaques 1-4, plaque 1- lc0, and plaque 3-lc. However, plaques 3 and 4 posed problems due to either thickness or concentration of specific chromophoric groups representing the hard segment and thus will not be discussed for this investigation.

The thin films for the two polyurethane elastomers were made by solution casting. The ESTANE® material was cast from a THF-solution onto a Teflon® surface. The excess solvent was later removed by vacuum. The PUUE elastomer was dissolved in DMF and then cast onto a Teflon® surface. This solution was allowed to stand overnight in a hood and then the excess solvent

was removed by vacuum at 50°C. The concentration of both solutions was approximately 0.015g/cc and the resulting film thickness was in the range of 0.5 to 1.0 mils.

Collection of IR-spectra

A Nicolet 5DXB FTIR Spectrometer with $4cm^{-1}$ resolution was used. A background spectrum was first taken with the FTIR chamber empty. After placing the stretching device(no sample) and the polarizer into the FTIR chamber, two reference spectra were taken. The reference spectra were taken with the polarizer at 0° (parallel to stretch direction) and after rotating it 90° (perpendicular to stretch direction). After placing the sample in the stretching apparatus, the sample spectra were then collected for 25 scans at the two polarization positions from which the dichroic ratio data were calculated.

Deformation-IR Dichroism Experiments

Three different types of deformation experiments were performed by utilizing the above Rheo-optical stretching apparatus. They were stress-strain, cyclic deformation, and stress relaxation. All three of these experiments were controlled by separate Basic computer programs with operator input. An example of one of the programs is given in Appendix B for a stress-strain experiment. A brief description is given below for each experiment describing the dichroic measurements as well as the mechanical aspects of each experiment.

The stress-strain experiment for IR-dichroism was utilized to evaluate the orientation-elongation behavior. It involved stretching a sample at increments of 10, 20, or 25% elongation depending on the type of sample. Extension rates of 6.706%/sec (400%/min) and 10%/sec (601%/min) were used and this includes the movement of both motors. At the end of each increment the dichroic measurements were obtained after "stress equilibration" was reached. This usually took 1 to 5 minutes depending on the sample and the strain level. The dichroic measurement involved taking

two IR spectra at 25 scans each with the polarizer parallel and perpendicular to the stretch direction as described above. This procedure of increasing the strain by stepping at a given increment and then making the necessary dichroic measurements was continued until the sample broke. During the experiment the mechanical behavior was also monitored at each increment of strain. Thus, at the end of the test the "stress-strain" behavior was obtained for the entire elongation period. All of the compression molded plaques mentioned above were used in this experiment.

The cyclic deformation test was used to describe the orientational hysteresis behavior. This experiment also involved stretching a sample at a given increment of strain and then making the necessary dichroic measurements as discussed above. First, the sample was stretched to a fixed initial elongation. After reaching this initial elongation, the sample was returned in an increment manner to one increment before 0 percent elongation and then re-stretched until the sample broke. During this experiment the stress strain behavior was followed in the two loading cycles and the one unloading cycle; thus giving the mechanical hysteresis behavior. Only plaque 2 and the PUUE elastomer were tested by this experiment. The other plaques were not tested due to difficulties in making more thin films (plaque 1) and no interest existed in obtaining such behavior for plaques 1-lc0 and 3-lc.

The stress relaxation experiment was used to provide an indirect indication of the orientation behavior with time. This test involved stepping to a given strain and then making the dichroic measurements with time. Only 10 scans for each polarization direction were used in order to obtain as many dichroism values as possible. Using this method it took 30 to 35 seconds to obtain one data point. For consistency, the spectrum with the polarizer in the parallel position was collected first and followed by the perpendicular measurement. The mechanical response was also followed simultaneously with time. Plaques 1 and 2 as well as the PUUE elastomer were evaluated using this method. Plaque 3-lc has been tested using this method, but there were some problems with the absorbances being too high for the samples tested. With this in mind, plaque 1-lc0 was not tested.

CHAPTER V

5.0 Results and Discussion

5.1 Stress Relaxation

The stress relaxation in flexible foams is an important property due to its relation to the recoverability in the foam's shape and strength. As discussed earlier, one variable that influences the relaxation behavior of foams is the hard segment content. The hard segment content in foams 1-4 and their respective plaques was varied by changing the amount of water and the diisocyanate appropriately, while keeping the other component additions constant. The weight and volume percent hard segment contents for these foams are shown in Table 5.1.

5.1.1 Foams

The stress relaxation behavior in tension is shown in Figures 5.1 and 5.2 for foams 1-4 stretched parallel($\sigma_{\parallel}$) and perpendicular($\sigma_{\perp}$) to the blow direction, respectively. In accounting for the differ-

ences in density of foams 1-4, the stress values were multiplied by density factors. The density factors were obtained by dividing the densities of foams 1-4 by the density of foam 1 and these factors are shown in Table 5.1 along with the densities of the foams. The stress relaxation behavior appears to be similar under either the parallel or perpendicular conditions with the only noticeable difference being in the level of stress (see Figures 5.1 and 5.2). The stress level is higher when stretching parallel to the blow direction due to the anisotropic cell structure. As shown earlier in Figure 2.7, the cells are ellipsoidally shaped. Thus, when deforming the foam parallel to the blow direction, the cells are elongated along the major axis which is the structurally stronger direction. In Figures 5.1 and 5.2, the stress decay occurs for the most part over a short a time period (10-20 minutes) and then approaches an asymptotic or "equilibrium" stress which indicates a stable crosslinked system (see Figures 5.1 and 5.2). Furthermore, the degree of stress relaxation appears greater for the foams with higher hard segment. For example, under the parallel or perpendicular conditions for the three hour testing period, foam 1 has approximately an 18 percent loss in stress, while foam 4 has about a 30 percent loss.

The stress relaxation shows a near linear relationship between the log of stress and the log of time in Figure 5.3 for foams 1-4 evaluated under parallel conditions. Similar behavior was also obtained for foams 1-4 stretched perpendicular to the blow direction, but is not presented. As discussed earlier, a linear relationship was also observed for stress relaxation in compression for flexible foams (44-45) as well as for a 2,4 TDI based polyurea-urethane elastomer (22). The slopes which give an indication of the rate of stress decay, σ_d, are given for both parallel and perpendicular conditions for foams 1-4 in Table 5.2. As shown in Figure 5.4 these σ_d values increase systematically with hard segment content. Furthermore, the rate of stress decay does not depend significantly on whether the experiment is carried out parallel or perpendicular to the blow direction (see Figure 5.4). Thus, it appears the stress relaxation behavior is independent of the anisotropic nature of the cells for flexible water-blown foams. The stress relaxation is therefore governed by the molecular structure which comprises the cell-wall struts and windows, and may be attributed to several factors. Generally, one important factor is the relaxation of the soft segments which begins upon stretching and

continues after reaching a constant level of strain. However, the relaxation of the soft segments does not appear to account for the differences between the observed stress relaxation of these foams. This belief is based on the stress relaxation increasing with hard segment content or decreasing with soft segment content which suggests that the difference in the stress relaxation behavior of foams 1-4 is related to other factors.

Three possible factors that could contribute to the differences between the stress relaxation of foams 1-4 are the differences in a) the local strains on the soft segments, b) disruption of hydrogen bonds and c) chain slippage. All three factors are, of course, related to some extent. A localized strain on the soft segment end near the interface of the hard segment is proposed, since the soft segments always relax quickly in comparison to the hard segments. This strain is also thought to increase with increasing hard segment content and is shown schematically in Figure 5.5. This proposed type of local strain on the soft segments is likely to exert a force on the hard segments which could eventually lead to the disruption of the hard domains as well as the polyurea aggregates (see Figure 2.10 for morphological structures). This disruption can be related to the dissociation of hydrogen bonds between the hard segments of the hard domains as well as the aggregates, but they are thought to reform quickly. The reformation of hydrogen bonds has been suggested by Cooper et. al. for polyurethane elastomers. They reported observing with infrared spectroscopy very small changes in the hydrogen bonded $C=O$ absorbance level as a function of strain. The disruption of hydrogen bonds could also facilitate local chain slippage. Since there is an increase in the hydrogen bonding content with increasing hard segment content for foams 1- 4, there should also be a possibility for an increase in the local strain on the soft segments, an increase in the disruption of hydrogen bonds, and an increase in the local chain slippage.

There are less important factors that could affect the stress relaxation in foams 1-4. It is also possible that the local strain on the soft segments can promote the breakage of chemical linkages such as urethane and biurets which are known to be weaker. Also, hydrogen bonds exist to a smaller extent between the ether linkages of the soft segments and the urethane N-H groups. These hydrogen bonds are most likely disrupted upon stretching the sample.

In summary, the results strongly suggest that the disruption of hydrogen bonds and the local chain slippage due to the local strain on the soft segments contribute the most to the differences in stress relaxation in foams 1-4. Similar trends have also been observed by other investigators who have studied the influence of hard segment content on the viscoelastic properties in flexible foams. The differences in the viscoelastic properties have also been generally attributed to hydrogen bonding effects. Examples of this behavior were given earlier in the literature review.

5.1.2 Compression Molded Plaques

In further evaluating the stress relaxation dependence on the solid portion of the foam, the stress relaxation behavior of plaques 1-4 was obtained. This behavior is shown in Figure 5.6 for plaques 1-4 for a 25 percent constant level of strain. The stress relaxation behavior of plaques 1-4 follows the same trends as that of foams 1-4 (see Figure 5.1 and 5.6).

The near linear relationship between the log stress-log time also exists for the plaques and there is also a systematic increase in the rate of stress decay, σ_d, with hard segment content (see Table 5.3). In comparison to their respective foams, the σ_d values are about 20-25 percent higher for plaques 1-3 and 40 percent higher for plaque 4. The foams and their corresponding plaques were stretched to different strain levels which resulted in their different stress decay rates. Recall that the different strain levels were used due to the sensitivity of the load cell and furthermore to obtain the stress relaxation behavior for all of foams 1-4 or plaques 1-4 at the same strain level.

In confirming the above difference in the stress decay rates between the foams and their plaques, foams 2 and 4 were tested parallel to the blow direction at 25 percent strain instead of the usual 40 percent. The rate of stress decay results which are given in Table 5.2 indicate that foam 2 and plaque 2 exhibit similar stress relaxation behavior at the same strain level. In contrast, the stress decay rate of plaque 4 was about 20 percent higher than that of foam 4. This suggests that there is

possibly some structural difference between foam 4 and its plaque due to the compression molding process.

The difference between the stress relaxation behavior of the foams and their respective plaques are not significant, except for the small difference in the stress decay rates of foam 4 and its plaque. Thus, it can be concluded that the plaques are a fairly good representation of the stress relaxation behavior of the foams. This is consistent with the earlier morphological investigations by Armistead et. al.(19) which reveal only a few differences between the plaques and the foams. This conclusion also supports the earlier observation that the material which comprises the cell-wall struts and windows is governing the stress relaxation behavior of the flexible foams. Therefore, it is thought that the stress relaxation in the plaques is caused by similar factors to those mentioned above for the foams.

A further understanding of the greater stress relaxation with increasing hard segment (HS) content in the plaques as well as the foams, can also be obtained by recalling the mechanical hysteresis and permanent set results that have been reported by Armistead (18). He showed for plaques 1-4 that the permanent set and the mechanical hysteresis increased with HS content. Furthermore, the permanent set values, and in some cases, the mechanical hysteresis increased with initial cycle elongation. These results suggest that with higher HS content, more chain slippage is taking place between the hard segments of the domains and aggregates which allows for stress relaxation to occur. The permanent set values also suggest that the hard segments are not relaxing back to their original state and thus the local strain on the soft segment could be increased. This last effect would of course be greater at higher elongations and higher HS contents (18).

5.1.3 Temperature Effects

The effects of temperature on the stress relaxation for foams 1-4 deformed parallel to the blow direction and their respective plaques have also been investigated. The stress relaxation behavior at 75°C as well as at ambient conditions is shown in Figures 5.7 and 5.8 for foam 4 and its plaque, respectively (behavior at 125°C discussed later). The other foams and their plaques also exhibited similar stress relaxation behavior at the two different conditions in comparison to the behavior shown in Figures 5.7 and 5.8, but are not presented. The values for the stress decay rates at 75°C of the foams and the plaques also show the same systematic increase with hard segment content as shown earlier at ambient conditions (see Tables 5.2 and 5.3).

Several comments can be made about the behavior at 75°C in comparison to ambient conditions presented in Figures 5.7 and 5.8. First, the initial stress levels are lower at 75°C which indicates more stress relaxation is taking place during sample stretching at this temperature. Second, less stress relaxation is observed at 75°C. These two observations suggest stress relaxation at 75°C is approaching equilibrium conditions faster.

At longer relaxation times approaching "equilibrium" conditions, the stress level is higher at 75°C in comparison to ambient conditions (see Figures 5.7 and 5.8). This is consistent with rubber elasticity theory which predicts a 15 percent increase in the level of stress with temperature at equilibrium conditions. A 7.5 and 10 percent increase in stress were observed at the longer relaxation times in Figures 5.7 and 5.8, respectively, which is slightly lower than the predictions given by theory. This same behavior was also observed by foams 1-3 and their respective plaques. One possibility for the small deviation from predictions given by rubber elasticity theory is that a perfect network does not exist and thus the existing entanglements are not thoght to be at equilibrium conditions. The small deviation from predictions also suggests that there is a possible increase in the disruption of hydrogen bonds at 75°C.

In support of this hypothesis, an increase in the disruption of hydrogen bonds with temperature has been detected by several investigators by infrared spectroscopy for polyurethane elastomers (64,74-76). Several of these investigators have suggested that at temperatures beginning with 20°C and up to 150°C the dissociation of hydrogen bonds occurs between the soft segment ether group and the N-H group of the hard segment as well as to a smaller extent between the hard segments (64,74-76). However, these investigators have also reported observing at higher temperatures a transition in this behavior such that the dissociation of the hydrogen bonding between the hard segments was thought to dominate (64,74-75). The temperature of this transition generally ranged from 50°C to 150°C depending on the segmental composition and the diisocyanate used (64,74-75).

The stress relaxation behavior was also evaluated at a higher temperature of 125°C as shown in Figures 5.7 and 5.8 for foam 4 and plaque 4, respectively. The initial stress levels are the lowest at 125°C. This observation indicates more stress relaxation is taking place during sample stretching at 125°C. The level of stress is lower at 125°C than at 75°C for the longer relaxation times which suggests the "equilibrium" stress at 125°C clearly deviates from the predictions given by rubber elasticity theory (see Figures 5.8 and 5.9). This deviation from theory is most likely caused by a significant increase in the disruption of hydrogen bonds between the hard segments as discussed above for polyurethane elastomers. In addition, rubber elasticity theory does not account for secondary forces (e.g. hydrogen bonds) between the chains (73, 74)

In comparing the stress relaxation behavior at 125°C for foam 4 and plaque 4, it appears there is more stress decay occuring in foam 4 (see Figures 5.8 and 5.9). This difference in stress relaxation behavior could be attributed to several factors. One is the difference in the constant strain level which is higher in foam 4. Another is the compression molding process which could have altered the molecular structure in plaque 4 by causing more network points to be formed.

In summary, several general observations can be drawn from the stress relaxation results at the different temperatures for foams 1-4 and their plaques. First, stress relaxation increases with hard segment content at temperatures up to 75°C. Secondly, the disruption of hydrogen bonds appears

to increase significantly from 75°C to 125°C. This suggests a possible transition in hydrogen bonding-temperature behavior and this significant increase is thought to occur mainly between the hard segments of the hard domains and the polyurea aggregates as has been indicated by infrared-thermal studies of polyurethane elastomers. Thirdly, the factors that bring about stress relaxation in the foams and the plaques also appear to be about the same up to temperatures of 75°C. Finally, the stress relaxation is taking place at a faster rate for the foams and plaques at 75°C in comparison to ambient conditions. However, at 125°C it is difficult to say whether the last comment holds due to only evaluating the stress relaxation behavior for foam 4 and plaque 4. Thus, before drawing any conclusions to this effect, the stress relaxations for all the foams and plaques must be obtained at 125°C and preferably at the same strain level.

5.2 Characterization of Samples used in the IR-Dichroism Study

Before discussing the results from the IR dichroism study, an overview of most of the samples investigated by this technique is necessary. Therefore, this section will concentrate on analyzing the effects of pretreatment method on the compression molded plaques, and providing some characterization of the polyurea-urea elastomer-PUUE, and plaques 1-lc0 and 3-lc.

5.2.1 Pretreatment Effects on Plaques

The effects of the pretreatment process on the resulting plaques were evaluated by utilizing stress relaxation, wide angle x-ray scattering (WAXS), and dynamic mechanical spectroscopy (DMS). The results from these techniques are given for plaque 2-DMF along with plaque 2 for comparison.

Recall that plaque 2-DMF was made by pretreating foam 2 with DMF before the compression molding process.

The results for the stress relaxation of plaque 2-DMF are shown with plaque 2 in Figure 5.9. One difference in the two plaques is that the initial stress level for plaque 2 is higher than that of the plaque 2-DMF. However, the stress relaxation behavior does appear to have the same general trend as shown in Figure 5.9. This observation is further supported by the similar values for the stress decay rates for plaque 2-DMF and plaque 2 (see Table 5.3).

In Figure 5.10, the storage modulus - temperature behavior is shown for plaques 2 and 2-DMF for which there appears to be some differences. The most significant difference is the modulus for plaque 2-DMF in the rubbery plateau region is approximately a factor of 2 lower than that of plaque 2. Furthermore, plaque 2-DMF softens at about 190°C which is 10°C lower than the softening temperature of plaque 2.

The WAXS patterns for plaques 2 and 2-DMF are shown in Figure 5.11. All of the plaques exhibit a diffuse halo and an apparent diffraction peak at 0.45 nm. Armistead et. al., as stated earlier, have attributed the amorphous halo to the randomness associated with the hard and soft segments (19). On the other hand, the apparent diffraction peak at 0.45 nm is an indication of increased order in the hard segments and is probably caused by paracrystalline ordering of the hard segments through hydrogen bonding (19). This diffraction peak as shown in Figure 5.11 appears to be slightly sharper for the untreated plaque 2 in comparison to its pretreated plaque 2-DMF. A similar result, but with a more distinct difference, was reported by Armistead et. al. for plaque 4 after swelling in DMF (19).

The above results for plaques 2 and 2-DMF suggests that some changes occured due to the pretreatment process. First, the WAXS results indicate that possibly some of the polyurea phase is extracted during the pretreatment of the foams and/or disruption of the hydrogen bonding has taken place. The IR results from the extraction studies of foams 1-4, reported by Armistead(discussed earlier), have also suggested that the polyurea phase was possibly extracted (18). The decrease in

storage modulus and the decrease in initial stress level are believed to be caused by the partial extraction of the polyurea precipitates (or at least free urea containing moieties). These results suggest the precipitates could be acting as filler particles to strengthen the plaque. Another possibility for the decrease in stress and modulus is the disruption of the hydrogen bonding in the hard domains and the aggregates. This disruption is possible, due to DMF interacting with the hard segments during the pretreatment process.

In summary, the pretreatment process does not appear to greatly alter the morphology or the physical properties of plaque 2-DMF. It also appears that the same conclusion would also hold true for the other pretreated plaques. This belief is based on the small changes observed for plaque 2-DMF in comparison to that of plaque 2 and the other results related to solvent treatment of the foams or plaques discussed earlier in the literature review. However, a more in depth study on all the pretreated plaques is necessary in order to obtain a clearer understanding of the effects of the pretreatment process. Such a study should not only consist of the techniques used on plaque 2-DMF, but other techniques (e.g. small angle x-ray scattering and transmission electron microscopy).

5.2.2 Polyurea-urethane Elastomer-PUUE

The polyurea-urethane elastomer, PUUE, was used in this investigation for the purpose of comparison to plaques 1-4. It was made from the same diisocyanate and a difunctional polyol which was made from the same cyclic oxide as that of the foams. The PUUE elastomer has a linear segmented morphology while the plaques contain a covalent segmented network. The PUUE elastomer also has approximately a 31 weight percent hard segment content which is comparable to that of foam 3 and its plaque. In characterizing the cast PUUE elastomer, WAXS and DMS were utilized. These results are given along with some comparisons to the plaques.

The storage modulus and the tan delta behavior are shown as a function of temperature in Figure 5.12 for the PUUE elastomer. The storage-modulus temperature behavior is similar to that of the plaques as expected. The tan delta curve in Figure 5.12 is somewhat broad at the soft segment glass transition region and suggests that there is possibly a higher level of phase mixing present in the PUUE elastomer. This however, was not observed for the plaques which have been reported as showing a much sharper tan delta peak and furthermore, a soft segment glass transition temperature about 15°C lower (20).

The WAXS pattern shown in Figure 5.13a for the PUUE elastomer is similar to that of the plaque 3 as shown in Figure 5.13b. The pattern for the PUUE elastomer has an amorphous halo and an apparent diffraction peak at 0.45 nm. The diffraction peak at 0.45 nm is not as distinct in comparison to that of plaque 3 (see Figure 5.13 a,b). Thus, there appears to be some hard segment order in the PUUE elastomer, but to a lesser extent than in plaque 3.

5.2.3 Plaques 1-lc0 and 3-lc

Plaques 1-lc0 and 3-lc were compression molded from their respective foams. Their foams differ slightly in that foam 3-lc has an extra proprietary component in its formulation. However, they have the same hard segment content which is the same as that of plaque 3 (see Table 5.1). In providing some characterization of plaques 1-lc0 and 3-lc, their WAXS patterns along with discussion of their transmission electron microscopy (TEM) results are given.

Wide-angle diffraction patterns are shown in Figure 5.14 for plaques 1-lc0 and 3-lc. These patterns exhibit similar characteristics to those of plaques 2 and 3 (see Figure 5.11 and 13). The apparent diffraction peak at 0.45 nm is slightly sharper in plaque 1-lc0 in comparison to that of plaque 3- lc. This dissimilarity could be due to the small difference in chemistries of foams 1-lc0 and 3-lc which in turn results in a better hard segment order in plaque 1-lc0. This difference in hard segment order

has been implied by the TEM results which reportedly showed plaque 1-lc0 as having large polyurea aggregations present, while no sign of any microphase separation down to the 10 nm level was observed for plaque 3-lc (73). As mentioned earlier, large aggregations were observed in the TEM micrographs for plaques 2-4 and these aggregates are believed to be formed from precipitated polyurea rich regions (19). Thus, the TEM results for plaque 1-lc0 and 3-lc suggest that plaque 1-lc0 is more likely to have a sharper diffraction pattern due to the presence of the polyurea aggregates. However, the above TEM and WAXS results do not confirm that the polyurea aggregates are absent in plaque 3-lc. As will be discussed later, it is possible that the aggregates in plaque 3-lc are smaller and more disperse.

5.3 IR-Dichroism with Mechanical Response

The results obtained from the IR-dichroism experiments are subdivided into two sections. The first section consists of evaluating the performance of the rheo-optical stretching apparatus with a polyether urethane (ET-2000-30) and comparing the results to those obtained with a chemically similar polyether urethane reported in the literature. In the second section, the IR-dichroism data for the compression molded plaques are given and discussed. Furthermore, comparisons to the PUUE elastomer are also made within the second section. Before presenting the results from these two sections, the means by which the IR and the mechanical data were analyzed will be explained.

5.3.1 Treatment of IR and Mechanical Data

Band Assignments

The objective behind using IR-dichroism is its ability to differentiate the orientation of the different segments in these polyurethane systems. In doing so, well-characterized absorption bands must be available to represent the chemically different segments. The band assignments for ET-2000-30 are similar to the assignments discussed earlier for the polyether urethane elastomers and are given in Table 3.1. For a review, the $N-H$ and the $(C=O)_b$ groups in the urethane linkage were utilized to characterize the hard segment orientation. The $(C=O)_f$ represents the interface of the hard and soft segments. The stretching vibrations for the carbonyl groups ($(C=O)_b$ and $(C=O)_f$) were used and both have a reported transition moment equal to 79°. The $N-H$ stretching vibration was used and has a reported transition moment of 90°. The soft segment orientation was characterized by the CH_2 group which has wagging(ω) and stretching(ν) vibrations with reported transition moments of 0° and 90°, respectively. Once again the different absorbing frequencies along with their respective transition moments are given in Table 3.1. An IR spectra of ET-2000-30 is shown in Figure 5.15 with the important absorption bands being designated.

For the compression molded plaques and the PUUE elastomer, the absorbing groups used were similar to the ones mentioned earlier for the urea-urethane elastomers. The $\nu(N-H)$ and in some cases the $\nu(C=O)_{ur}$ were used to characterize the hard segment orientation. The $\nu(C=O)_f$ was used to represent the orientation at the interface while the $\omega(CH_2)$ and the bending(δ) CH_2 were used to represent the soft segment orientation for the plaques. The $\nu(CH_2)$ and the $\omega(CH_2)$ were utilized to characterize the soft segment orientation of the PUUE elastomer. The same transition moment angles were used as given above and a transition moment angle of 90° was employed for $\delta(CH_2)$ as reported by earlier workers (50). These absorbing groups along with their absorbing frequencies

and transition moments angles are summarized in Table 5.4. An IR spectra is shown in Figure 5.16 for the PUUE elastomer with the important absorption bands being specified.

IR Sample Spectra and Dichroic Measurements

After collecting a sample spectrum with the polarizer parallel or perpendicular to the stretch direction, the respective polarizer absorption was subtracted. This was necessary because the absorbance spectrum of the polarizer is different at 0°(∥) and 90°(⊥). The baseline in most cases was raised slightly due to scattering of radiation caused by the sample. Therefore, for each spectrum the baseline was leveled which involved lowering the baseline by a constant absorbance across the entire infrared spectrum. By lowering the baseline and depending on the absorbance level, a $\pm$ 5 to 10 percent change in the dichroic ratio was observed.

The peak heights were measured assuming a flat baseline across the entire spectrum and by using a peak picker routine from a Nicolet software package. In some instances, the IR spectra were also smoothed before obtaining the peak heights to improve the signal to noise ratio. The smoothing technique was used most often for the $N-H$ region (see Figures 5.15 and 5.16) and resulted in a $\pm$2 to 7 percent change in the dichroic ratio. The peak heights used to calculate the dichroic ratio (eq.[3.3]) for ET-2000-30 and the PUUE elastomer were normally in the range of 0.2 to 1.2 absorbance units or 60% to 8% transmission which is comparable to the suggested absorbance or transmission levels given in the literature for IR dichroism (48,50). However, the peak heights for the plaques, as will be discussed in more detail later, were generally higher. After calculating the dichroic ratio, the second moment orientation function was then calculated using eq. [3.7]. As stated earlier, these measurements were made as a function of time and elongation for the different polyurethanes.

Mechanical Evaluation

The evaluation of the mechanical data was done by the use of a Basic computer program (see Appendix B). The force readings were converted into stress by inputting the cross sectional area at the beginning of a given experiment. The strain exerted on a thin film was calculated by multiplying the velocity of the combined motors by the time of motor travel. This time was obtained from the internal clock of the computer and was also collected simultaneously with the force readings. The time lapsed during stress relaxation was also monitored by the internal clock of the computer. The stress-strain data and the stress relaxation data were stored in data files at the end of the experiment, where at a later time they were plotted.

5.3.2 Evaluation of Rheo-Optical Stretching Apparatus

The rheo-optical stretching apparatus was tested with a polyether urethane elastomer, ET-2000-30. The orientation-elongation behavior and the simultaneous mechanical response for the ET-2000-30 sample are shown in Figures 5.17 and 5.18. The results of the orientation-elongation behavior represent an average of 3 different samples. The error in the orientation function was about 5 to 10 percent for all of the absorbing groups and is represented by the error bars shown in Figure 5.17 for the $(C=O)_f$ group. Furthermore, as shown in Figure 5.17 at zero deformation, there are some small deviations from no orientation which is unexpected for an isotropic system. These deviations are within experimental error for all the representative absorbing groups, except for the $\omega(CH_2)$ group. The slightly larger deviation at zero deformation for the $\omega(CH_2)$ orientation function is believed to be due to assuming a flat baseline when measuring the peak heights for this particular part of the IR spectrum (see Figure 5.15).

The orientation-elongation behavior for all of the absorbing groups is very similar to the results discussed earlier and reported by Seymour et. al. (60-61). For comparison purposes, the results for

one of Seymour et. al.'s samples, ET-1000-31, are shown in Figure 5.19. As one may observe, the trends for the different absorbing groups in Figures 5.17 and 5.19 are the same. The hard segment orientation is higher than the orientation at the interface of the hard and soft segments as well as the soft segment. This difference in orientation behavior is caused by the soft segments relaxing quickly and the hard segments retaining their orientation upon deformation. The orientation function for the $(C=O)_f$ group is greater than that of the CH_2 group because the $(C=O)_f$ groups are influenced by both the hard and the soft segments.

The $(C=O)_b$ and the $N-H$ groups did exhibit some negative orientation at lower elongations for the ET-2000-30 sample as shown by the orientation function for the $(C=O)_b$ group in Figure 5.19. Small amounts of negative orientation have also been reported by Seymour et. al. (57) as well as by Bonart and Hoffman for polyether urethane elastomers (58). The negative orientation has been attributed often to the presence of lamellae structured hard domains which could have been the reason for the negative orientation observed in the hard segments of the ET-2000-30 sample.

The simultaneous mechanical response during one of the orientation elongation test for ET-2000-30 is shown in Figure 5.18. The "equilibrium" stress-strain represents the stress level when the dichroic measurements were made. Note also in Figure 5.18, that the relaxation of the initial stress value increases with strain as expected.

In evaluating the performance of the stretching device to obtain a mechanical response, the stress-strain behavior was monitored by the stretching device and then compared to that obtained by an Instron tensile tester. For this experiment, only one motor of the stretching device was moved instead of moving both simultaneously. The stress-strain tests were done on the same shape dog-bone specimen and at an extension rate of 480 percent per second. Similar stress-strain behavior was obtained by the two instruments as shown in Figure 5.20. There are some small differences in the initial modulus behavior and the stress levels. However, for the most part the stress strain behavior obtained from the stretching device compares well with that of the Instron tensile tester.

In summary, the orientation-elongation behavior obtained with the assistance of the rheo-optical stretching device is similar to the results reported in the literature. Furthermore, the stretching device appears to work well mechanically.

5.3.3 IR-Dichroism Studies of Compression Molded Plaques and the PUUE Elastomer

The orientation behavior as a function of elongation, time following stretching, and cyclic deformation are discussed in this section for the plaques and the PUUE elastomer for comparison purposes. The orientation data as well as the mechanical data are represented by single experimental measurement and not an average over many experimental measurements. However, the experiments have been repeated for all samples and the same general behavior has been reproduced.

It was difficult to obtain very thin (1-1.5 mils) films by pressing the foams. The foams are of course crosslinked systems and could not be solvent cast as in the case of the PUUE elastomer which is comprised of linear chains. As mentioned earlier, the thinnest films (1-2 mils) were usually obtained by using the pretreatment method before pressing the foams. Furthermore, as indicated earlier, by using this method to prepare the thin films or plaques, the properties as well as the morphology of the plaques were not thought to be greatly changed.

In most cases after using the pretreatment method, the thin films that were obtained resulted in absorbance levels that were low enough to make the necessary dichroic calculations. When calculating the dichroic ratio for the plaques, peak heights with absorbances of 2 (1% transmission) and lower were normally used. This is higher than the suggested absorbance levels in the literature (48,50), but it did not appear to affect the reproducibility of the orientation behavior. In a few instances, absorbance levels greater than 2 were used and these instances are mentioned in the discussion of the results.

The greatest difficulties with the absorption measurements arose at the lower elongations for many of the absorbing groups (e.g. $\nu(C=O)_{ur}$, $\nu(N-H)$, $\omega(CH_2)$). However, at the higher elongations the plaques become thinner and did not generally create a problem with the absorption measurements. Very few difficulties were experienced in obtaining the orientation results for the PUUE elastomer. In the following section, the orientation behavior upon deformation by utilizing linear dichroism theory is given along with the simultaneous mechanical response for plaques 1, 2, 1-lc, and 3-lc as well as the PUUE elastomer.

Orientation-Elongation Behavior

Plaque 2 and PUUE Elastomer

The orientation-elongation behavior for plaques 2-DMF and 2-THF are shown in Figures 5.21 and 5.22, respectively. As expected, the general orientation behavior of the absorbing groups is similar for plaques 2-DMF and 2-THF (see Table 5.4 for details). The orientation level of the soft segments as well as at the interface of the hard and soft segments is small as shown in Figures 5.21 and 5.22 (more explanation is given later). The hard segments, however, exhibit significant amounts of negative or transverse orientation represented by the $(C=O)_{ur}$ and the $N-H$ absorbing groups. The orientation function for the $(C=O)_{ur}$ groups is given as a relative value due to the error caused by the high absorbance of polarized radiation parallel to the stretch direction ($A_{\|}$). This behavior is reproducible, but the magnitude of the orientation function is questionable as shown by the difference in the orientation function of the $(C=O)_{ur}$ groups for plaques 2-DMF and 2-THF. However, one would expect the orientation function of the $\nu(C=O)_{ur}$ to be less than that of the $\nu(N-H)$ due to the presence of $N-H$ groups in both the urethane and urea linkages. The urethane groups which are at the interface of the hard and soft segments exhibit positive orientation. This behavior suggests that the orientation level of the $N-H$ groups should be more positive than that of the $(C=O)_{ur}$ groups. Thus, the orientation elongation behavior of the $(C=O)_{ur}$ groups

shown in Figure 5.21 appears more characteristic of the expected hard segment orientation behavior.

The hard segment orientation behavior for plaque 2-DMF (see Figure 5.21) is further supported by the hard segment orientation behavior shown in Figure 5.23 at elongations less than 100% for the PUUE elastomer. This is consistent with the results from the DMS and WAXS studies which are comparable for the two different polyurea-urethanes.

The results given in Figure 5.21 and 5.23 also compare well with the orientation-elongation behavior reported for urethane and urea-urethane elastomers that contain lamellar structured hard domains (33,66-70). These lamellar hard domains have been reported as normally having paracrystalline or crystalline order, but they also can be amorphous (58,69-70). As indicated earlier, the WAXS patterns suggests that there is probably some paracrystalline order present in the hard segments that is induced by hydrogen bonding for plaque 2-DMF as well as for the PUUE elastomer. Thus, it is speculated for plaque 2 that the postulated large polyurea aggregates that are shown in Figure 2.10 are not spherically shaped, but possess a lamellar or rodlike texture somewhat as schematically portrayed in Figure 3.5. Further explanation of the PUUE elastomer is given later.

The lamellar texture is further suspected for the polyurea aggregates in plaque 2 since investigators have predicted the formation of the polyurea aggregates in the later stages of the foaming reaction where the gelling reaction becomes more effective (6,8,12). This timing of events in the foaming reaction suggests that the gelling reaction (i.e., urethane formation) would tend to limit the chain extension for the polyurea chains that precipitate. It would also suggest that the formation of lamellar textured polyurea aggregates consists of short hard segments. Furthermore, the shorter hard segments are more likely to form longer hard domains due to less hindrance created by the irregular structure of 2,4 TDI.

By assuming that the polyurea aggregates in plaque 2 possess structures similar to the lamellar hard domains shown in Figure 3.5, the negative hard segment orientation (see Figures 5.21 and 5.22) can

be explained in a similar fashion to that of the urethane and urea-urethane elastomers. That is, the polyurea rich lamellae orient as a whole with their long axis preferably in the stretch direction. The smaller domains or microdomains pictured in Figure 2.10 and Figure 3.5 are more likely to align in the stretch direction. However, the larger lamellae-like aggregates appear to be dominating the orientation behavior of the hard segments. As discussed earlier, Bonart and Hoffman have suggested a similar explanation for the orientation-elongation behavior of a polyurethane elastomer (58).

The lamellar hard segment domains are also suspected to be present in the PUUE elastomer due to the two-step reaction method used to make this elastomer. The formation of these lamellar hard domains also appears to be driven by the symmetrical structure of its chain extender, MOCA. The structure of MOCA (see Figure 2.6) is similar to that of MDI(see Figure 2.3) which is also thought to promote the formation of crystalline or paracrystalline domains. Furthermore, Khranovskii and Gul'ko have reported observing similar orientation behavior to that shown in Figure 5.23 for a urea-urethane elastomer that possesses hard segments made from 2,4 TDI and a chain extender with the same structure as that of MOCA. However, as mentioned earlier, these authors did not attribute the negative orientation to the presence of lamellar structured domains in their samples, but to conformation transitions in the hard segments based on the results from their deformation-WAXS studies. This explanation, although possible, does not seem realistic. Thus, the orientation behavior exhibited in Figure 5.23 for the $N-H$ and $(C=O)_{ur}$ groups of the PUUE elastomer, is attributed here to the hard segments possessing lamellar domains and is explained more fully in the following paragraph.

The transverse orientation shown in Figure 5.23 also appears to be due to the lamellar hard domains orienting as a whole with their long axis aligned in the stretch direction (remember the long axis is perpendicular to the hard segment axis). At or near elongations of 100%, a positive upturn in the hard segment orientation level is observed (see Figure 5.23). This change in orientation behavior suggests that some of the lamellar hard domains are disrupted and possibly form smaller hard domains. These smaller domains are more likely to align with the hard segment axis in the stretch direction; this event would give rise to positive orientation behavior. Other investigators of

MDI-based polyurea-urethane elastomers have also suggested that the positive upturn in the hard segment orientation level is due to some disruption in the lamellar hard domains (33,66-70). As discussed earlier, the actual mechanism by which the lamellar hard domains are disrupted and the hard segments of these domains align more in the stretch direction is not fully understood.

In Figure 5.23, the orientation function of the $\nu(C=O)_{ur}$ for the PUUE elastomer is below the lower limit of -0.5 defined by linear dichroism theory for uniaxial orientation. As mentioned earlier in the linear dichroism section, Bonart and Hoffman also observed negative orientation values below -0.5 for a MDI-ED-PTMO urea-urethane elastomer (66-67). The authors in this case implied that biaxial orientation existed in the hard segments of their polymer upon deformation. It is also thought that upon deforming the PUUE elastomer the hard segments are oriented biaxially. The derivation for the dichroic ratio using linear dichroism theory is based on a random distribution of the chains about the stretch direction and the transition moments for $(C=O)_{ur}$ groups about the chains (see Figure 3.2b). By considering a case of non-random distribution for either situation and re-inspecting the derivation of the dichroic ratio, the experimental values obtained for the dichroic ratio giving orientation function values less -0.5 can be estimated (see Appendix D). This method by which the experimental dichroic ratios were obtained suggests one of two things. The hard segments are preferentially aligned at a angle to the film surface which also suggests the hard segments are biaxially oriented. Alternatively, the transition moments of $(C=O)_{ur}$ are at a angle or are non-randomly distributed about the chain axes. For more details of the above reasoning -see Appendix D. An example is shown in Appendix D, for both cases (hard segments or transition moments) for which the hard segments are assumed to be aligned transverse to the stretch direction. Two cases were considered: (1) The transition moments are symmetrical about the chain axis while the hard segments are not symmetrical about the stretch direction, and (2) The hard segments are symmetrical about the stretch direction and the transition moments are not symmetrical about the chain axis. In both cases, after re-inspecting the derivation for the dichroic ratio when the orientation function was less than -0.5, it was determined that either the chains or transition moments were oriented at a 50° angle about their respective axes. The case for which the hard segments align at

an angle of 50°, is possible since these hard segments are thought to be a part of lamellar domains. In other words, the lamellar domains as a whole could be aligning at an angle to the surface of the film as well as transverse to the stretch direction. The case for which the transition moments align at an angle of 50°, is also possible due to the rigidity of the hard segments. This rigidity as well as the hydrogen bonding between the hard segments could contribute to the transition moments of $(C=O)_{ur}$ groups being aligned at an angle about the chain axes or taking a non-random distribution such that the angle about the chain axes is heavily weighted towards 50°.

Until this point, very little has been mentioned about the soft segment orientation as well as the orientation at the interface for plaque 2 and the PUUE elastomer. Both of these orientation levels are small as shown in Figures 5.21 through 5.23 for both plaque 2(DMF and THF) and the PUUE elastomer. The soft segment orientation was difficult to follow for plaque 2 due to the high absorbances for the common absorbing groups that are normally reported for urethane and urea-urethane elastomers. Thus, the CH_2 bending(δ) vibration was utilized because of its lower absorbances. The orientation level obtained by using the $\delta(CH_2)$ group is inconsistent for plaques 2-DMF and 2-THF, but the magnitude of the two does suggest very little soft segment orientation. Furthermore, at the higher elongations, the magnitude of the orientation values obtained by the $\omega(CH_2)$ group are comparable to that of $\delta(CH_2)$ group. This small amount of orientation exhibited by the orientation function of the CH_2 groups is consistent with the nature of the soft segments to relax quickly. It also suggests that the soft segments return to their random orientation upon deformation. This random orientation is possible since the soft segments make up the matrix of the network polymer system.

The soft segment orientation of the PUUE elastomer (see Figure 5.23) is positive for the most part and slightly higher than that of plaque 2 (see Figure 5.21). This difference in the orientation level upon deformation is thought to be attributed to the different functionalities of the polyols for the two polyurea-urethanes. The PUUE elastomer is made from a difunctional polyol and therefore comprised of linear chains which enables the soft segments to align more in the stretch direction. In contrast, plaque 2 is made from a trifunctional polyol which promotes a network structure. As

suggested above, the network structure results in the soft segments being more randomly oriented. Finally, the soft segment orientation level as a function of elongation in the PUUE elastomer is comparable to the soft segment orientation level reported in the literature for similar composition urea-urethane elastomers (33,69).

The orientation level at the interface as a function of elongation is positive for both plaque 2 and the PUUE elastomer (see Figures 5.21-5.23). In addition, this orientation level is slightly higher than that of the soft segment orientation for the same strain level. This behavior is consistent with reports from the literature for both urethane and urea-urethane elastomers (33,69). The $(C=O)_f$ groups also appear to be influenced more by the soft segments and to a smaller extent by the hard segments in both of these urea-urethanes (see Figures 5.21 and 5.23).

The "stress-strain" behavior followed during the orientation measurements is shown in Figure 5.24 for plaque 2-DMF. The stress-strain behavior was obtained for 10 percent increments of strain and the stress was allowed to relax for approximately 1 to 2 minutes at the lower strain levels (10 to 40 percent) and approximately 3 minutes at the higher strain levels (greater than 40 percent) before making the dichroic measurements which generally took one and half minutes. The stress relaxation is almost negligible at the lower strains and is slightly greater at the higher strains (see Figure 5.24). The simultaneous "stress- strain" behavior was obtained for 20 percent increments of strain for the PUUE elastomer as shown in Figure 5.25. The stress relaxation is much greater for the elastomer in comparison to plaque 2. This observation possibly explains why there is only a small difference in the soft segment orientation levels for the two polyurea-urethanes.

Plaque 1

The orientation-elongation behavior is shown in Figure 5.26 for plaque 1-THF. The orientation function for the $(C=O)_{ur}$ groups is not shown in Figure 5.26 because the absorbances were too high thereby producing results with unrealistic behavior. The orientation-elongation behavior exhibited in Figure 5.26 is similar to that of the plaque 2 (see Figures 5.21-5.22). The soft segment

orientation is almost negligible as shown in Figure 5.26. The results for the soft segment orientation were obtained using the $\omega(CH_2)$ groups which consistently gave high absorptions for all elongations. The soft segment orientation behavior was confirmed by the orientation function for the $\delta(CH_2)$ groups obtained for other plaque 1 samples at higher elongations. The orientation behavior at the interface is positive and higher than the soft segment orientation as expected (see Figure 5.26).

As shown in Figure 5.26, the hard segments for plaque 1-THF exhibit negative orientation as in the case for plaques 2-DMF and 2-THF. However, in comparison to plaque 2 at higher elongations, the orientation function for the $N-H$ group on average (i.e., an average of all the plaque 1 and 2 samples tested) appears to be about 0.1 orientation units smaller in plaque 1. Thus, it is thought that the polyurea aggregates present in plaque 1 are dominating the transverse orientation as was described for plaque 2, but to a lesser extent. This observation is consistent with TEM results which show plaque 1 possessing smaller polyurea aggregates in comparison to plaque 2. Furthermore, this observation also suggests that the fraction of hard segments that makes up the polyurea aggregates is less in plaque 1 than in plaque 2.

Earlier it was indicated, by the results of various techniques, that the pretreatment method has little effect on the morphology of the plaques. These results are further supported by the similar orientation-elongation behavior shown in Figure 5.27 for plaque 1 (no solvent treatment) in comparison to that of plaque 1-THF (see Figure 5.26). The absorbances that were used to calculate the orientation function for the $N-H$ groups in Figure 5.27 were high except at 50% elongation. However, the general orientation behavior is consistent with plaque 1-THF and thus, suggests that the pretreatment method has little or no effect on the orientation behavior in the plaques.

Plaques 1-lc0 and 3-lc

As mentioned earlier, the TEM micrographs that have been observed for plaques 1-lc0 and 3-lc showed plaque 3-lc having no sign of polyurea aggregates on the 10 nm level. However, the TEM micrograph of plaque 1-lc0 does indicate that the large hard segment aggregates that were described

earlier for foams 2-4 are present on the 250 nm level. Thus, plaques 1-lc0 and 3-lc were also studied to hopefully obtain a clearer understanding of the role of the polyurea rich aggregates in the hard segment orientation behavior of plaques 1 and 2.

The results of the orientation-elongation behavior for plaques 1- lc0(DMF) and 3-lc are shown in Figures 5.28 and 5.29, respectively. Generally speaking, the orientation behavior of the two plaques does not appear to be that different. The orientation behavior at the interface is positive for both plaques and also comparable to the results shown above for plaques 1 and 2. The orientation function for the soft segment is less than that at the interface and is slightly negative at the higher elongations (see Figure 5.28 and 5.29). The negative orientation is questionable since the results of the $\nu(CH_2)$ groups (not presented) exhibited a small amount of positive orientation at higher elongations where the orientation function of the $\nu(CH_2)$ groups could be evaluated. This result suggests a possible problem in the baseline chosen to measure the peak heights for the $\omega(CH_2)$ group (see Figure 5.16). However, the magnitude of the orientation level for the soft segments, obtained by using both of the absorbing groups, is small and less than that of the $(C=O)_f$ groups (see Figures 5.28 and 5.29).

The orientation of the hard segments as shown in Figures 5.28 and 5.29 exhibits very unusual behavior. This same behavior has been reproduced for both plaques on several occasions. For these two samples, the orientation function is not shown at zero deformation and at 10% in the case of plaque 1-lc0(DMF) due to very high and unrealistic absorbance levels perpendicular to the stretch direction (see Figure 5.28 and 5.29). However, at zero deformation considerable positive orientation for the hard segments has been observed for thinner samples. In addition, positive orientation at zero deformation was observed at different positions along the thinner samples which suggests that there is not a concentration effect. In short, there is not a reasonable explanation for the positive orientation behavior at zero deformation. It can only be said that this unusual orientation behavior has not been observed to any great extent in the other thin films studied; therefore, experimental error does not appear to be a likely explanation.

A more important result is the transverse orientation behavior of the hard segments shown in Figures 5.28 and 5.29 for plaques 1-lc0(DMF) and 3-lc, respectively. This behavior is similar for the two plaques which was unexpected due to the different TEM results for these two plaques. One would expect to observe transverse orientation for plaque 1-lc0 due to the polyurea aggregates orienting transverse to the stretch direction as described earlier for plaques 1 and 2. On the other hand, the transverse orientation behavior was not expected in plaque 3-lc since the polyurea aggregates are not observed in its TEM micrograph. As suggested earlier the polyurea aggregates are not assumed to be displaced in plaque 3-lc because the technique of transmission electron spectroscopy did not detect any microphase separation down to the 10 nm level. Since foam 3-lc is a high water content foam (see Tables 4.2 and 5.1), the polyurea aggregates are thought to be present. It appears the proprietary component used in the formulation of foam 3-lc controls the size of the aggregates. Furthermore, this component could have possibly dispersed the aggregates in the network structure of the foam 3-lc. With the above in mind, it is suggested that the polyurea aggregates are still present in plaque 3-lc, but are smaller in size and more randomly dispersed in comparison to plaque 1-lc. The orientation results for the hard segments suggest the polyurea aggregates are present in the same quantity for the two plaques (see Figures 5.28 and 5.29). This belief extends from the results of the orientation level for the $N-H$ groups of several samples being comparable for plaques 1-lc0 and 3-lc at about the same strain level (see Figures 5.28 and 5.29). Thus, the transverse orientation observed for the hard segments in these plaques is speculated to be attributed to the polyurea aggregates as explained earlier for plaque 2.

The stress-strain behavior for plaques 1-lc0(DMF) and 3-lc are shown in Figure 5.30. The stress levels for the two are comparable with plaque 3-lc being slightly higher. The difference could be due to plaque 1-lc0(DMF) using the pretreatment method. The most noticeable difference between the two plaques is the greater stress relaxation observed after each increment of strain for plaque 3-lc (see Figure 5.30). This greater amount of stress relaxation is thought to possibly be related to plaque 3-lc possessing smaller and more disperse polyurea aggregates. However, the actual mech-

anism by which this occurs is not fully understood and thus should be subject to future investigation.

In summary, the orientation-elongation behavior for the plaques and the PUUE elastomer has provided some new insight into the morphological structure of the polyurea aggregates present in the plaques. This structure is also thought to hold true for their respective foams. Thus, a modification to the earlier proposed morphological model (Figure 2.10) for the foams and their plaques is shown in Figure 5.31. The model in Figure 5.31 suggests that the aggregates (specified polyurea) contain short polyurea chains which are stacked to form lamellar-like domains. In addition to the larger polyurea domains, the smaller hard segment domains are also believed to be present as was discussed earlier in the literature review (18-19). The orientation-elongation behavior of the PUUE elastomer also suggested that similar morphological textures i.e., lamellar hard domains are present. Thus, the plaques appear to contain some similar morphological characteristics to the urea-urethane elastomers as suggested by the similar orientation-elongation behavior exhibited by the plaques (1, 2 , 1-lc0, and 3-lc) and the PUUE elastomer.

Orientational Hysteresis Behavior

The orientational hysteresis behavior and the simultaneous mechanical response were evaluated for plaque 2-DMF and the PUUE elastomer. Such behavior was obtained by stretching a sample to a fixed initial strain, then returning it to one increment(10 percent) before zero percent strain and finally restretching the sample until break. The orientation and the simultaneous cyclic stress-strain behavior are shown in Figures 5.32 and 5.33, respectively for plaque 2-DMF. The orientation function for the $(C=O)_f$ groups shown in Figure 5.32 is reversible upon cyclic deformation. The soft segment orientation behavior was also reversible, but is not shown here. The hard segment orientation exhibits reversible behavior upon cyclic deformation, except for a small deviation at 10% strain upon unloading. This small deviation from reversible behavior in the hard segment orientation might be expected since the soft segments relax quickly and cause the hard segments

of the hard domains and the polyurea aggregates to align more in the stretch direction. This near reversible behavior of the hard segment orientation also suggests that the hard segments do not retain their initial orientation as their rigid nature might imply. This behavior is thought to be attributed to the elastic nature of the network which contain the hard segments. This orientation behavior for the hard and soft segments as well as at the interface of plaque 2-DMF, is reflected in the small amount of mechanical hysteresis shown in Figure 5.33.

The orientational hysteresis behavior for the PUUE elastomer is shown in Figure 5.34. The $(C=O)_f$ groups exhibit similar behavior to that of plaque 2-DMF as well as to reports in the literature for urea-urethane elastomers (66,69). The soft segment orientation was reversible, but the data is not shown here. However, the hard segment orientation behavior for the PUUE elastomer in comparison to plaque 2-DMF exhibits more irreversible behavior upon unloading (see Figures 5.32 and 5.33). As mentioned above, the hard domains and the polyurea aggregates in plaque 2-DMF are thought to exhibit reversible behavior due to the true covalent elastic network in the plaques. On the other hand, the hard domains in the PUUE elastomer are part of a linear segmented system which would suggest these hard domains are less likely to retain their initial orientation upon unloading. This difference in orientation behavior can also be attributed to the hard domains and polyurea aggregates of plaque 2-DMF retaining their structure upon deformation while apparently some of the lamellar hard domains in the PUUE elastomer are disrupted at the higher strains during loading. Therefore, it is thought that the disrupted hard domains of the PUUE elastomer do not reform immediately or at all during the unloading period due to the soft segments relaxing quickly. By relaxing fast, the soft segments exert a force on the hard segments; thus causing the hard domains to align more into the stretch direction. It also appears that only a small percentage of the hard domains in the PUUE elastomer was disrupted during the initial loading period. This belief is based on the orientation behavior for the second loading period practically retracing that of the unloading period (see Figure 5.33).

The mechanical response shown in Figure 5.35 was obtained during cyclic deformation of the PUUE elastomer. The orientation behavior of the $(C=O)_{ur}$ groups(see Figure 5.33) compares well

with this cyclic stress-strain behavior shown in Figure 5.35. Thus, the large amount of mechanical hysteresis appears to be related to the re-orientation of the hard segments during cyclic deformation.

Ishihara et. al. as well as Bonart and Hoffman have reported observing significant irreversible orientation behavior for polyurea-urethanes at ambient conditions (66-70). They also showed upon stretching to initial elongations of 200 percent and greater that the irreversible behavior becomes larger. Furthermore, for the same experiment they reported observing a decrease in the transverse orientation upon restretching the sample (66-70). Similar behavior is thought to have resulted during cyclic deformation of the PUUE elastomer by stretching to higher initial elongations (200 percent). It is also possible that greater irreversible orientation behavior for the hard segments of plaque 2 would have been obtained by stretching to higher initial elongations. It is even more likely that greater irreversible hard segment orientation behavior will be observed for the higher hard segment plaques due to the report of an increase in the mechanical hysteresis with hard segment content in plaques 1-4 (18). However, the above have not been evaluated for the PUUE elastomer and the plaques at higher elongations due to sample failure or difficulties in obtaining thin enough films (e.g. plaques 3 and 4). Thus, by overcoming these difficulties, the above studies are potential ways to obtain a more complete comprehension of the orientational hysteresis behavior for the plaques and hopefully an understanding of important properties in flexible foams such as compression set and fatigue.

Orientation Time Study

The viscoelastic nature of plaques 1 and 2 as well as the PUUE elastomer was evaluated after imposing a constant level of strain and then by periodically following the orientation of the different absorbing groups and the stress relaxation. The orientation change with time at a constant strain level of 30 percent for plaques 1-THF and 2-DMF is shown in Figures 5.36 and 5.37, respectively. Figures 5.36 and 5.37 reveal that the orientation relaxation for the hard segments and at the interface of the hard and soft segment groups is very small, if significant at all. Furthermore, it is as-

sumed the orientation relaxation of the soft segments is small with respect to the time frame of the experiment (recall-30 seconds to obtain one data point) and to be related to the small changes observed for the orientation function for the $(C=O)_f$ group. The small changes that are observed in the orientation functions for the $(C=O)_f$ and $N-H$ groups mainly result from small fluctuations in the peak heights for the absorbance spectra. These small fluctuations in the peak heights are thought to be the result of the absorbance levels being in the range of 1.5 to 2 for $\nu(N-H)$ and 1 to 1.5 for $\nu(C=O)_f$.

The stress relaxation for plaque 2-DMF which was followed simultaneously with the orientation behavior is shown in Figure 5.38. Most of the stress decay in plaque 2-DMF takes place in the first 10 to 20 minutes. However, this stress decay does not appear to be in agreement with the orientation-time behavior shown in Figure 5.37 as discussed in the previous paragraph. As discussed earlier, the stress relaxation in the plaques is thought to be attributed to several factors. Furthermore, these factors do suggest that some orientation changes could possibly be observed in the hard segments. Therefore, the possibility exists that either the average of the orientation of the hard segments is not changing or the hard segments do re-orient with time, but the changes are small and within experimental limitations($\pm$ 5-10 percent).

A similar study was also performed on the PUUE elastomer after imposing a 100 percent constant level of strain. The orientation relaxation and the simultaneous stress relaxation for the PUUE elastomer are shown in Figures 5.39 and 5.40, respectively. The CH_2 and the $(C=O)_f$ groups exhibit very little change in orientation with time, while the orientation functions for the $N-H$ and $(C=O)_{u_r}$ groups decrease gradually over time. The behavior of the different groups suggests several things about the viscoelastic nature of this material. First, the soft segments possibly relax in such a short time frame that the change in orientation was not detected during the experimental time frame. Secondly, the orientation time dependence of the $(C=O)_f$ group is similar to that of the soft segment orientation behavior which suggests the free carbonyl groups are influenced more by the soft segments possibly due to their($(C=O)_f$ groups) location at the interface. Thirdly, similar behavior to that of the hard segments in the PUUE elastomer has also been observed by Seymour

and Cooper for a polyether urethane (57). It appears the decrease in the orientation function with time is due to the hard segments relaxing much slower in comparison to the soft segments. This behavior, of course, is consistent with the rigid nature of the hard segments.

The stress relaxation shown in Figure 5.40 for the PUUE elastomer is greater than that of plaque 2-DMF(see Figure 5.38) as expected. One reason is there are no apparent orientation changes observed with time in the hard segments of plaque 2-DMF (see Figure 5.37). On the other hand, the hard segments of the PUUE elastomer possess a time dependent orientation level as shown in Figure 5.39. Furthermore, this difference in stress relaxation behavior is thought to be attributed to the linear chains in the PUUE elastomer permitting more chain slippage to take place in comparison to the covalent network in plaque 2-DMF.

5.4 Summary

A set of flexible polyurethane foams and their respective plaques as well as a chemically similar polyurea-urethane elastomer, PUUE, were studied to better understand the molecular orientation and relaxation behavior in these systems. Foams 1-4 and their corresponding plaques varied in hard segment content from 21.1 to 33.8 percent by weight with foam 1 having the lowest hard segment content and foam 4 the highest. Foams 1-lc and 3-lc were of the same hard segment content (30 percent by weight), but foam 3-lc has an extra proprietary component in its formulation. Compression molded plaques were also made from all of the above foams by applying pressure for 10 minutes at 204°C. In order to make very thin plaques, the foams in some cases were pretreated with DMF or THF before compression molding. The PUUE elastomer had a 30 percent by weight hard segment content. A polyether urethane elastomer, ET-2000-30, was also used for purposes of testing the capabilities of the recently built rheo-optical stretching apparatus due to this system being highly studied in the literature (56,57).

Stress relaxation in tension was carried out on foams 1-4 stretched parallel and perpendicular to the blow direction as well as their corresponding compression molded plaques. The stress relaxation increased with hard segment content for the foams (parallel and perpendicular conditions) as well as the plaques. This behavior was supported by the systematic increase in stress decay rates with hard segment content. The stress decay rate, σ_d, was obtained from the slope of the linear relationship between log time and log stress. The similar σ_d values for foams 1-4 at the parallel and perpendicular conditions revealed that the stress relaxation behavior was independent of the anisotropic cell geometry and therefore dependent on the solid material that makes up the cell-wall struts and windows. Furthermore, the stress decay rates of the plaques were similar to that of their respective foam which also suggested the stress relaxation of the foams was governed by the material comprising the cell-wall struts and windows.

The stress relaxation in foams 1-4 and their corresponding plaques were thought to be attributed to several factors. The most important factors were the relaxation of the soft segments, the local strain on the soft segments, disruption of the hydrogen bonds, and local chain slippage. The difference in the stress decay appears to be related to the different levels of hydrogen bonding in foams 1-4.

At 75°C, the stress relaxation behavior evaluated when stretching foams 1-4 parallel to the blow direction and for their plaques exhibited slightly lower and similar initial stress levels in comparison to that at ambient conditions. The observed stress relaxation for the foams and plaques was less at 75°C in comparison to ambient conditions. These results suggested that by increasing the temperature (up to 75°C) the stress relaxation behavior reached the "equilibrium" stress level faster. The stress relaxation also increased with hard segment content for foams 1-4 and their plaques.

At the longer relaxation times approaching "equilibrium" conditions, the stress level at 75°C deviated about 8 percent from predictions given by rubber elasticity theory. A much larger deviation from predictions given by theory was observed at 125°C. These deviations from theory were thought to have been caused mainly by disruption in hydrogen bonding either between the ether

carbonyl of the soft segment and the $N-H$ group of the urethane linkage or between the hard segments of the hard domains and the polyurea aggregates.

The results from the stress relaxation, DMS, WAXS, and IR-dichroism studies on the plaques pressed after the pretreatment method of the foams indicated only small changes in their morphology and their properties compared to the plaques (no treatment process of the foams). The changes observed by some of these different techniques for plaque 2-DMF were lower initial stress level and lower storage modulus as well as less order in the hard segments. A possible reason is that some of the polyurea precipitates were extracted from the foams during swelling in the solvent. Furthermore, these small changes suggested the possibility that the hydrogen bonding was disrupted due to the interaction with DMF during swelling. The results from the IR-dichroism study exhibited similar orientation-elongation behavior in the hard segments as well as at the interface for plaque 1 and plaque 1- THF.

Dynamic mechanical spectroscopy and wide angle x-ray diffraction were utilized to characterize the PUUE elastomer as well as to aid in the comparison to the plaques. The DMS spectrum for the PUUE elastomer was similar to that of the plaques and revealed a phase separated system with a reasonably sharp soft segment glass transition region region as well as hard segment softening and degradation near temperatures of 180°C. Furthermore, the tan delta-temperature behavior suggested some phase mixing was present in the PUUE elastomer. The WAXS pattern for the PUUE elastomer showed an amorphous halo and an apparent diffraction peak at 0.45 nm. The diffraction peak for the PUUE elastomer was not as sharp as that of plaque 3 which contains a similar hard segment content by weight percent.

The WAXS diffraction patterns for plaques 1-lc and 3-lc also showed an apparent diffraction peak at 0.45 nm. This diffraction peak was sharper for plaque 1-lc which suggested better hard segment ordering as compared to plaque 3-lc. The TEM results reported for these two plaques indicated that the difference could be due to the observation of large polyurea aggregates in plaque 1-lc and no sign polyurea aggregates by TEM in plaque 3-lc down to the 10 nm level.

The orientation-elongation behavior for ET-2000-31 was comparable to that reported in the literature for a chemically similar polyether urethane (56,57). Furthermore, the error in the orientation function for the different representative chromophoric groups was about $\pm$5-10 percent for an average of three different samples. The stress-strain behavior that was obtained by the stretching apparatus for ET- 2000-30 was comparable to the behavior obtained by an Instron tensile tester. The above results suggested that the recently constructed rheo-optical stretching apparatus was capable of assisting in obtaining orientation behavior upon deformation as well as the mechanical response.

The orientation-elongation behavior for all the plaques (2-DMF, 2-THF, 1-THF, 1, 1-lc(DMF), and 3-lc) exhibited significant transverse orientation for the hard segments and a small amount of orientation for the soft segments as well as at the interface of the two domains. The orientation at the interface was positive upon deformation and appears to be affected mostly by the soft segments. The magnitude of the soft segment orientation was smaller than the orientation at the interface for the same level of strain. The small change in soft segment orientation function with strain suggested the soft segments maintained their random orientation due to their quick relaxation.

The hard segment orientation upon deformation was usually negative, except for plaques 1-lc and 3-lc at lower elongations. It was speculated that the negative orientation behavior exhibited by the hard segments was due to the polyurea aggregates possessing a lamellar-like structure and thus orienting as a whole with the long axis of the lamellae in the stretch direction. With this in mind, a modification (see Figure 5.30) was made to the proposed morphological model. The smaller hard segment domains as shown in Figure 5.30 were expected to orient in the stretch direction giving rise to positive orientation. However, the larger polyurea aggregates appeared to be dominating the orientation of the hard segments. A similar explanation was reported by Bonart and Hoffman in explaining the transverse orientation behavior of hard segments for a polyurethane elastomer (58).

The orientation function for the $N-H$ group appeared to exhibit more transverse behavior for the higher hard segment plaque 2 as compared to plaque 1. This difference was thought to be attributed to the larger polyurea aggregates present in plaque 2. Based on the orientation elongation behavior

of plaque 3-lc and the above speculation for transverse orientation behavior, it was suggested that the polyurea aggregates are present in plaque 3-lc, despite the TEM results suggesting otherwise.

The PUUE elastomer exhibited similar orientation-elongation behavior to that of the plaques (up to 100 percent elongation for hard segments) as well as to reports in the literature for most polyurea-urethane elastomers (33,56-72). The transverse orientation observed for the hard segments was attributed to the formation of large lamellae- like domains. Such domains were suspected due to the symmetrical structure of the MOCA chain extender and due to the two step reaction used in making the cast elastomer. At higher elongations some of the lamellar hard domains were thought to be disrupted thereby giving rise to a positive upturn in the hard segment orientation behavior. The negative orientation for the hard segments of the PUUE elastomer did go below the lower limit set by linear dichroism theory for uniaxial orientation; thus biaxial orientation of the hard segments was suggested and shown to be a likely possibility. In confirming this possibility, a recommendation for a possible study will be made later in this thesis.

The orientational hysteresis behavior for the soft segments and at the interface of the hard and soft segments for plaque 2-DMF and PUUE was reversible. The hard segment orientation upon cyclic deformation for plaque 2-DMF was practically reversible for an initial elongation of 50%, while that of PUUE exhibited irreversible behavior for a much higher initial elongation of 125%. The near reversible behavior for the hard segments of plaque 2-DMF was attributed to the elastic network as well as the stable (cohesive) hard domains and polyurea aggregates. This behavior was also reflected in the small amount of mechanical hysteresis. The irreversible orientation behavior for the hard segments in the PUUE elastomer was thought to be caused by some disruption in the hard domains and the relaxation of the soft segments exerting a tension on the hard segments. This irreversible orientation behavior was reflected in the large amount of mechanical hysteresis for the PUUE elastomer.

After imposing an increment of 30 percent strain on plaques 1-THF and 2-DMF the orientation level changed very little over time for the hard and soft segments as well as at the interface. The

simultaneous stress-relaxation for plaque 2-DMF did exhibit some stress decay over the first 20 minutes. Therefore, it was suggested either the average of the orientation of hard segments was not changing or the hard segments do re-orient, but the changes are small and within experimental limitations.

At a 100 percent increment of strain, the PUUE elastomer did exhibit orientation changes with time for the hard segments, but very little for the soft segments and at the interface. These changes in orientation were reflected in the simultaneous stress relaxation observed for the PUUE elastomer. These differences in viscoelastic behavior for plaque 2-DMF and the PUUE elastomer were thought to be related to the plaque possessing a covalent network structure, while the elastomer consists of a linear segmented morphology.

5.5 Conclusions and Recommendations

5.5.1 Conclusions

- Stress relaxation in foams 1-4 and their respective plaques increases with hard segment content. This trend is thought to be related to the increasing amounts of hydrogen bonding with higher hard segment content in these materials. The stress relaxation in the foams appears to depend very little on its anisotropic cell geometry and mainly on the material comprising the cell-wall struts and windows.

- By increasing the temperature(up to 75°C), the stress relaxation is accelerated in foams 1-4 and their respective plaques. This conclusion is supported by the smaller amount of stress relaxation observed at 75°C and the lower or equivalent initial stress levels at 75°C in comparison to that at ambient conditions. Between 75°C and 125°C, the difference in the deviations from predictions given by rubber elasticity theory at "equilibrium" conditions for the stress relaxation behavior of foam 4 and plaque 4 increases. This difference suggests an increase in the disruption of hydrogen bonds between the hard segments of the hard domains and the polyurea aggregates is taking place.

- The pretreatment process used to make thinner compression molded plaques does not appear to greatly effect the morphology and properties of the plaques. This conclusion is supported by the results from stress relaxation, DMS, WAXS, and IR-dichroism studies on some of the pretreated plaques and their respective plaques (no pre-treatment).

- The rheo-optical stretching apparatus which was constructed for the purpose of obtaining deformation-orientation behavior with a simultaneous mechanical response gives comparable results to that reported in the literature for chemically similar materials. Furthermore, the stretching apparatus obtains a comparable mechanical response to that of an Instron tensile tester.

- To the author's knowledge, the segmental orientation measurements made on the plaques are the first to be made on a polyurethane foam material.

- The orientation changes upon deformation in the soft segments are small for the compression molded plaques 1, 2, 1-lc, and 3-lc and slightly larger than the plaques for the PUUE elastomer. The orientation at the interface of the hard and soft segments is influenced more by the soft segments in the plaques and the PUUE elastomer. Furthermore, the orientation level at the interface is higher than the soft segment orientation level for the plaques and the PUUE elastomer. Significant transverse orientation upon deformation is observed in the hard segments

of the plaques and up to elongations of 100 percent for the PUUE elastomer. Based on this transverse orientation in the plaques, the polyurea aggregates in the foams and their plaques are thought to possess a lamellar-like structure. Other investigators of urethane and urea-urethane elastomers have attributed the transverse orientation behavior in the hard segments to lamellar hard domains being present in these elastomers (33,56-58,65-70). Thus, the orientation-elongation behavior of the plaques pressed from the polyurethane foams is apparently controlled by similar forces to those of the polyurethane elastomers; despite the plaques possessing a covalent network morphology and the elastomers a linear segmented system.

- The hard domains and the polyurea aggregates of plaque 2-DMF are part of an elastic network and appear to remain cohesive upon cyclic deformation to initial strain levels of 50 percent. This is supported by the orientation behavior upon cyclic deformation for plaque 2-DMF. Furthermore, the small mechanical hysteresis appears to correlate with the orientational hysteresis behavior of the different components for plaque 2-DMF.

- Some of the lamellar hard domains in the PUUE elastomer are thought to be disrupted at the higher strains which likely gives rise to the large mechanical hysteresis. This is supported by the orientational hysteresis behavior with its mechanical response as well as orientation-elongation behavior.

- The orientation changes with time are possibly not observed in the plaques 1 and 2 either due to the average in the orientation of the chains not changing or because the changes in the orientation of the chains are small and are within experimental limitations. The stress relaxation in the PUUE elastomer is thought to be related to the orientation changes observed in the hard segments. This difference in the observed orientation-time behavior for these two polyurea-urethanes is believed to be related to the covalent network structure of the plaques and the linear segmented system of the PUUE elastomer.

5.5.2 Recommendations

Future work should begin with continuing the present investigation of obtaining a better understanding of the relaxation and orientation-deformation behavior in the foams and their plaques. The present investigation has provided a base to build on and furthermore, given direction for the next steps to be taken in order to hopefully achieve the above objectives more completely. The recommendations for future work will now be given.

- The stress relaxation results at 75°C indicated the stress relaxation was accelerated or in other words occurred on a different time scale in comparison to ambient conditions. This observation suggests the possibility of applying time- temperature superposition to foams 1- 4 or their plaques since both exhibit similar stress relaxation behavior.

- An important factor that influences the viscoelastic properties of flexible foams is humidity. For example, Harrington and Klarfeld have shown an increase in humid aged compression set with hard segment content for a set of flexible molded foams (36). With this in mind, stress relaxation of foams 1-4 under humid conditions would be an ideal study.

- Some molecular origins of stress-relaxation have been considered for the foams and their respective plaques, but were not confirmed. One molecular origin was the disruption of hydrogen bonds which could possibly be confirmed by following the stress relaxation with FTIR. One way to determine this would be to stretch a *thin* plaque (e.g. 1-4) to a constant strain level with the rheo-optical stretching apparatus inside the FTIR chamber and monitor the $\nu(N-H)$absorbance level. Furthermore, a similar test could be carried out at high temperatures(125°C or greater) in the thermal chamber built for the rheo-optical stretching apparatus. One could determine if an increase in the dissociation of hydrogen bonds is taking place at the higher temperatures. One is also more likely to observe some changes in hydrogen bonding at these higher temperatures as discussed earlier.

- The effects of temperature on the orientation behavior of the plaques for different modes of deformation would be a useful study. For example, Cooper et. al. have reported observing for polyurethane elastomers that the hard segment orientation-elongation behavior goes through a maximum with temperature (56,60). It is also likely that some changes in the hard segment orientation for the plaques would be observed at the higher temperatures. Such tests would be carried out by utilizing the rheo-optical stretching apparatus along with the thermal chamber. The high temperature surroundings should be used while obtaining the orientation behavior upon elongation, cyclic deformation, and as a function of time after reaching a constant level of strain.

- The orientation-elongation behavior of plaques 1 and 2 have indicated that the the orientation level of the hard segments is affected by the hard segment content. Before confirming this result, the orientation-elongation behavior of plaque 3 and possibly plaque 4 also need to be obtained. This may call for better techniques to make thinner films in order to obtain such behavior for these higher hard segment plaques. Furthermore, by obtaining the orientation-elongation behavior for plaques 3 and 4 would help confirm the speculation that the polyurea aggregates are causing the transverse orientation in the hard segments.

- The orientation behavior upon cyclic deformation needs to be investigated more thoroughly for all of the plaques if possible. This investigation is necessary because these results would hopefully lead to a better understanding of some important foam properties such as compression set and fatigue. In addition to the studies suggested earlier, the residual orientation or the orientation at no load after cyclic loading a thin plaque would also be a useful result to help understand the compression set.

- Another useful study would be to investigate the effects of unsymmetrical 2,4 TDI versus that of symmetrical 2,6 TDI on the hard domains of the plaques pressed from the polyurethane foams. It appears the symmetrical 2,6 TDI would produce a foam and its respective plaque with more cohesive and possibly larger domains. This could be investigated by making two different

foams (lower water content preferably) and utilizing the techniques mentioned in this thesis to obtain their deformation-orientation behavior.

- It would be interesting to determine if similar deformation-orientation behavior would be obtained for the foams as shown for that of their respective plaques. One would think so, since the morphology of the solid material in the foams is similar to that of their compression molded plaques. One possible way to investigate this, is to utilize IR-microscopy along with the appropriate deformation stage and focus on a cell strut in the foam. This experiment, although difficult, would indicate if the plaques are representative of the deformation-orientation behavior in the foams.

- Biaxial orientation of the hard segments was suggested as the reason for the hard segment orientation function reaching a value below the lower limit for uniaxial orientation defined by linear dichroism theory. One possible method to confirm this suggestion, is to obtain the orientation-elongation behavior of the hard segments with the sample tilted at different angles to the IR beam. Therefore, if the orientation-elongation behavior is different at the various angles, there is a good chance biaxial orientation of the hard segments is taking place.

References

1. G. Woods, "The ICI Polyurethanes Book," ICI and John Wiley & Sons, Netherlands, (1987).

2. G. Woods, "Flexible Polyurethane Foams: Chemistry and Technology," Applied Sci. Plublishers, LTD, New Jersy (1982).

3. Dow Chemical Co., "The Flexible Foam Handbook," Dow Chem. USA, Urethane Dept., Midland, MI.

4. K.C. Frisch and J.H. Saunders, "Plastics Foams: Part 1," Marcel Decker, Inc., New York (1972).

5. R.D. Duffy and R.D. Whittman, *J. Cell. Plastics,* 14(3), 161 (1978).

6. G. Burkhart, H.J. Kollmeier and H.H. Schloens, *J. Cell Plastics,* 19, 441 (1983).

7. P.S. Zurer, *Chemical and Engineering News,* 66, 16 (1988).

8. G. Rossmy, H.J. Kollmeier, W. Lidy, H. Schator and M. Wiemann, *J. Cell. Plastics,* 17(6), 319 (1981).

9. G. Rossmy, W. Lidy, H. Schator, M. Wiemann and H.J. Kollmeier, *J. Cell. Plastics,* 13(1), 26 (1977).

10. B. Kanner and T.G. Decker, *J. Cell. Plastics,* 4, 32 (1969).

11. B. Kanner, B. Prokai, C.S. Eschbach, and G.J. Murphy, *J. Cell. Plastics,* 15, 315 (1979).

12. F.E. Bailey and F.E. Critchfield, *J. Cell. Plastics,* 17, 333 (1981).

13. G. Hauptman, K.H. Dorner, J. Hocker and G. Pfister, *Proceedings of the 5th. International SPI- Conference,* 1980.

14. J. Hocker, *J. Appl. Polym. Sci.,* 25, 2879 (1980).

15. H.W. Illeger, K.H. Dorner, H. Hettel, *Polyurethane World Congress,* 305 (1987).

16. R.L. Rowton, *J. Cell. Plastics,* 16, 287 (1980).

17. P. Van Gheluwe and J. Leroux, *J. Appl. Polym. Sci.,* 28, 2053 (1983).

18. J.P. Armistead, MS Thesis, Virginia Polytechnic Institute and State University, Chemical Eng. Dept., Blacksburg, VA (1985).

19. J.P. Armistead, G.L. Wilkes and R.B. Turner, *J. Appl. Polym. Sci.,* 35, 601 (1988).

20. R.B. Turner, H.L. Spell, G.L. Wilkes, *SPI 28th Annual Technical/Marketing Conference,* 244 (1984).

21. J.W.C. Van Bogart, A. Lilaonitkul and S.L. Cooper, *Adv. Chem.,* 176, 3 (1979).

22. C.S. Paik Sung, C.B. Hu and C.S. Wu, *Macromol.,* 13, 111 (1980).

23. D. Tyagi, Ph.D. Thesis, Virginial Polytechnic Institute and State University, Chemical Eng. Dept., Blacksburg, VA (1985).

24. R. Bonart, L. Morbitzer and E.H. Muller, *J. Macromol. Sci. Phys.,* B9(3), 447 (1974).

25. G.L. Wilkes and S. Abouzahr, *Macromol.,* 14, 458 (1981).

26. J.T. Koberstein and R.S. Stein, *J. Polym. Sci., Polym. Phys. Ed.,* 21, 1439 (1983).

27. A.N. Gent and A.G. Thomas, *J. Appl. Polym. Sci.,* 1, 107 (1959).

28. A.N. Gent and A.G. Thomas, *Rubber Chem. Tech.,* 36, 597 (1963).

29. M.F. Ashby, *Mettalurgical Trans.,* 14A, 1755 (1983).

30. L.J. Gibson and M.F Ashby, *Proc. R. Soc. Lond.,* 382, 43 (1982).

31. Hilyard, "Mechanics of Celluar Solids," Applied Sci. Publishers, LTD, New Jersey, 1980.

32. K.C. Rusch, *J. Appl. Polym. Sci.,* 13, 2297 (1969).

33. C.B. Wang and S.L. Cooper, *Macromol.,* 16, 775 (1983).

34. W. Patten and D.C. Priest, *J. Cell. Plastics,* 8, 134 (1972).

35. W. Patten and C.G. Seefried, *J. Cell Plastics,* 12, 41 (1976).

36. R.M. Herrington and D.L. Klarfeld, *Proceedings of the SPI-6th International Tech./Marketing Conf.,* 177 (1983).

37. K. Saomtome, K. Matsurbara, and T. Yatomi, *J. Cell. Plastics,* 13, 203 (1977).

38. S.M. Terry, *J. Cell. Plastics,*12, 156 (1976).

39. F.J. Dywer, *J. Cell. Plastics,* 12, 104 (1976).

40. R.P. Kane, *J. Cell Plastics,* 7, 5 (1971).

41. W.M. Lee, *Proceedings of the SPI-30th Annual Tech./Marketing Conf.,* 138 (1985).

42. W.J. Dzierza, *J. Appl. Polym. Sci.,* 27, 1487 (1982).

43. R.W. Seymour, G.M. Estes, D.S. Huh, and S.L. Cooper, *J. of Polym. Sci.,* 10(A-2), 1521 (1972).

44. D.J. Doherty and G.W. Ball, *J. Cell. Plastics,* 3(5) (1967).

45. E.A. Meinecke and R.C. Clark, "The Mechanical Properties of Polymeric Foams," Technomic Publishing Co., Inc., Westport, Conn (1973).

46. J. Miltz and O. Raman, *Polym. Eng. and Sci.,* 26, 1305 (1986).

47. M. Peleg, *J. Rheology,* 24, 451 (1980).

48. R.S. Stein, *Rubber Chem. and Tech.,* 44, 458 (1976).

49. G.L. Wilkes, *J. Macromol. Sci. Review Macromol. Chem.* 10(2), 149 (1974).

50. H.W. Siesler, "Infrared and Raman Spectroscopy of Polymers," New York: Marcel Dekker (1980).

51. R.D.B. Fraser, *J. Chem. Phys.,* 21, 1511 (1953).

52. I.M. Ward, "Structure Properties of Oriented Polymers," Appl. Sci., London (1975).

53. R.S. Stein , personal communication

54. J.L. White and J.E. Spruell, *Polym. Eng. Sci.,* 21, 859 (1981).

55. J.L. White, *J. Polym. Eng.,* 5, 277 (1985).

56. R.W. Seymour, A.E. Allegrezza and S.L. Cooper, *Macromol,* 6, 896 (1973).

57. R.W. Seymour and S.L. Cooper, *J. Polym. Sci. Symposium,* 46, 69 (1974).

58. R. Bonart and K. Hoffman, *Colloid and Polym. Sci.,* 260, 268 (1982).

59. R. Bonart, L. Morbitzer, and G. Hentze, *J. Macromol. Sci.,* B3, 337 (1969).

60. A.E. Allegreza, R.W. Seymour, N.H. Ng and S.L. Cooper, *Polymer,* 15, 433 (1974).

61. G. M. Estes, R.W. Seymour and S.L. Cooper, *Macromol.,* 4, 452 (1971).

62. H.W. Siesler, *Polymer Bull.,* 9, 557 (1983).

63. H.W. Siesler, *Pure and Appl. Chem.,* 57(11), 1603 (1985).

64. V.W. Shrichatrapimuk and S.L. Cooper, *J. Macromol. Sci. Phys.,* 15, 267 (1978).

65. R. Bonart, L. Morbitzer, and E.H. Muller, *J. Macromol. Sci.-Phys.,* B9(3), 337 (1974).

66. K. Hoffman and R. Bonart, *Makromol. Chem.,* 184, 1529 (1983).

67. K. Hoffman and R. Bonart, *Colloid and Polym. Sci.,* 262, 1 (1984).

68. R. Bonart, *J. Macromol. Sci.-Phys.,* B2(1), 115 (1968).

69. I. Ishihara, I. Kimura, K. Saito and H. Ono, *Macromol. Sci.-Phys.,* B10(4), 591 (1974).

70. I. Kimura, H. Ishihara, H. Ono, N. Yoshihara, S. Nomura, and H. Kawai, *Macromol.,* 7, 355 (1974).

71. C.S.P. Sung and C.B. Hu, *Macromol.,* 14, 212 (1981).

72. V.A. Khranovskii and L.P. Gul'ko, *J. Macromol. Sci.-Phys.,* B22(4), 497 (1983).

73. J.J. Alklonis and W.J. MacKnight, "Introduction to Polymer Viscoelasticity," John Wiley and Sons, New York, (1983).

74. P.J. Flory, "Principles of Polymer Chemistry," Cornell University Press, Ithaca and London, (1953).

75. R.B. Turner, personal communication

76. C.S.P. Sung and N.S. Scheider, *Macromol.,* 10, 452 (1977).

77. C.S.P. Sung and N.S. Scheider, *J. of Mat. Sci.,* 13, 1689 (1978).

78. G.A. Senich and W.J. MacKnight, *Macromol.,* 13, 106 (1980).

79. D.J. Jones, personal communication

Table 3.1. Absorbing Frequencies for Polyurethane Elastomers*

Frequency (cm^{-1})	Assignment**	Transition Moment Angle (°)	Component Representation
3320	$\nu(N-H)$	90	Hard Segment(ET)
3320	$\nu(N-H)$	90	Hard Segment(ES)
2935	$\nu(CH_2)$	90	Soft Segment(ET)
2960	$\nu(CH_2)$	90	Soft Segment(ES)
2850	$\nu(CH_2)$	90	Soft Segment(ET)
1730	$\nu(C=O)_f$	78	Interface(ET)
1700	$\nu(C=O)_b$	78	Hard Segment(ET)
1370	$\omega(CH_2)$	0	Soft Segment(ET)

* taken from references 56-58,61

** ν - stretching vibration, ω - wagging mode

Table 3.2. Absorbing Frequencies for Polyurea-urethane Elastomers*

Frequency (cm^{-1})	Assignment**	Transition Moment Angle (°)	Component Representation
3320	$\nu(N-H)$	90	Hard Segment
2940	$\nu(CH_2)$	90	Soft Segment
2860	$\nu(CH_2)$	90	Soft Segment
1730	$\nu(C=O)_f$	78	Interface
1700	$\nu(C=O)_b$	78	Interface
1640	$\nu(C=O)_{ur}$	78	Hard Segment
1370	$\omega(CH_2)$	0	Soft Segment

* taken from references 33,69

** ν - stretching vibration, ω - wagging mode

Table 4.1. Formulation Components for Flexible Water-Blown Foams

Isocyanate	T-80, 80:20 mixture of 2,4- and 2,6- isomers of toluene diisocyanate (Dow Chemical)
Polyol	Voranol 3100, a 3000 MW propylene oxide glycerine initiated polyether polyol; approximately trifunctional (Dow Chemical)
Water/ Blowing Agent	Deionized water - no chemical blowing agent used
Catalysts	T-9, a tin catalysts commonly known as stannous octate (MET Chemical) DABCO 33LV, an amine catalyst which is triethylenediamine in dipropylene gycol (Air Produts)
Surfactant	BF-2370, a silicone surfactant (Goldschmidt)

Table 4.2. Formulation Amounts for the Foams

Component	Foam #					
	1	2	3	4	1-lc	3-lc
Voranol 3100	100	100	100	100	-	-
Water	2	3	4	5	4	4
T-80	30.79	41.43	52.06	62.70	-	-
Surfactant	1.0	1.0	1.0	1.0	-	-
Tin Catalyst	0.15	0.15	0.15	0.15	-	-
Amine Catalyst	0.3	0.3	0.3	0.3	-	-

Comments:
1. Formulations based on 100 parts by weight of polyol.
2. An isocyanate index of 110 was used for Foams 1-4.
3. Formulation amounts are not given for Foams 1-lc and 3-lc due to proprietary reasons.
4. Compression molded plaques were made by applying pressure for 10 minutes at 204°C.
5. Foam 3-lc has additional propietary component to the ones listed above.

Table 5.1. Composition and Density of Foams

Foam	pp H_2O	Density(lb/ft_3)	Density Factor	wt% HS	vol% HS
1	2	2.85	1	21.1	17.5
2	3	1.92	1.48	25.8	21.4
3	4	1.43	1.99	30.1	25.0
4	5	1.24	2.30	33.8	28.0
1-lc	4	-	-	30.1	25.0
3-lc	4	-	-	30.1	25.0

Comments
1. Density measured by weighing known volume of foam.
2. Calculations for compositions neglected excess isocynate. If not neglected approximately 10% higher in each case.
3. Everything between the urethane ether oxygen is considered as hard segment.
4. Volume fractions are based on densities of 1.016 g/cc for soft segment and 1.22 g/cc for hard segment(HS).
5. Approximate compositions are given for foams 1-lc and 3-lc.
6. Density factors were obtained by dividing the densities of foams by density of foam 1.

Table 5.2. Stress Decay Rates for Foams 1-4

Foam	Stress Decay Rates* at Different Temperatures (°C)			
	$25(\sigma_{\perp})$	$25(\sigma_{\parallel})$	$75(\sigma_{\parallel})$	$125(\sigma_{\parallel})$
1	2.07	1.94	1.70	
2	2.44	2.35	2.06	
3	2.91	2.75	2.34	
4	3.13	3.01	2.41	3.5
2**		2.95		
4**		3.5		

* Stress decay rates, σ_d have been multipied by -1 x 10^2
** Obtained for 25 percent strain level; other values obtained at 40 percent strain level

Comments: 1. The error varied from ± 3 to 8 percent for the stress decay rates, σ_d.
2. The correlation functions for the log-log relationship between time and stress were equal to 0.995 to 0.999 except at 125°C.
3. $\sigma_{\parallel}$ and $\sigma_{\perp}$ represent the foams that were stretched parallel and perpendicular to the stretch direction, respectively.

Table 5.3. Stress Decay Rates for Plaques 1-4

	Stress Decay Rates* at Different Temperatures (°C)		
Plaque	25	75	125
1	2.44	1.92	-
2	2.82	2.66	-
3	3.50	3.30	-
4	4.30	4.09	3.41
2-DMF	2.80	-	-

* stress decay rates have been multiplied by -1 x 10^2

Comments: 1. The error varied from ± 5 to 10 percent for the stress decay rates, σ_d.

2. The correlation functions for the log-log relationship between time and stress were equal to 0.995 to 0.999 except at 125°C.

3. All σ_d were obtained values from tests performed at a 25 percent strain level.

Table 5.4. Absorbing Frequencies for Plaques and the PUUE Elastomer

Frequency (cm^{-1})	Assignment*	Transition Moment Angle (°)**	Component Representation
3300	$\nu(N-H)$	90	Hard Segment
2940	$\nu(CH_2)$	90	Soft Segment
2860	$\nu(CH_2)$	90	Soft Segment
1730	$\nu(C=O)_f$	78	Interface
1640	$\nu(C=O)_{ur}$	78	Interface
1475	$\delta(CH_2)$	90	Soft Segment
1370	$\omega(CH_2)$	0	Soft Segment

* ν - stretching vibration, ω - wagging mode, δ - bending mode

** taken from references 33, 50

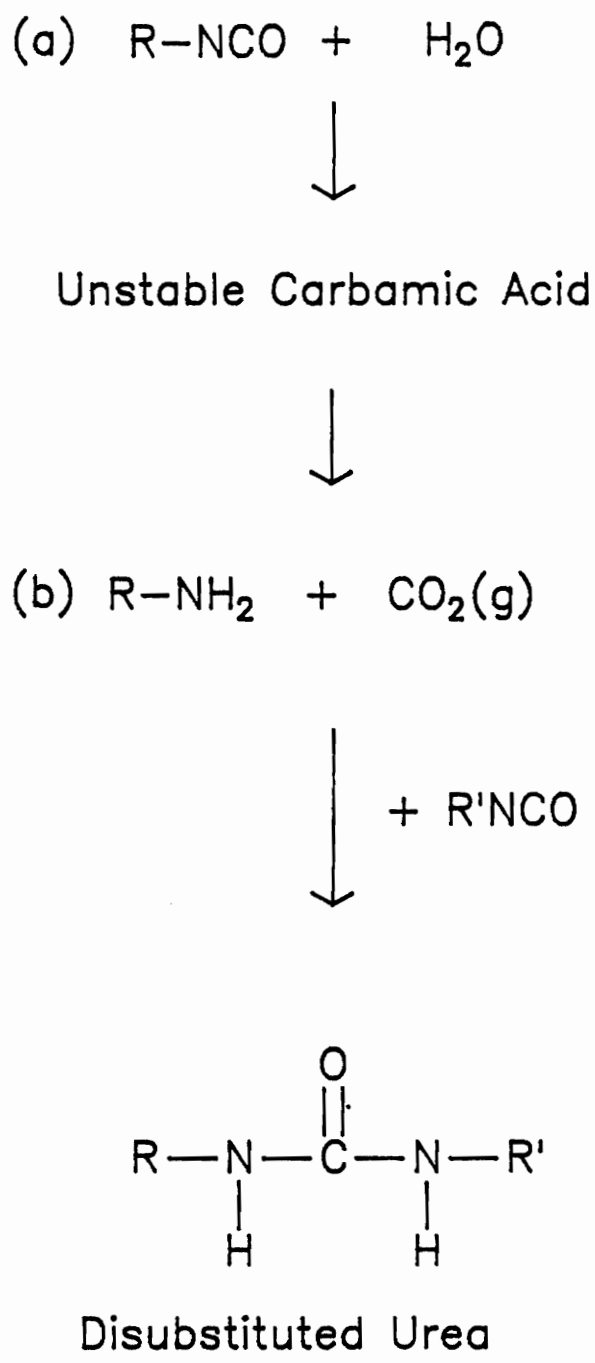

Figure 2.1. Primary Reactions in Flexible Foam Formation: (a) blowing reaction (b) chain extension (c) gelling reaction (next page)

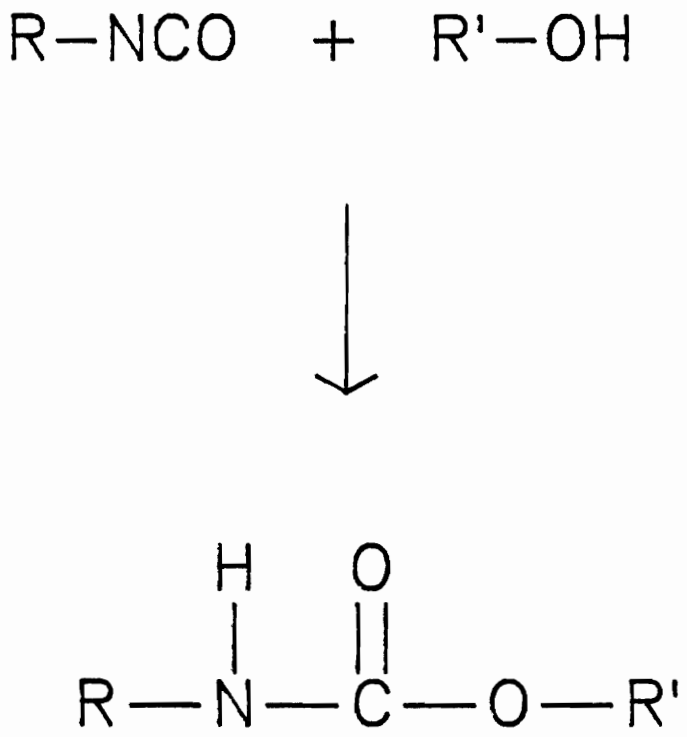

Figure 2.1, cont'd: Gelling Reaction

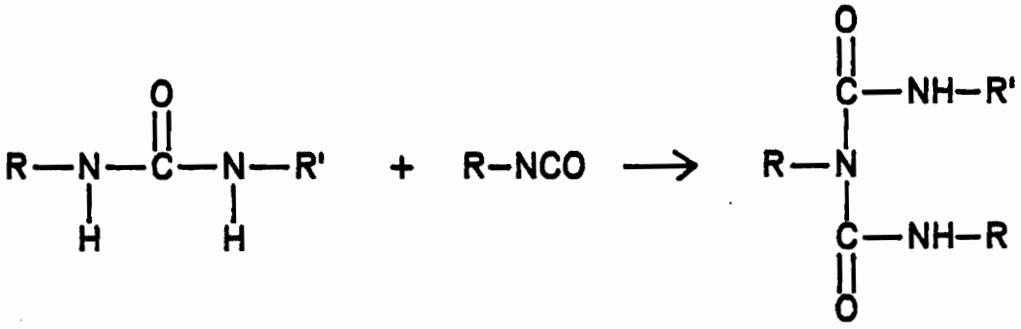

Biuret

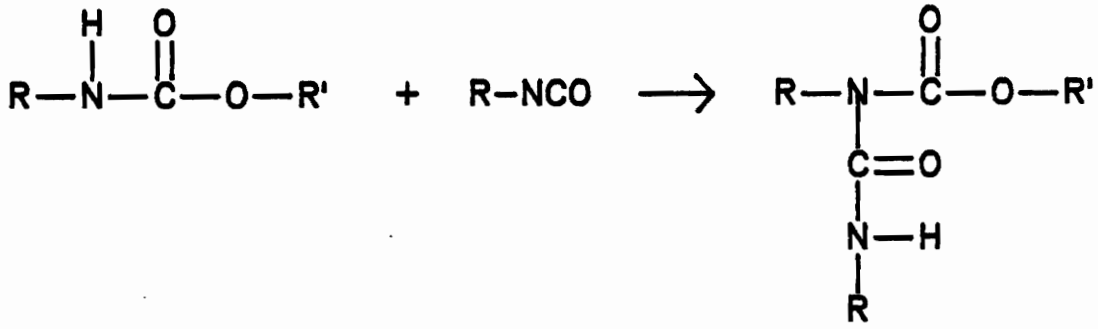

Allophanate

Figure 2.2. Secondary Reactions in Flexible Foam Formation

Toluene–diisocyanate (TDI)

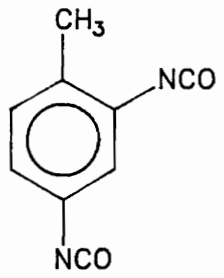

2,4 isomer

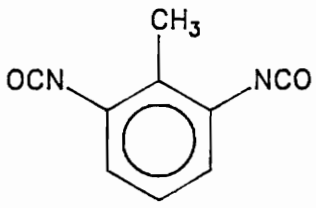

2,6 isomer

4,4'–diphenylmethane diisocyanate (MDI)

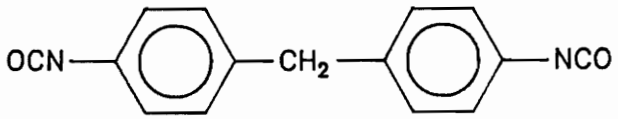

Polymeric MDI

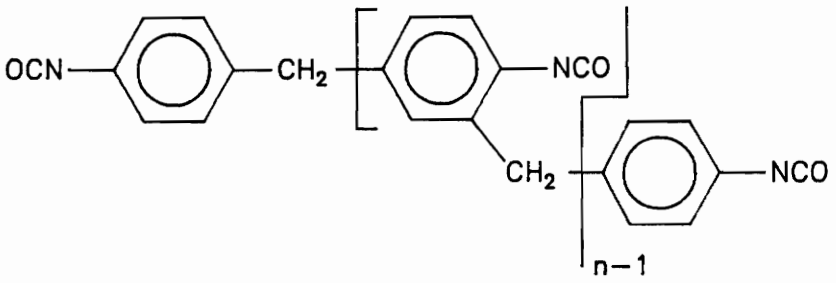

Figure 2.3. Stuctures of Diisocyanates Commonly Used in Manufacture of Foams and Elastomers

(a) Polypropylene oxide (PPO)

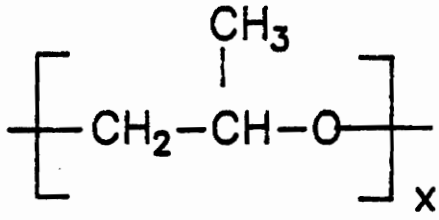

Polyethylene oxide (PEO)

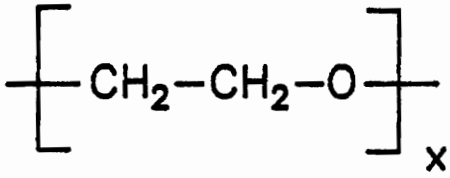

(b) Poly(tetramethylene oxide) (PTMO)

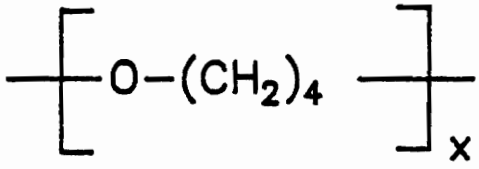

Figure 2.4. **Repeat Units for the Most Common Polyether Polyols:** (a) flexible foams and (b) elastomers

(a) Poly(oxydiethylene adipate)

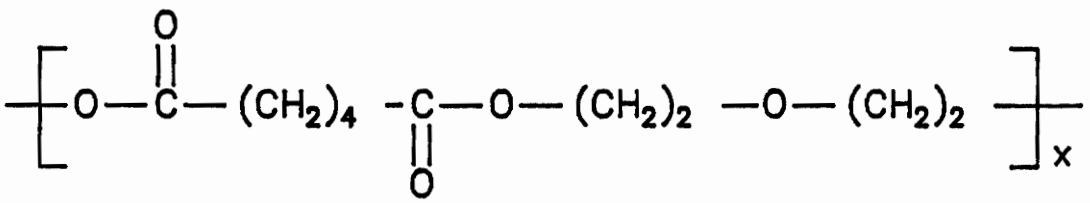

(b) Poly(tetramethylene adipate)

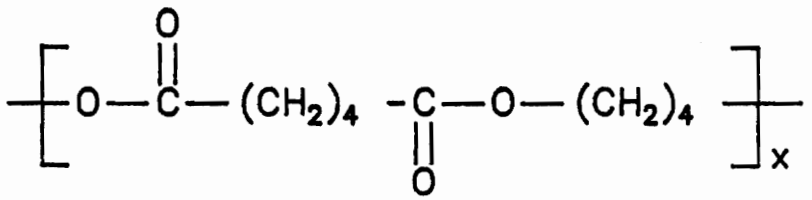

Figure 2.5. Repeat Units for Most Common Polyester Polyols: (a) flexible foams and (b) elastomers

1,4 Butanediol (BD)

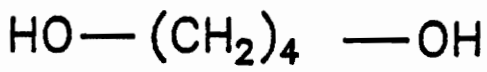

Ethyldiamine

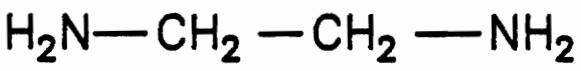

Methylene–bis(2–chloroaniline) (MOCA)

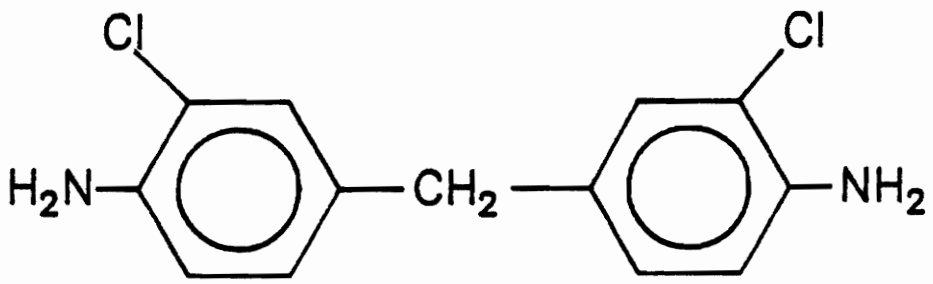

Figure 2.6. Most Common Chain Extenders Used in Manufacture of Elastomers

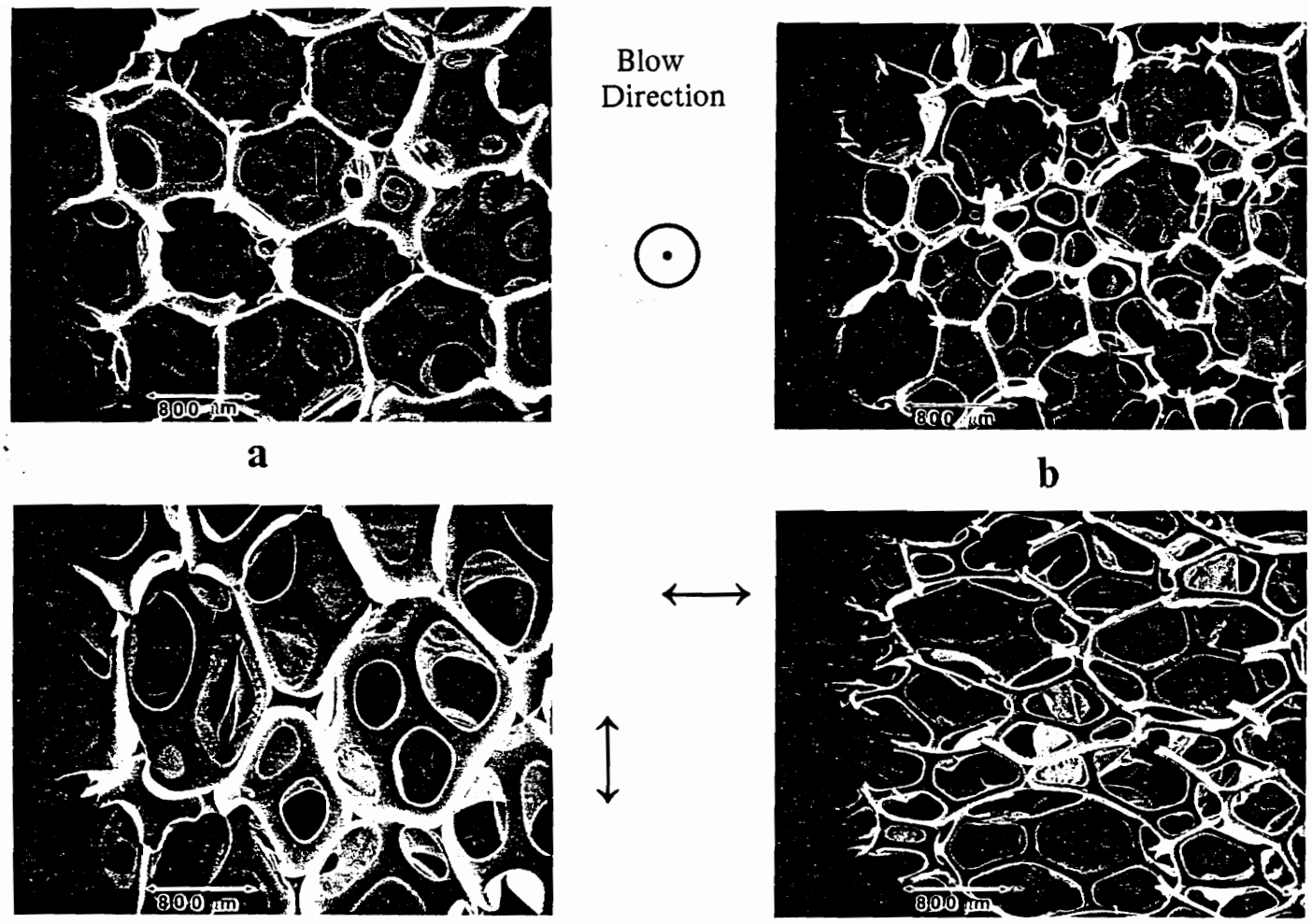

Figure 2.7. **SEM Micrographs of Foam 1(a) and 4(b):** observation direction is perpendicular(bottom) and parallel(top) to the blow axis (ref. 19)

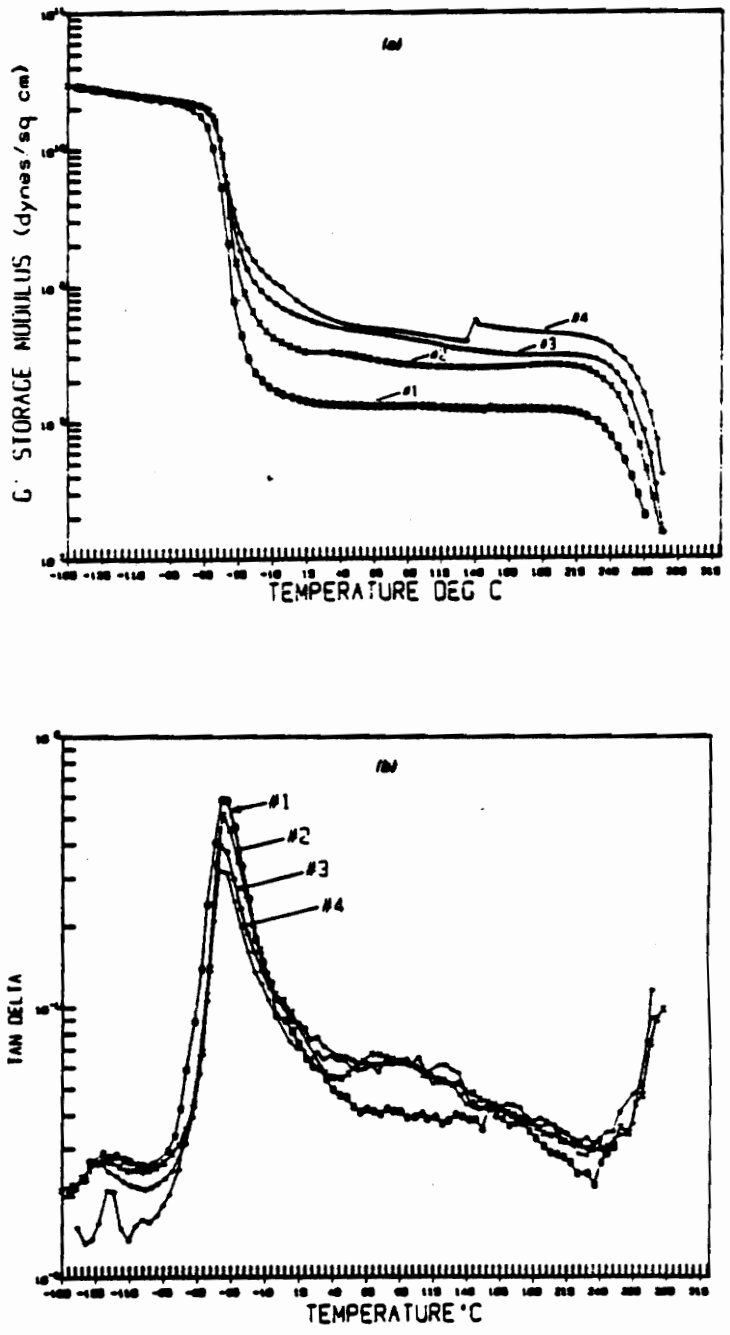

Figure 2.8. **Storage Moduli(a) and Tan Delta(b) Curves for Foams 1-4:** The storage moduli are normalized at -160°C based on a typical polyurethane plaque in the glassy state (ref. 20).

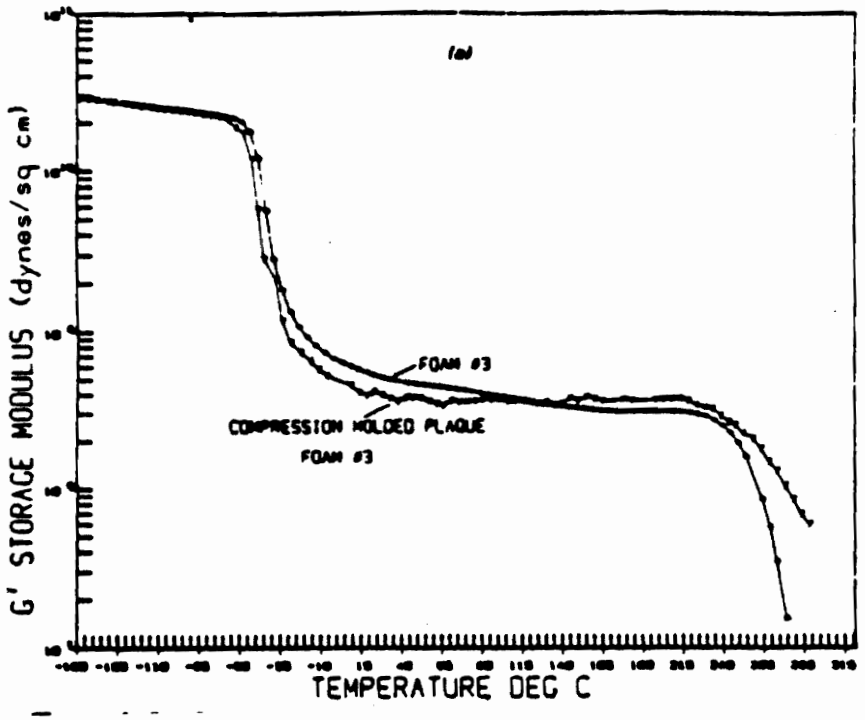

Figure 2.9. Comparison of DMS spectra for Foam 3 and its Compression Molded Plaque:

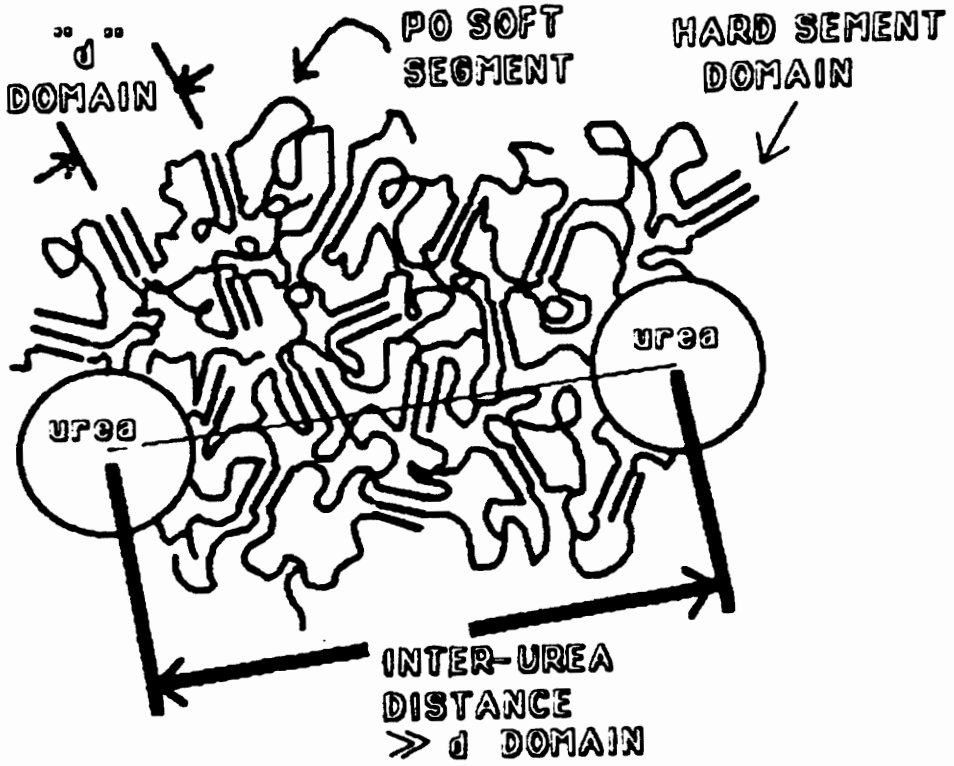

Figure 2.10. **Proposed Morphological Model for the Solid Portion of Flexible Water-Blown Foam:** The urea represents the polyurea aggregates; "d" is the interdomain distance between the smaller hard domains represented by the "sticklike" hard segments (ref. 19)

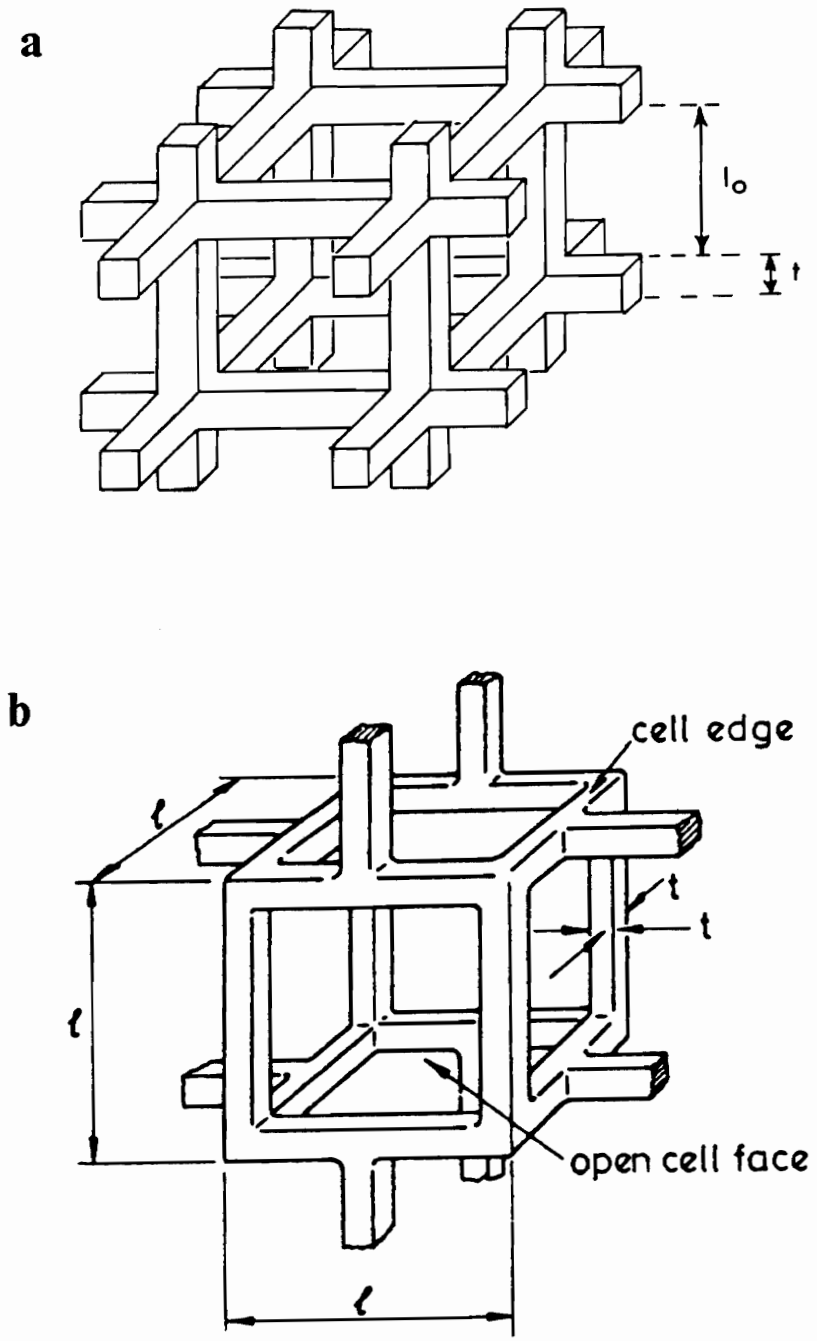

Figure 2.11. Cubic Models for Open-Celluar Materials: (a) Gent and Thomas (ref. 27) and (b) Gibson and Ashby (ref. 30)

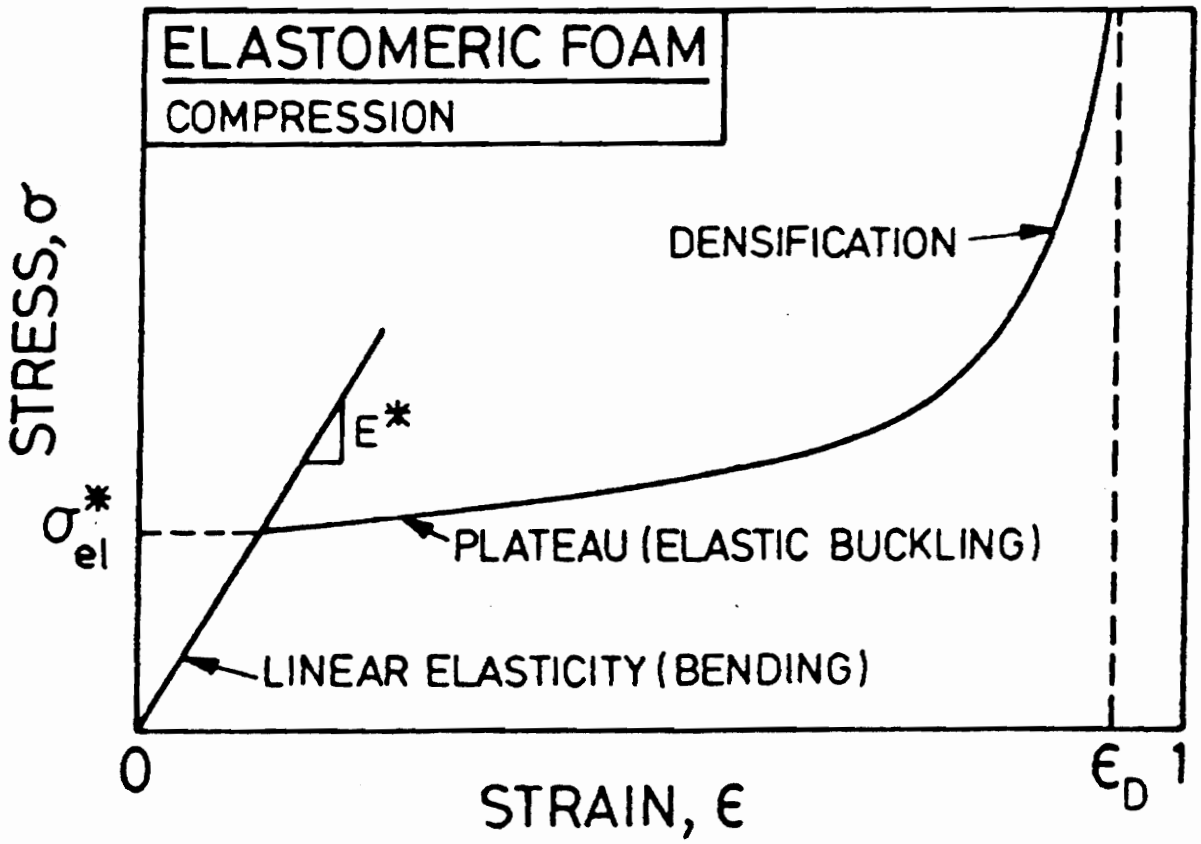

Figure 2.12. Typical Shape of the Compressive Stress-Strain Curve for a Foam: taken from ref. (29)

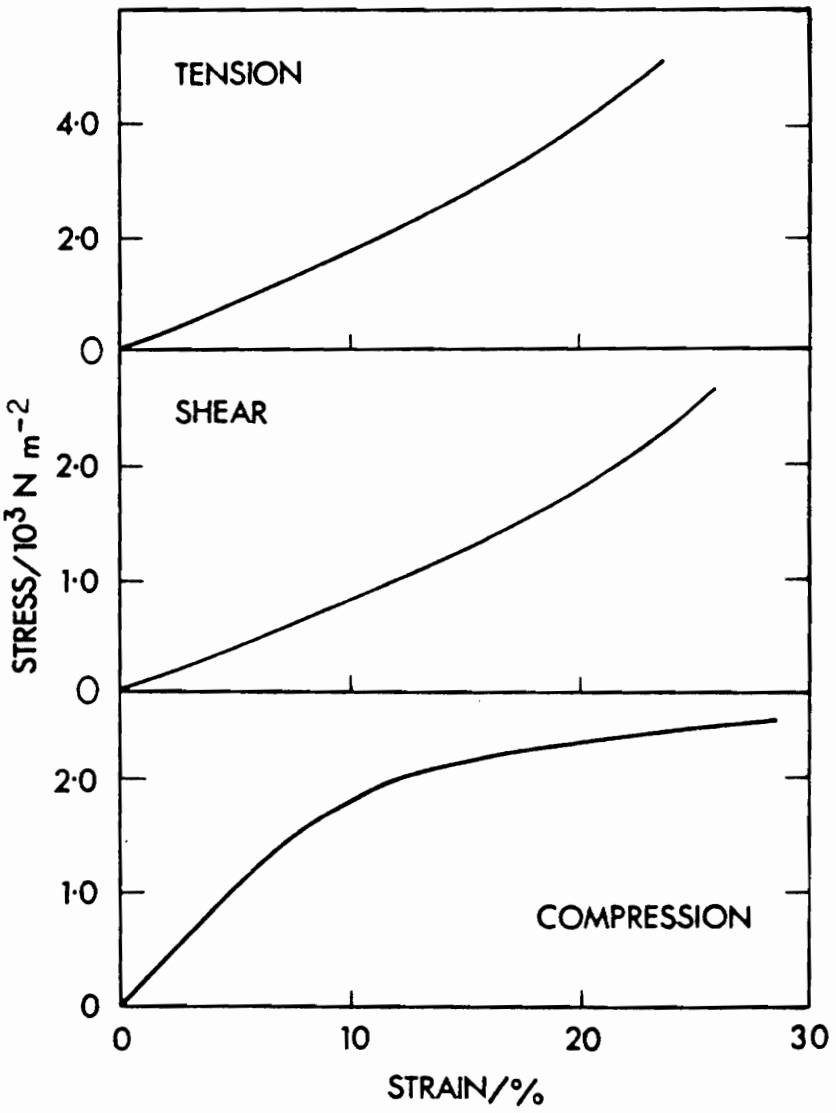

Figure 2.13. **Stress-Strain Behavior for Flexible Foams in Compression,** Shear, and Tension: taken from ref. (31)

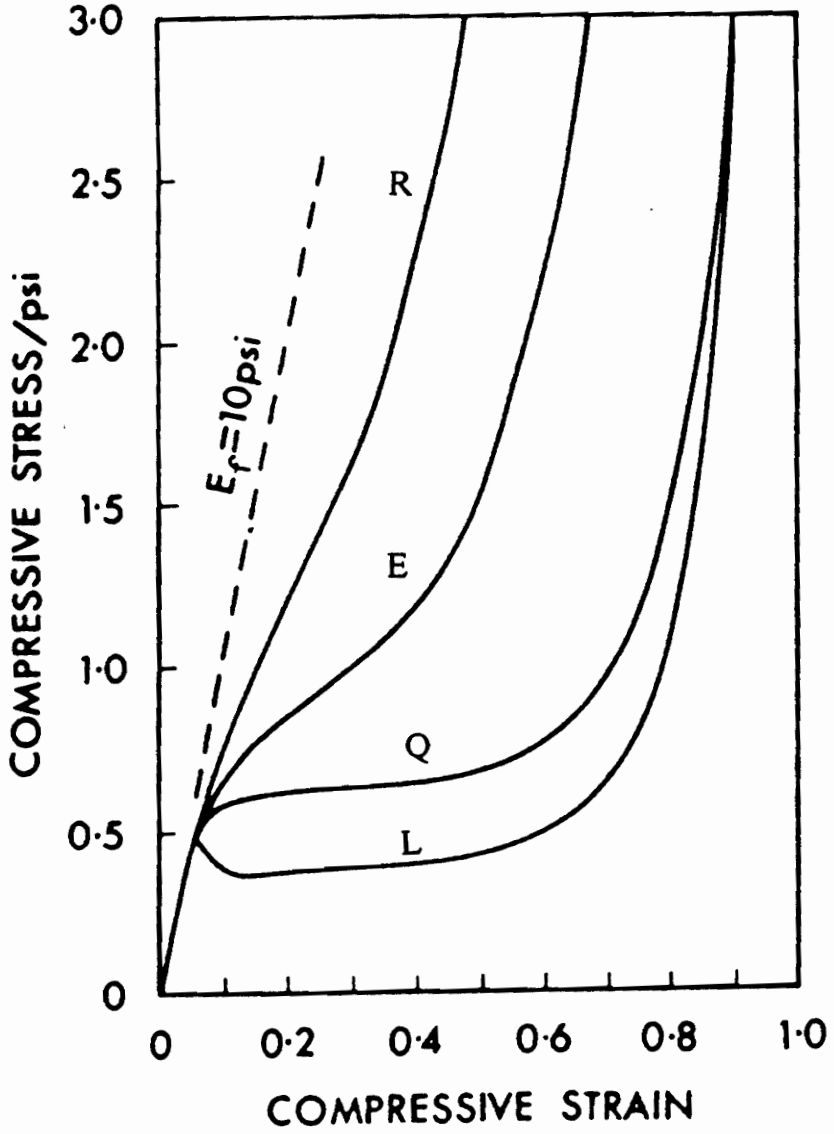

Figure 2.14. **Compressive Stress-Strain Curves for Four Different Flexible Foams:** taken from ref. (32)

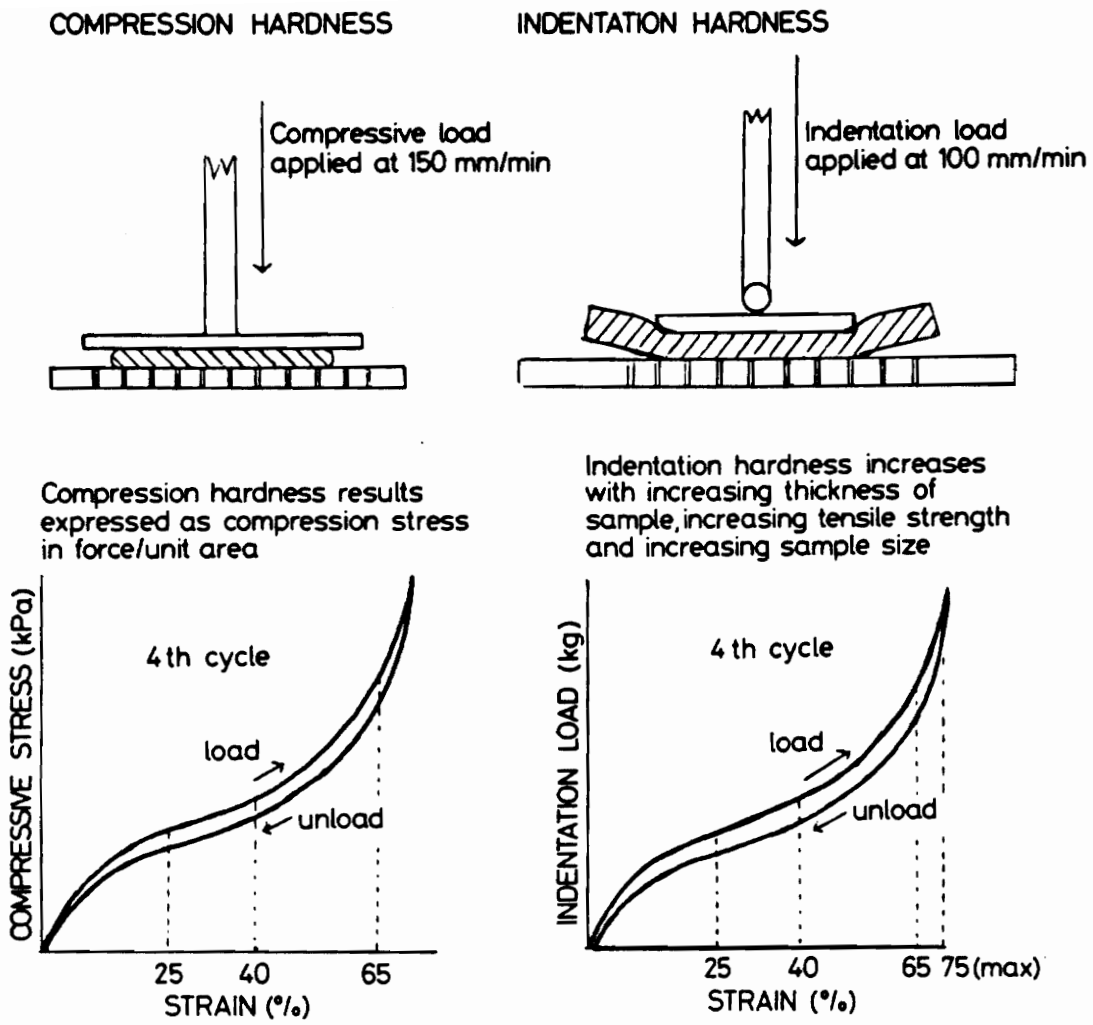

Figure 2.15. Characteristics of Compression Hardness and Indentation Hardness in Flexible Foams: taken from ref. 2

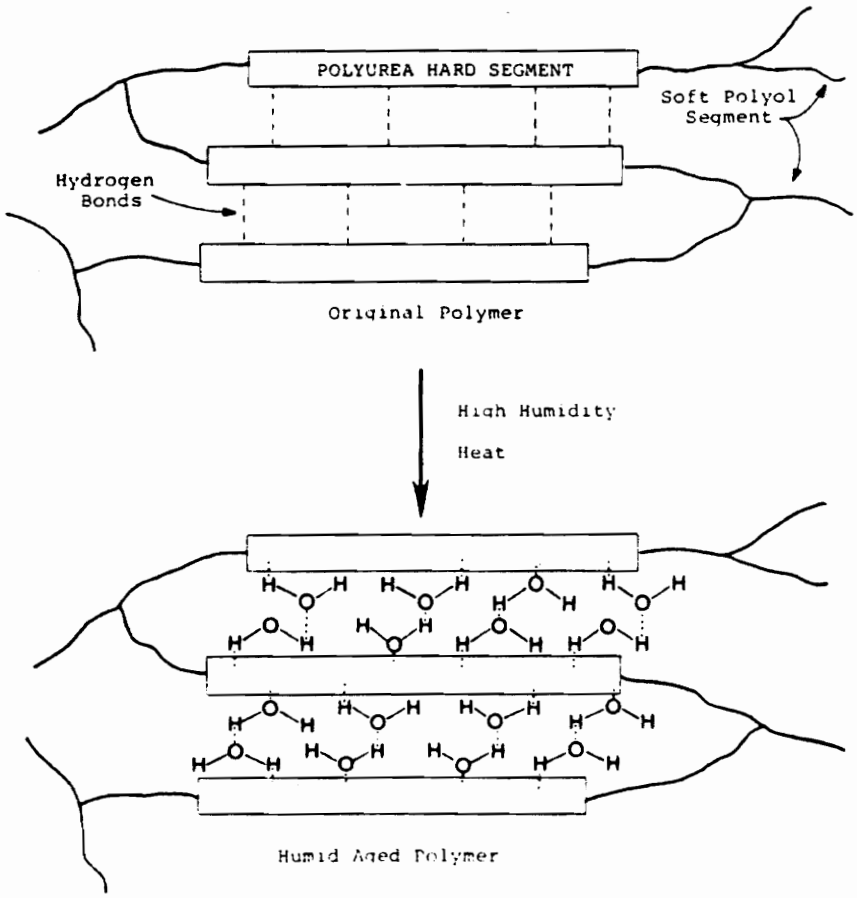

Figure 2.16. Proposed Model for Humid Aged Flexible Foam: taken from ref. 36

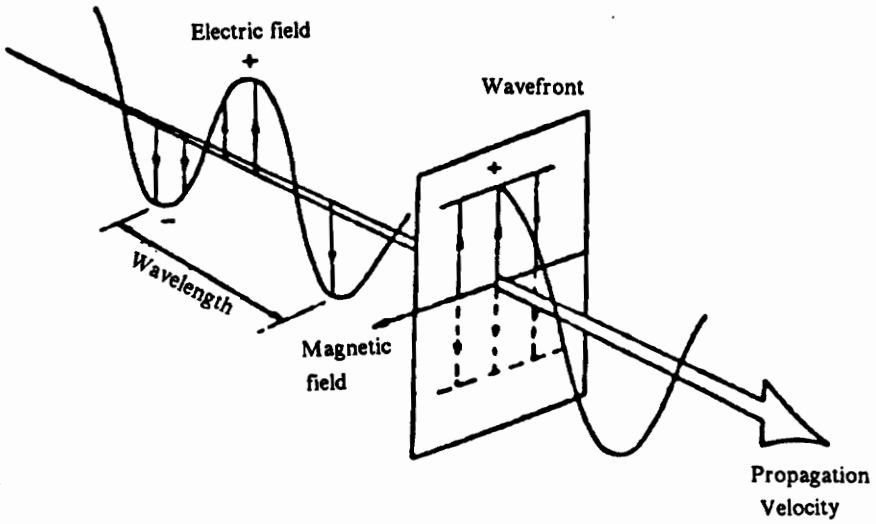

Figure 3.1. The Electric and Magnetic Fields for Plane Polarized Light: taken from ref. 48

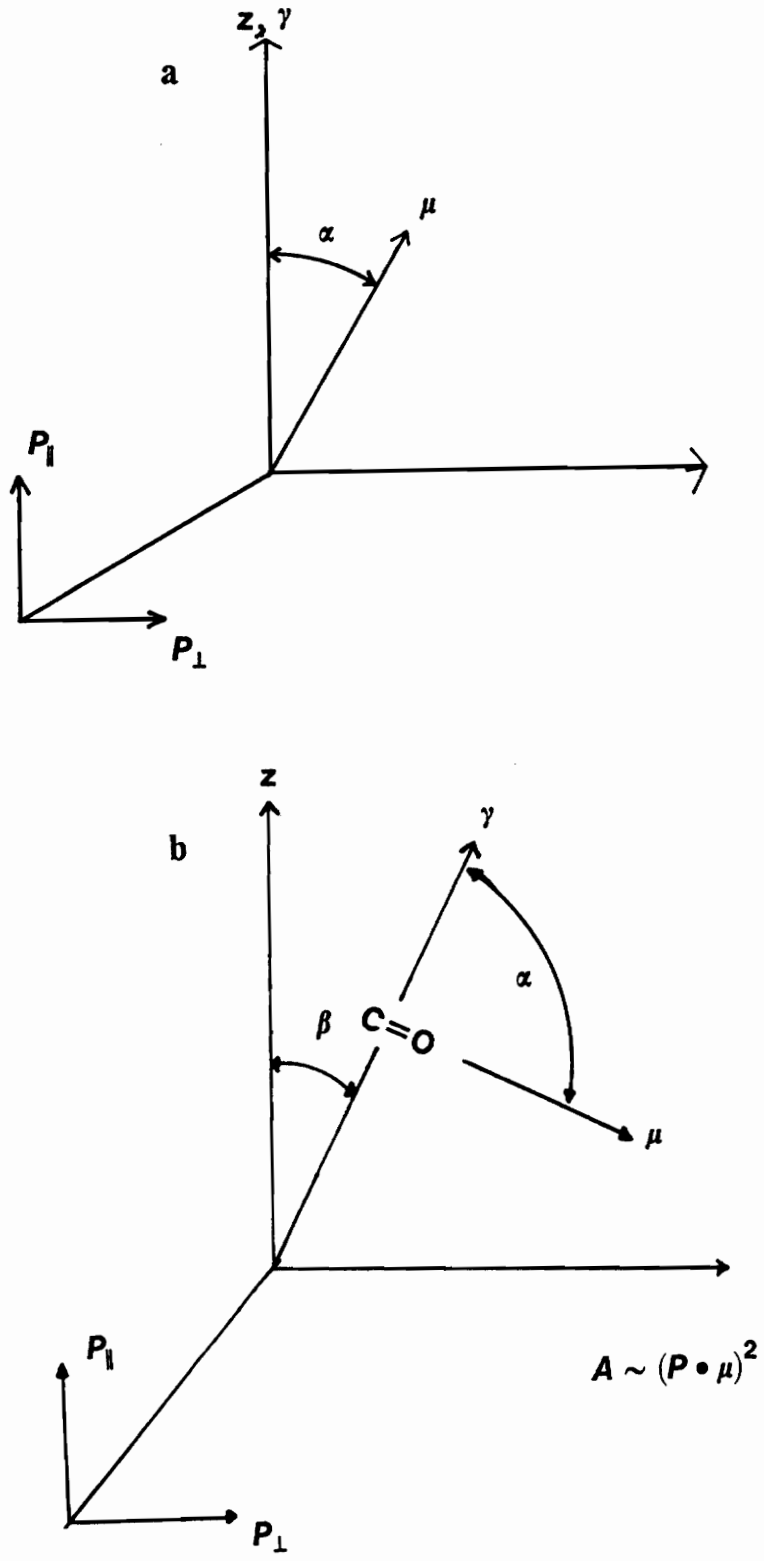

Figure 3.2. Coordinate Systems for Linear Dichroism: (a) perfect uniaxial order and (b) chain axis in relation to deformation axis (z is the stretch axis, γ is the chain axis and μ is the transition moment)

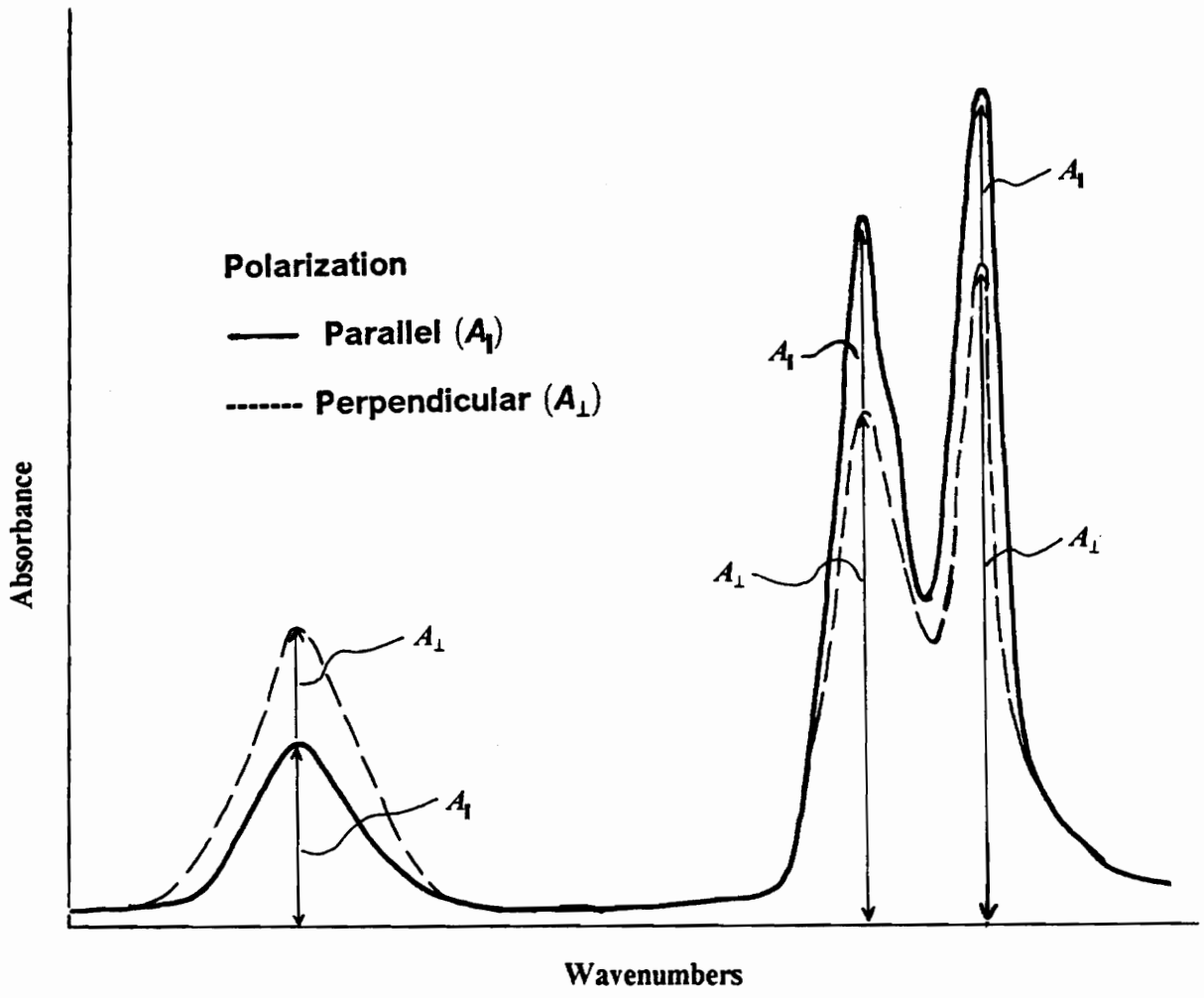

Figure 3.3. Two Spectra Technique for Measuring IR Dichroism

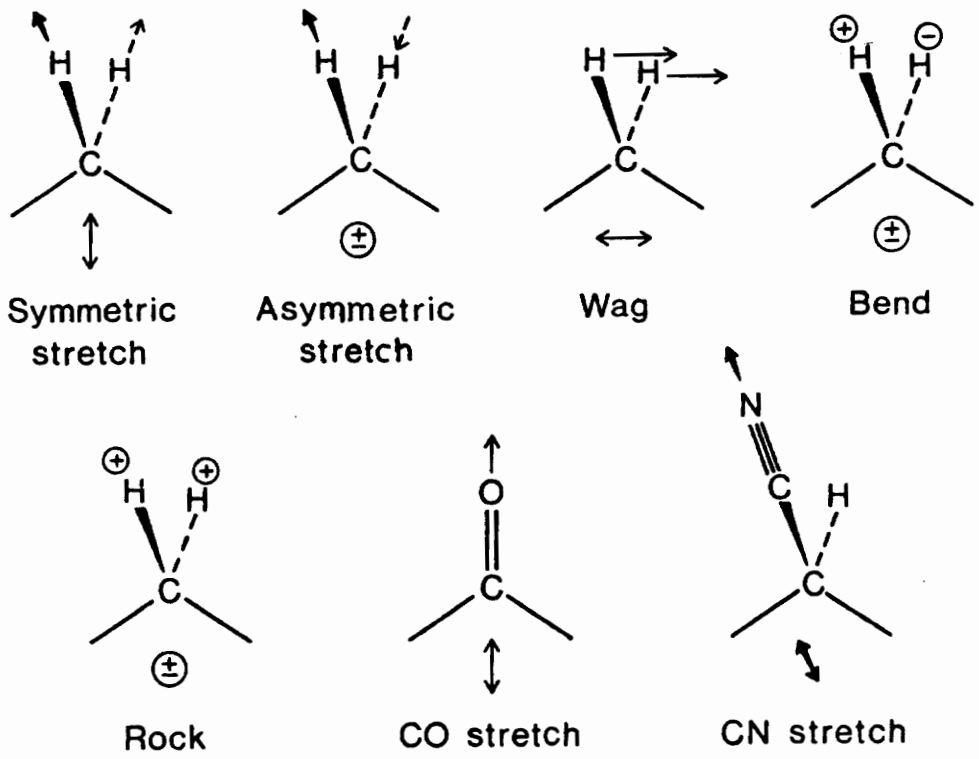

Figure 3.4. Examples of Transition Moments: Transition directions are indicated below each chromophoric group; ⊕ indicates movement perpendicular to page (52)

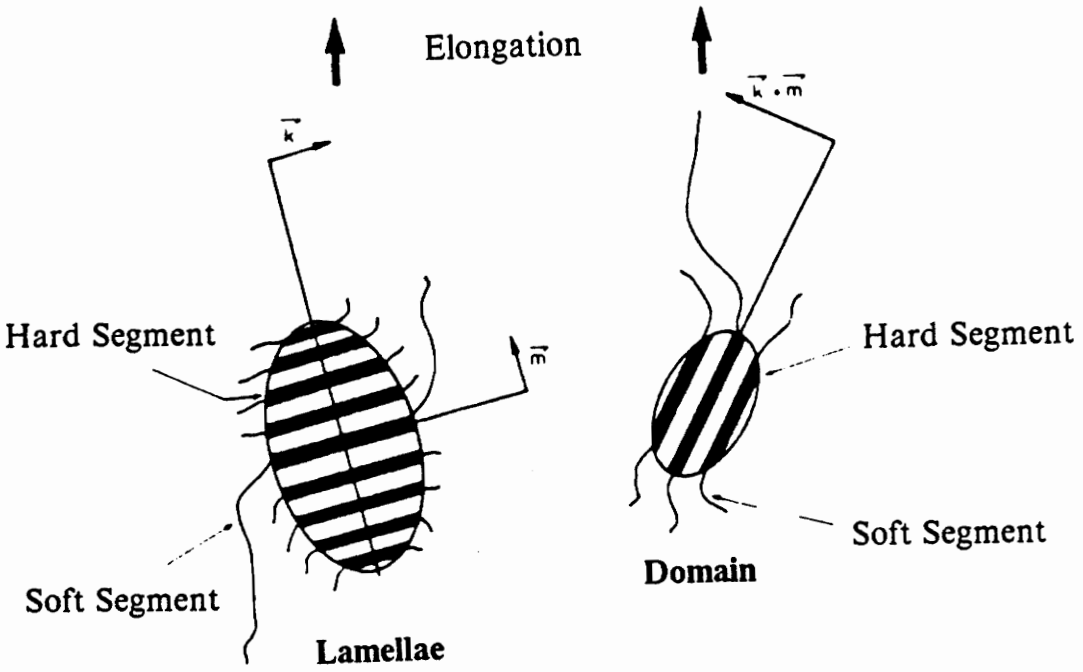

Figure 3.5. Schematic Representation of Hard Domains in Polyurethane Elastomers: The lamellar domain and the smaller hard segment domain are shown (58).

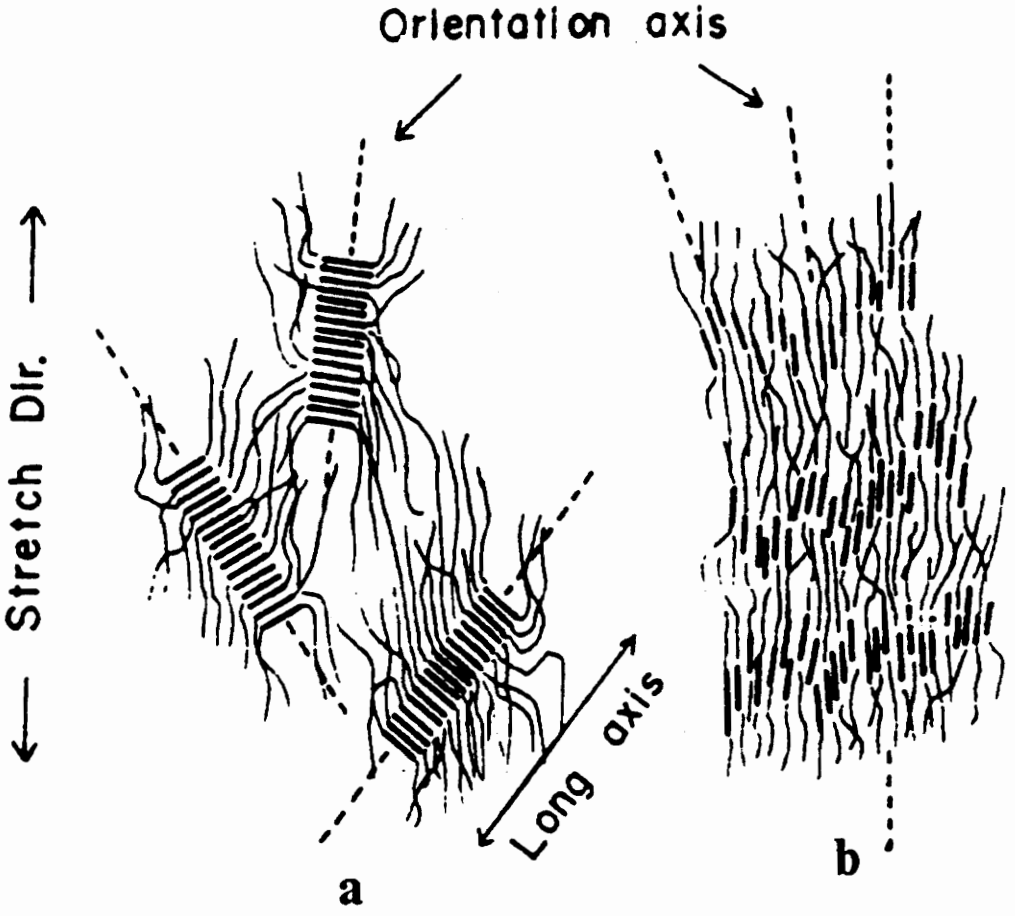

Figure 3.6. Proposed Mechanism for Deformation of Lamellar Hard Domains: (a) small elongations and (b) higher elongations (70)

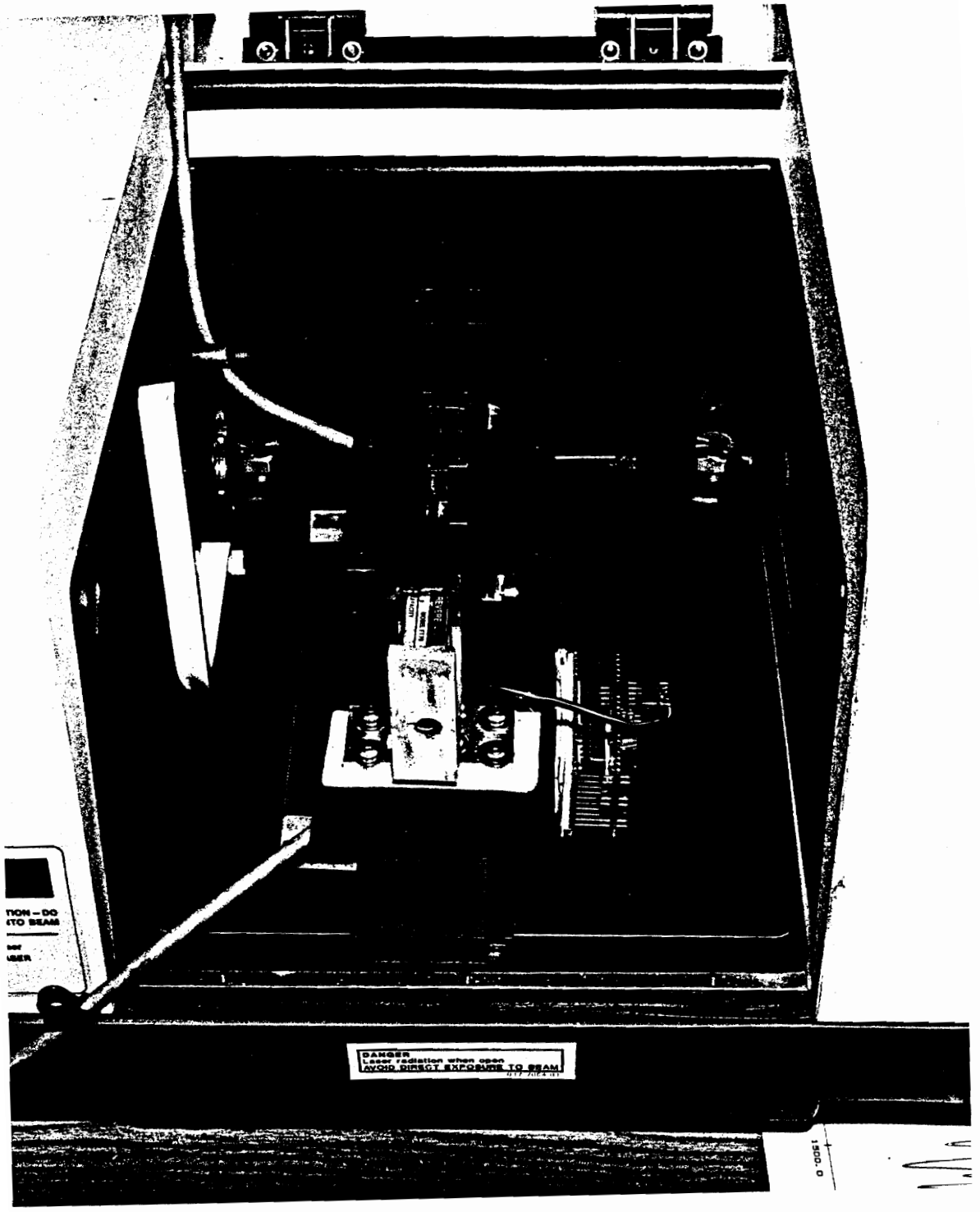

Figure 4.1. Rheo-Optical Stretching Device in Nicolet 5DXB FTIR Chamber

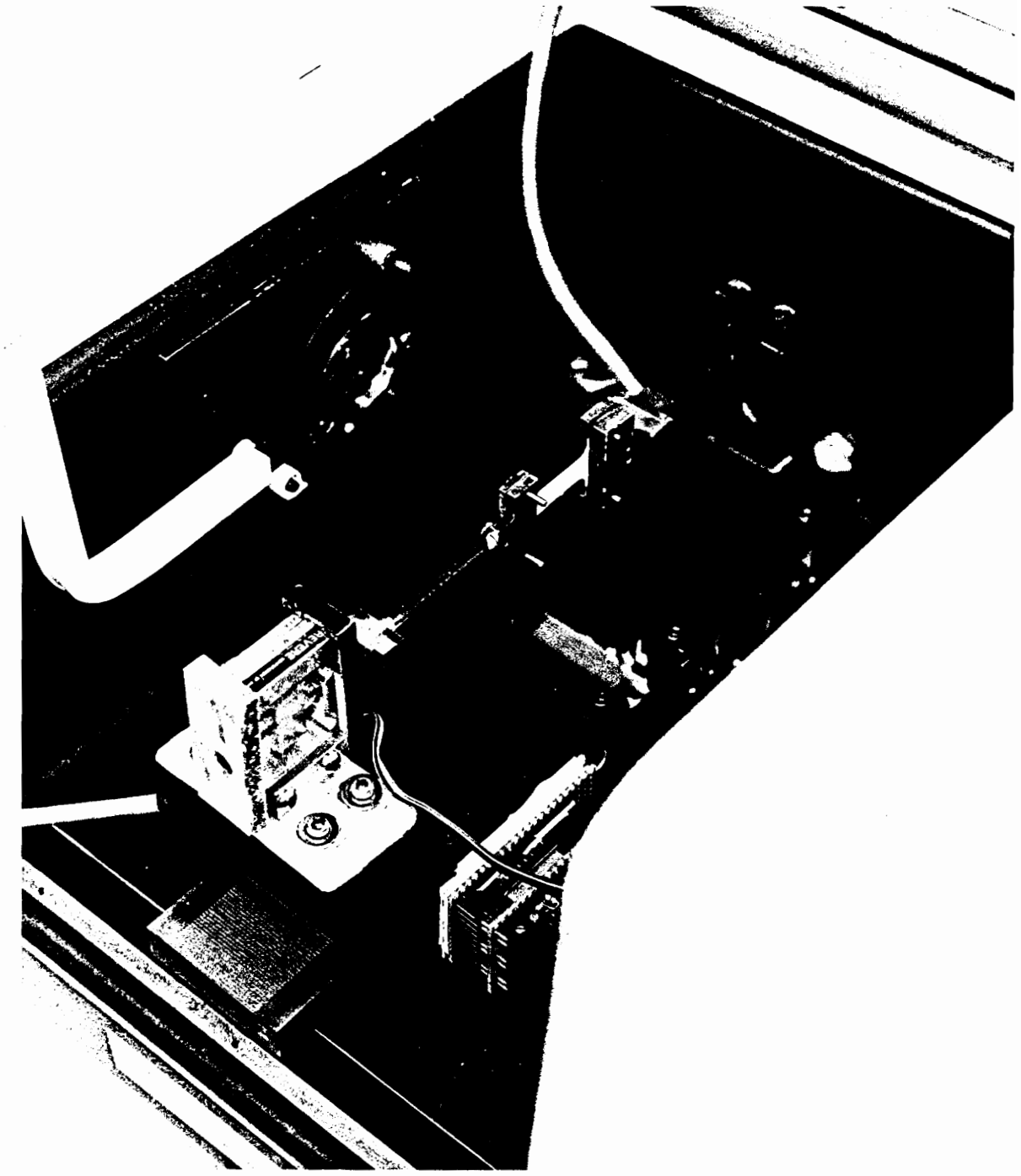

Figure 4.2. Rheo-Optical Stretching Device in Nicolet 5DXB FTIR Chamber

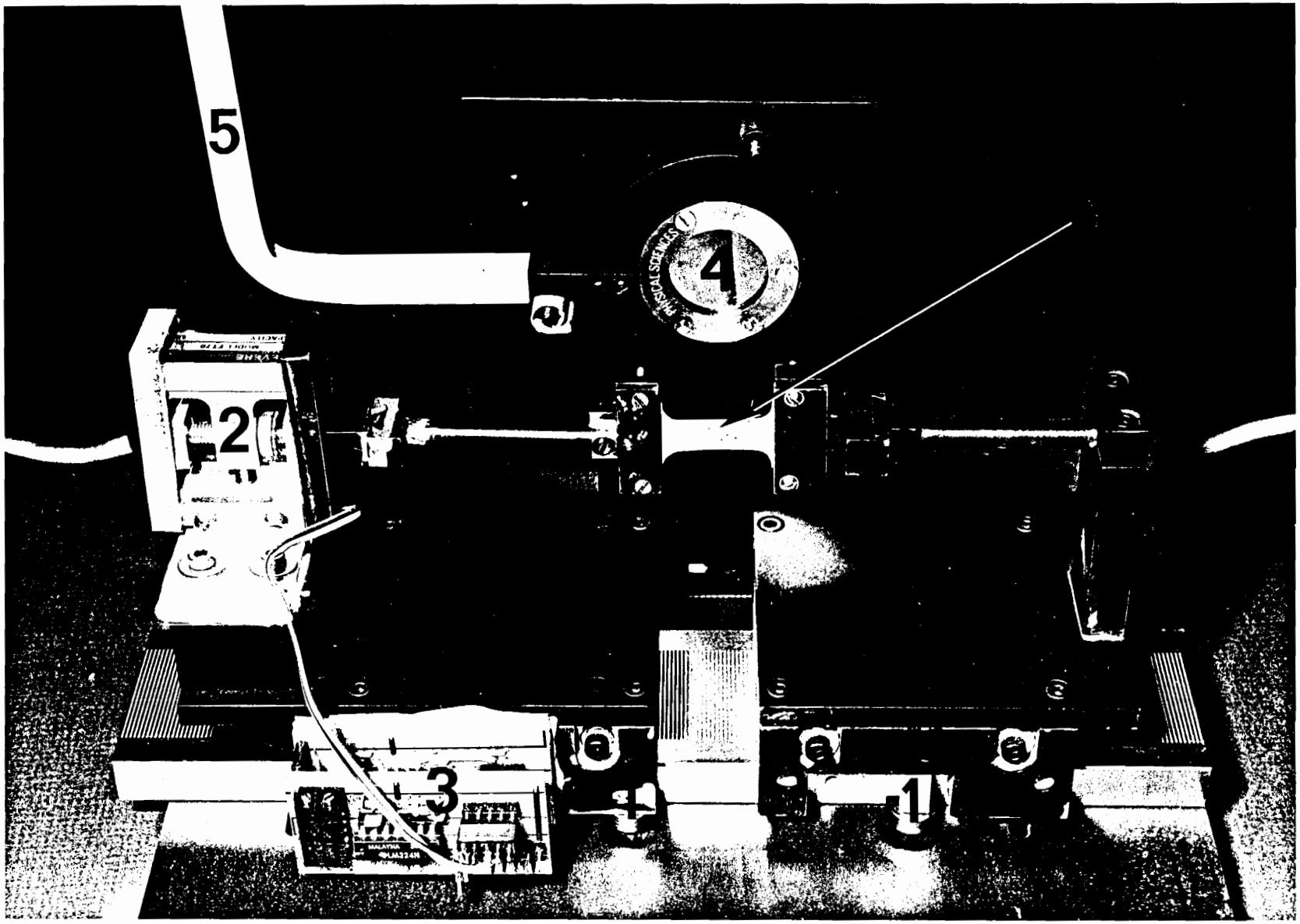

Figure 4.3. **Rheo-Optical Stretching Device:** (1) Linear motors, (2) Load cell, (3) Amplifier, (4) Grid polarizer, (5) Arm to rotate polarizer and (6) Sample

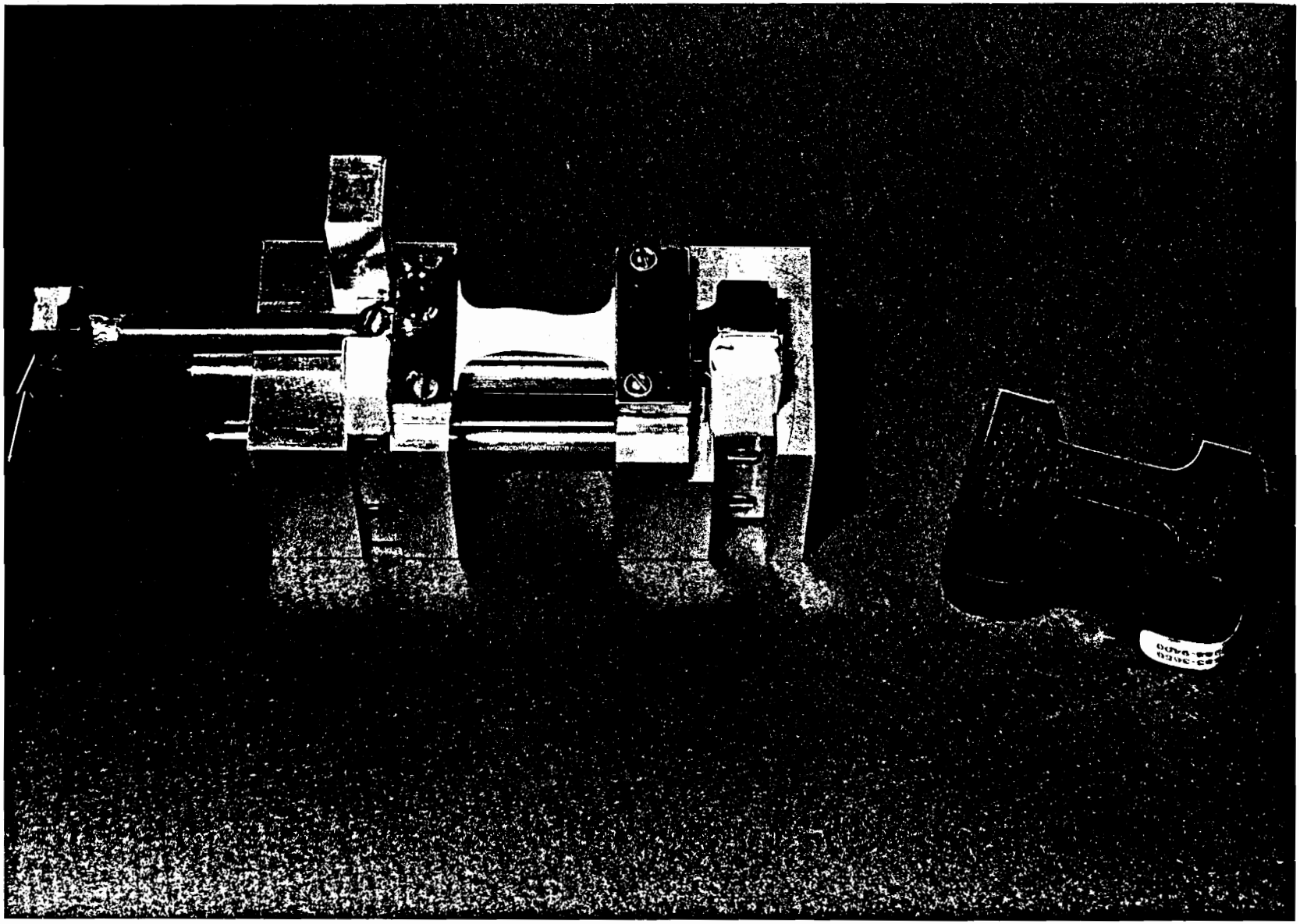

Figure 4.4. Sample Preparation Holder and Dogbone Die Cutter

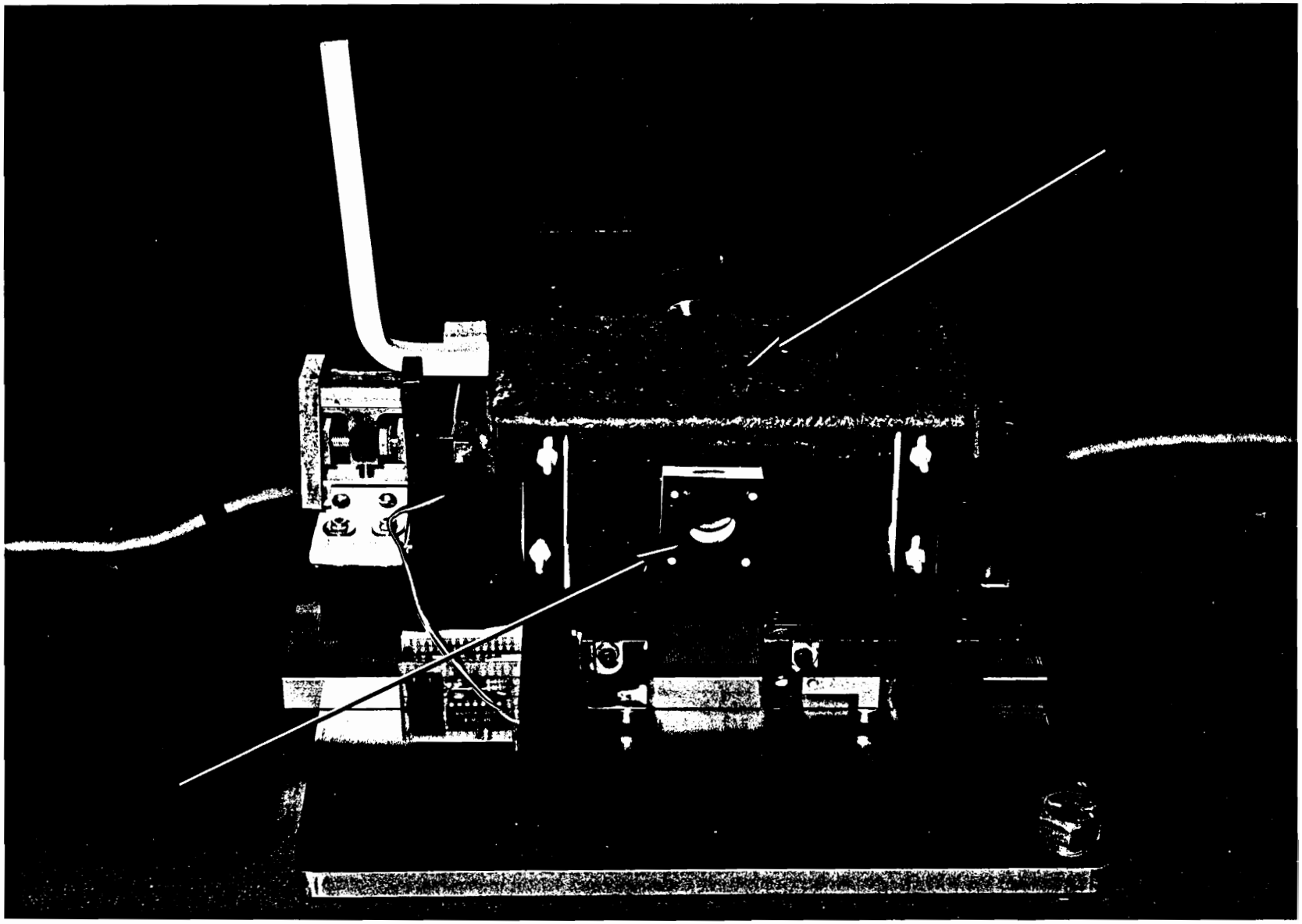

Figure 4.5. Thermal Chamber with Stretching Device: (1) Removable lid and (2) Teflon holder for salt plate window

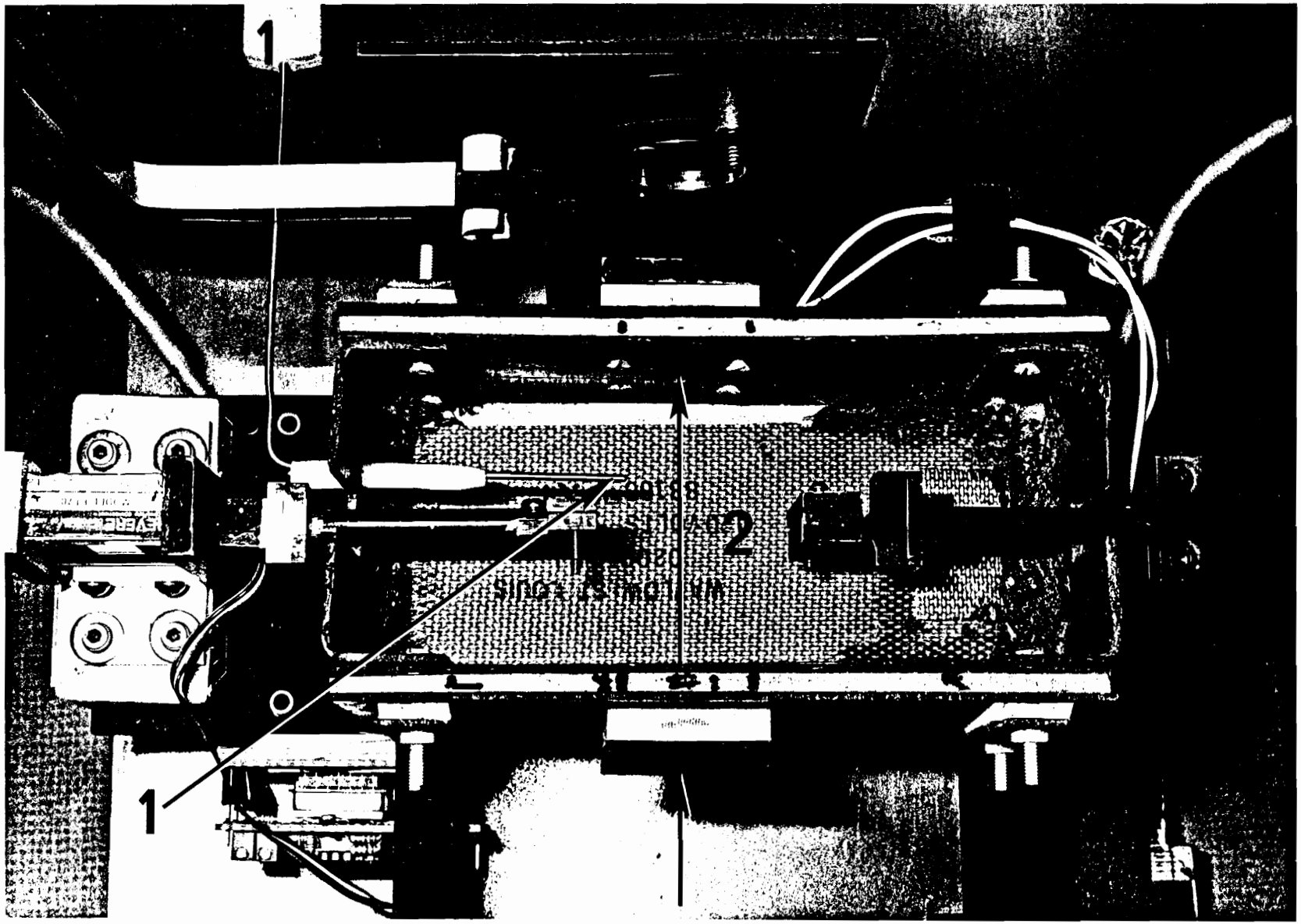

Figure 4.6. Top View of Thermal Chamber with Stretching Device: (1) thermocouple and (2) flexible heater

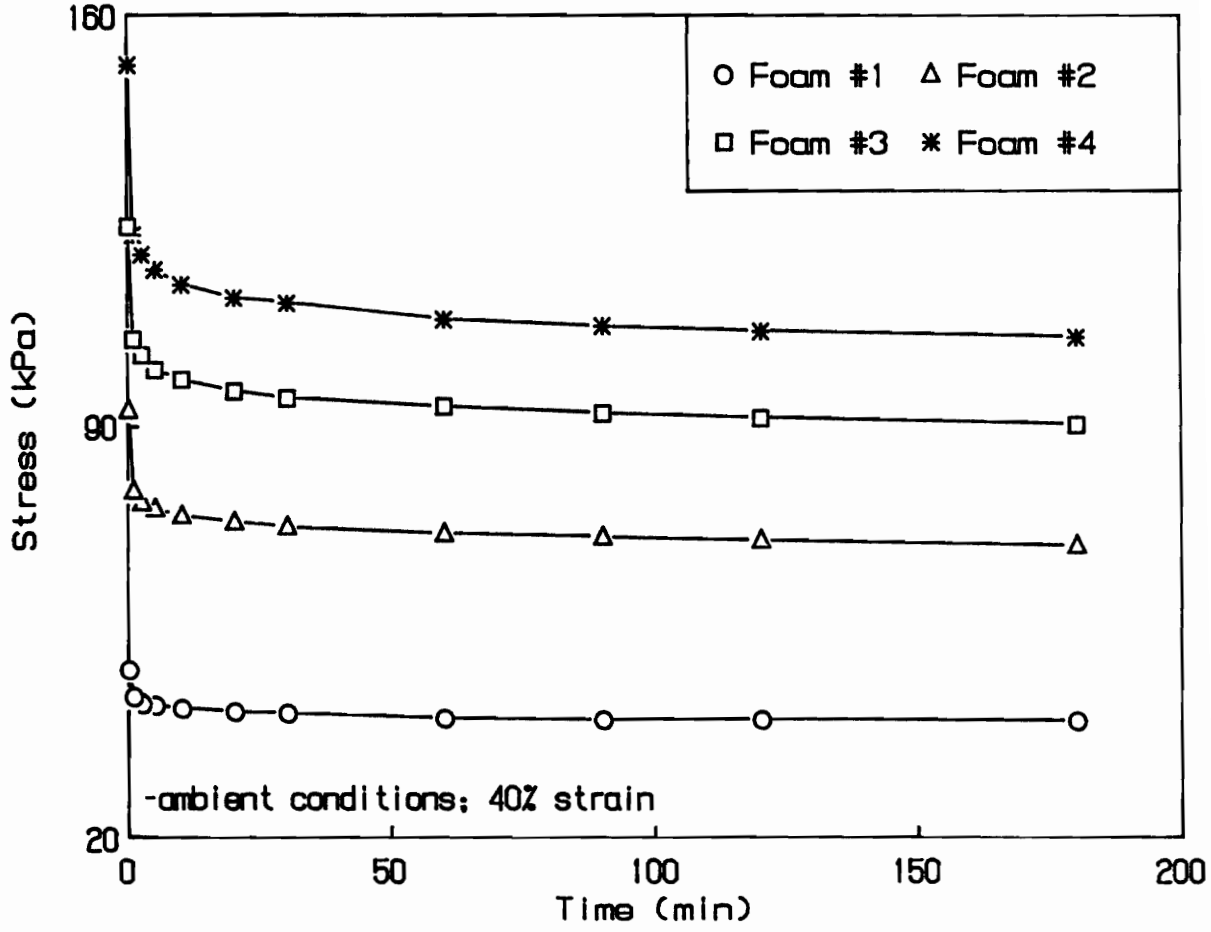

Figure 5.1. Stress Relaxation Behavior for Foams 1-4 Stretched Parallel to Blow Direction: Stress values have been multiplied by density factors to adjust for differences in density of the foams

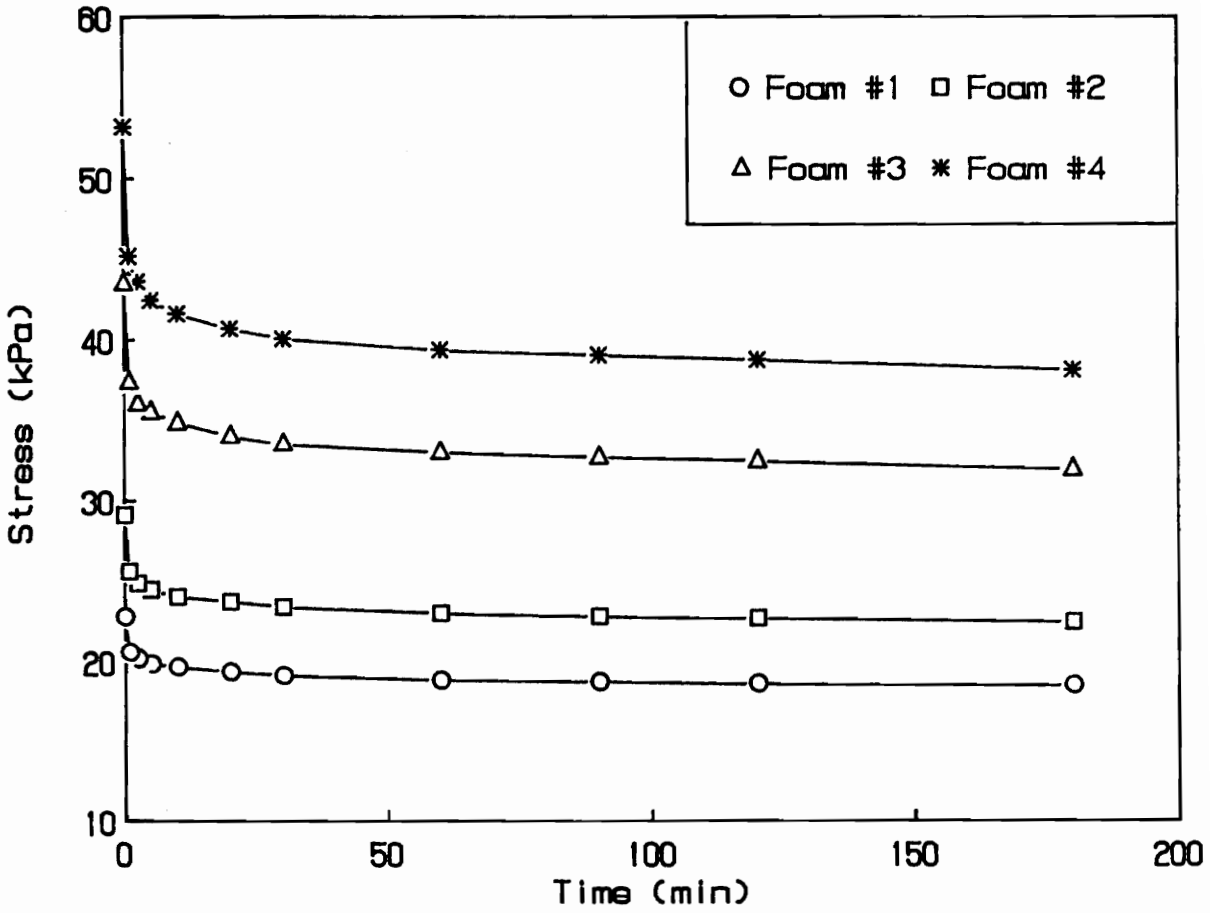

Figure 5.2. Stress Relaxation Behavior for Foams 1-4 Stretched Perpendicular to Blow Direction

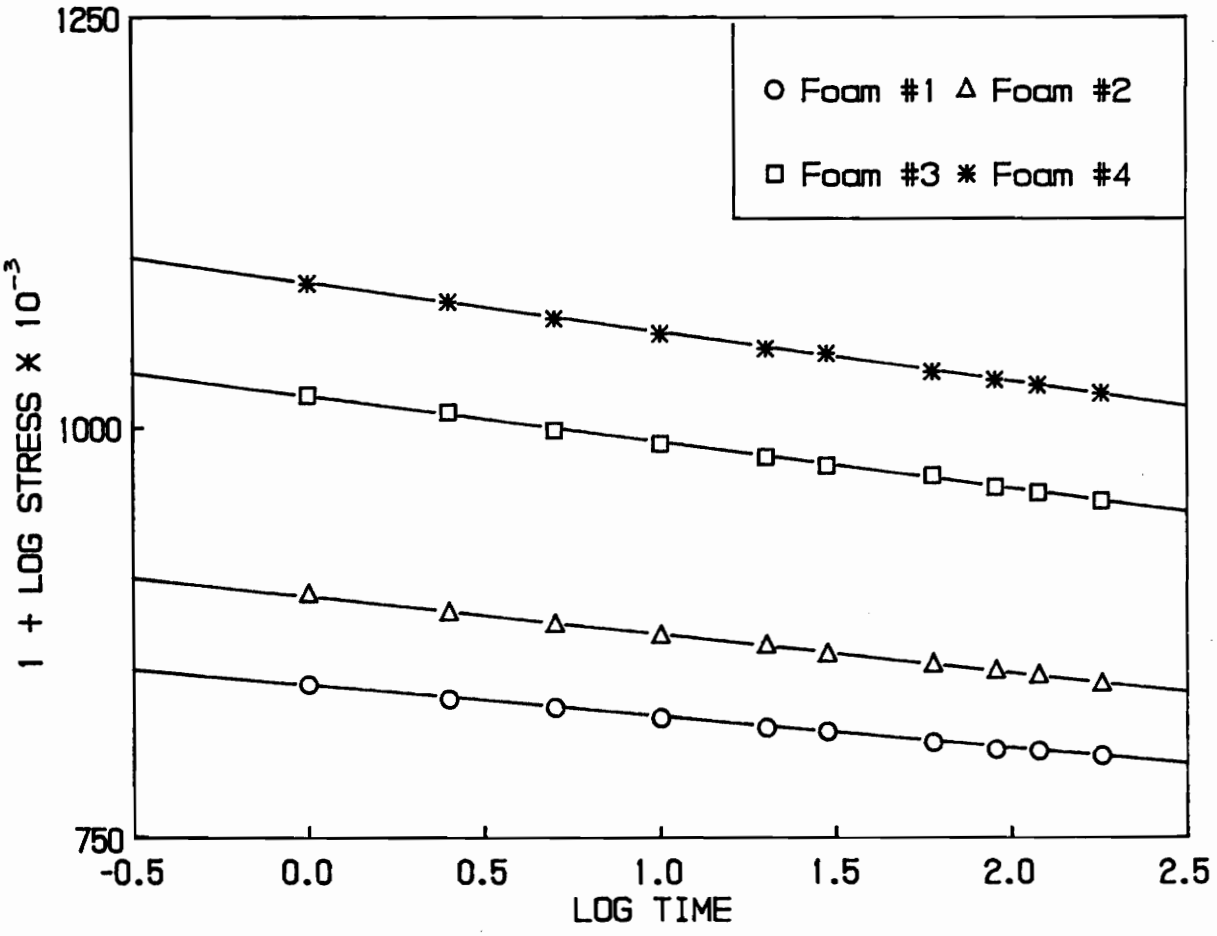

Figure 5.3. Linearized Stress Relaxation Behavior for Foams 1-4: For foams stretched parallel to blow axis

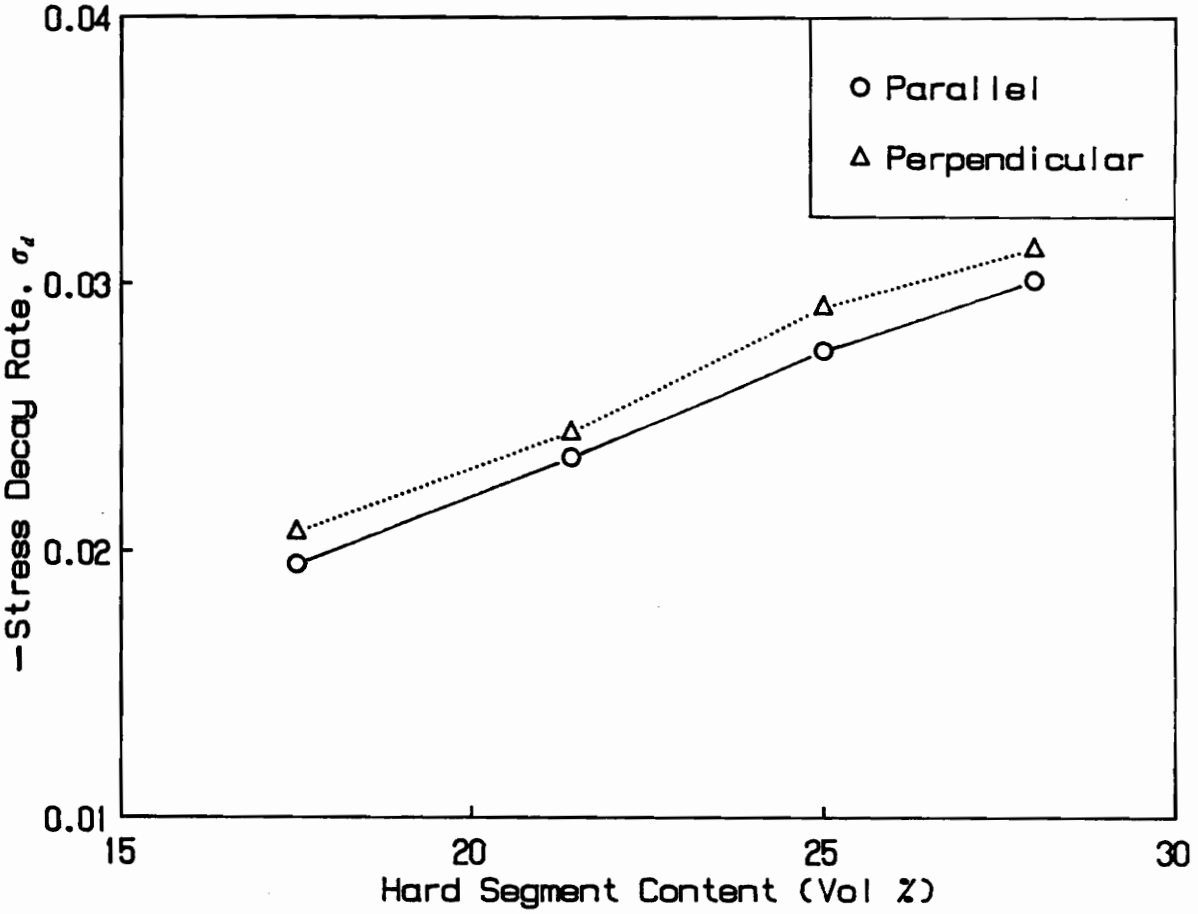

Figure 5.4. Effect of Hard Segment Content on Stress Decay Rates for Foams 1-4

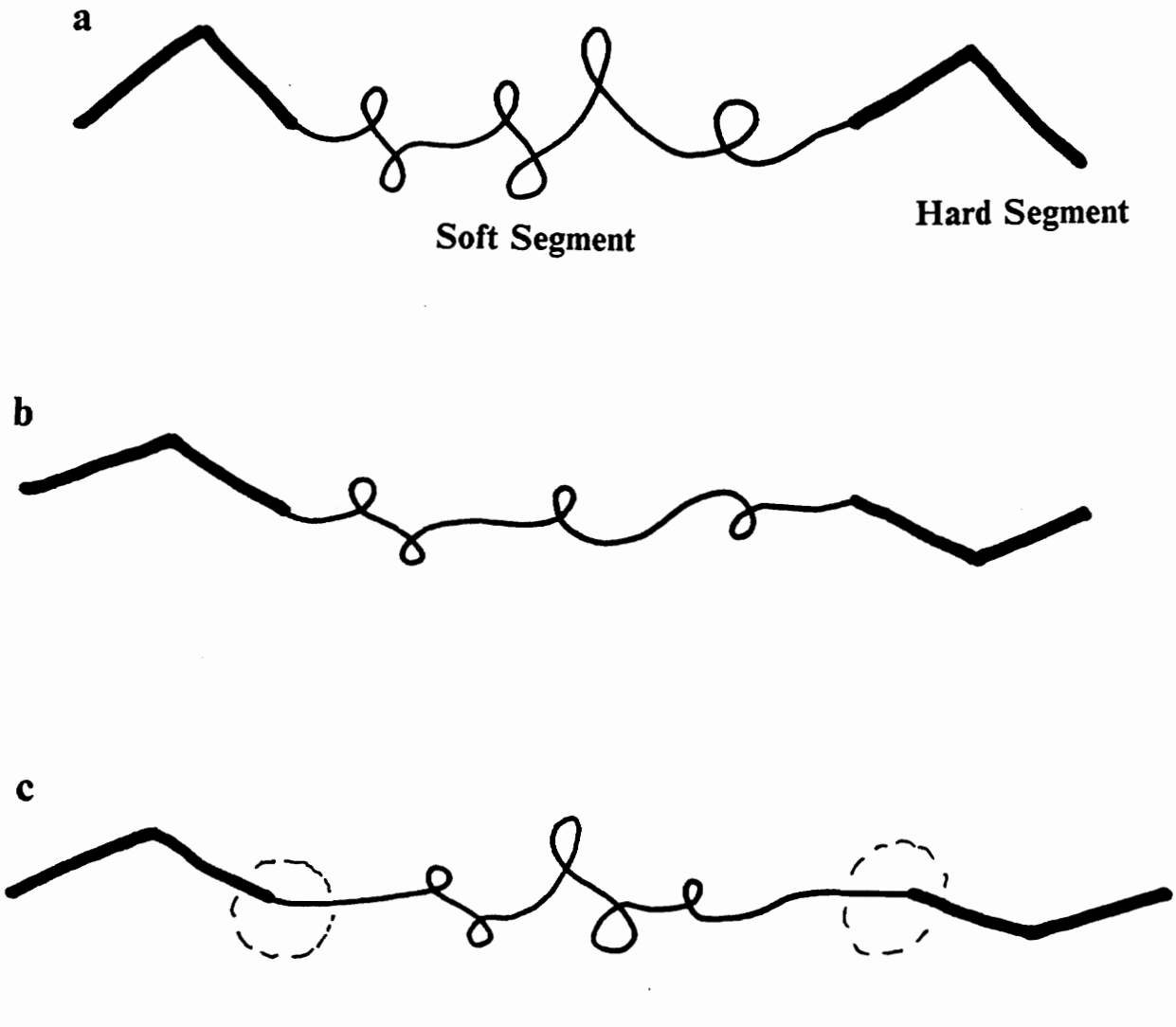

Figure 5.5. **Proposed Mechanism for Local Strain on Soft Segments during Stress Relaxation:** (a) zero deformation, (b) immediately after reaching a constant level of deformation and (c) some time after reaching a constant level of deformation (dotted circles indicate localized area of strain)

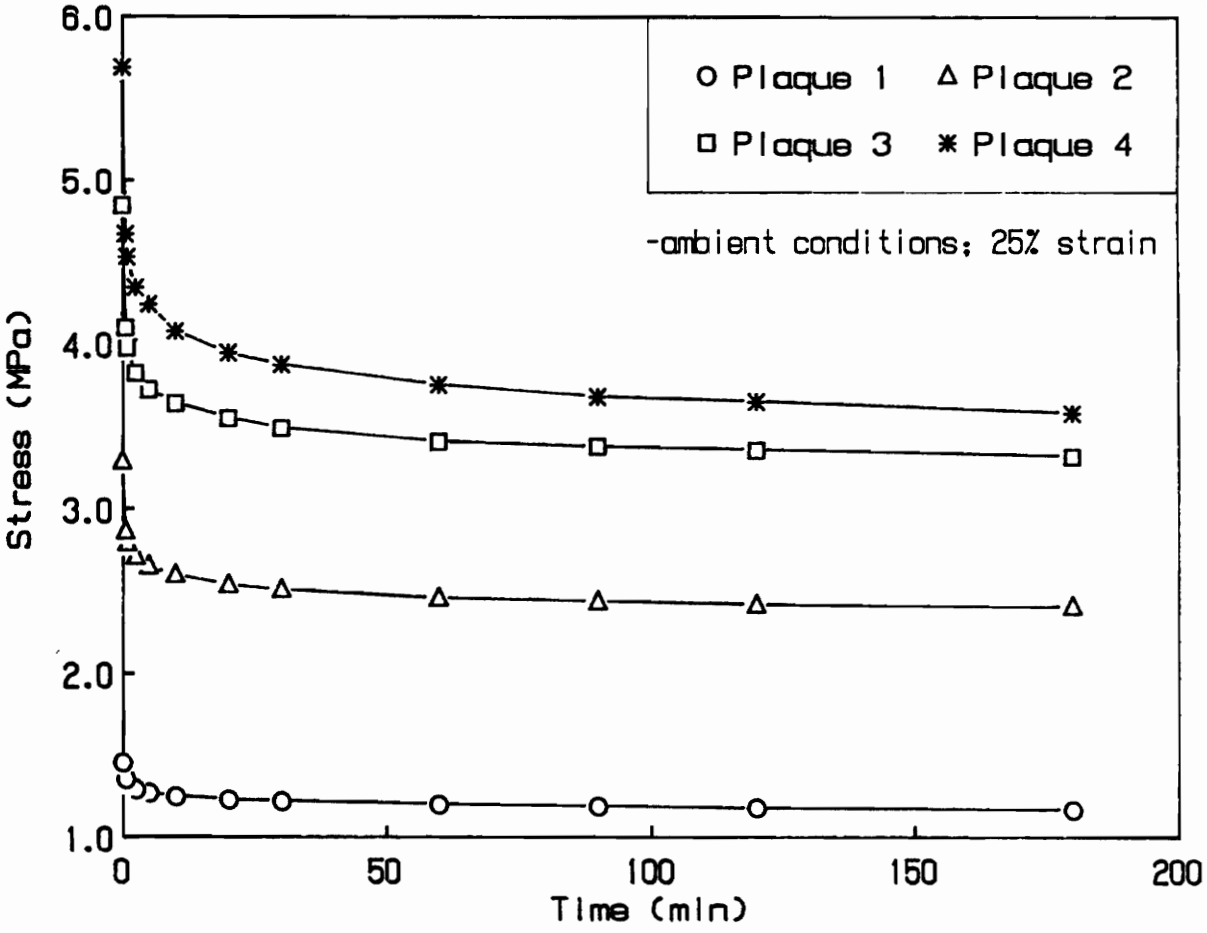

Figure 5.6. Stress Relaxation Behavior for Plaques 1-4

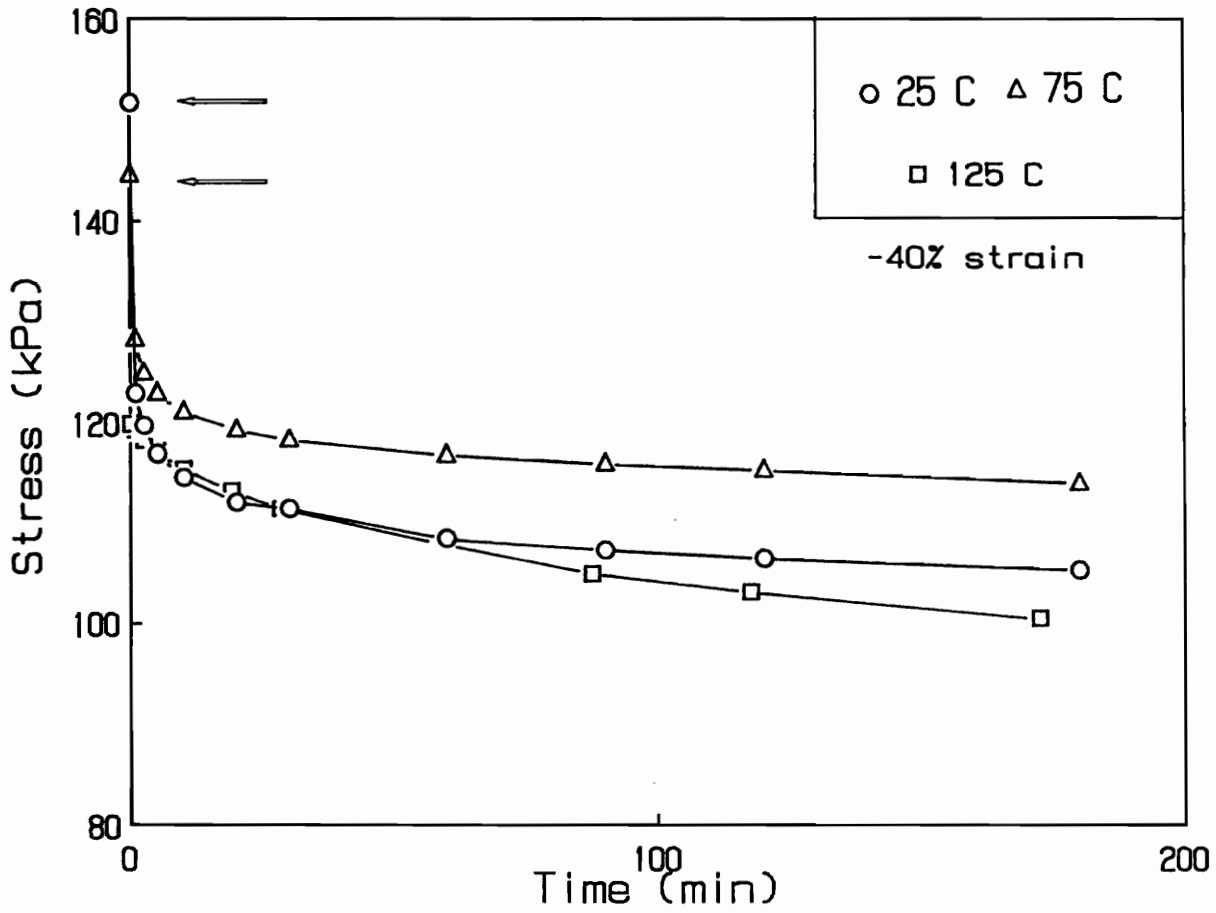

Figure 5.7. Stress Relaxation Behavior for Foam 4 at Different Temperatures: Stretched parallel to blow axis; arrows indicate initial stress levels

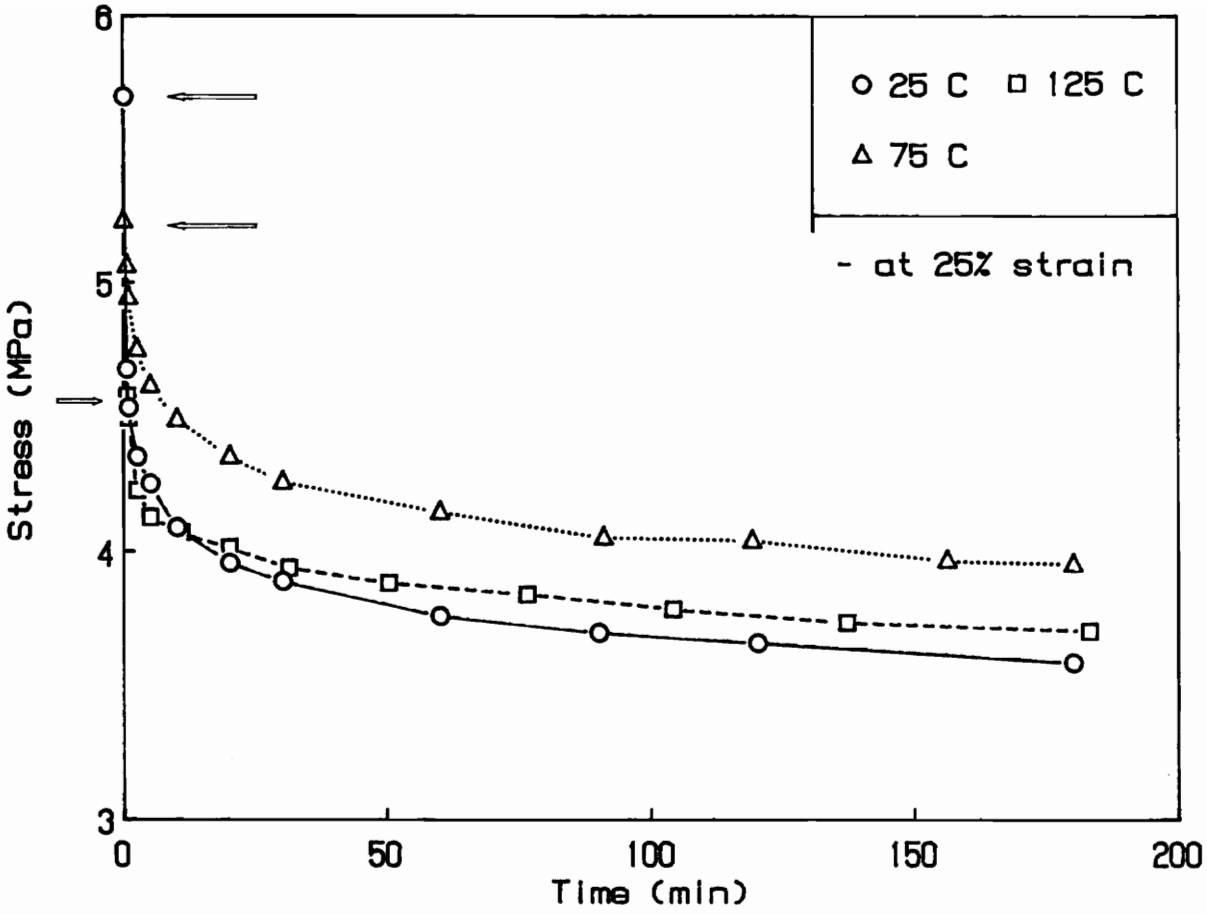

Figure 5.8. **Stress Relaxation Behavior for Plaque 4 at Different Temperatures:** arrows indicate initial stress level

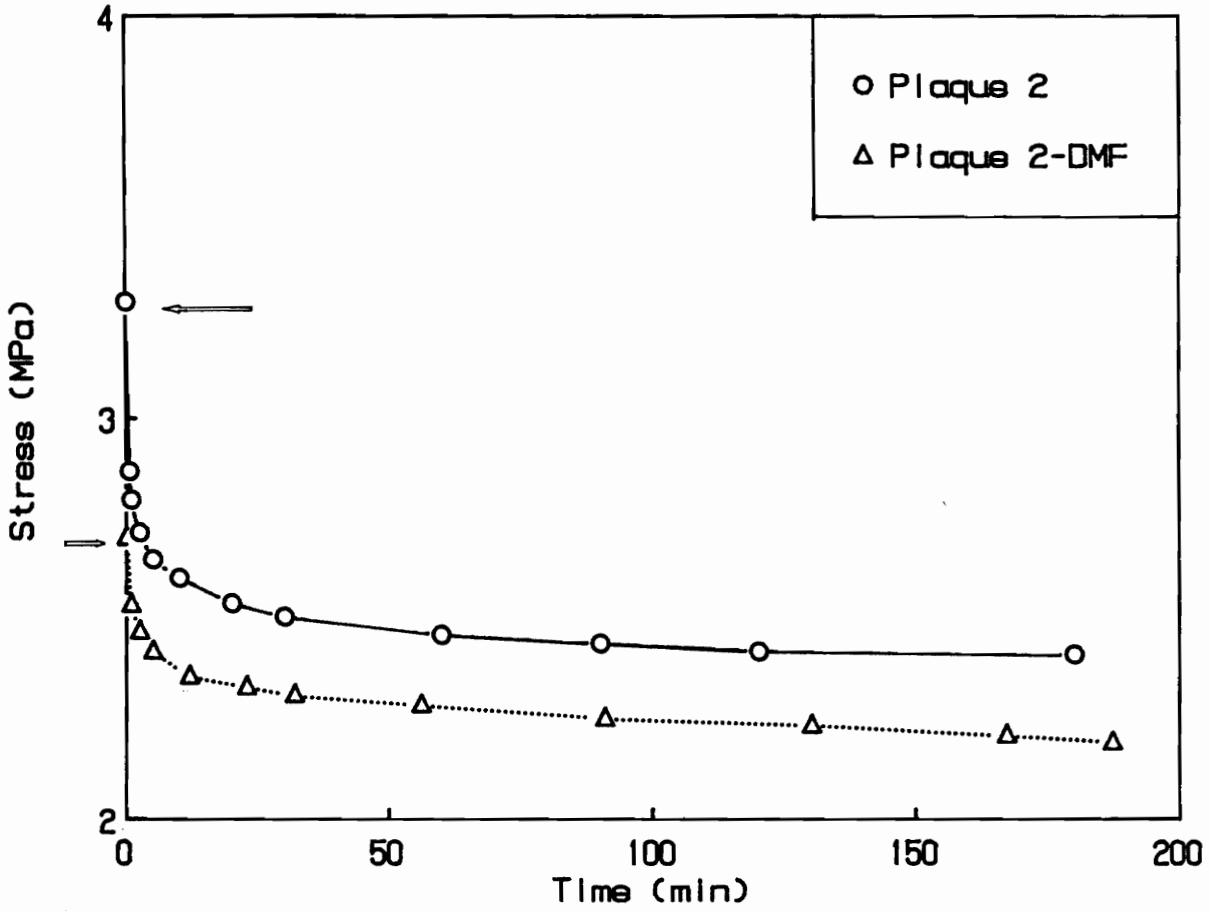

Figure 5.9. Stress Relaxation Behavior for Plaque 2 and Plaque 2-DMF: tests performed at 25 percent strain; arrows indicate initial stress levels

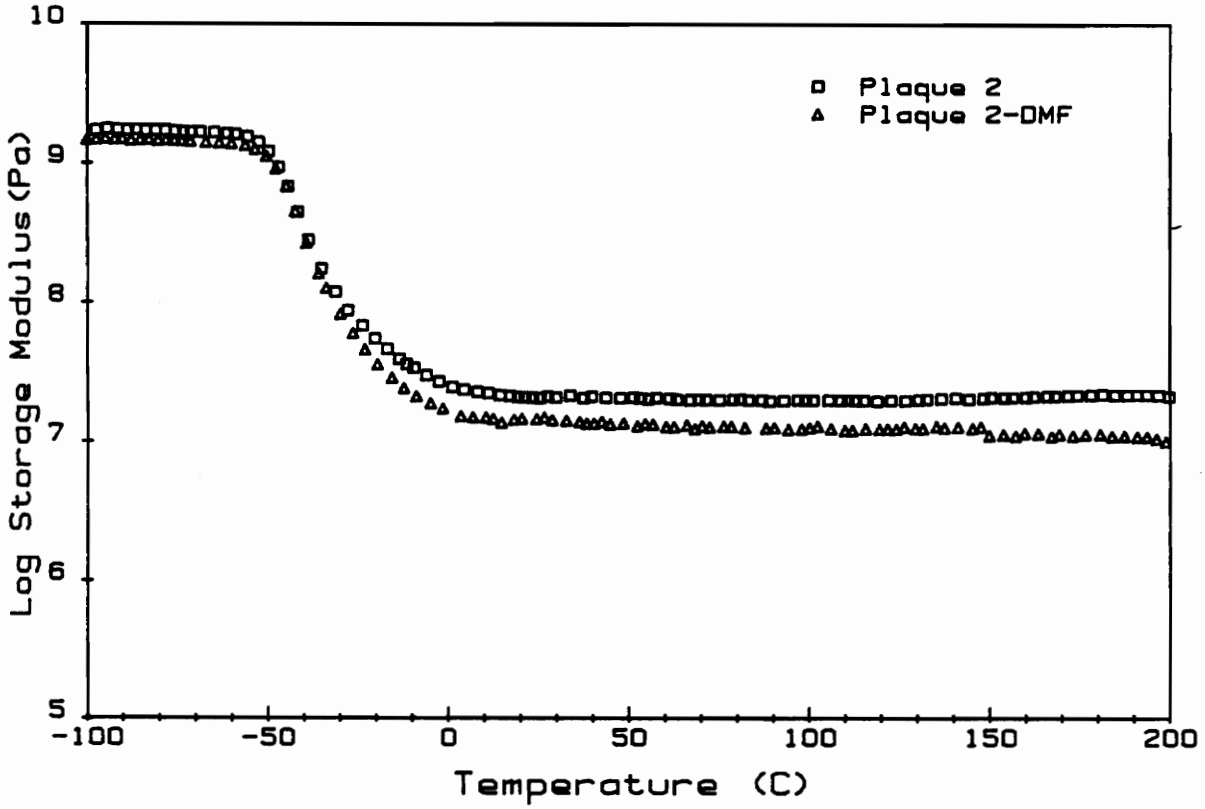

Figure 5.10. Storage Modulus Curves for Plaques 2 and 2-DMF: Frequency is equal to 11 hertz

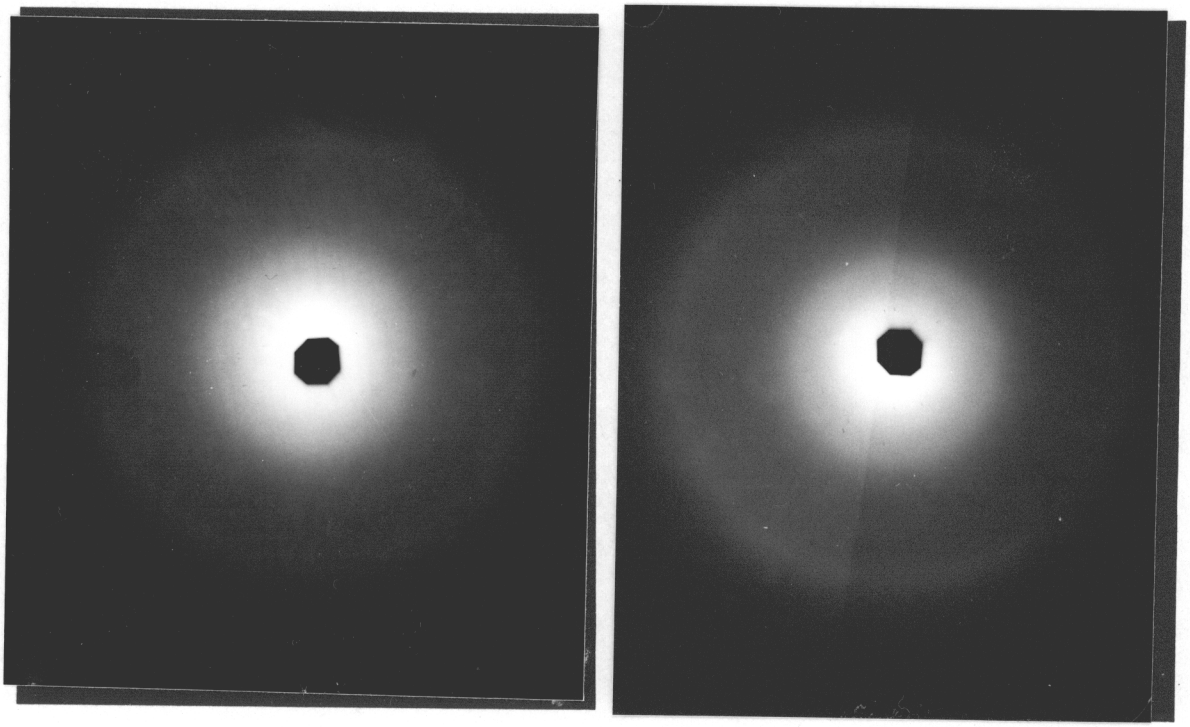

Figure 5.11. WAXS Patterns for Plaques 2(a) and 2-DMF(b)

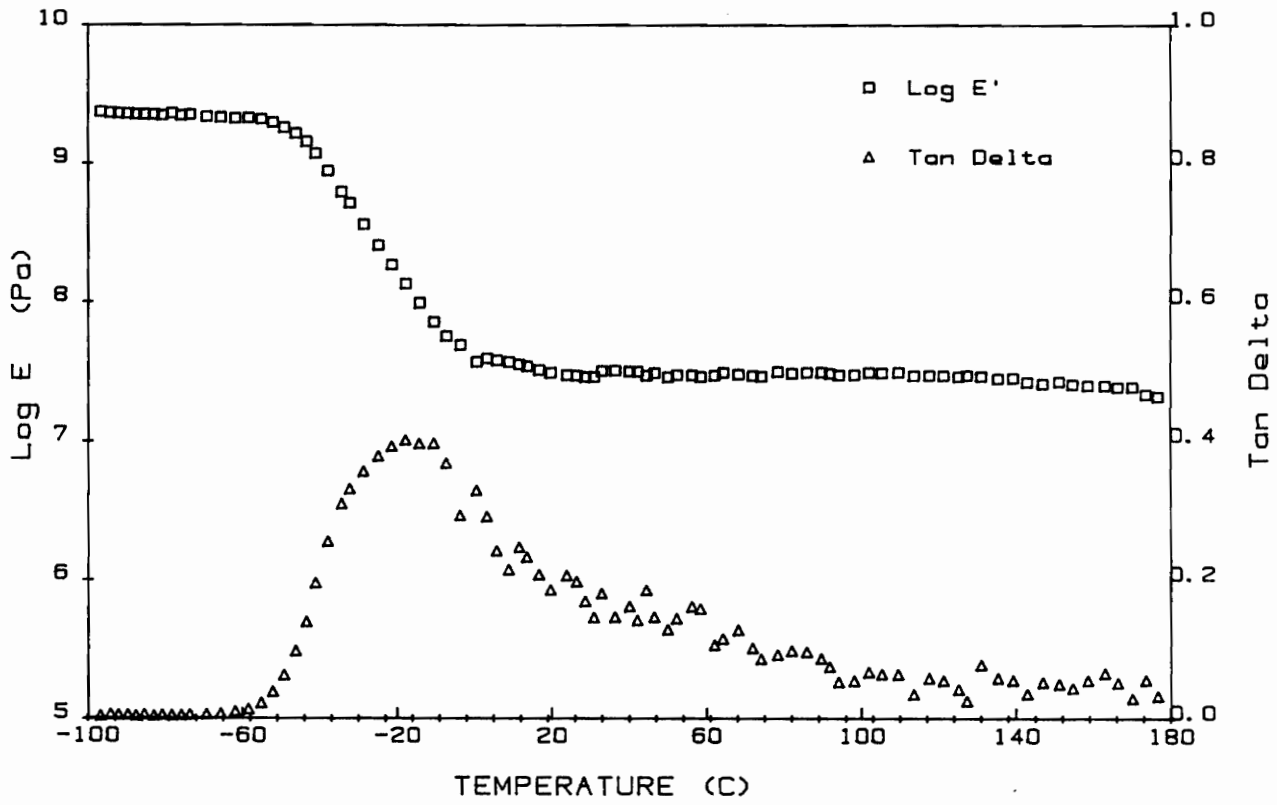

Figure 5.12. Storage Modulus and Tan Delta Curves for the PUUE Elastomer: The frequency is 11 hertz

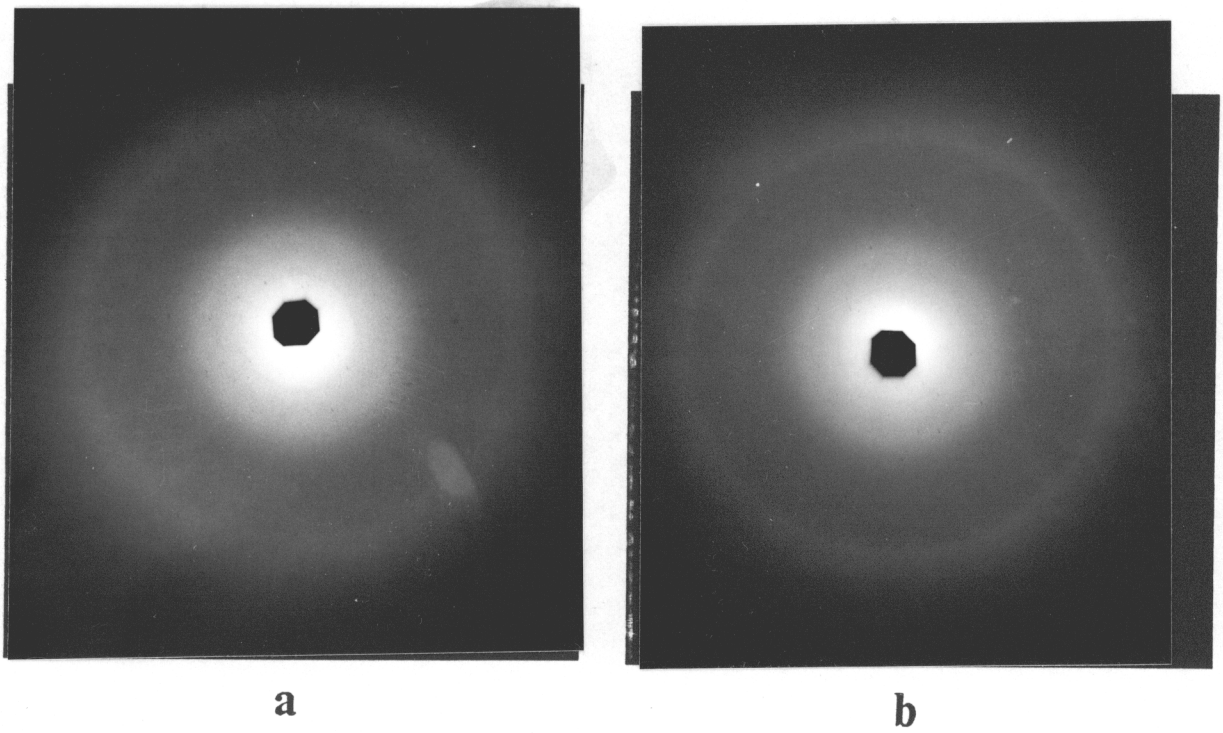

Figure 5.13. WAXS Patterns for the PUUE Elastomer(a) and for Plaque 3(b)

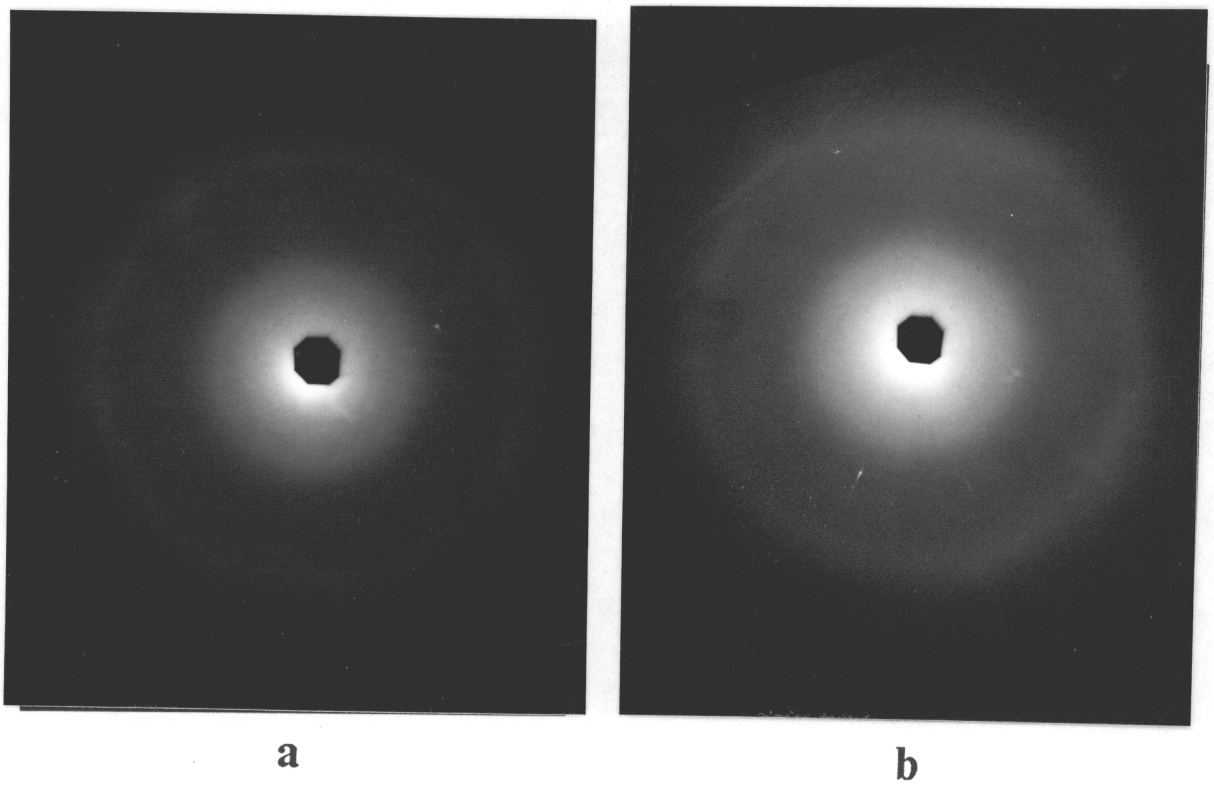

Figure 5.14. WAXS Patterns for Plaques 1-lc(a) and 3-lc(b)

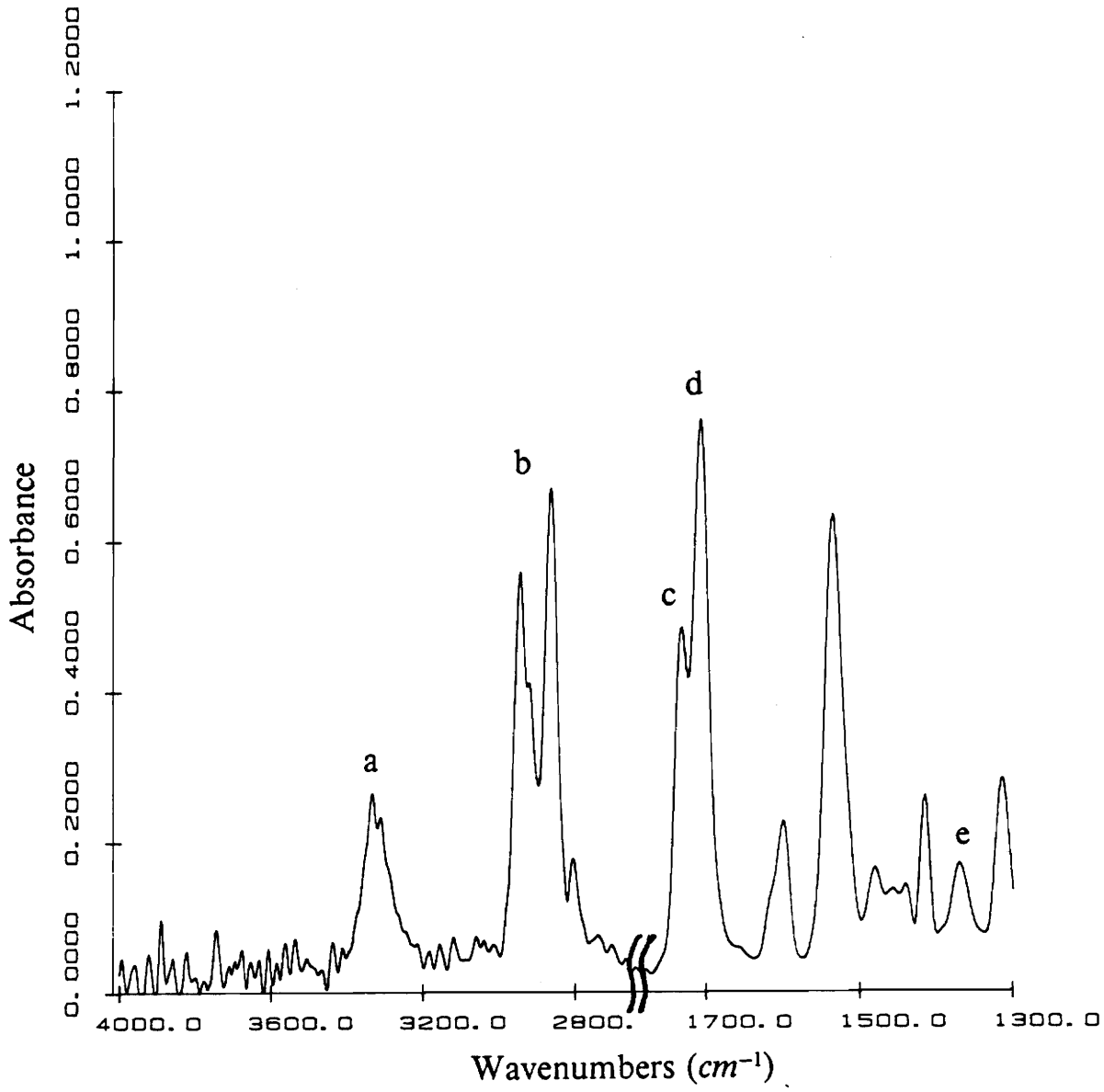

Figure 5.15. **Infrared Spectrum of a Polyether Urethane Elastomer:** ET-2000-30 (ESTANE®) cast film; absorbing groups are (a) $\nu(N-H)$, (b) $\nu(CH_2)$, (c) $\nu(C=O)_f$, (d) $\nu(C=O)_b$ and (e) $\omega(CH_2)$ -for further details see Table 3.1

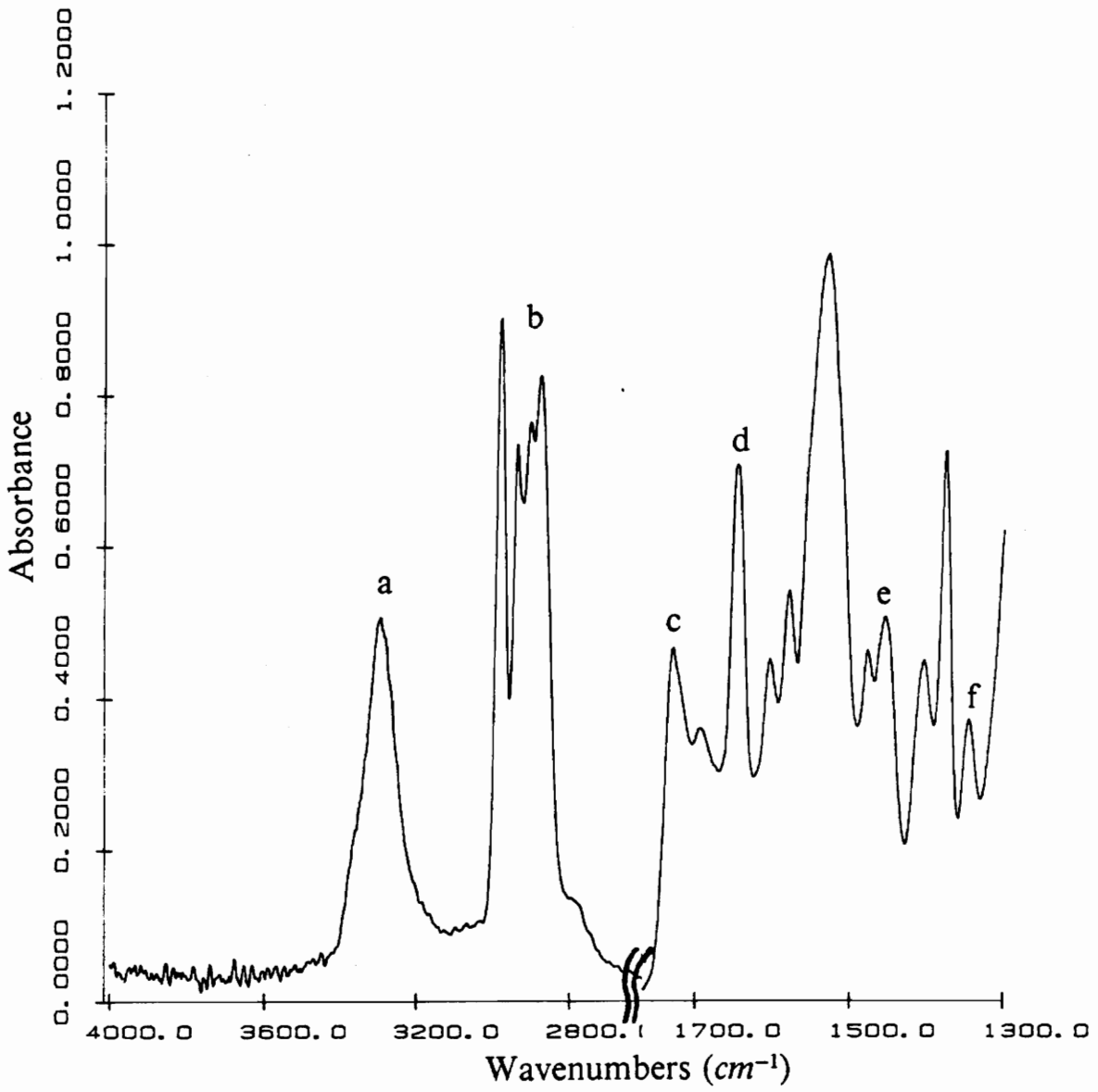

Figure 5.16. **Infrared Spectrum of Polyurea-urethane:** Absorbing groups are (a) $\nu(N-H)$, (b) $\nu(CH_2)$, (c) $(C=O)_f$, (d) $(C=O)_{ur}$, (e) $\delta(CH_2)$ and (f) $\omega(CH_2)$ -for further details see Table 5.4

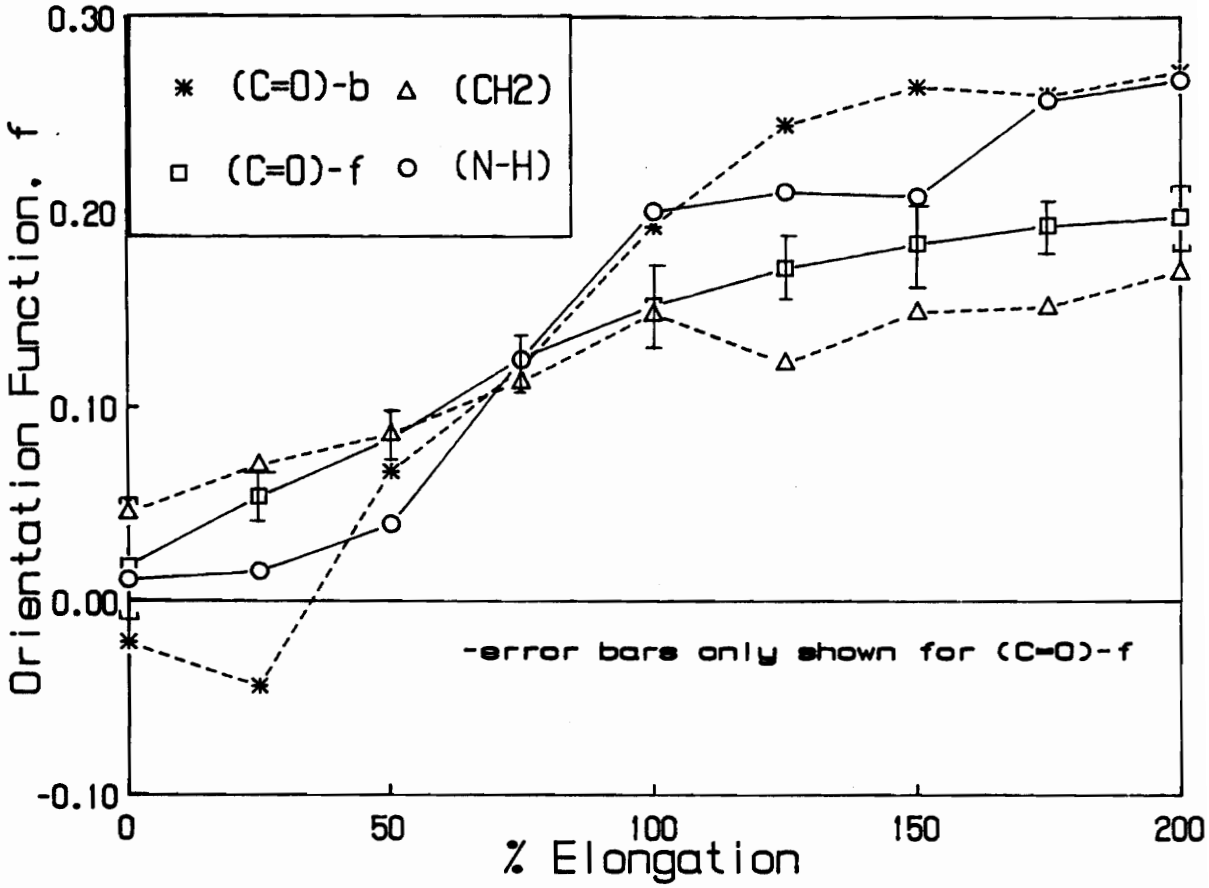

Figure 5.17. Orientation-Elongation Behavior for ET-2000-30: Carried out in 25 percent increments of strain with an extension rate equal to 600 %/min

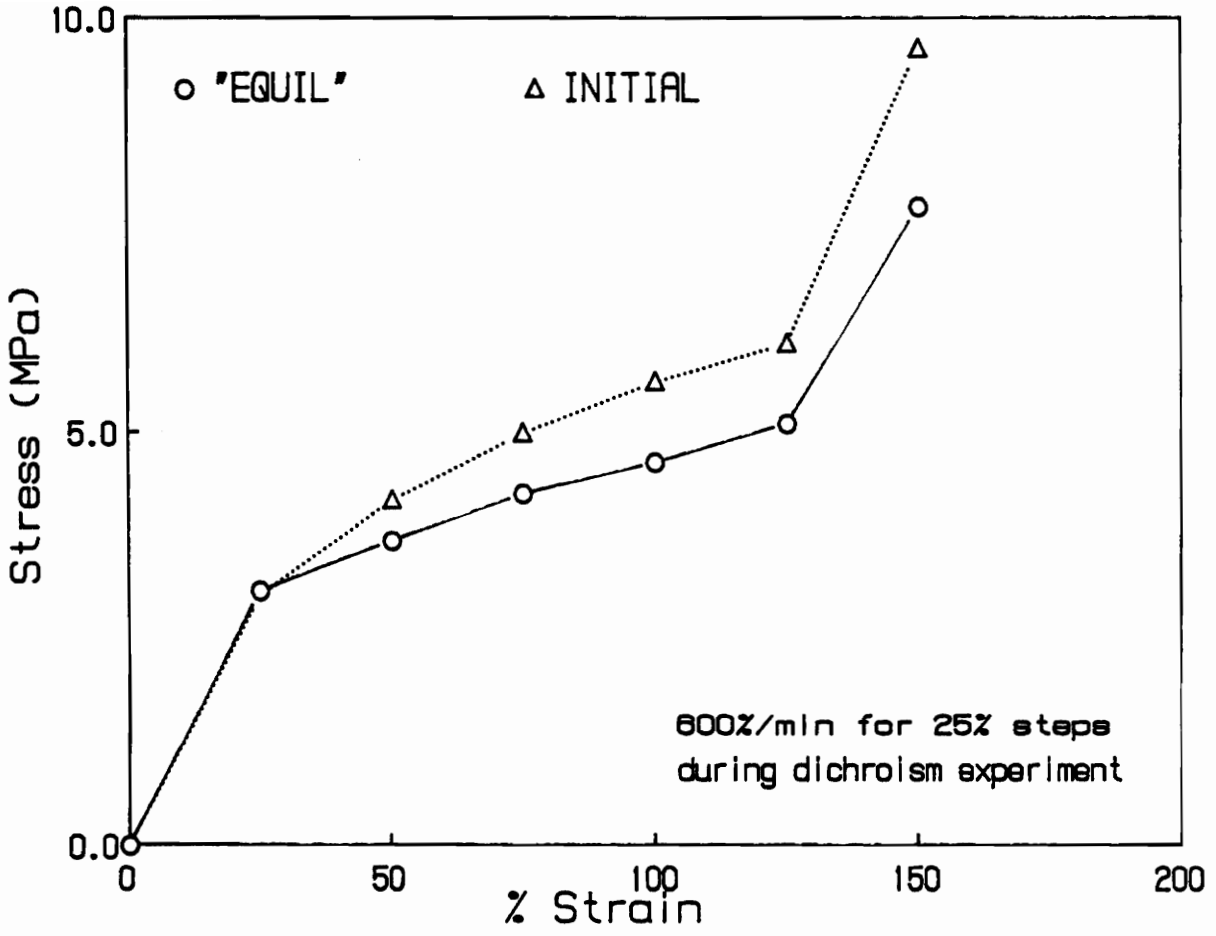

Figure 5.18. Simultaneous Stress-Strain Behavior for ET-2000-30: stress-strain behavior obtained during orientation- elongation experiment

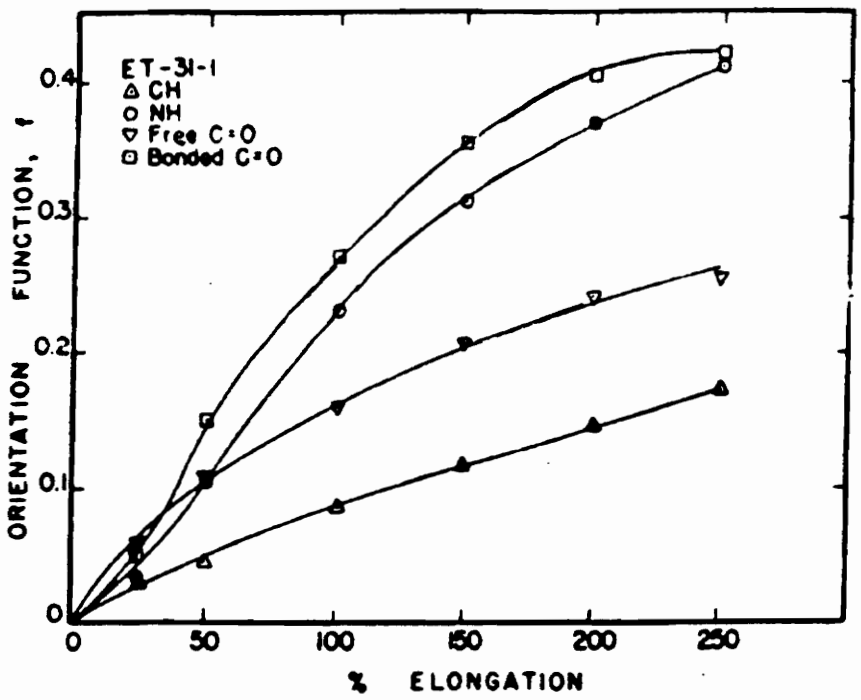

Figure 5.19. **Orientation-Elongation Behavior for ET-1000-31:** taken from ref. 56 for a chemically similar material to that of ET-2000-30

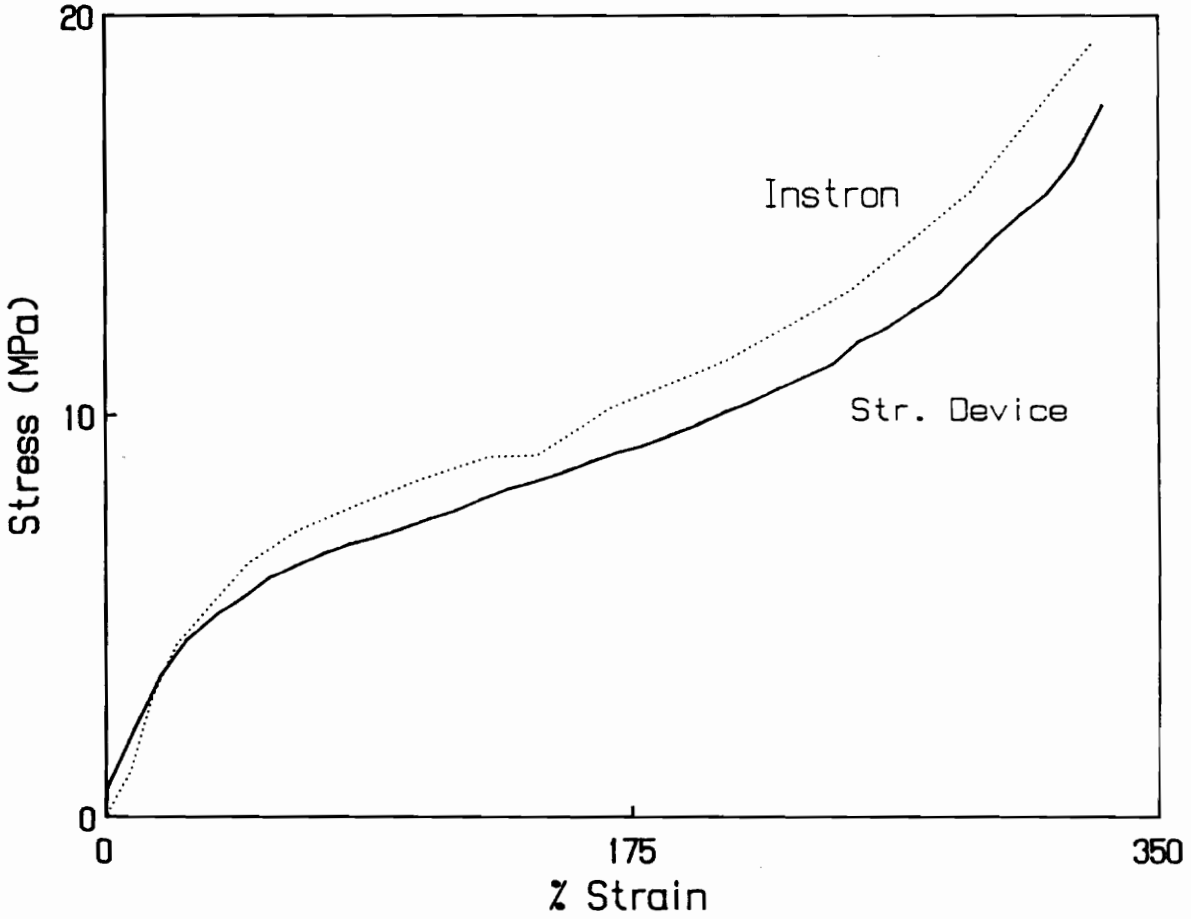

Figure 5.20. Mechanical Evaluation of Stretching Apparatus

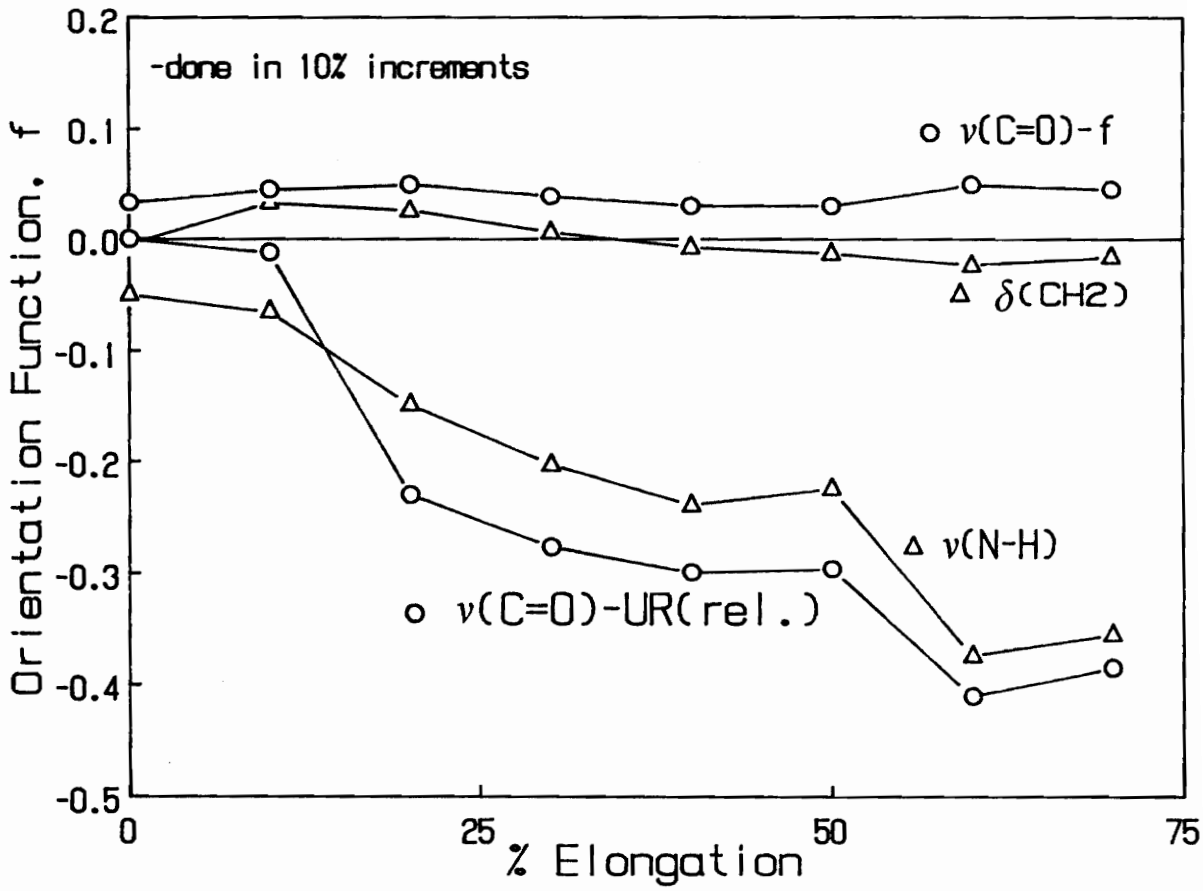

Figure 5.21. Orientation-Elongation Behavior for Plaque 2-DMF: extension rate equal to 400%/min,

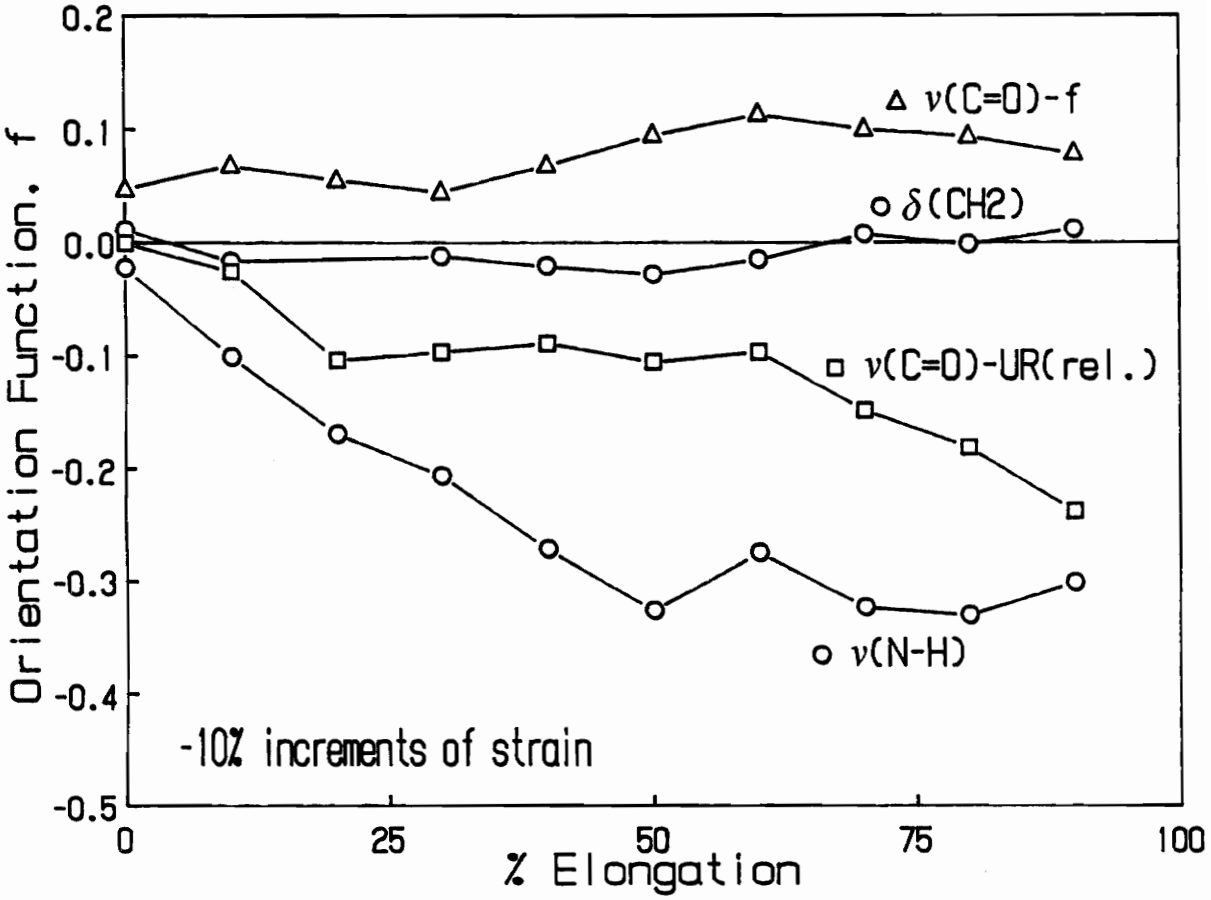

Figure 5.22. **Orientation-Elongation Behavior for Plaque 2-THF:** extension rate equal to 400%/min

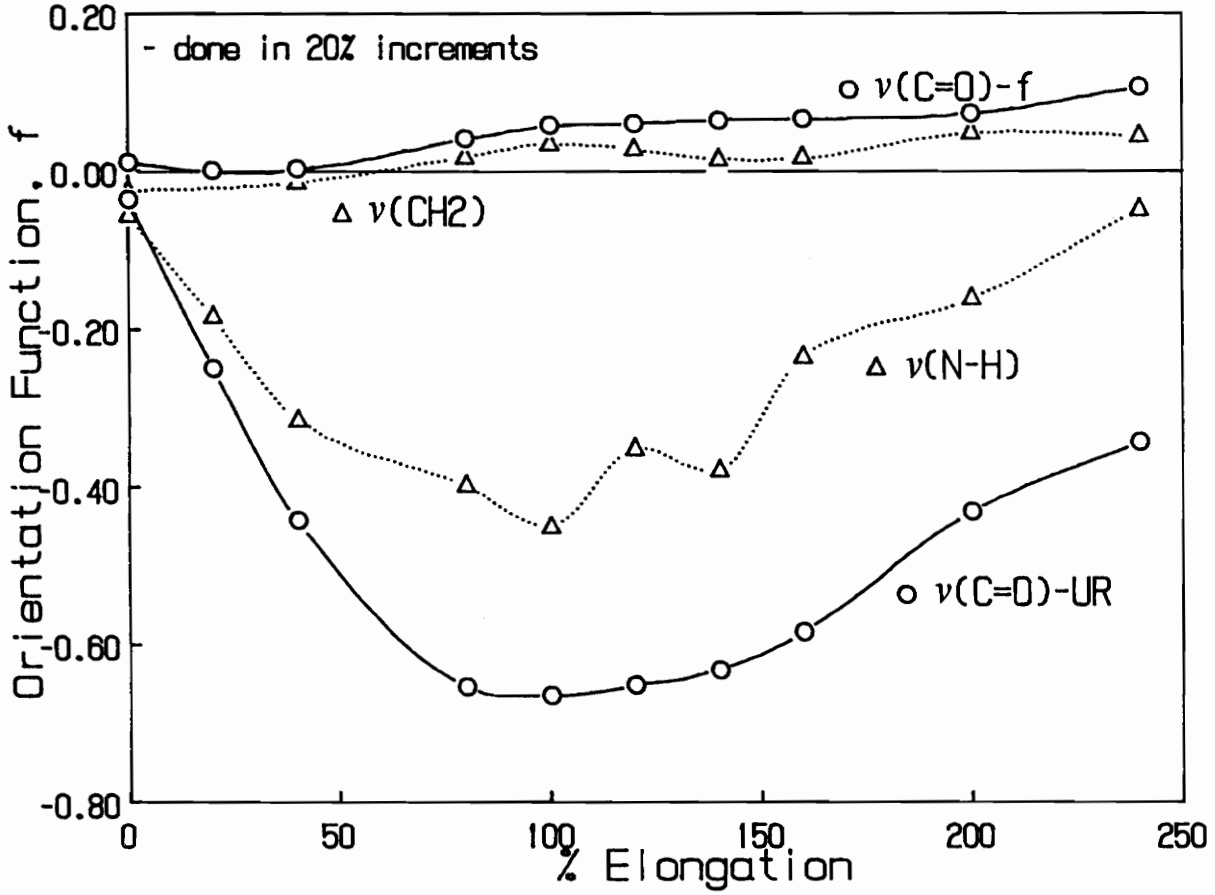

Figure 5.23. **Orientation-Elongation Behavior for PUUE Elastomer:** extension rate equal to 400 %/min

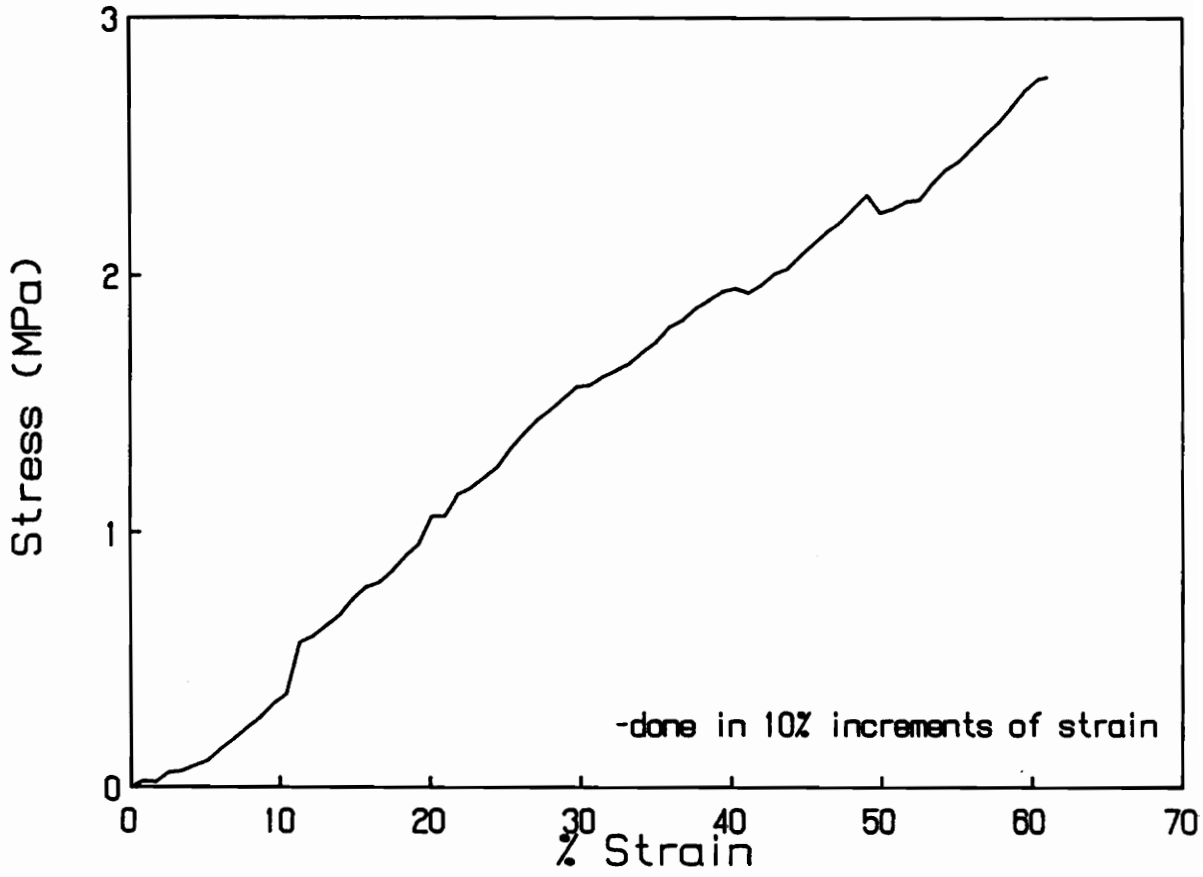

Figure 5.24. **Simultaneous Stress-Strain Behavior for Plaque 2-DMF:** evaluated during orientation elongation test; drop in stress indicates relaxation of sample (due to noise in transducer the stress-strain curve is not very smooth in places)

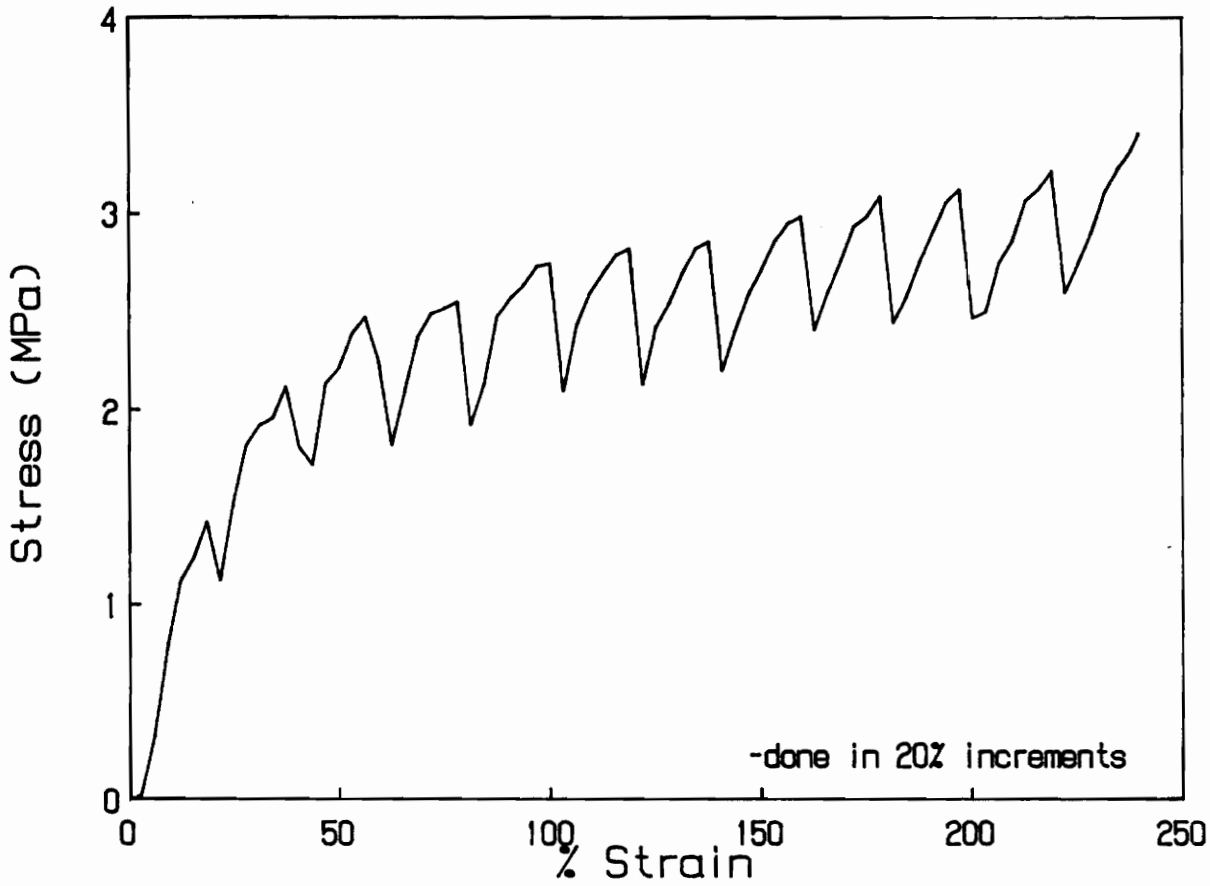

Figure 5.25. Simultaneous Stress-Strain Behavior for PUUE Elastomer: drop in stress indicates relaxation of sample

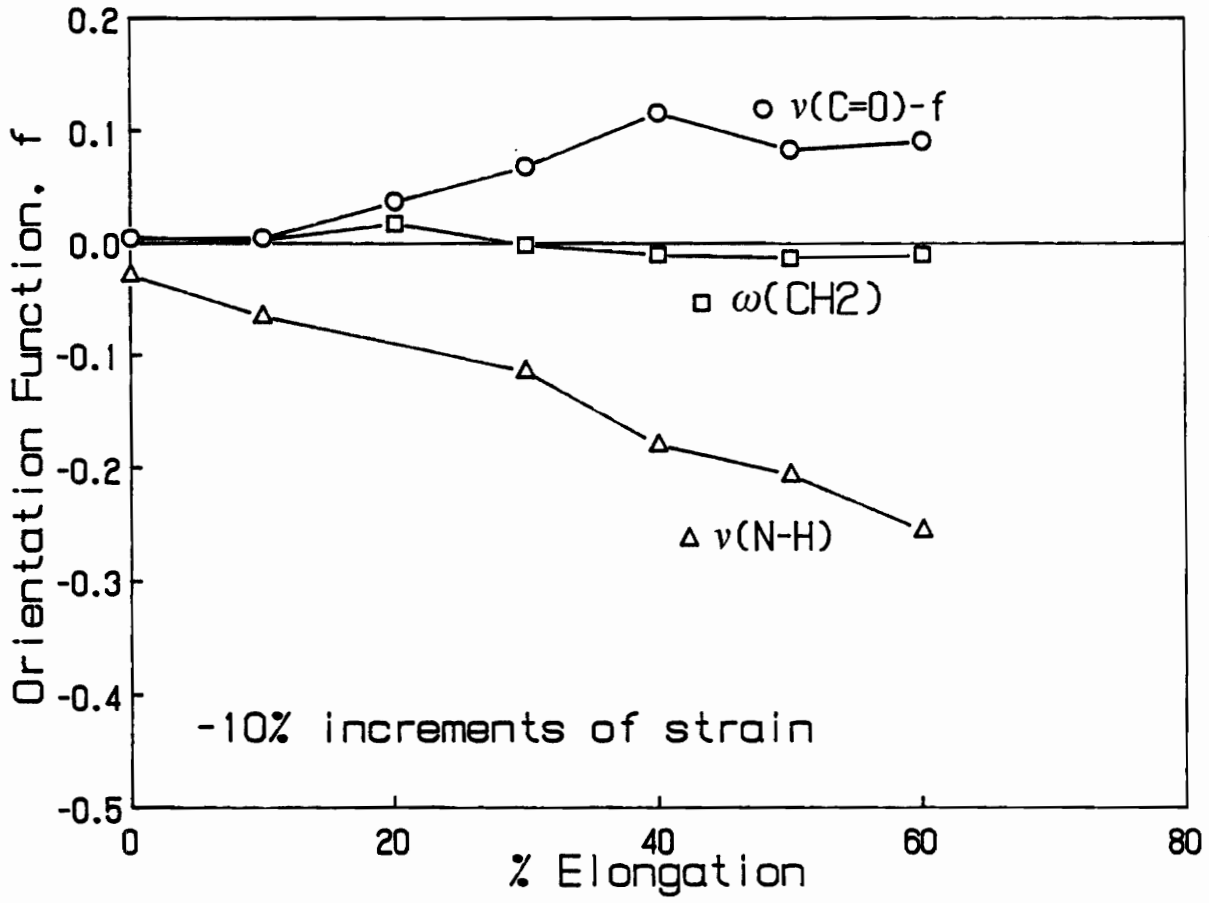

Figure 5.26. Orientation-Elongation Behavior for Plaque 1-THF: extension rate equal to 400 %/min

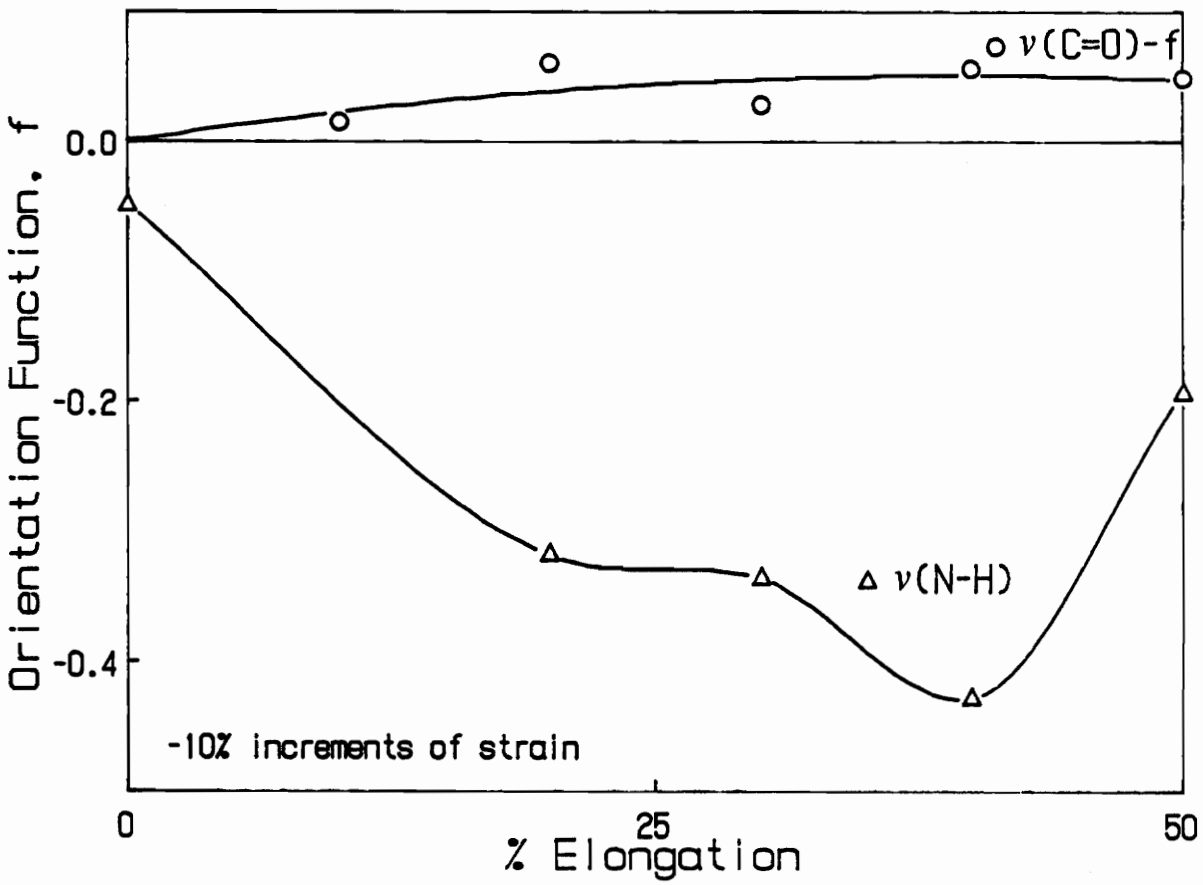

Figure 5.27. Orientation-Elongation Behavior for Plaque 1: extension rate equal to 400%/min

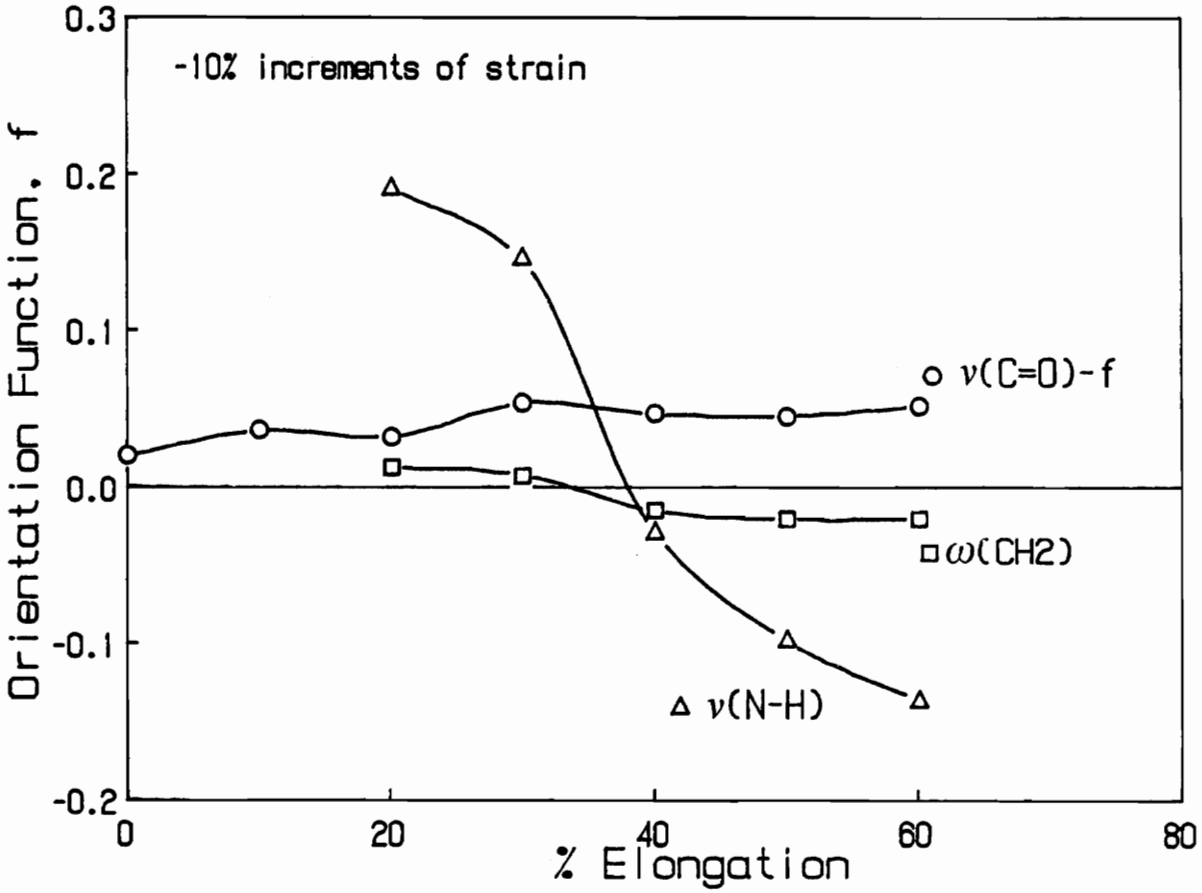

Figure 5.28. **Orientation-Elongation Behavior for Plaque 1-lc(DMF):** $f_{(N-H)}$ and $f_{(CH_2)}$ are not shown at 0% and 10% elongation due to large absorbances; extension rate equal to 400%/min

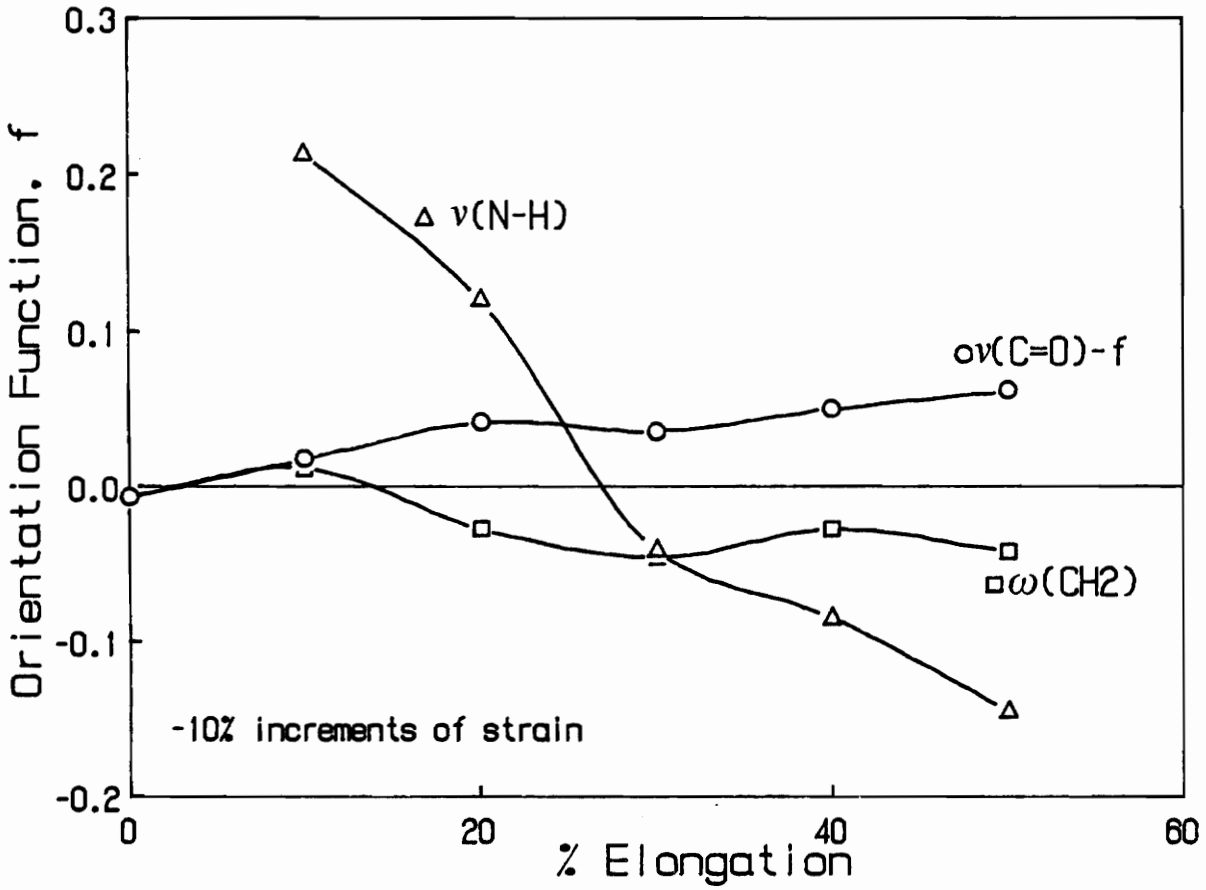

Figure 5.29. **Orientation-Elongation Behavior for Plaque 3-lc:** $f_{(N-H)}$ is not shown at 0% elongation due to large absorbances; extension rate equal to 400%/min

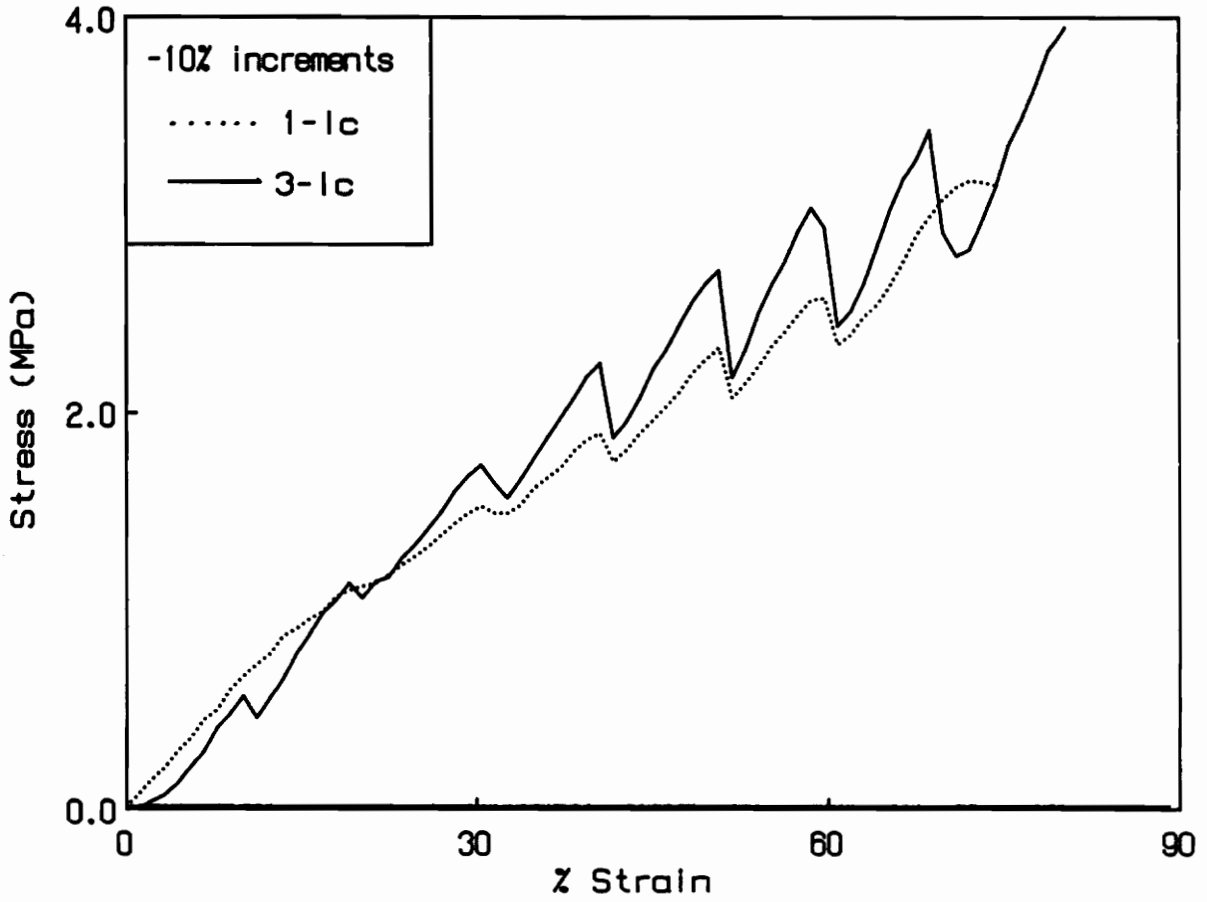

Figure 5.30. Simultaneous Stress-Strain Behavior for Plaques 1-lc(DMF) and 3-lc

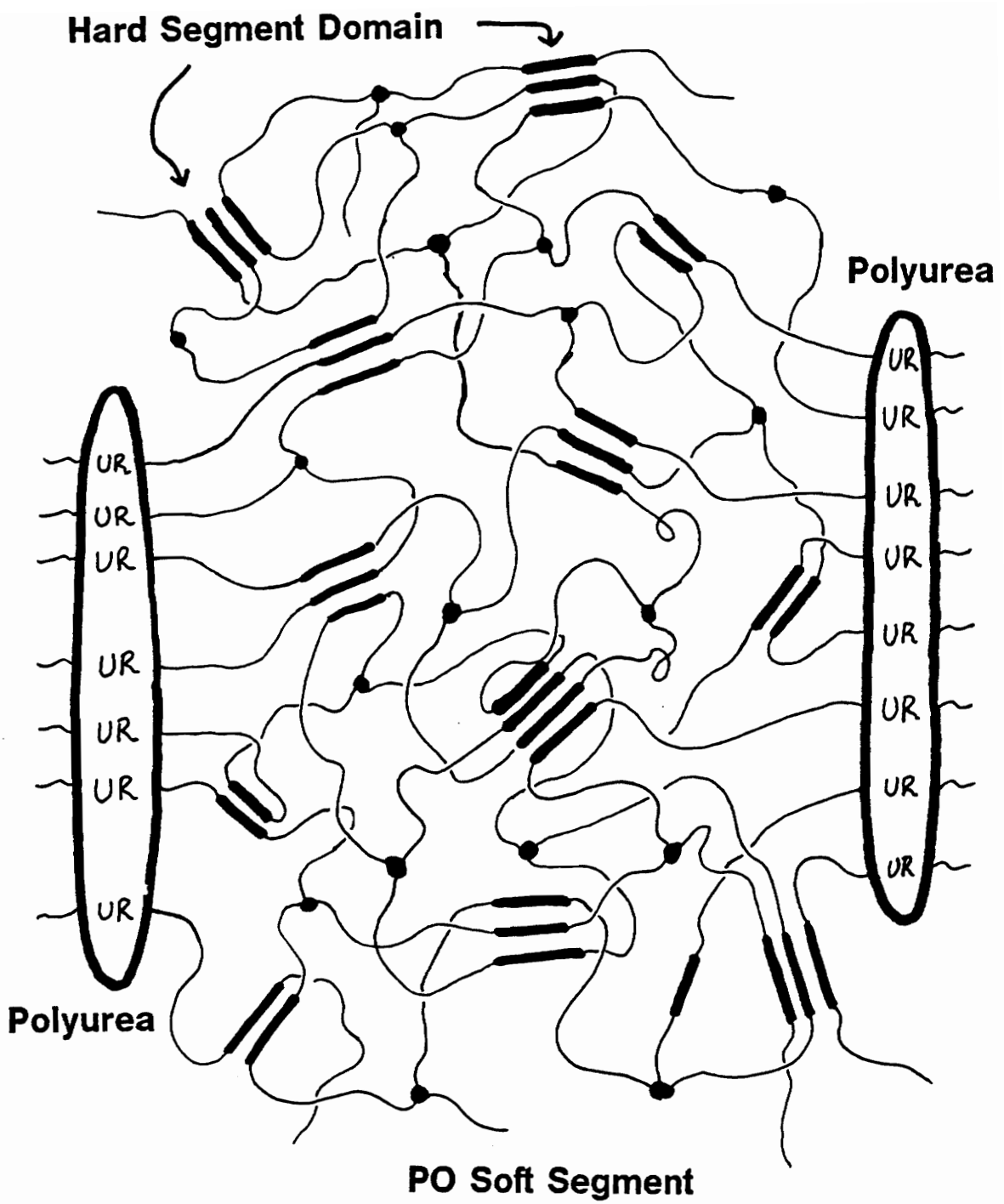

Figure 5.31. **Suggested Modification of Proposed Morphological Model:** earlier model given in Fig. 2.10; the only change suggested is the polyurea aggregates have a more elongated structure

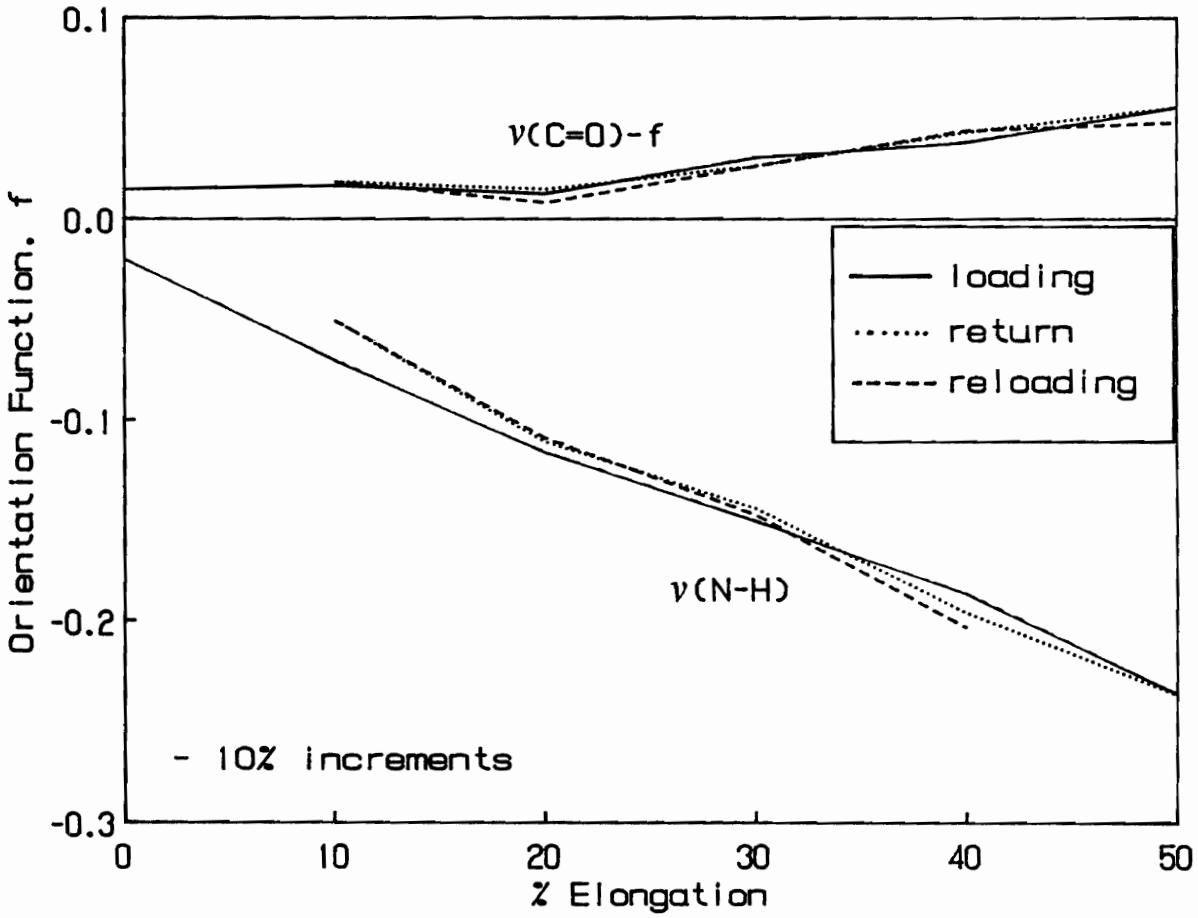

Figure 5.32. **Orientational Hysteresis Behavior for Plaque 2-DMF:** extension rate equal to 400 %/min; $f_{(CH_2)}$ is not shown, but behavior similar to $f_{(C=O)f}$

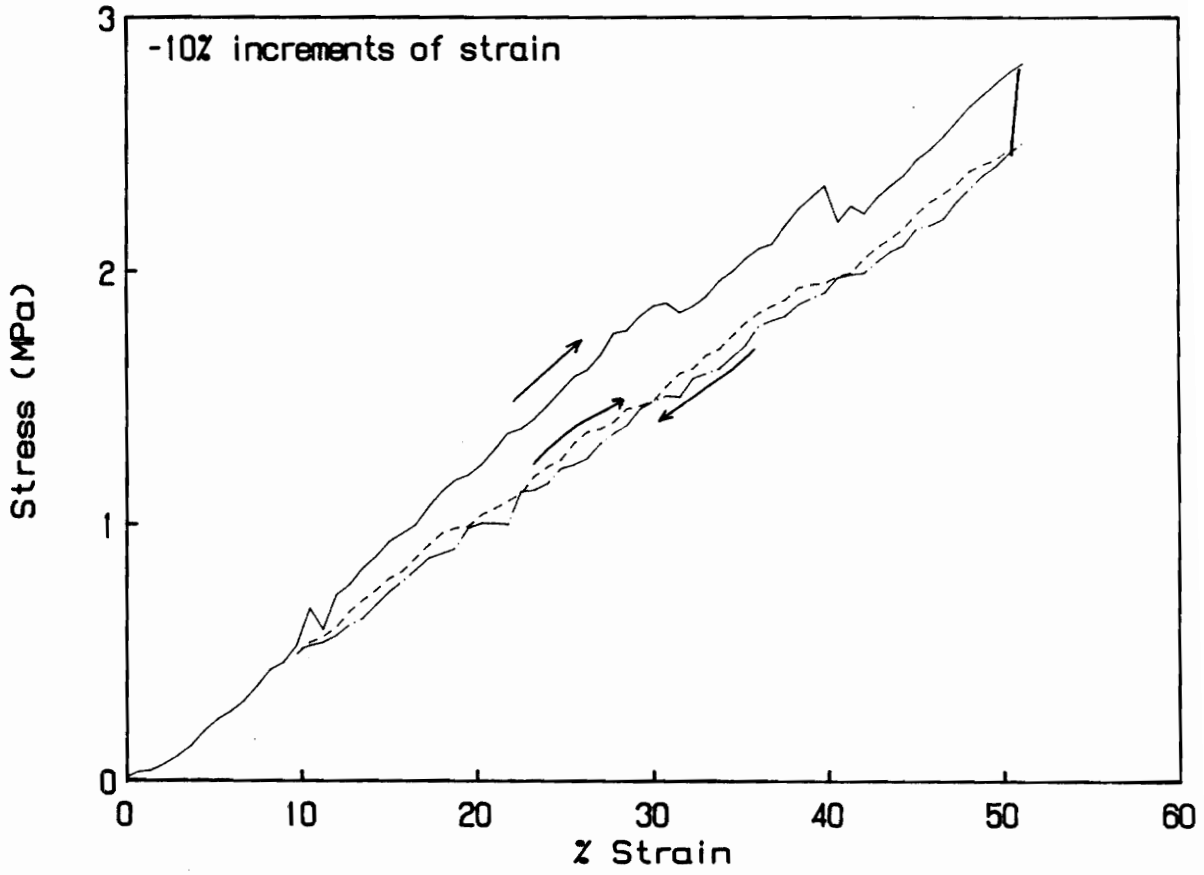

Figure 5.33. **Mechanical Response for Plaque 2-DMF during Cyclic Deformation:** (due to noise in the transducer the stress-strain curve is not smooth in some places)

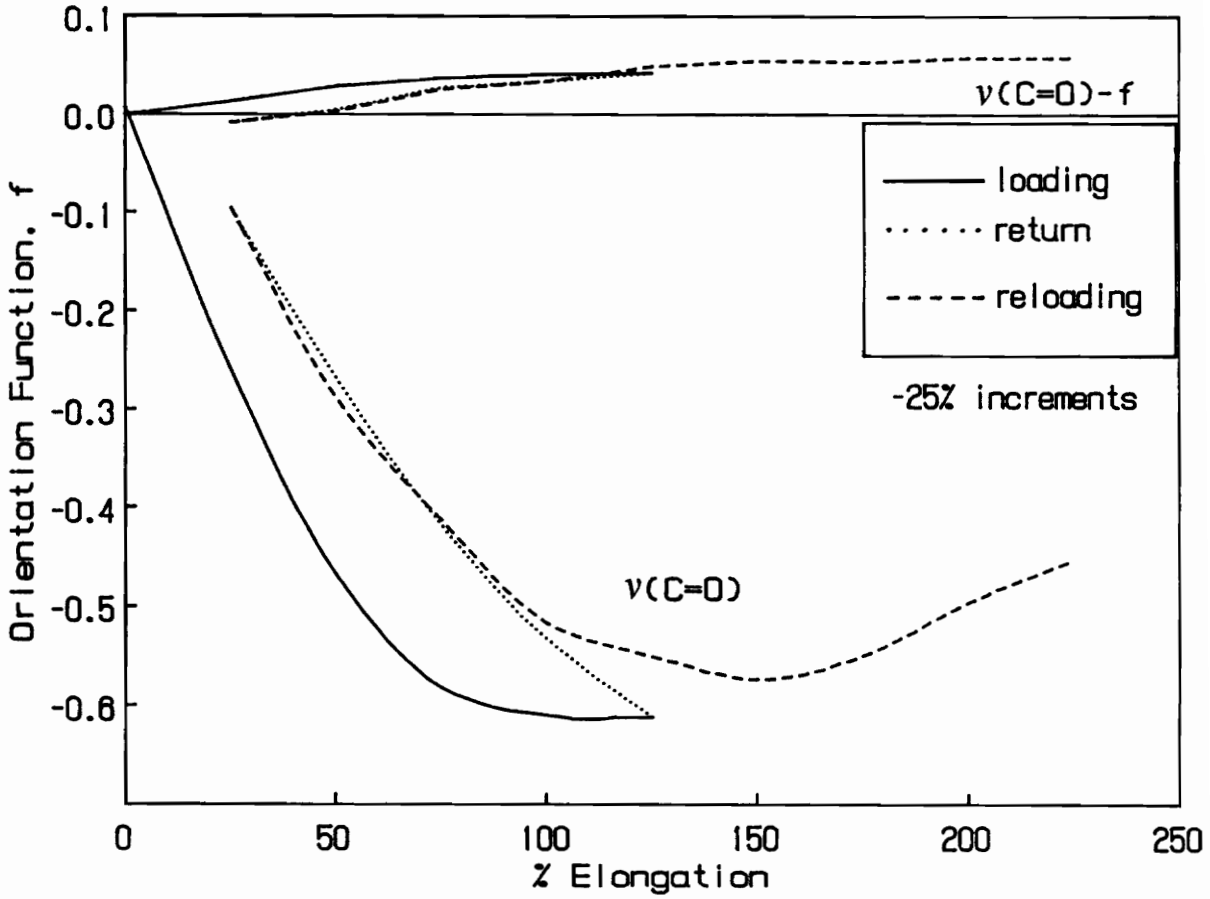

Figure 5.34. Orientational Hysteresis Behavior for the PUUE Elastomer: extension rate equal to 400 %/min; $f_{(CH_2)}$ not shown, but exhibits reversible behavior; $f_{(N-H)}$ also not shown, but exhibits behavior similar to $f_{(C=O)ur}$

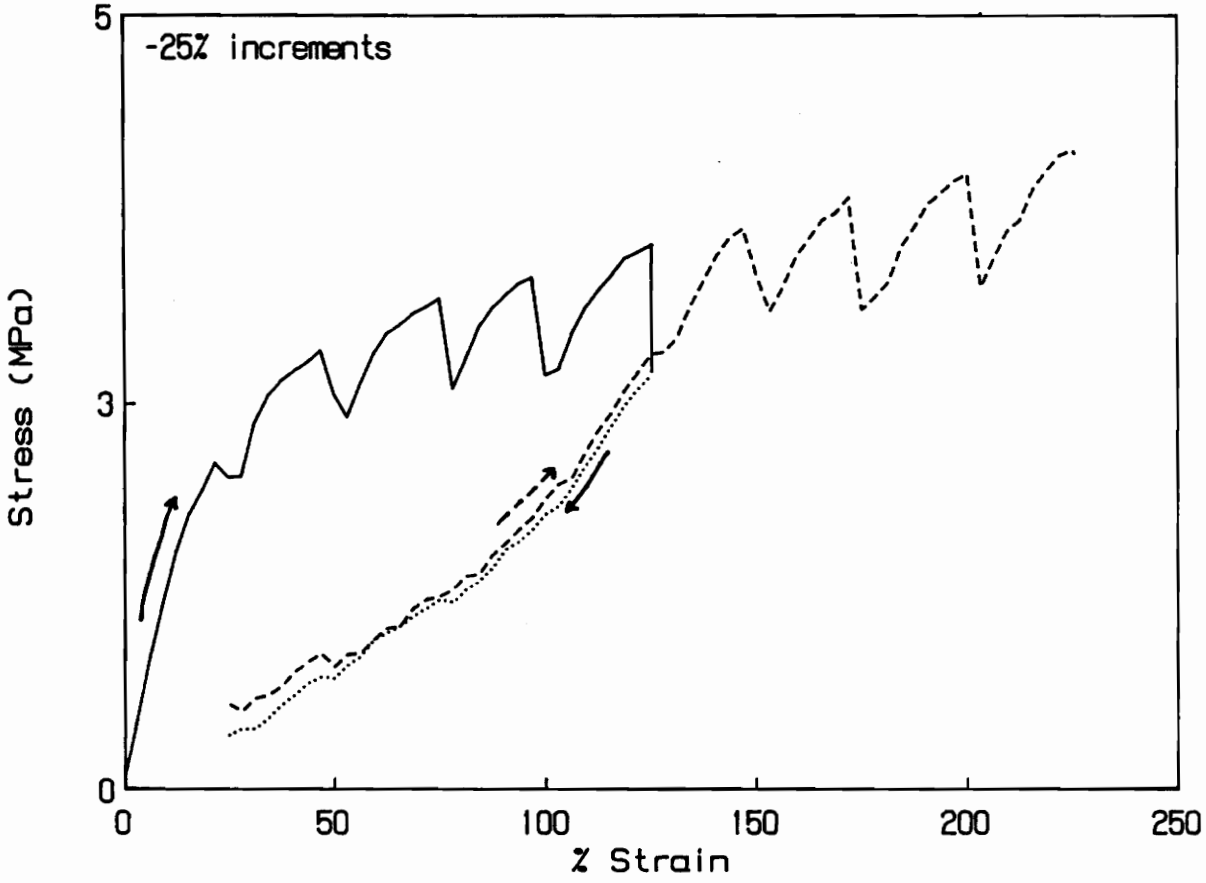

Figure 5.35. Mechanical Response for the PUUE Elastomer during Cyclic Deformation

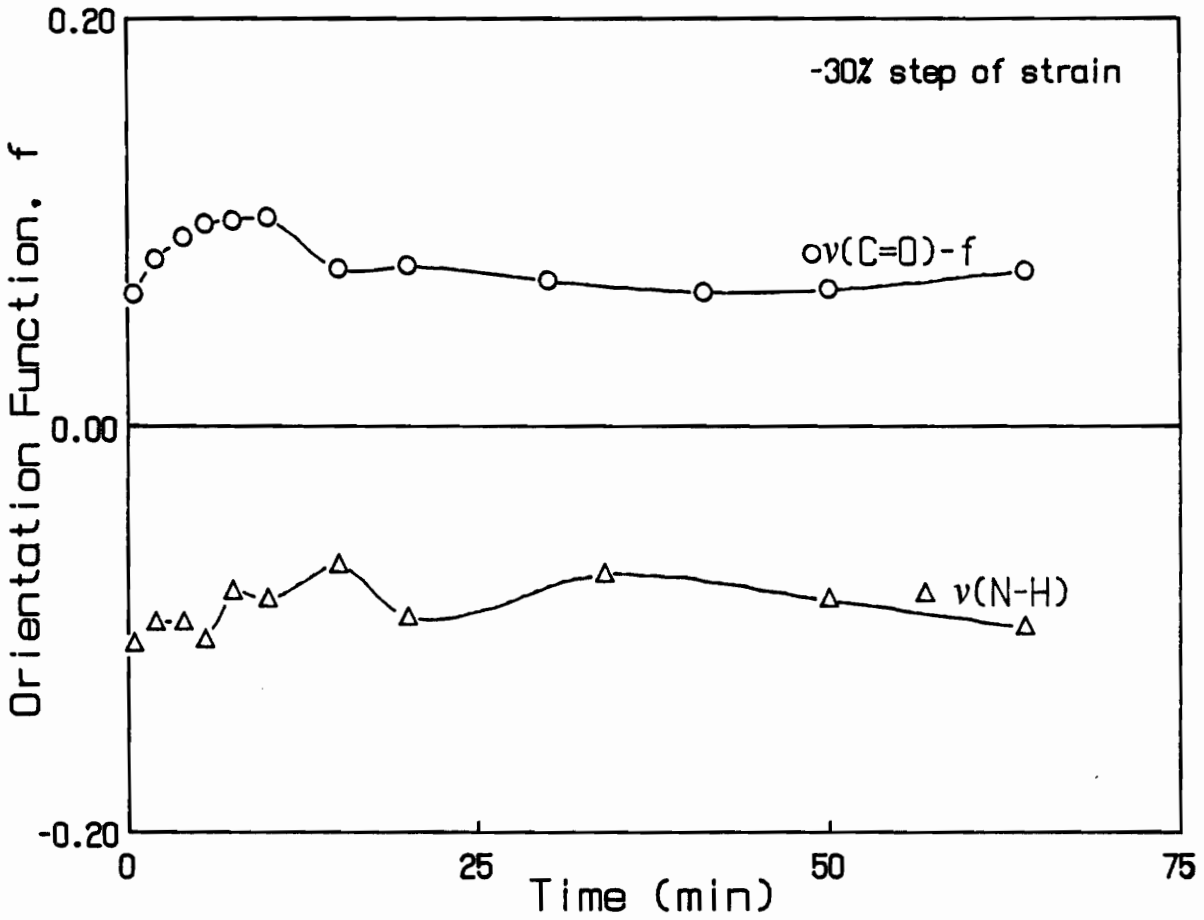

Figure 5.36. Orientation Time Behavior for Plaque 1-THF

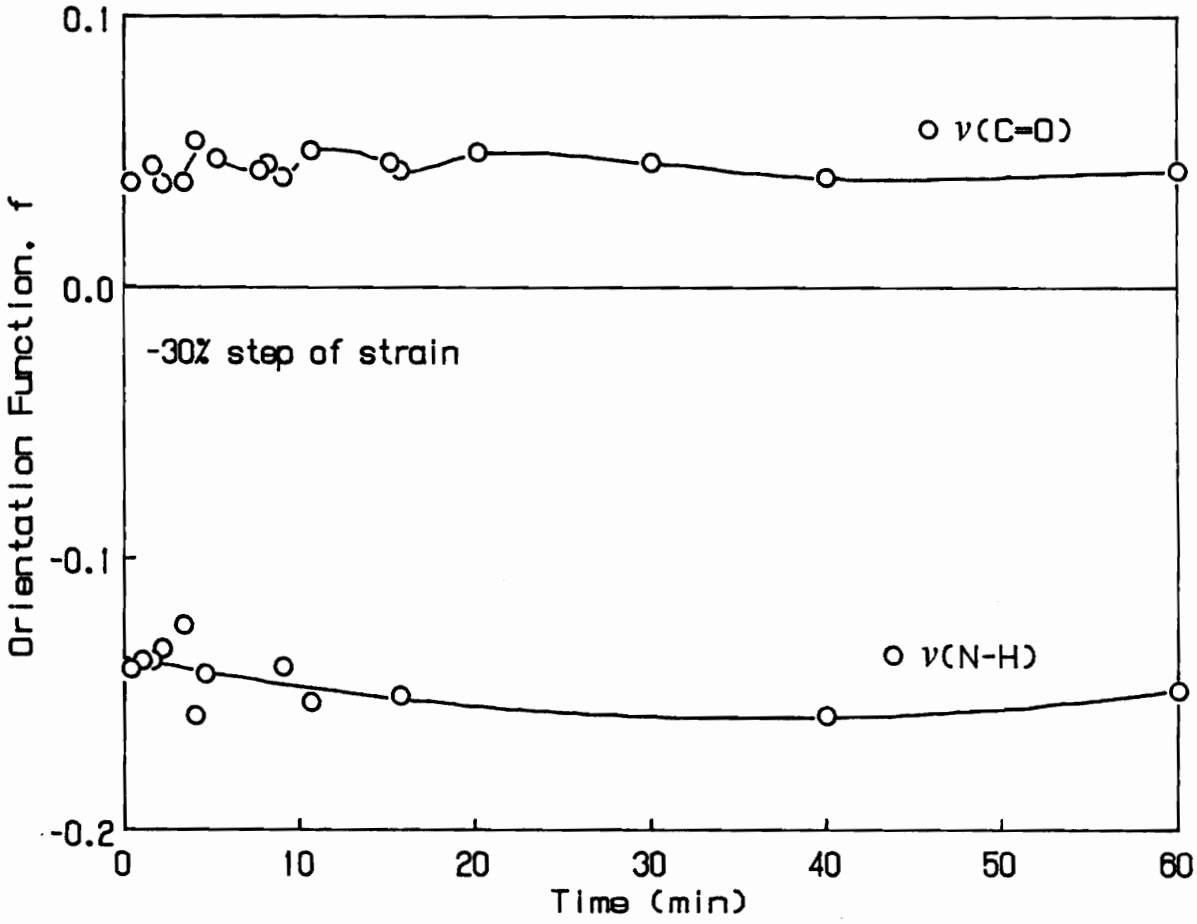

Figure 5.37. Orientation Time Behavior for Plaque 2-DMF

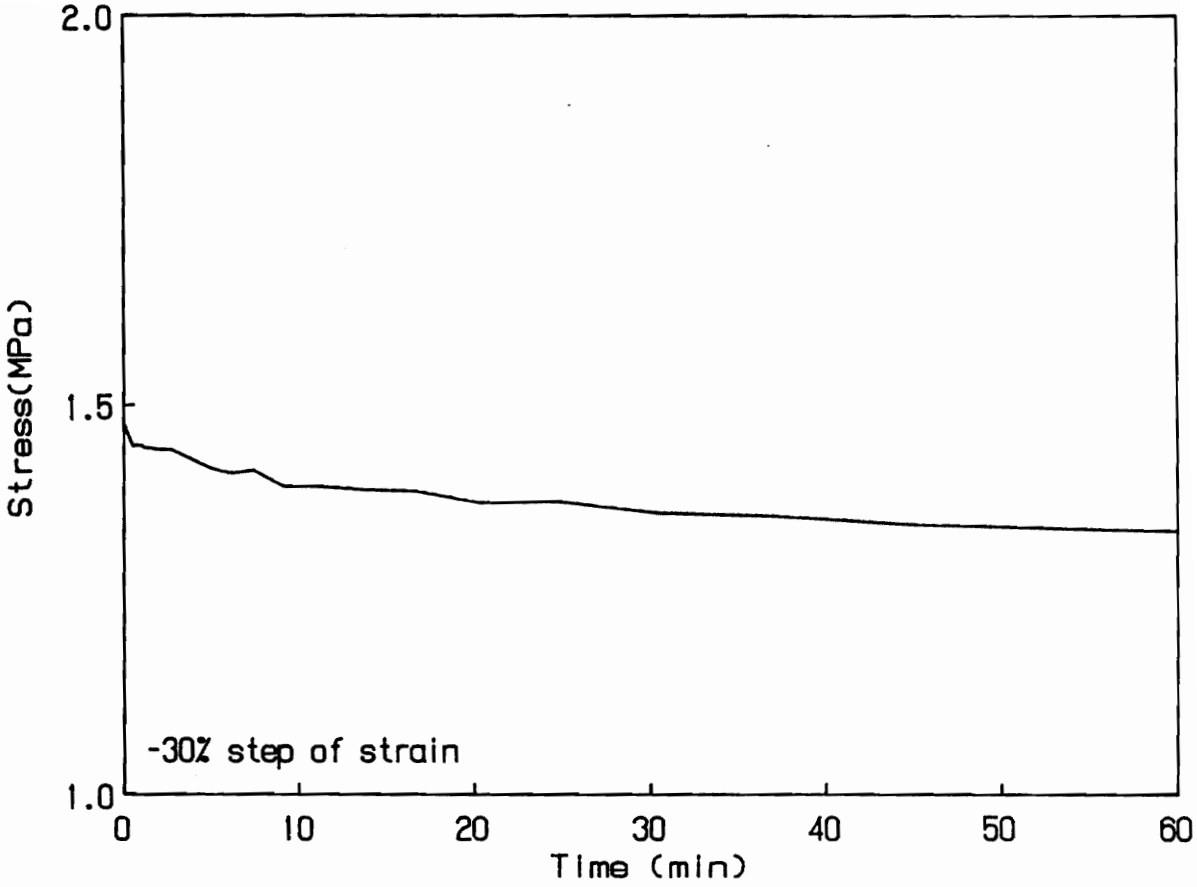

Figure 5.38. Simultaneous Stress Relaxation Behavior for Plaque 2-DMF

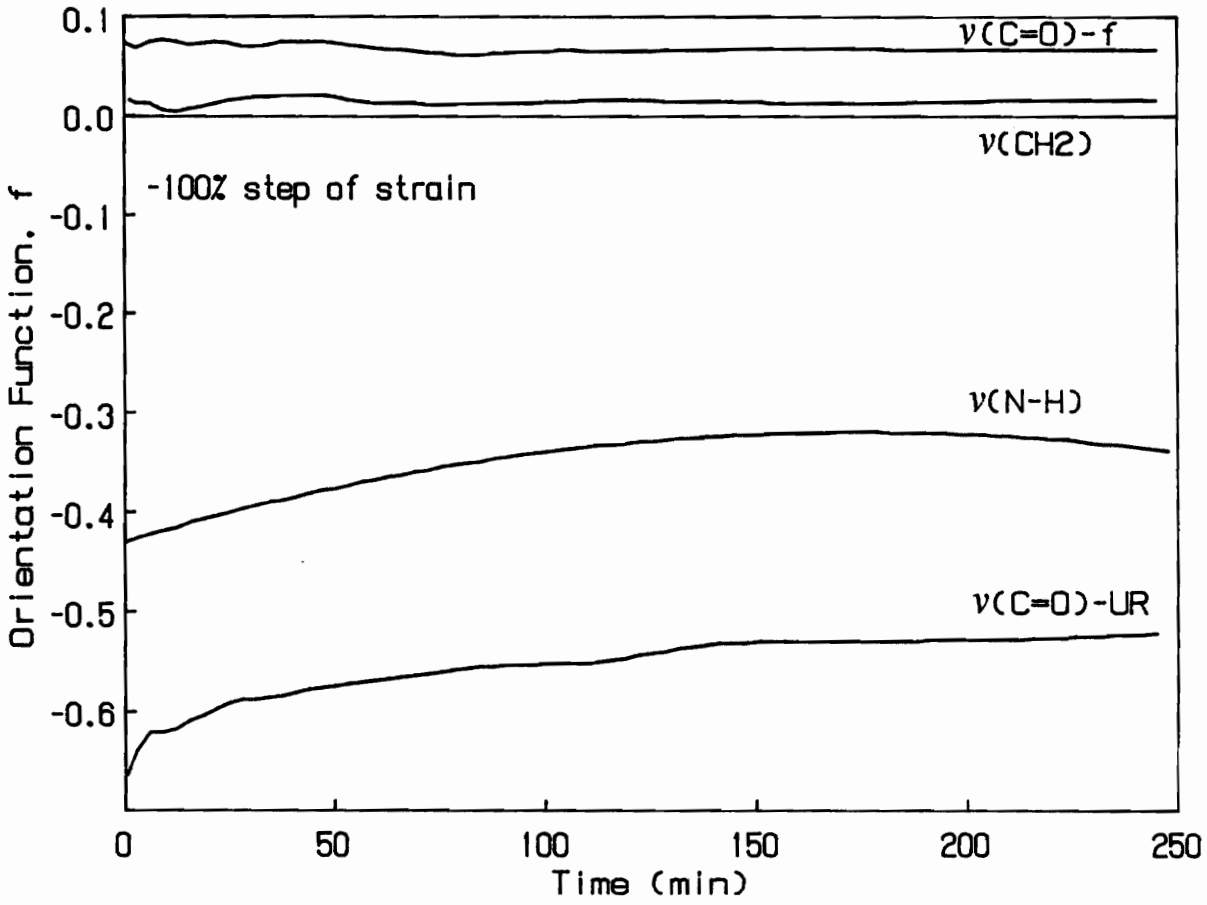

Figure 5.39. Orientation Time Behavior for the PUUE Elastomer

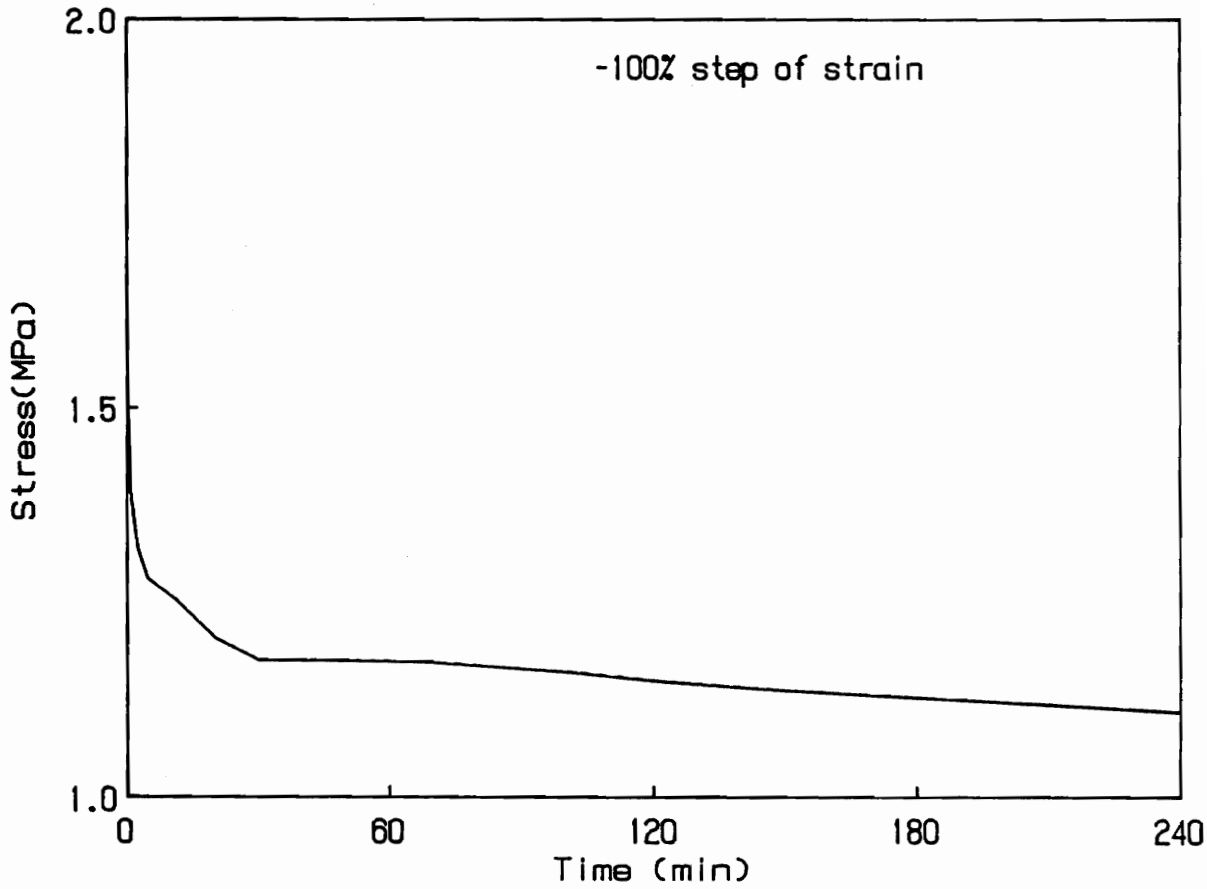

Figure 5.40. Simultaneous Stress Relaxation Behavior for the PUUE Elastomer

BLANK PAGE

Appendix A

Components for Stretching Apparatus

1. Linear Motor System (F-L5A)

   Manufacturer: Compumotor Corp.

   Parts: (1) 2 linear motors
   (2) 2 microstepping drives
   (3) platen
   (4) PC23 computer card

2. Load Cell (FT70-2)

   Manufacturer: Revere

   Description: A 1 kg force translator sensor which delivers better than 0.1% overall accuracy; contains a maximum safe load of 10kg

3. Analog to Digital Converter(ADM12-10)

   Manufacturer: Qua Tech, Inc.

   Description: The ADM12-10 is a 12-bit A/D conversion module and is used in conjunction with a PXB-721 Parallel Expansion Board. By using the software package, it is capable of a throughput rate of 24 kHz.

4. Polarizer (IGP-225)

   Manufacturer: Molectron Detector Corp.

   Description: Infrared grid polarizer with KRS-5 substrate material and 70% maximum transmission

5. Computer

Manufacturer: Ultra-Comp

Description: A pc/xt compatible with two disk drives, 448K memory, and monochrome monitor

6. Amplifier

Manufacturer: Constructed at Virginia Tech by Riley Chang

Description: Functions as a means to amplify voltage from load cell, as a signal conditioner and as a power source for load cell; has 1% non-linearity

7. Dogbone Die

Manufacturer: The Hudson Die Group

Description: See Figure 4.4; heat treated forged clicker die; dimensions: gage length = 25mm and cross sectional width = 8mm

Appendix B
Computer Program for Stretching Device

```
5000 REM THIS PROGRAM IS USED TO OBTAIN ORIENTATION-ELONGATION
5005 'DATA FOR PLAQUES
5010 REM this program is called calirssf
5020 REM NUMBER OF POINTS FOR STRESS-STRAIN = 15:
5025 'VELOCITY= 1.6764 MM/SEC
5030 INPUT "NUMBER OF POINTS";N,O
5040 INPUT "NUMBER OF DATA POINTS FOR STRESS-STRAIN
5045 RATE AND CROSS SEC. AREA";MM,EX,AX
5050 INPUT "DELAY";B
5060 INPUT "STRESS STRAIN FILENAME";FILE2$
5070 OPEN "B:"+FILE2$+".DAT" FOR OUTPUT AS #2
5080 INPUT "STRESS RELAXATION FILENAME";FILE$
5090 OPEN "B:"+FILE$+".DAT" FOR OUTPUT AS #1
5100 '
5110 'CALLING TO COLLECT LOAD READINGS TO ZERO LOAD CELL
5120 '
5130 ADDRESS%=&H260
5140 CALL ADC.SETUP(ADDRESS%)
5150 CHANNEL%=0
5160 FOR I= 1 TO 20
5170 CALL INADC12.S(CHANNEL%,ARRAY3%)
5180 PRINT ARRAY3%
5190 NEXT I
5200 INPUT "BINARY READING => xx=-(120-binary reading)";XX
5210 FOR II=1 TO 15
5220 '
5230 'CALLING MOTOR ADDRESS AND THEN SENDS COMMAND
5235 'TO MOTORS TO MOVE ONE INCREMENT
5240 '
5250 ADDRESS%=&H300
5260 CMD$ = "1V.033 2v.033 1d-1230 2d-1230 ps 1g 2g c
5270 GOSUB 1000
5280 '
5290 'CALLING UP A/D CONVERTER TO BEGIN RECORDING LOAD READINGS
5300 '
```

```
5310 ADDRESS%=&H260
5320 CALL ADC.SETUP(ADDRESS%)
5330 CHANNEL%=0
5340 REM IF (TIMER-A) => B THEN 5170
5350 REM GOTO 5120
5360 A=TIMER
5370 FOR I=1 TO MM
5380 '
5390 ' CALCULATION OF STRAIN GIVEN THE VELOCITY OF THE MOTORS
5395 'AND TIME OF TRAVEL
5400 '
5410 E(I)= (TIMER-A)*EX/.25 + 10*(II-1)
5420 CALL INADC12.S(CHANNEL%,ARRAY2%(I))
5430 ARRAY2%(I)= ARRAY2%(I)-XX
5440 PRINT E(I),ARRAY2%(I)
5450 NEXT I
5460 A=TIMER
5470 '
5480 'DO LOOP FOR STRESS RELAXATION BEHAVIOR AFTER REACHING
5485 'END OF INCREMENT
5490 '
5500 FOR J=N TO O
5510 AD=920
5520 FOR K=1 TO 5
5530 CALL INADC12.S(CHANNEL%,ARRAY%(K))
5540 ARRAY%(K)=ARRAY%(K)-XX
5550 F=TIMER-A-B
5560 ATIME = ATIME + F
5570 ALOAD = ALOAD + ARRAY%(K)
5580 NEXT K
5590 AVGT(J)=ATIME/5 : AVGL(J)=ALOAD/5
5600 PRINT AVGT(J),AVGL(J)
5610 ATIME=0 : ALOAD=0
5620 AD=AD-1
5630 IF AD=0 THEN 5640 ELSE 5620
5640 NEXT J
5650 INPUT "DO YOU WANT TO CONTINUE WITH STRESS RELAXATION
5655 (N,O,P PRINT)";D$,N,O,P
```

```
5660 IF D$="Y" THEN 5500 ELSE 5700
5670 '
5680 ' CALCULATION OF STRESS FROM LOAD READINGS OBTAINED
5685 'DURING STRESS RELAXATION
5690 '
5700 FOR L=1 TO P STEP 2
5710 IF AVGL(L) =< 800 THEN 5740 ELSE 5720
5720 STRESS = AVGL(L)*.111071317#+14.1
5730 GOTO 5750
5740 STRESS=AVGL(L)*.14129685#-10.08
5750 STRESS1=98.1*STRESS*AX/1000000!
5760 TIME=AVGT(L)/60
5770 ' WRITING STRESS RELAXATION DATA TO DATA FILE
5780 WRITE #1, TIME,STRESS1
5790 NEXT L
5800 '
5810 ' LOOP FOR CALCULATION OF STRESS OBTAINED DURING SAMPLE
5815 'STRETCHING
5820 '
5830 FOR NN=1 TO MM
5840 IF ARRAY2%(NN) =< 800 THEN 5870 ELSE 5850
5850 STR=ARRAY2%(NN)*.111071317#+14.1
5860 GOTO 5880
5870 STR=ARRAY2%(NN)*.14129685#-10.08
5880 STR1=98.1*STR*AX/1000000!
5890 WRITE #2, E(NN),STR1
5900 NEXT NN
5910 INPUT "DO YOU WANT TO ELONGATE FURTHER";E$
5920 IF E$="Y" THEN 5930 ELSE 5940
5930 NEXT II
5940 CLOSE #2 : CLOSE#1
5950 END
```

Appendix C
Components for Thermal Chamber

Materials

1. Ryton® Polyphenyl Sulfide Advanced Thermoplastic Composite
   Manufacturer: Phillips Petroleum
   Description: graphite fiber reinforcement; service temperatures up to 300°C

2. Absestos Free Milboard
   Description: 1/8 of an inch in thickness; insulating material with service tempertures up to 930°C

3. Nylon Machine Screws
   Description: #4-40 screw; maximum service temperture of 150°C

4. Salt Plates
   Manufacturer: Aldrich
   Description: Sodium Chloride; 25 mm in diameter, 4mm in thickness

Temperature Components

1. Miniature Microprocessor Temperature Controller
   Manufacturer: Omega
   Description: PID approach control; ± 0.1°C resolution up to 200°C

2. Type K, Chromel-Alumel Thermocouple
   Manufacturer: Omega
   Description: 6 inch subminiature thermocouple

3. Silicone Rubber Flexible Heater
   Manufacturer: Watlow
   Description: Maximum surrounding temperature of 220°C; 120 volts and 5 watts/in; heater is 5″ by 2″ and 1/16 of an inch in thickness

Appendix D
Possible Explanation for Biaxial Orientation

Problem: Some of the orientation values obtained for $(C=O)_{ur}$ groups were greater than -0.5. The lowest value was about -0.6 which corresponds to a dichroic ratio, D, equal to 2.35 assuming $\alpha = 90°$ (α defined on pg.194 in Fig. 1).

The dichroic ratios are of course determined from the experimental values of $A_{\parallel}$ and $A_{\perp}$ and then by taking the ratio of $A_{\parallel}$ to $A_{\perp}$. Thus, in determining why the dicroic ratio is greater than 2 or the orientation function is less than -0.5, the derivation of D given by Fraser will be examined (51).

In doing so, it will be assumed that the chains(hard segments) are aligned transverse to the stretch direction. This of course corresponds to a dichroic ratio equal to 2 and likewise an orientation function equal to -0.5. Furthermore, this calculation for the orientation function from the experimental dichroic ratio is based on the chains being symmetrical about the stretch direction(z) and the transition moment for $(C=O)_{ur}$ being symmetrical about the chain axis (see Fig 1). Thus, if D > 2, this suggests that the chains or the transition moments are not symmetrical about their respective axes. In the pages following, both cases will be considered in the derivation for the dichroic ratio.

Recalling that $A \propto (P \bullet \mu)^2$, one needs to find μ with respect to Q, b, a such that

$$\mu = \cos\alpha\hat{Q} + \sin\alpha\cos\psi\hat{a} + \sin\alpha\sin\psi\hat{b} \qquad [1]$$

for $P = P_{\parallel}$

$$P \bullet \hat{Q} = \cos\beta$$

$$P \bullet \hat{a} = 0$$

$$P \bullet \hat{b} = -\sin\beta$$

therefore,

$$(P_{\parallel} \bullet \mu)^2 = \cos^2\alpha \cos^2\beta + \sin^2\alpha \sin^2\psi \sin^2\beta \qquad [2]$$

for $P = P_{\perp}$

$$P \bullet \hat{a} = -\cos\phi$$

$$P \bullet \hat{Q} = \sin\beta \sin\phi$$

$$P \bullet \hat{b} = \cos\beta \sin\phi$$

therefore,

$$(P_{\perp} \bullet \mu)^2 = \cos^2\alpha \sin^2\beta \sin^2\phi + \sin^2\alpha \cos^2\psi \cos^2\phi + \sin^2\alpha \sin^2\psi \cos^2\beta \sin^2\phi \qquad [3]$$

D is a $f(\phi, \alpha, \beta)$ and D is given as a ratio of the average of $|P_{\parallel} \bullet \mu|^2$ over the average of $|P_{\perp} \bullet \mu|^2$. Averaging for this paticular coordinate system consist of averaging over all angles of ϕ (chain axis about stretch direction) and ψ (μ about the chain axis) -see Fig. 1 (79).

If the assumption is made that the chains lie at one angle, ϕ, and all possible orientations over ψ[1] , then

$$D = \frac{\frac{1}{2\pi}\int_0^{\pi} d\psi \, |P_{\parallel} \bullet \mu|^2}{\frac{1}{2\pi}\int_0^{\pi} d\psi \, |P_{\perp} \bullet \mu|^2} \qquad [4]$$

and substituting in eq.'s [2] and [3] in eq. [4]; D becomes

---

[1] probability that a given bond lies in the region $d\psi$ is $\frac{d\psi}{2\pi}$

$$D = \frac{\cos^2\alpha \cos^2\beta + 0.5 \sin^2\alpha \sin^2\beta}{\cos^2\alpha \sin^2\beta \sin^{\phi} + 0.5 \sin^2\alpha(\cos^2\phi + \cos^2\phi \sin^2\phi)} \quad [5]$$

If one lets $\alpha = 90°$ (close for $(C=O)_{ur}$) and $\beta = 90°$ ($\beta = 90°$ - corresponds to all chains being aligned transverse to the stretch direction), then

$$D = \frac{1}{\cos}^2\phi \qquad \phi = \cos^{-1}(\frac{1}{D})^{0.5}$$

and for $D = 2.35 \rightarrow \phi \geq 50°$.

If the assumption is made that the transition moments for $(C=O)_{ur}$ lie at an angle ψ and all possible orientations over ϕ are valid, then

$$D = \frac{\frac{1}{2\pi}\int_0^{\pi} d\phi \, |P_{\parallel} \bullet \mu|^2}{\frac{1}{2\pi}\int_0^{\pi} d\phi \, |P_{\perp} \bullet \mu|^2} \quad [6]$$

and substituting in eq.'s [2] and [3] in eq. [6]; D becomes

$$D = \frac{\cos^2\alpha \cos^2\beta + \sin^2\psi \sin^2\alpha \sin^2\beta}{0.5 \cos^2\alpha \sin^2\beta + 0.5 \sin^2\alpha(\cos^2\psi + \cos^2\psi \sin^2\phi)} \quad [7]$$

Again if one lets $\alpha = 90°$ and $\beta = 90°$, then

$$D = 2\tan^2\psi \qquad \psi = \tan^{-1}(\frac{D}{2})^{0.5}$$

and for $D = 2.35 \rightarrow \phi \geq 50°$.

In both cases (ϕ,ψ), for D equal to 2.35, the azimuthal angle for which the chains or transition moments are oriented is equal to 50°. The case for which the hard segments align at an angle of 50° or the distribution of chains are preferentially aligned at or near to the film surface, is possible

since these hard segments are part of lamellar domains. In other words, the lamellar domains as a whole could be aligning at an angle to the surface as well as transverse to the stretch direction.

The case for which the transition moments align at a 50° angle about the chain axes, is also possible due to the rigidity of the hard segments. This rigidity as well as the hydrogen bonding between the hard segments could contribute to the transition moments of $(C=O)_{ur}$ being aligned at an angle about the chain axes or taking a non-random distribution such that the angle about the chain axes is heavily weighted towards 50°.

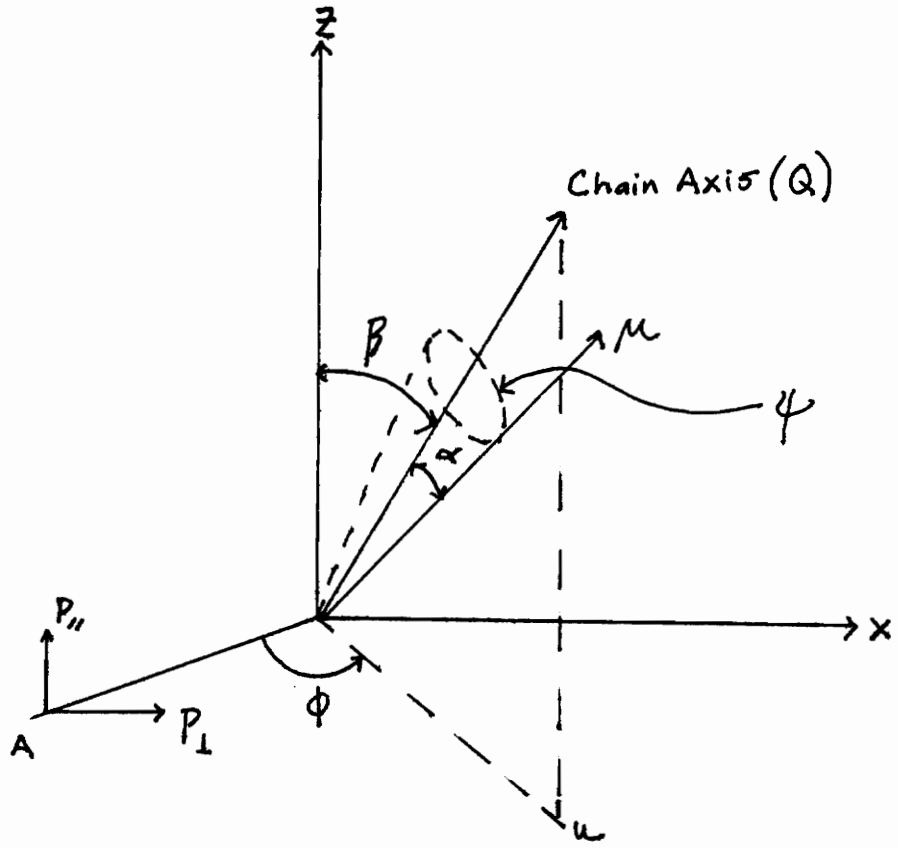

Using a right-handed frame, such that the chain axis is its z-axis, μ can be related to Q, b, and a

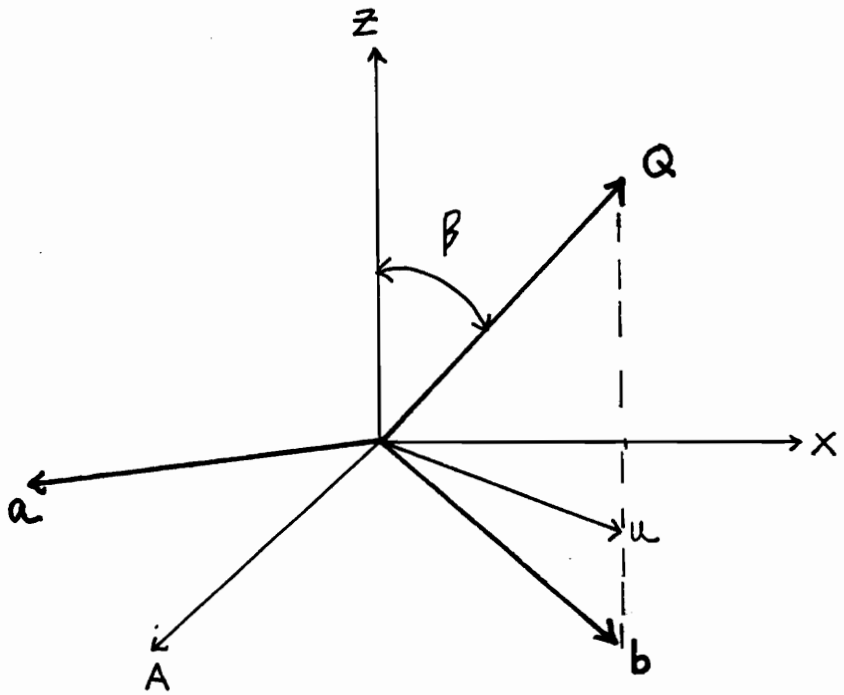

Figure 1: Coordinate Systems for Derivation of Dichroic Ratio

Vita

John Calloway Moreland was born on August 19, 1963 to Dr. and Mrs. Charles G. Moreland in Gainesville, Florida. He grew up in Raleigh, N.C. where he attended Needham B. Broughton High School. In 1986, Cal obtained his Bachelor of Science degree in chemical engineering from North Carolina State University. He then entered Virginia Tech and in February, 1989 received his Master of Science in chemical engineering. Cal is presently working on his Doctorate in chemical engineering under the guidance of Dr. G.L. Wilkes at Virginia Tech.